NEW FLEXIBLE MOLDABLE ION-EXCHANGE POLYMERS AND THEIR ANALYTICAL APPLICATIONS

by

FERESHTEH MALEKI

Presented to the Faculty of the Graduate School of The University of Texas at Arlington in Partial Fulfillment of the Requirements

for the degree of

DOCTOR OF PHILOSOPHY

THE UNIVERSITY OF TEXAS AT ARLINGTON

August 2021

I dedicate this dissertation to my parents,

Mohammad Javad Maleki and Fatemeh Maleki

Because of all their sacrifices that they made for me and my brothers to provide everything for us to grow up in an environment full of love and peace. They value everyday learning, education and science and they always support our backs to achieve what we are wishing for.

To love of my life,

Dr. Seyed Amir Jafari Ghoreshi

Who was beside me all the way in gaining my Ph.D.

And my kind, wise and joyful son,

Liam Aryo Jafari Ghoreshi

Who was my best companion from the moment he started his life in this world

To my brothers,

Majid and Hamid Maleki

For all the laughter they bring to me when I feel lonely or tired.

For their efforts to make me feel that my parents are not alone while I am very far away.

Acknowledgments

I feel extremely fortunate to have Dr. Dasgupta as my mentor in my long journey of PhD program. He is a great professional analytical chemist whose unlimited supports, new ideas, enthusiasm, passion always kept me motivated to learn more and break my boundaries to achieve more. What I have achieved as a graduate student is all because of him and his efforts and contributions to make me successful. He is not only my academic mentor but also my life mentor as well. His big heart and generosity are unique about him which cannot be found in everyone easily. He is always there when I need a kind support like my father.

When I became mom during my PhD studies, he understood me, supported me, and helped me to keep going and achieve the best. He is like a grandfather to my son and even my 2.5-year-old son loves him like his grandpas.

I would like to thank my committee members, Dr. Frank Foss, Dr. Daniel Armstrong, and Dr. Saiful Chowdhury for their time and valuable suggestions.

I would like to thank Dr. Charles Shelor (Phillip) for all his professional and friendly supports. I was so lucky to find him as one of my best friends.

Abstract

NEW FLEXIBLE MOLDABLE ION-EXCHANGE POLYMERS AND THEIR ANALYTICAL APPLICATIONS

Fereshteh Maleki

The University of Texas at Arlington, 2021

Supervising Professor: Purnendu K. Dasgupta

This dissertation aims to improve the functionality of open tubular capillary ion chromatography (OTIC) in terms of the lower limit of detection (LOD) and higher sensitivity by fabricating a microchannel suppressor and integrating it into an OTIC system. To reach the goal, an ion-exchange membrane (IEM) was formulated and developed using aqueous solutions environmentally friendly chemicals. The PVA-SS polymer is made from poly vinyl alcohol (PVA) as the polymer matrix and styrene sulfonate sodium salt (SS) as the ionic functional group (the salt-form polymer is eventually converted to acidic form), referred to here mostly as PVA-SS polymers. The new IEM has high ion-exchange capacity (IEC), at the high end, 2 times more than best known commercial cation exchange membrane, Nafion®. The PVA-SS prepolymer solution can be uniquely cast around fine wires as mandrels, polymerized, and thus generate a smooth circular micro-size channel after removing the wire. This allowed us to succeed in fabricating

suppressors with diameters size close to those of actual OT columns in use sizes.

The second chapter of the dissertation reviews the broad area of analytical applications of ion-exchange membranes (IEM) including their applications in IC in fabricating suppressors, the main focus of this dissertation. It provides a complete history of IEM-based suppressors in IC and how they have been evolved. It reviews different geometries of chemically and electrodialytically regenerated suppressors from macro to micro size. In addition, it covers other analytical applications of IEMs, such as electrodialytic eluent generation, water purification, charge detection, matrix isolation, and reagent introduction, Donnan dialysis separation, and preconcentration.

Chapter 3 discuses formulating, developing, and characterizing PVA-SS as a novel moldable strong cation-exchange polymer. It centers on the synthesis of PVA-SS polymers and their characterization for water sorption capacity, specific conductance values, and ion-exchange capacities across the different polymer compositions. IEMs exhibit anisotropy regarding their electrical conductance. The two different specific conductance values of IEMs (normal and tangential) were thoroughly discussed including experimental values of PVA-SS and compared with those for several commercial IEMs. PVA-SS polymers were found to absorb water (as moles of water/mole H^+) 5- 10 times greater than does Nafion. The IEC of PVA-SS polymers at the high SS-content end is $>$ 2x of Nafion.

The PVA-SS polymers survive hour-long boiling in water and alcohols and maintains their high IECs over repeated regeneration cycles. This chapter also describes the fabrication of microchannel $\sim$ 30 μm in diameter from casting the prepolymer solution around the 25 μm wire as a mandrel. The microchannel permitted facile flow of water and was shown to withstand at least 300 psi pressure.

Chapter 4 covers how a fabricated 45 μm bore microchannel in a PVA-SS polymer was utilized as a microsuppressor in OTIC. The microsuppressor was characterized using tandem mass spectrometry (MS) and conductance measurements to determine any potential leaching of the polymer or its monomeric components. A commercial electrodialytically regenerated suppressor was also characterized in a similar manner by MS. The PVA-SS microchannel suppressor showed that with rare exceptions (possibly in the m/z range of 675-750), no significant leachates over blank water were observed for the whole range of m/z 30-1500. The blank was water that went directly through the system bypassing the suppressor. However, for the commercial suppressor, the story was completely different. The PVA-SS polymer simply has far less detectable MS background to permit extended use in mass spectrometry. The microsuppressor was next integrated with the column and detector to realize its practical application as a chemically regenerated suppressor in an OTIC system. The microsuppressor was placed between an admittance detector and a conductivity following the separation column. The two separate detectors

provide orthogonal information about the analytes and also permit evaluation of the dispersion caused by the microsuppressor. The results indicated that the induced dispersion is perceptible even with the suppressor of this bore and the additional dispersion of a 700 μm long suppressor can discerned over that caused by a 400 μm long suppressor. However, the considerable increase in peak height and decrease in baseline noise in suppressed IC results indicate that adding the microsuppressor leads us to the lower LOD and higher sensitivity. A 700 μm long microsuppressor was tested at a flow rate of 168 nL/min (typical of flow rates currently used in OTIC) for its ability to suppress (quantitively exchange K^+ for H^+) a KOH solution. The microsuppressor could suppress 30 mM KOH; comparison, most practical eluent concentrations in OTIC is less than 10 mM. The capabilities of a PVA-SS microsuppressor is therefore adequate.

The last chapter addresses potential future work in this area. Ways to improve the performance by modifying PVA-SS microsuppressors are suggested and discussed.

TABLE OF CONTENT

LIST OF ILUSTRATIONS

LIST OF TABLES

Chapter 1

INSTRODUCTION

This dissertation covers a two-part project: (a) developing a new class of moldable ion exchange polymer and (b) its application as a microsuppressor in open tubular ion chromatography. The dissertation starts with a comprehensive review on analytical applications of ion-exchange membranes in analytical chemistry in general and ion chromatography in particular. This review article, title, Dasgupta, P. K.; Maleki, F. *Talanta*, **2019**, 204, 89-137 comprises chapter 2.

Chapter 3 focuses on the first part of the project, namely synthesizing and developing a moldable strong cation exchange polymer and initial attempts towards microchannel fabrication. This article, title, Maleki, F.; Dasgupta, P. K. *Analytical Chemistry*, **2020**, 92, 13378-13386, centered on how the ion exchange polymer (IEP) was synthesized, characterized and how the microchannel was fabricated with the novel IEP.

Chapter 4 covers the fabrication of the microsuppressor and its application in OTIC. Detailed characterization of the microsuppressor regarding leaching of ionic and nonionic material by mass spectrometry and conductance measurements have been included in this article, Moldable Capillary Suppressor for Open Tubular Ion Chromatography Based on Polymeric Ion Exchanger, Maleki, F.; Chouhan, B.; Shelor, C. P.; Dasgupta, P. K., presently being submitted. I carried out the polymer synthesis part, microsuppressor fabrication, and wrote the first draft of the manuscript. Dr.

Bikash Chouhan performed all IC experiments with the microsuppressor. Dr. Charles Shelor performed the leaching studies on the microsuppressor via mass spectrometry and conductance measurements.

Ion chromatography (IC) was introduced in 1975 based on a novel idea, column effluent conductivity suppression.[1] Few small ions, inorganic or organic, can be selectively determined by optical absorption.[2] In favorable cases they have to be derivatized. Similarly, while potentiometric methods exist for some ions, they are often not successfully selective. Ions that can be determined electrochemical redox processes or luminescence methods are fewer still. On the other hand, electrical conductivity is an universal trait for all ions and should be an ideal detection method for ions that are chromatographically separated. But ion (exchange) chromatography (IC) intrinsically requires highly conductive ionic eluents. Detecting trace ionic analytes conductometrically on such a background would normally be impossible. IC owes its success to the suppressor. The suppressor is an ion exchanger device that is placed between the column and the detector in IC to reduce the conductivity background and simultaneously enhance the analyte signal. For anion chromatography (as an example), the suppressor is a cation-exchanger that exchanges eluent cations (typically Na^+ or K^+) in a KOH or NaOH eluent with H^+. This results in a background of poorly conductive H_2O while analytes like Cl^-, NO_3^-, SO_4^{2-} etc. enter the detector as highly conducting corresponding acids.

Taking IC to the open tubular scale is a challenge, particularly in fabricating a small enough membrane suppressor. The fabrication of the first capillary suppressor began with making ~ 40 μm diameter crack by a 300 μm needle in minute blocks of Nafion perfluorosulfonate Catex material.[3] Both because of the lack of availability of this material in this form and the fact that the “cracks” change their flow resistance over time, something closing up altogether, alternatives to building a capillary suppressor were sought. The next chapters detail this effort.

Chapter 2

ION EXCHANGE MEMBRANES IN ION CHROMATOGRAPHY AND RELATED APPLICATIONS

2.1. Introduction

Ion exchange membranes (IEMs) have major industrial applications, from the large-scale use in the chemical process industry to miniature cells/batteries used by individual consumers; several books have been written on the topic. However, it is also true that there are many unique (and some major) applications in the analytical sciences that would not exist in the present form without IEMs; such an account has not appeared anywhere to our knowledge, with one exception. That exception is ion sensing; however, sensing membranes used in such applications (mostly potentiometry) are rarely conventional IEMs. This area is not covered here. The areas covered are detailed in the abstract. Briefly, perhaps because of the senior authors' predilection, the use of IEMs in all areas of ion chromatography (IC) is thoroughly covered, including their use in sample preparation. Some unique properties of IEMs, specifically a H^+-form cation exchange membrane (CEM), namely their high affinity and permeability to water, have led to equally unique applications, facilitated by the ready availability in tubular form.

2.2. Ion exchange Membranes in Ion Chromatography

Ion chromatography is an important subset of liquid chromatography and is presently the benchmark technique for ion analysis, especially anion

analysis, with a worldwide annual market exceeding US $300 million. Small, Stevens and Baumann[1] invented IC in 1975. While separation of ions on a packed bed of ion exchange media has been known for a long time prior to this, the problem has always been sensitive detection. Analyte ions must be pushed through the column with ionic eluents, creating a highly conductive ionic background. This made it difficult to detect analyte ions through changes in the solution electrical conductivity, the hallmark property of ions that distinguishes them from uncharged molecules. Small et al. provided an ingenious solution to this problem: For the separation of cations, they used a strong acid eluent (e.g., HCl) and a cation exchange (CEX) column for the separation of target alkali and alkaline earth cations, this column was followed by a strong base type anion exchange (AEX) column in OH^- form. The second column converted the eluent HCl to poorly conducting water while the analyte cations emerged from this column as fully ionized and strongly conducting LiOH, NaOH, KOH, etc., and were sensitively detected by a conductivity detector (CD). The second column, initially called a “stripper” was later termed a “suppressor”, as it suppressed the eluent conductivity, while amplifying the analyte conductance compared to the original analyte conductance. Anion chromatography using the same principles was deemed to be more valuable from the very beginning - after all atomic spectrometric techniques were already available to determine the metal cations but this was not the case for anions.

Although the obvious choice for anion chromatography would have been the obverse of what was done for cation chromatography, namely using an AEX separation column with an alkali hydroxide eluent and use an H^+-form strong acid CEX column as the suppressor, for a variety of reasons, it was not initially possible to use hydroxide as the eluent in anion chromatography. Anion chromatography was first commercialized with a mixture of sodium carbonate and bicarbonate as eluent; this was neutralized to carbonic acid by the suppressor. While carbonic acid did not provide as low a conductivity background as water, it was still rather weakly conducting and permitted sensitive detection of ions making anion chromatography an immediate commercial success.

2.3. IEM-Based Suppressors in IC

In its introductory section, a recent paper [4] provides an excellent account of the evolution of IC suppressors over time; this account is strongly recommended.

2.3.1. Chemically Regenerated Suppressors

While the invention of the suppression scheme was a *tour de force* in ingenuity, the use of a packed column as a suppressor was not without problems. A packed column has a finite capacity, the H^+-form suppressor used in anion IC is converted during use to the Na^+-form by the $NaHCO_3/Na_2CO_3$ bearing eluent and eventually must be regenerated to the H^+-form before re use. In its first commercial incarnation, the packed column

suppressor was made large enough to last for a typical workday (8 h) with the recommended eluent and flow rate combination. The sizable suppressor column induced considerable band dispersion, deteriorating chromatographic performance. Two suppressors had to be present in the system; when one got exhausted, the other one, already regenerated and washed, was switched in its place but still required significant time to equilibrate with the eluent from its water-washed state. Another unforeseen aspect of a high-capacity gel-type CEX resin column in H^+-form as a suppressor is that it also behaves as a chromatographic element. Moderately weak acid ions like acetate are neutralized by the suppressor to acetic acid, the unionized fraction of this has no charge, is not subject to the Donnan barrier and can partition to the water phase in the interior of the gel-type resin. This retention is quantitatively different for the H^+-form vs. the Na^+-form resin, due to the different amounts of water held in the gel-phase. As a result, when the suppressor is fresh (i.e., mostly in the H^+-form, an analyte ion like acetate exhibits a greater retention time than when the suppressor is nearly exhausted and is mostly in the Na^+-form. The retention in the separation column does not change but that in the suppressor decreases as the latter is converted to the Na^+-form. As such, the retention time, the primary marker used for analyte identification in chromatography, changes as a function of how long the suppressor has been used.

Stevens et al. [4] provided a solution in the form of a suppressor made from a tubular IEM. They sulfonated polyethylene capillaries, 300 µm in

bore, to convert the tube to a CEM. The principle is illustrated in Figure 4-1; the $NaHCO_3/Na_2CO_3$ eluent flowed inside the fiber while the exterior was bathed by a countercurrent flow of dilute H_2SO_4. Driven by the proton gradient across the membrane, H^+ was transported to the lumen of the membrane while Na^+ was carried outside to waste. Anion transport across the membrane was inhibited by the Donnan barrier. Thus, this IEM-based suppressor was continuously regenerated and did not need to be taken off-line for regeneration. The state of the suppressor remained unaltered at all times, preventing any retention drift of analytes like acetate.

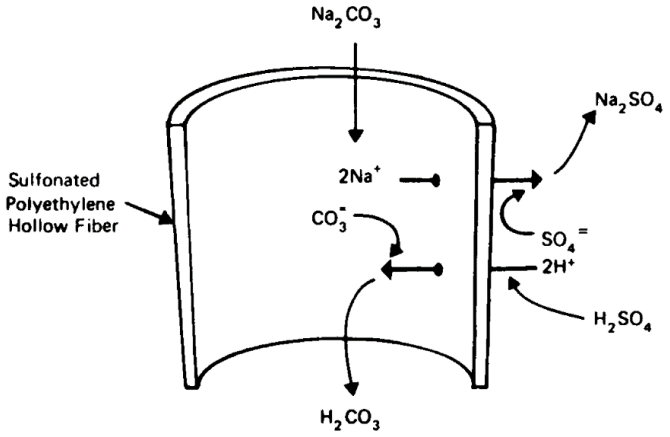

Figure 2- 1.Operating principle of first IEM-based continuously regenerated suppressor. Reprinted from reference [4] with permission from the American Chemical Society.

This IEM-based suppressor was never commercialized. Even with a wall thickness as littles 40 µm, sulfonated polyethylene made relatively poor IEMs. The capillary bore represented a significant pressure drop. As many as 8 hollow fibers, each ~2 m length, needed to be used in parallel to

achieve suppression of a 3 mM $NaHCO_3$/2 .4 mM Na_2CO_3 eluent flowing at 1.1 mL/min. Because it is impossible to achieve identical residence times in eight fibers, band dispersion in this suppressor was considerable. The first commercialized IEM based suppressor utilized commercially available Nafion perfluorosulfonate ionomer tubing, wet i.d. ~0.9 mm. The IEM tube was packed with solid beads in a pearl string configuration (bead diameter approximately equal to 60 % of the tube i.d.) to improve mass transfer and reduce the unacceptable dispersion caused by such a large bore tube on [5]. This device enjoyed some commercial use but exhibited relatively poor durability. This was not as much a fault of the design as the imperfection of ancillary equipment. Early pumps used in IC exhibited considerable pulsation and Nafion tubes are significantly elastic, resulting in beads becoming packed together in some places in the tube, leaving large voids in others and eventually bursting. This problem was also solved eventually by tightly packing the exterior of the membrane with beads; this made any movement of interior beads far more difficult [6]. Others had since shown that if the packing beads are appropriate ion exchangers themselves in intimate contact with the IEM, the exchange capacities can be significantly increased [7] but neither of the above configurations ever became commercial. Hanaoka et al. [8] thermally stretched available Nafion tubing to 400 µm i.d. and found acceptable dispersion without any bead packing, even for a 5-m length used as a suppressor. The Nafion tube was surrounded by an external jacket tube through which the regenerant acid flowed. The stretching resulted in

the wall of the Nafion tube being much thinner and promoted undesired penetration of the regenerant acid. These authors were the first to advocate the use of large counter ion acids (e.g., dodecylbenzenesulfonic acid) to minimize the penetration.

2.3.1.1. Filament-Filled Tubular Suppressors

A different physical configuration was proposed by Dasgupta for the construction of IEM-based tubular suppressors: He theoretically [9] and experimentally [10] examined the performance of the same Nafion tubes used in the commercial suppressors but filled them with a tightly fitting nylon monofilament and wound into a small diameter coil. The helical geometry induces secondary flow that improves mass transfer to the wall as well as flattens the parabolic profile of laminar flow, thus reducing dispersion. In all performance indices (the maximum concentration of an alkali hydroxide that could be exchanged at any given flow rate at steady state, induced band dispersion and the asymmetry of an injected band), this design substantially outperformed the pearl string reactor configuration. Subsequently Gupta and Dasgupta [7] showed that other configurations of a filament filled IEM tube where laminar flow is disrupted, e.g., by tying small diameter knots alternating in direction, were also very effective as suppressors in IC. There are many other ways to minimize dispersion and improve radial mass transport: A filament-filled IEM tube woven on a screen support in a 3D-Serpentine II configuration [11] makes a very low dispersion suppressor. The utility of a filament-filled IEM tube deliberately deformed geometrically to

improve radial mass transport and reduce axial dispersion has stood the test of time - the design is still commercially available [12], some three decades after its original introduction.

2.3.1.2. Dual Tubular Filament Filled Suppressors

The filament filled helical (FFH) design was exploited to increase available membrane area in the same basic geometry by inserting one filament-filled IEM tube inside a second slightly larger IEM tube. The whole was then coiled into a helix and put in an external jacket [13]. The eluent passed between the two tubes while regenerant acid flowed through the outer and innermost channels, as shown in Figure 2-2. The larger available membrane area is especially useful when large ions like tetraethyammonium or tetrapropylammonium, that diffuse relatively slowly through an IEM must be transported [14].

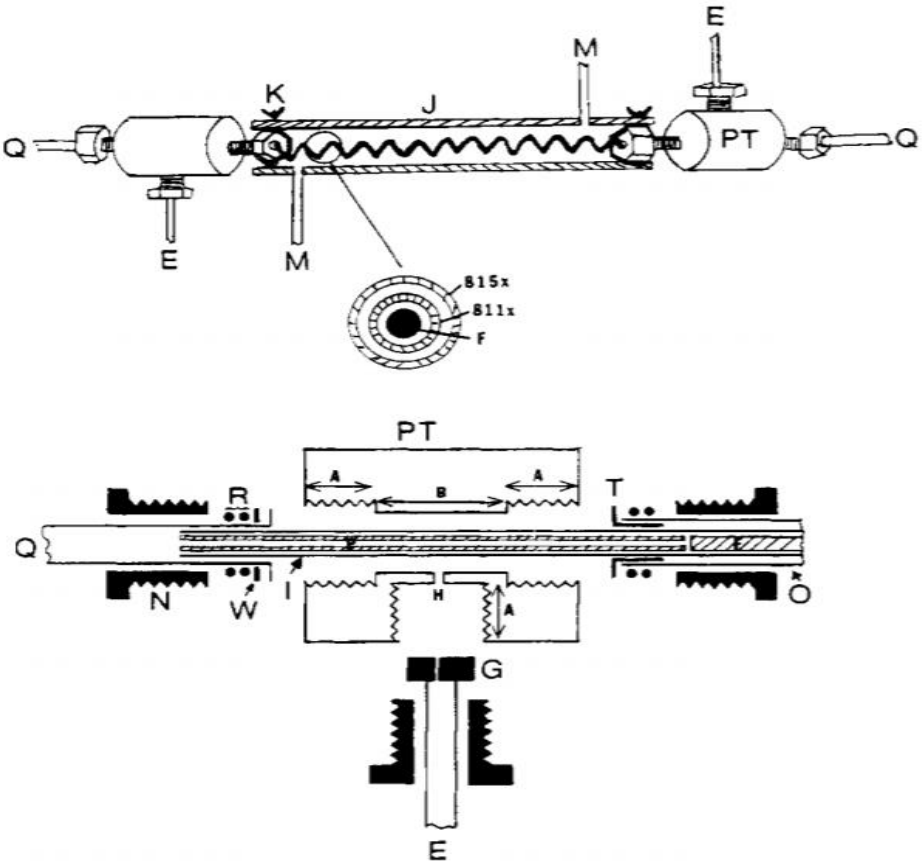

Figure 2- 2. Top: Complete dual membrane annular helical suppressor. Q, PTFE inlet/outlet tube for Inner channel regenerant; E, PTFE tube for column effluent outlet/inlet; M, PVC Inlet/outlet tube for outer channel regenerant; K, wire crimp; J, Tygon® jacket tube; PT, polypropylene tee. Inset shows cross section of filament filled dual membrane assembly. Bottom: Details of polypropylene tee and connections: W, washer; G, gripper fitting; other legends as above. Dimension A is 1 cm; dimension B is exaggerated, should be as small as possible; hole H is 0.5 mm in diameter. Drawings are not to scale, gaps are exaggerated for clarity. Reprinted from reference [13] with permission from the American Chemical Society.

2.3.1.3. Planar Suppressors

The majority of IEM- based suppressors have followed a planar design based on sheet membranes, since the mid-80's [15]. Much as with the dual tubular membranes, the eluent flows in between the two membranes while regenerant flows countercurrent on the outer side of each membrane. To achieve this in a low-volume, the design must be ingenious: A gasket between the two membranes essentially forms the eluent channel, which is accessed through a hole at each end of one of the membranes (Figure 2-3). Except for packing elements in the eluent channel, such as an ion exchange screen, or beads (ion exchange functionalized or not), or improvement of backpressure tolerance by hardware design, fundamentally such suppressors have not changed since their inception. The dual membrane configuration in a planar suppressor provides for a significant membrane area and allows for significant continuous ion exchange capacity, even for relatively large ions. For example, one common use for such a device is as a suppressor for ion exclusion chromatography, where a large ion must be transported, as detailed in section 3.1.5.

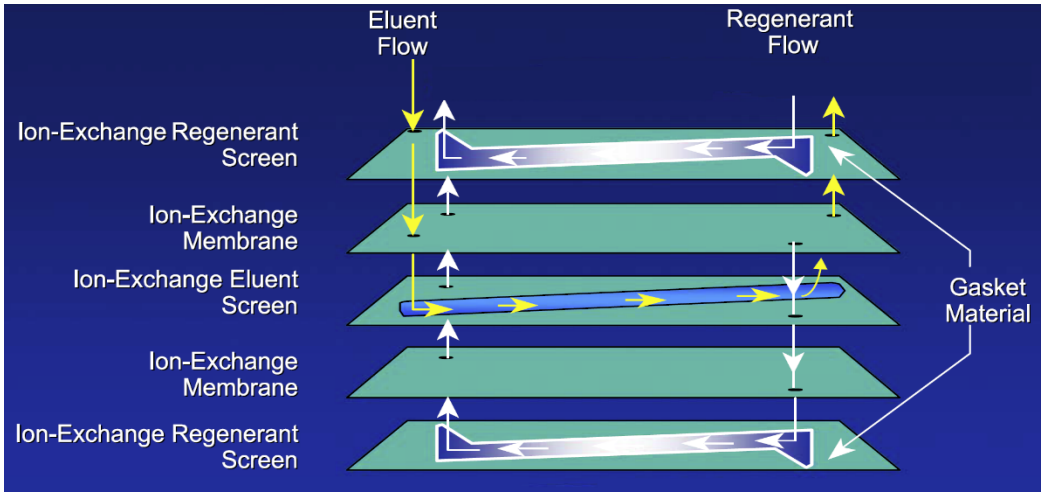

Figure 2- 3. The classic design of a planar membrane suppressor. There are three flow channels, each of which contains an ion exchange screen. The same source of regenerant flow is directed through both the top and bottom channels and has a common exit. The central channel where the eluent flows through is flanked by two IEMs. Adapted with alteration from reference [16].

2.3.1.4. Capillary IC Suppressors

Although the planar/sheet IEM design has dominated macroscale IC, in the capillary scale, the tubular IEM design rules: A smaller volume and low-dispersion connection to the separation column is much easier to attain. As early as 1983, Rokushika et al. [17] connected a 10-mm long 0.2 mm ϕ Nafion IEM tube to a 190 µm ϕ packed AEX column and showed the feasibility of suppressed IC in this scale. More than a decade later, Sjögren et al. [18] used much smaller diameter (80 µm ϕ) Nafion IEM tubes in a nearly identical configuration with 180 µm packed columns. Shortly thereafter, Boring et al. [19] demonstrated a field-portable IC centered on a 180 µm

packed column connected to a 50 µm ϕ, 19-mm long radiation-grafted, CEX-functionalized PTFE tube serving as the suppressor. The applicability of this instrument to measure atmospheric trace gases was CEX subsequently demonstrated as well [20].

Kuban and Dasgupta inserted a 50 µm wire between the ends of two 75 µm ϕ capillaries and cast a membrane on this junction using a colloidal Nafion solution, for use as a suppressor in open tubular IC (OTIC) [21]. While functionality was demonstrated, IEMs undergo large dimensional changes upon wetting; it is difficult to take a once-dried device and not have it leak while wetted.

Huang and Dasgupta [22] took an entirely different approach. They synthesized a monolith around the wire mandrel - by controlling the amount of porogen added during the synthesis of monolithic polymers derived from ethylene dimethacrylate – glycidyl methacrylate (the polymers were subsequently converted to an anion exchanger by treating with trimethylamine), it was possible to obtain rigid ion exchange polymers that behaved like IEMs and allowed only one charge type of ions to pass through. Successful open tubular (OT) cation chromatography suppressor performance was demonstrated with these monolithic suppressors. Subsequently, these authors similarly fabricated monolithic suppressors integrated to capillary columns for suppressed OT anion chromatography [23].

2.3.1.5. IEM Suppressors in Ion Exclusion Chromatography

Ion exclusion chromatography (often called ICE, ion chromatography in the exclusion mode) utilizes gel type CEX resins in the separation column. A low concentration of a large anion strong acid, e.g. perfluorobutanoic acid, is used as the eluent and results in weak acids mostly being undissociated. As previously discussed for acetic acid behavior in a packed column suppressor (Section 3.1), these can then partition into the interior of the resin and be separated based on their different affinities. An ICE suppressor simply exchanges H^+ in the eluent for a large cation like tetrabutylammonium (NBu_4OH is used as the "regenerant") the effluent background is then tetrabutylammonium perfluorobutanoate, a relatively low conductivity salt (because both the constituent ions are large and thus of low mobility) while the weak acids like acetate or formate elute atop this background as the corresponding tetrabutylammonium salt [24]. Exchanging H^+ with much lower mobility NBu_4^+ results in the background conductance from 1 mM octanesulfonic acid eluent (~230 μS/cm) to be reduced to 45-55 μS/cm.[25,26] While "suppression" in this case does not lower the eluent conductivity background quite as much as in the case of suppressed IC, it *does* lower the background. Importantly, it vastly improves the linearity of conductometric analyte response: While the conductivity of a weak acid after conventional proton exchange suppression is understandably nonlinear, that for the tetrabutylammonium salt is linear. This remains the state of the art in ICE

suppression and detection: while detection of UV absorbance at 190-200 nm of aliphatic carboxylic acids is possible, it is not nearly as sensitive and is plagued with interference by other UV absorbing compounds. In fact, the sensitivity of UV absorption detection is also improved with a suppressor as the analyte acids are more absorbing in the ionized form.

2.3.1.6. Other IEM-Based Alternatives in ICE Detection

Altogether different approaches have been used in detection in ICE where IEMs play an important role. While UV absorption detection for aliphatic carboxylic acids is not very sensitive as indicated, optical absorbance detection nevertheless holds a premier place in liquid chromatographic separations. Okada [27] initially attempted to use HI as an eluent and added H_2O_2 postcolumn to form nonconductive I_2. Significant amounts (10%) of HI remained, causing a high background and rendering gradients impossible. The introduction of H_2O_2 was carried out conventionally with a tee and a pump but such a reagent can be readily introduced through an IEM (see Section 12). Later, Okada and Dasgupta [28] devised an optical detection method that does not rely on the optical absorption of the weak acids themselves but on the acid-base properties of their fully neutralized alkali metal salts. A dilute solution of a strong acid, e.g., HNO_3, is used as the ICE eluent. The corresponding fully neutralized salt $NaNO_3$ is pH-neutral but the corresponding salt of a carboxylic acid analyte, e.g., Na-acetate, is alkaline. This change in pH can be sensed by a suitable indicator. They used a 360 μm i.d. Nafion IEM tube in the FFH

configuration to convert the acid to the Na-salt. Using NaOH alone as the conversion agent produces too much penetration, the best external solution for the desired conversion was a slightly alkaline NaCl solution. Also, unionized weak acids are not subject to the Donnan barrier and can be easily lost through the IEM. Once neutralized, the anions/salts are not subject to such losses. The penetration of NaOH is the greatest where it has the highest concentration, when the regenerant is fresh. As such, the solution in the lumen is more quickly neutralized and the analyte loss is lower when the lumen flow and the external reagent flow is co-current, rather than countercurrent. 4-nitrophenol (4-NP) was chosen as the indicator (pK_{In} plays an important role in the magnitude of the observed response, should be lower than $pK_{analyte}$) and this small molecule was introduced easily through another (much shorter than the sodium converter) Nafion IEM tube. The latter was immersed in a stirred solution saturated with 4-NP and $KClO_4$. If 4-NP was used alone, the Nafion will be in H^+-form and an undesirable exchange of the Na^+ in the lumen with H^+ on the membrane can occur. The KClO4 keeps the membrane in an alkali-metal form. The authors were able to use eluents as acidic as pH 2 and to perform gradient elution - neither was previously possible in conventional suppressed conductometric ICE. Very weak acids such as boric acid or HCN cannot be detected by either ICE methods above, whether using conductometric or optical detection.

2.3.2. Electrodialytically Regenerated Suppressors

Thus far, the suppressors discussed accomplish the desired process that is driven by a chemical concentration gradient. Often, it is possible to accomplish the same ends with an electrical potential gradient instead. Occasionally, the two approaches have been used in conjunction, although as will be seen, such a practice may not provide the best of either world.

Suppressors convert the ionized eluent to an essentially un-ionized low conductivity background and increase the analyte signal by converting them to a more conductive form [29]. Chemically regenerated suppressors do require a chemical regenerant to convert the eluent to the suppressed form. Concentration polarization can develop at the membrane surfaces and the diffusion of the eluent/regenerant ion to the membrane surface can become the rate determining process, thus limiting the maximum concentration of the eluent that can be suppressed. To a degree, deliberately introducing gas bubbles on the regenerant side of a membrane can disrupt such polarization [30]. Increasing regenerant concentration also helps, but with common regenerants, undesired penetration of regenerant counter-ions sets a practical limit. Tian et al [31] proposed an electrodialysis based device (Figure 2-4) to address these issues.

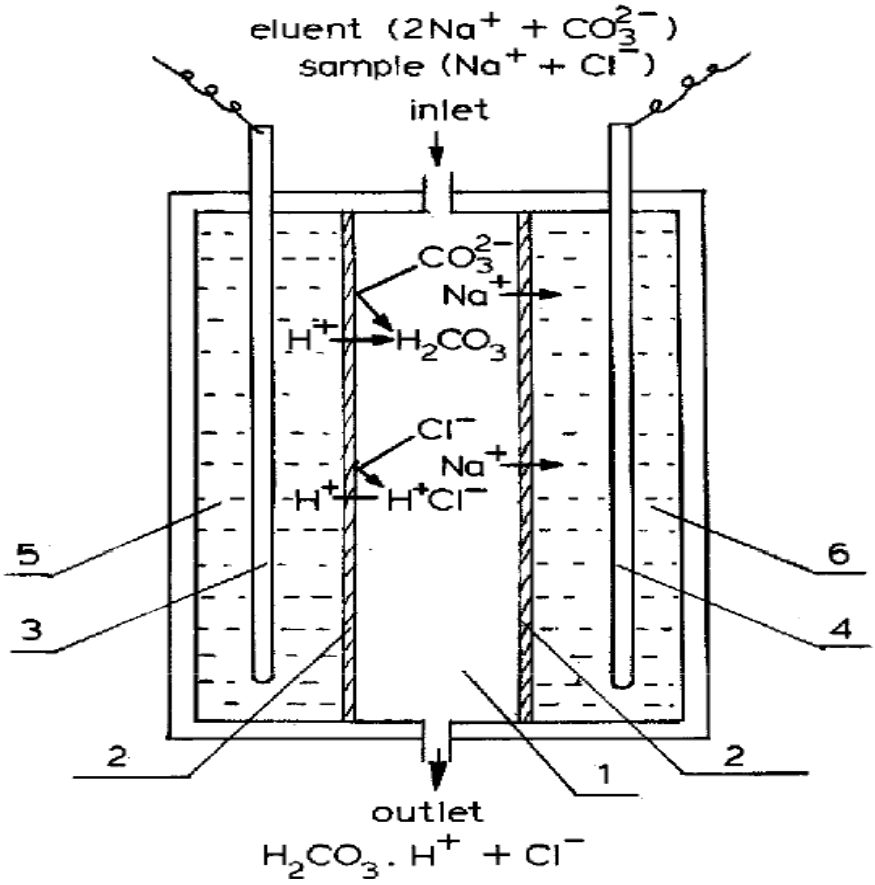

Figure 2- 4. Schematic of electrodialytic regenerated suppressor. 1: suppression chamber, 2: cation-exchange membrane, 3: anode, 4: cathode, 5: anolyte chamber, 6: catholyte chamber. Reprinted from reference [31] with permission from Elsevier.com

The suppressor, shown for use with a carbonate/bicarbonate-based eluent in anion chromatography, contained two CEMs, which between them, form the suppression channel. The 60-mm long 7-mm wide channel was packed with CEX resin beads to reduce the internal volume. Sulfuric acid (0.1 M) was used as a static solution on the outer side of each CEM; platinum-plated titanium electrodes were used. With 4 V applied to the

electrodes, 50 mA current resulted and the suppression of 2.4 mM Na_2CO_3 + 3 mM $NaHCO_3$ was demonstrated at flow rates up to 3.2 mL/min.

While one could regard this as the first literature report of an electrodialytic suppressor, how much electrodialysis really contributed to its operation is not clear. Given that a very substantial concentration of acid was already present, a large amount of the observed ion exchange must have been driven by the chemical concentration gradient present. The authors stated that the transmembrane sodium ion transport was aided by the applied potential. While this must be true, in a chemically regenerated configuration both membranes are available for sodium transport. In the described configuration, however, only the cathode membrane is effective for this purpose. Diffusive transport is made poorer in this design by an unspecified but seemingly large intermembrane distance compared to other sheet membrane suppressors, whether chemically regenerated [15] or subsequently introduced electrodialytic versions. The claimed suppression efficiency was 99.9%. It should be recognized that this performance is not especially good and a significant residual unexchanged eluent concentration remained. The Faradaic efficiency (different from suppression efficiency) of an electrodialytic device can be judged from the minimum theoretical current i_{th} necessary to transport a given equivalent of ions per unit time:

$$i_{th}, \text{mA} = FCQ/60 \quad ...(1)$$

where F is the Faraday constant (96,500 coulombs/equivalent), *C* is the concentration of the ion to be transported in eq/L and *Q* is the volumetric flow rate of the latter in mL/min. On this basis, it theoretically requires ~40 mA to transport 7.8 meq/L Na^+ @ 3.2 mL/min. With the stated 50 mA requirement, the device was 80% current-efficient. While this is respectable, it seems likely that most of the observed suppression was from the acid regenerant. As such, this does not represent the true current efficiency. The authors considered the static deployment of the external electrolyte (no flow required) to be an asset. Such a configuration is bound to fail long-term when enough Na^+ builds up in the catholyte.

This publication is not alone in the belief that the joint use of a chemical regenerant and applied potential is of benefit. The simultaneous use of a chemical regenerant during electrodialytic suppression can improve energy efficiency in certain demanding applications but often it is of no particular benefit and can occasionally be deleterious. In a planar perfluorosulfonate membrane-based device in which 25 mM H_2SO_4 was used as a flowing regenerant, Ohta et al [32] reported that the suppressed background conductance of a 1.6 mM Na_2CO_3/ 2 mM $NaHCO_3$ eluent (original conductance 570 µS/cm) dropped from 42 to 13 µS/cm upon application of 5 V across the membranes. This result makes it obvious that the major amount of suppression took place without any voltage application. Considering that devices of very similar geometry [15] have already fully suppressed such eluents routinely without any applied voltage, the device

likely suffered from poor transport to or through the membrane, as may result from an overly thick or poorly functionalized membrane.

Strong and Dasgupta [33] first reported electrodialytic suppressors which used only water as the regenerant, generating H^+ by electrolysis; no other chemical was needed. Although the authors showed that a single Nafion tube, with a platinum wire anode running through the lumen and a stainless steel (SS) jacket tube functioning as the cathode, adequately behaves as a suppressor (eluent runs through the lumen, water runs outside it in a countercurrent fashion), the suppressed eluent contains large amounts of electrolytic O_2 gas. This makes degassing necessary before detection. A more practical arrangement was a dual membrane helical design, similar to that previously described [13] except that there is a central Pt wire anode instead of a nylon monofilament and the dual IEM helix is put in an outer stainless steel jacket tube, functioning as the cathode. The outer jacket was further packed with conductive carbon granules to reduce electrical resistance. Water flows both through the inner tube and the outer jacket while the eluent flows between the two IEM tubes. The dual-membrane suppressor was not as current efficient as its single IEM counterpart but here the eluent stream was isolated from the anode and cathode by IEMs, preventing gas formation in the eluent stream. Excessive voltage/current, however, can result in gas formation in the eluent. A suppressor assembled from a 50-cm long IEM tube was able to suppress as much as 500 μequiv Na^+/min (0.5 M NaOH @ 1 mL/min).

Strong et al. [34] next used sheet IEMs to design a water-only planar electrodialytic suppressor using the hardware for a commercially available chemically regenerated planar suppressor (Figure 2-3). Figure 2-5 shows the principle of operation. Subsequently, such water-regenerant electrodialytic suppressors became commercially available – the only difference from the chemically regenerated suppressor depicted in Figure 2-3 was the presence of corrosion-resistant electrodes in the regenerant channels [16].

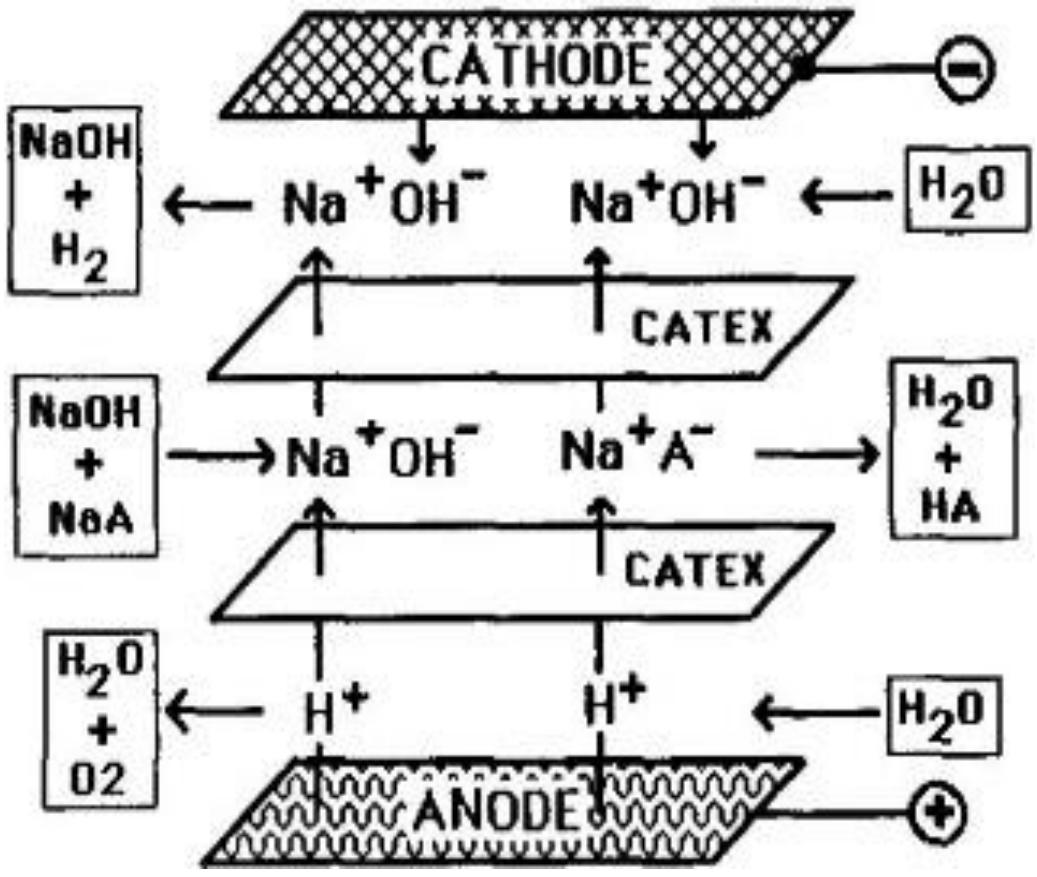

Figure 2- 5 Principle of electrodialytic suppressor using two CEMs. Note that the cathode IEM remains mostly in the Na^+-form while the anode IEM is in the H^+-form. It is advantageous for the anode IEM to extend beyond

the cathode IEM on the eluent exit side, so the effluent only contacts a H^+-form IEM before exit. Reprinted from reference [34] with permission from Elsevier.com.

2.3.2.1. Recycling of Detector Effluent as Suppressor Regenerant

With a hydroxide eluent in anion chromatography or a strong acid eluent in cation chromatography, the suppressed effluent is water. Even with a carbonate/bicarbonate eluent in anion chromatography, the suppressed effluent is poorly conducting carbonic acid. Instead of using fresh external water as the regenerant, it is possible to use the system effluent (carbonic acid or water) regenerant in an electrodialytic suppressor, this avoids the need for pumping regenerant water through the system and generates less waste. Rabin et al. [35] compared these two modes of electrodialytic suppressor operation (external water vs. recycling detector effluent) in terms of limits of detection (LODs) observed for different analyte ions (Table 2-1); these values are obviously inversely related to the observed detector noise.

Table 2- 1 Limits of detection (LOD) with electrodialytic regenerated suppressor.

Species	LOD, cell effluent recycle (μg/l)	LOD, external water (μg/l)
Anions[a]		
Chloride	4	2
Nitrate	12	5
Phosphate	44	17.5
Sulfate	18	8
Cations[b]		
Lithium	1	0.7
Sodium	4	2
Ammonium	5	3
Potassium	4	3
Magnesium	5	3
Calcium	8	4

[a]Column: AS4A-SC; eluent: 1.8 mM Na_2CO_3, 1.7 mM $NaHCO_3$, 2 mL/min; 50 μL sample; [b]Column: CS12; eluent: 20 mM CH_3SO_3H, 1 mL/min; 25 μL sample. Reprinted from reference [*35*] with permission from Elsevier.com.

Although external water flow provided better performance in all cases, the difference was not large. This remains true to date. The authors also pointed out that electrodialytic suppression cannot be used in all cases, it is incompatible with many organic solvents. Methanol oxidizes to formaldehyde and then to formic acid. This finds its way back to the eluent channel raising background conductance and noise. In cation

chromatography, high halide content samples lead to free halogens or hypohalites, these strong oxidants rapidly destroy IEMs, especially anion exchange membranes (AEMs). The lowest noise levels, even today, are observed with chemical suppression but the convenience of electrodialytic suppression has generally become the overriding consideration.

2.3.2.2. Combined Cation and Anion Suppressor

The group of Hu has had an early interest in electrodialytic suppressors and related devices for IC [31]. In 2003, Hu et al [36] reported a combined cation and anion suppressor that essentially put together a conventional CEX-based suppressor used in anion IC (Figure 2-6, Suppressor 1, left half) with an AEX-based suppressor used in cation IC (suppressor 2). In effect, they combined the negative electrode of suppressor 1 with the positive electrode of suppressor 2 into a single electrode located in a single flow-through compartment. The suppressors could be used alone or together. Simultaneous cation and anion chromatography were successfully conducted.

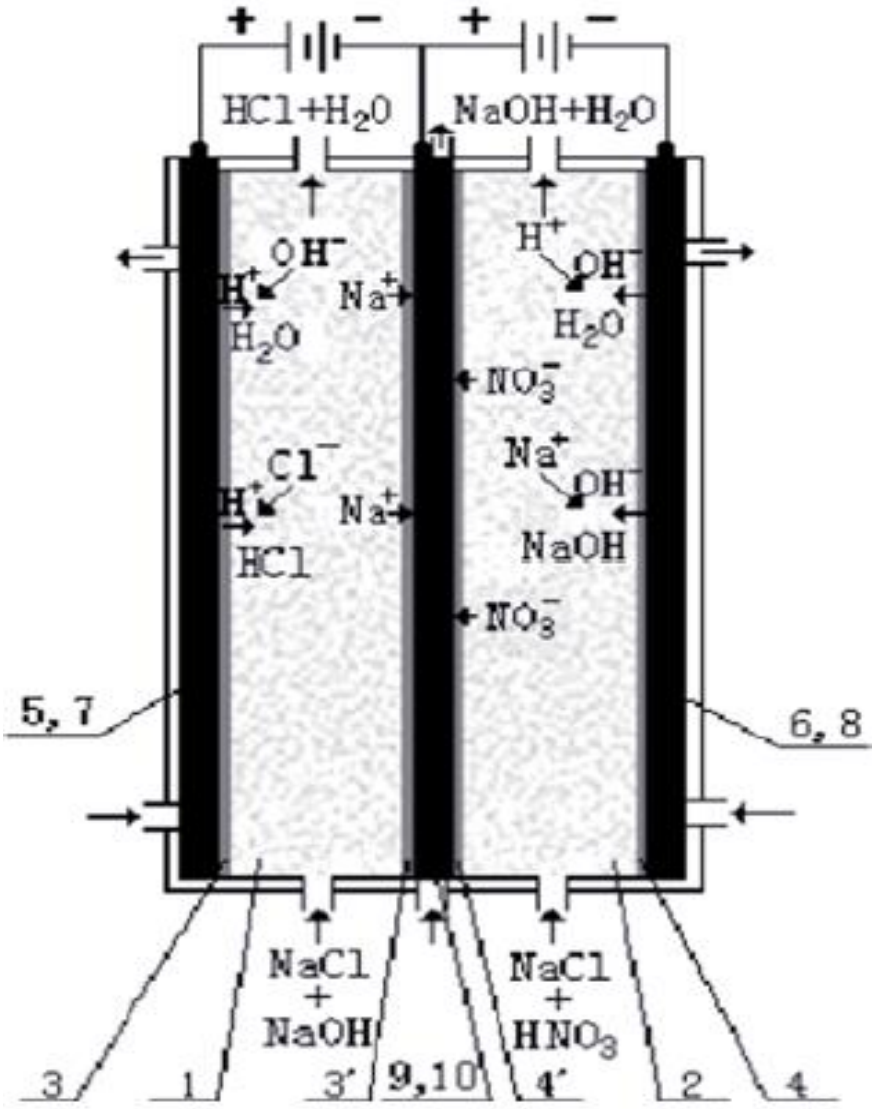

Figure 2- 6 Bifunctional suppressor. 1: CEX-based suppression chamber for anion IC, 2: AEX-based suppression chamber for cation IC, 3, 3': CEM, 4, 4': AEM, 5: anode chamber; 6: cathode chamber; 7, 8, 10: noble metal electrodes; 9: common electrode chamber. Reprinted from reference [36] with permission from Springer.com.

2.3.2.3. Porous Electrodes and Combined Suppressor-Resistivity Detector

Another paper from the Hu group [37] described very small suppressors in which a 10-mm dia. porous electrode was pressed against an IEM which was separated 7-14 mm from a second IEM backed by another porous electrode. The space between the two IEMs defined the thickness of the suppression channel; this was also packed with ion exchange resin. The eluent flowed through this bed. Applied voltage (increasing with the bed height) ranged from 11-25 V; successful cation chromatography was demonstrated with 6 mM CH_3SO_3H @1 mL/min.

In 2011, the same group [38] proposed combining the suppressor and the detector in the same device enclosure. Measuring resistivity of a bulk sample by a four-electrode arrangement is well-established. Solution CDs have also been designed using this principle. Typically, the four electrodes are placed in a linear configuration. The voltage between the two inner sensor electrodes is measured while a voltage is applied between the outermost electrodes. The same principle was used by Huang et al. [38] with a low µA-level constant current applied between the outer electrodes while the analyte solution flowed over the inner electrodes. The voltage across the sensor electrodes thus decreased as conductive suppressed analytes passed across the sensed channel (it functions as a resistivity detector). The detector itself was described previously [39]. The suppressor is essentially the same porous two-electrode, IEM based device with a resin-

packed center channel for eluent flow [37]. The detector, where the outer electrodes are also positioned behind IEMs, is then situated downstream with its own four electrodes. But the outer positive electrode is common with the suppressor anode, resulting in five electrode connections in all. Figure 2-7 shows the overall device construction and the equivalent circuit. Resistivity detection has the disadvantage that the linear relationship between the analyte concentration and the detector output signal is lost. Standard bipolar pulse conductance measurement [40] would have been just as easily applicable. Of note, in high resistivity backgrounds, conductivity can be measured with relatively low noise even with DC potential [41].

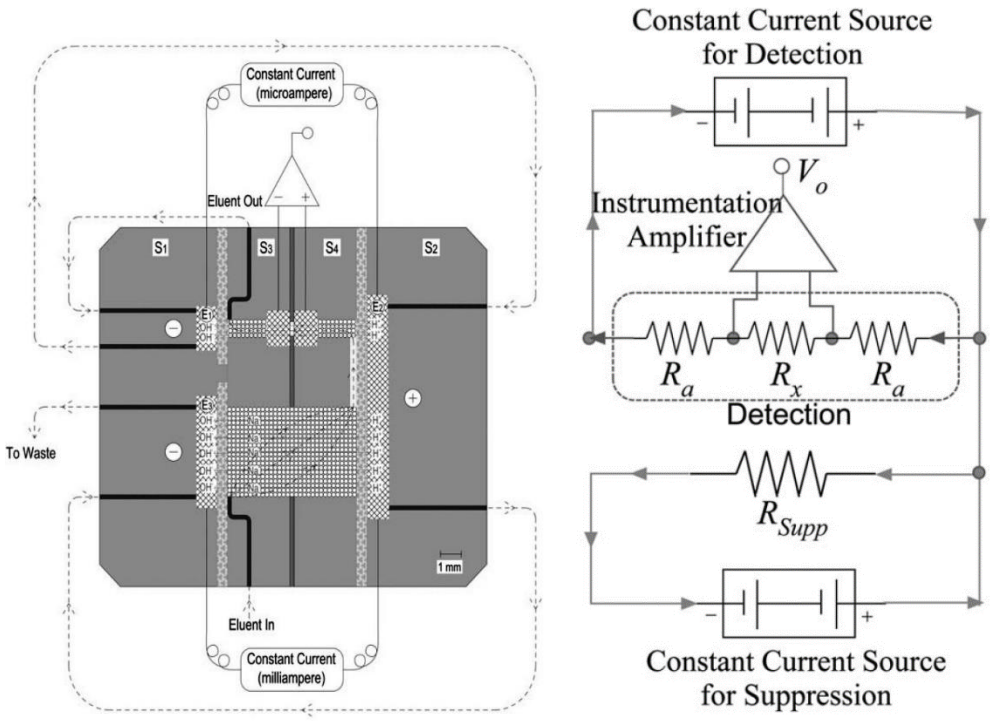

Figure 2- 7 Left: Combined suppressor- DC resistivity detector by Huang et al. [38]. The device consists of a suppression and a detection chamber,

three electrolysis electrodes (one common anode and the other two independent cathodes) and two sensor electrodes and three cation-exchange membranes defining the suppression and detection chambers. The suppression path (6 mm ϕ, 6.2 mm long) is filled with CEX resin Two other similar resin-packed connection channels connect the detection volume to the electrodes. All five electrodes are porous. Two constant current sources are in electrical communication with the cathodes and the common anode, respectively. Right: Electrical Circuit equivalent. Reprinted from reference [38] with permission from the Royal Society of Chemistry.

2.3.2.4. The Atlas^{TM}: A Suppressor Using Ion Exchange Disks and Membranes.

Small et al. [42] developed a continuous electrolytically regenerated packed-bed suppressor that became commercially available as the Atlas^{TM} suppressor. Referring to Figure 2-8, the key components constitute a suppression bed of 6 monolithic ion exchange disks (4-mm dia.), interspersed with five flow distributor disks and a total length of 10 mm. This assembly is sandwiched between two IEMs that separate the eluent chamber from the anode and cathode chambers of the suppressor. The flow distributor disks are impermeable to the liquid flow except via the small holes near their perimeters. In the anion suppressor configuration, cations migrate across the membrane in the suppressor bed under the electrical field. The flow distributor disks create a serpentine flow pathway to increase

the effective residence time of the eluent in the suppression bed. The suppressor has the advantage of rapid attainment of a stable baseline but its suppression capacity is limited.

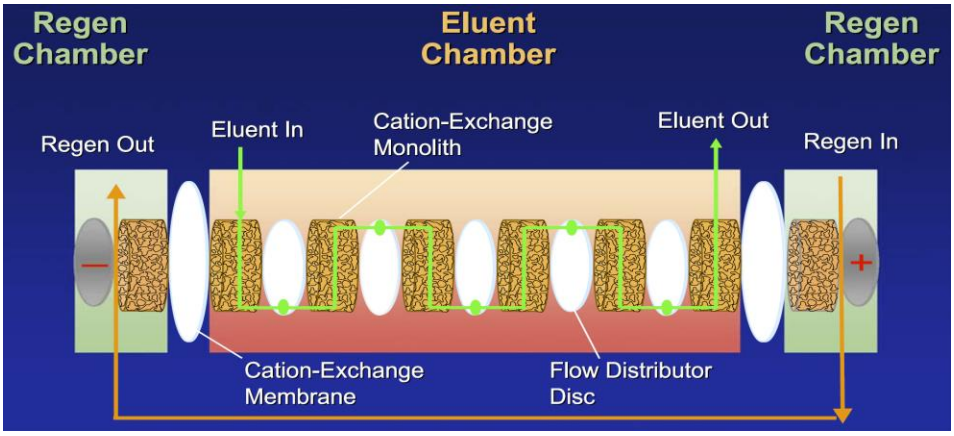

Figure 2- 8 The Atlas™ suppressor , consisting of 6 monolithic ion exchange disks, flow directing separators and terminal IEMs that separate the regenerant chambers from the eluent flow. Compared to a membrane suppressor, the electrode separation is larger and hence operating voltage is higher. Reprinted from ref. [16] with permission from Elsevier.com

2.3.2.5. Electrodialytic Suppressor Using both IEM Types

An unorthodox concept in electrodialytic suppressors was proposed by Masunaga et al. [43] in 2012. Thus far, in any given suppressor type for cation or anion chromatography, only one type of IEM (either CEX or AEX) has been used. Whether chemically or electrodialytically regenerated, a suppressor used in anion chromatography consists of CEMs, typically the flow paths in addition being packed with CEX resin beads and/or CEX functionalized screens. In a conventional electrodialytic suppressor,

presence of the CEX material in the anode compartment primarily serves to reduce the voltage drop (unless the electrode is in contact with CEM, in which case adding IEX material is superfluous). In the cathode compartment, the CEX material provides both steady state and transient surge capacity by taking up M^+ transported into the cathode compartment and thus preventing excess MOH buildup and eventual Donnan-forbidden leakage. The role a CEX screen/or resin in the eluent channel of an electrodialytic suppressor is more complex. While the presence of some CEX capacity in this channel does improve steady state and transient surge suppression capacities, it also leads to decreased current efficiency. A bridge of CEX material contacting two CEMs represents an ionic short-circuit, current can flow directly by anodically generated H^+ proceeding through this bridge, without the desired transport of M^+ [44].

To understand the electrodialytic suppression strategy of Masunaga et al., it is first necessary to understand the behavior of a bipolar membrane (BPM). A BPM consists of a CEM in contact with an AEM, as depicted in Figure 2-9 (with the interfacial water layer thickness being exaggerated) [45]. With voltage applied in the manner indicated, the water in the interfacial layer ionizes and H^+ and OH^- are transported in the manner indicated.

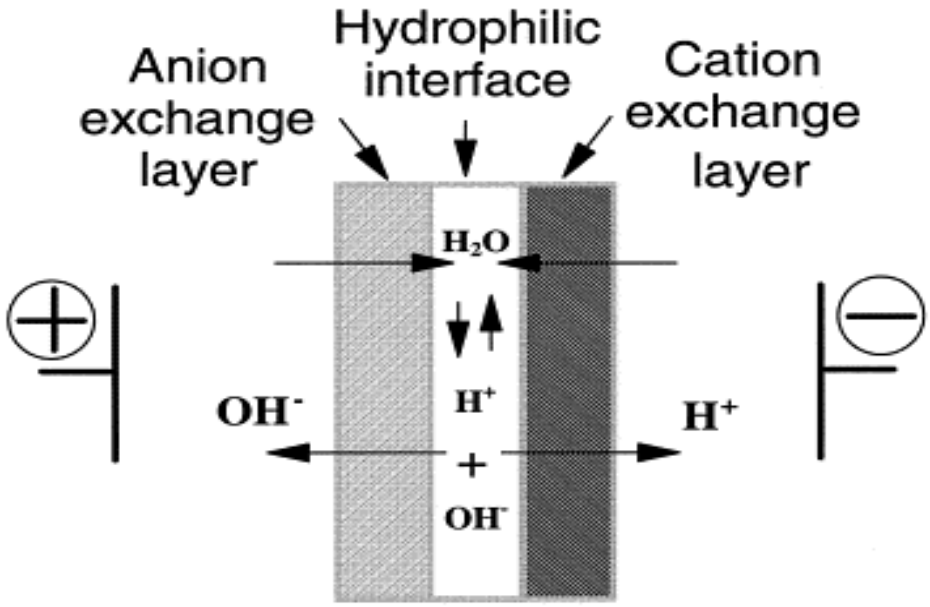

Figure 2- 9 Bipolar membrane (BPM) illustrating “water splitting”.

Reprinted from ref. [45] with permission from Elsevier.com

Now consider the suppressor for anion chromatography introduced by Masunaga et al. (Figure 2-10) [43]. The right half of this suppressor, consisting of a CEM and both the eluent and cathode compartment being packed with CEX resin, are substantially the same as most other suppressor designs proposed for anion chromatography. The left half of the suppressor is completely different, consisting of an AEM separating the anode compartment that in turn is filled with AEX resin. The CEX resin bed in the eluent channel in contact with the AEX IEM is *de facto* a BPM-like interface, resulting in water splitting. Although it is not addressed in the work [43], some chloride is in fact lost to the anode compartment in this device. However, a substantial amount remains to be detected as HCl in the central

compartment effluent. The primary driver for chloride or other anions to migrate through the AEM to the anode compartment is the electric field.

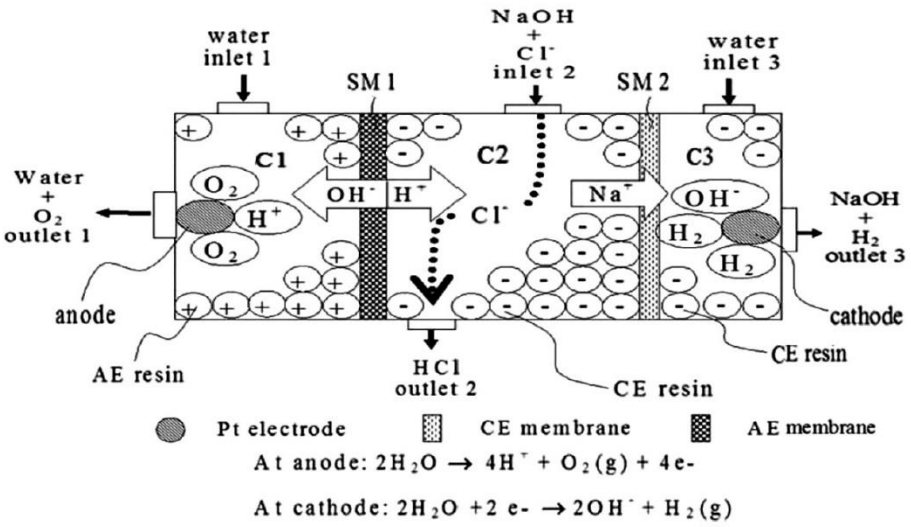

Figure 2- 10. Suppressor for anion chromatography (converts NaOH to water and NaCl to HCl) according to ref. [43]. Reprinted with permission from the Japan Society of Analytical Chemistry.

Several aspects of this suppressor design are noteworthy. Because the eluent entry and exit ports are asymmetrically located, the necessary transport distance is increased. By densely packing the central channel with CEX resin, H^+ and Na^+ in the resin phase carries much of the current, undesirably lowering the voltage drop/electric field across the eluent channel. However, unlike a double CEM suppressor, some loss of the analyte ion through the AEM can occur. The authors present data for an analogously constructed suppressor for cation chromatography in a subsequent paper and compare the suppressed and the non-suppressed response for various analyte cations [46]. The signal intensities are expected

respectively to be proportional to (λ_{M^+} + λ_{OH^-}) and (λ_{H^+} - λ_{M^+}) where λ_i represents equivalent conductance of ion *i*. The reported data indicate that the ratio of the non-suppressed to suppressed signal is substantially higher than the above expectations; this can be accounted for by the loss of M^+ from the eluent channel. While the approach of Masunaga et al. may be novel, much remains undiscussed by the authors. Providing a "short circuit" path between the two IEMs necessarily makes the overall suppression process current-inefficient, quite aside from analyte loss. In addition, all ion exchangers, resin beads and especially membranes, lose ionic oligomers over time, especially in an electrolytic environment. If different types of ion exchangers are used in the same device, AEX/CEX oligomer fragments will respectively poison CEX/AEX material over time, reducing current efficiency further and compromise the usable lifetime.

In this review, we largely focus on general principles of operation. Finer aspects, e.g., how to reduce noise in a suppressor, are not considered. One interesting case, however, deserves an exception. Noise in an electrodialytic suppressor arises from multiple sources. Applying more than the necessary current, for example, always increases the noise. With a Na_2CO_3/$NaHCO_3$ eluent, some of the carbonic acid can be and is lost through the suppressor membranes. This loss must be the highest near the eluent exit where the eluent has become essentially pure H_2CO_3 and one of the regenerant channels have become purely NaOH. Gas evolution in this region thus can perturb the loss process, generating noise. Minimizing

excess current towards the exit end of the cathode membrane can thus be conducive to lower noise. In a recently introduced electrodialytic suppressor expressly intended for carbonate eluents, the anode is a single electrode. But the cathode area is divided into two regions, the eluent exit zone being smaller than the eluent entry zone. The main voltage is applied to the entry cathode and this is connected by a resistor to the exit cathode, thus reducing the voltage applied to the exit zone. This device is capable of noise levels comparable to that produced by suppressed hydroxide eluents [47].

2.3.2.6. Electrodialytic Suppressors for Packed Capillary Chromatography

Overall, chromatography is moving to smaller dimensions, IC is no exception. The present commercial packed capillary chromatography format operates with 0.4 mm i.d. columns. It is very difficult to design sheet-IEM based suppressors that are of sufficiently low internal volume (and provide sufficiently low dispersion) to be usable in such applications. The present commercial suppressor designed for this application, shown in Figure 2-11, is based on an IEM capillary [48]. The jacket around the ~100-125 µm i.d. IEM tube is packed with ion exchange resin beads to increase the suppression capacity. Water flows countercurrent in the bed and a voltage is applied across the resin bed to regenerate the bed in a direction countercurrent to eluent flow. Predictably, the overall current efficiency in a system where the current regenerates a packed resin bed, and the bed then regenerates the IEM by chemical contact, is relatively poor. Figure 2-11

illustrates a suppressor for anion chromatography with a KOH eluent being suppressed.

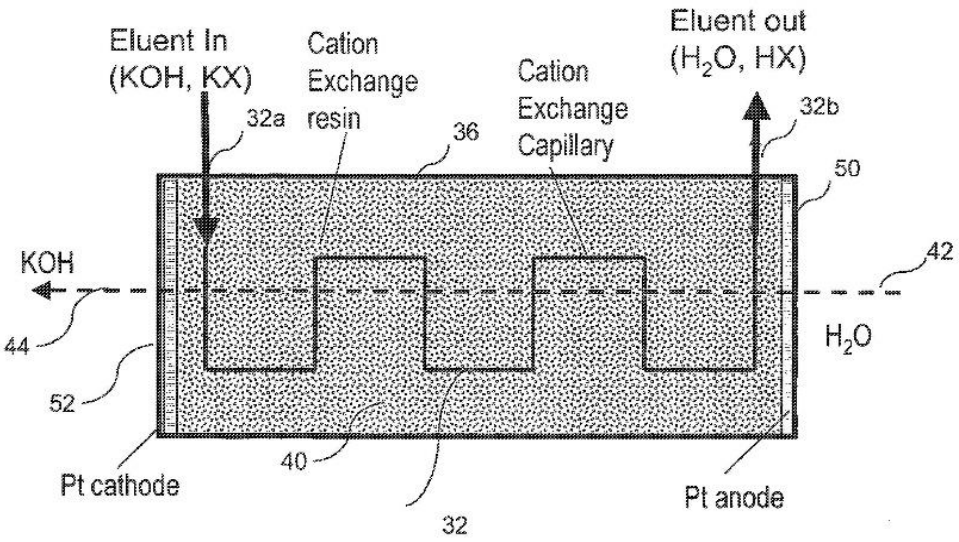

Figure 2- 11 Capillary IEM based suppressor for packed capillary ion chromatography.

2.3.2.7. Electrodialytic Suppressor for Open Tubular Ion Chromatography (OTIC)

Huang and Dasgupta [49] developed an electrodialytic suppression scheme for an even smaller scale, to work with OTIC columns of ~25-30 µm inner diameter. A general problem in designing suppressors for such columns is that the o.d. of the columns is typically 15x larger than the i.d. As such, even if a capillary IEM is somehow connected to such a column, the abrupt diameter change at the interface will lead to an unacceptable amount of dispersion. Three suppressor designs were investigated with

columns that were tapered at the end like a sharpened pencil. A 300 µm needle was inserted along the center of the long axis in a Nafion CEX polymer block (1 x 5 x 10 mm); see Figure 2-12. The crack made by the needle essentially self-heals after the removal of the needle. The tapered column end and a similarly tapered detection capillary were inserted into the block through the opposing ends of the crack, leaving a ~1 mm gap to function as the suppression channel. Assuming a cylindrical gap, 1 mm was computed to be long enough for 99.99% of the eluent cations to reach the Nafion walls by diffusion. Referring to Figure 2-12, in the best performing design (B), two other channels, 0.45 mm dia. (substantially larger than the "crack"), are drilled on either side of the suppressor channel and in parallel to it to provide flowing regenerant water or acid (putting acid as the anode regenerant improves current efficiency by increasing anolyte conductivity). The electrodes are exposed only in the locations corresponding to the suppression gap, the current efficiency is much better than the packed capillary suppressor depicted in Figure 2-11. With 28 µm i.d. cyclic olefin polymer (COP) capillary columns, sulfonated and coated with positively charged latex particles, plate counts >70,000 plates/m were observed at a flow rate of 170 nL/min (this flow rate is substantially higher than the van Deemter optimum).

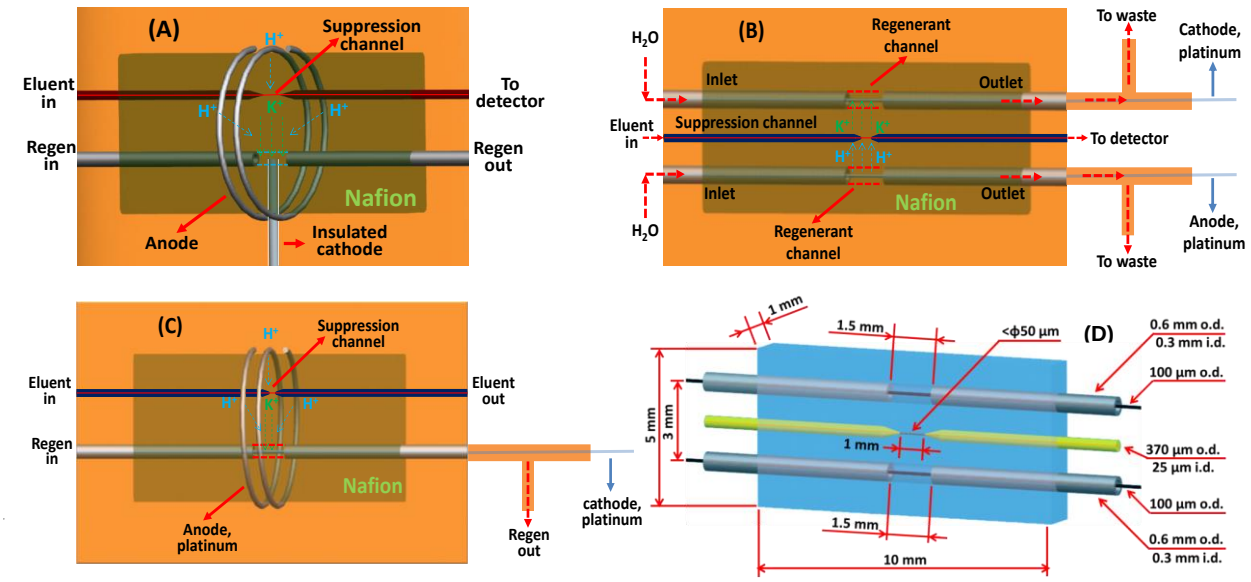

Figure 2- 12 Suppressor designs (A-C). Perspective and design drawing of design B is shown in panel D. In A and C, a platinum coil wrapped around the block serves as the anode. In A, the exterior insulated cathode goes through the block and is placed in a parallel water regenerant channel; in C, the cathode wire is inserted through a tee-junction at the suppressor terminus. In B, both electrode wires are inserted through tees, only the tip near the suppression gap is electrically exposed. Reprinted from reference [49] with permission from the American Chemical Society.

Design B permitted better current efficiency than designs A and B and could suppress 100 mM NaOH flowing at 100 nL/min. Dispersion is critical in such small systems, the separation column and the detector capillary were both inserted directly into the suppressor block.

2.4. Electrodialytic Suppression in Capillary Electrophoresis

The most common detection methods used in capillary electrophoresis (CE) are optical absorbance and conductivity (both contact and contactless, the latter more correctly called *admittance* detection [50]). A sodium tetraborate (borax) solution is a common background electrolyte (BGE) used in CE. When cation exchanged for H^+, very weakly conducting boric acid results and can thus form the basis of a very sensitive conductance/admittance detection method. Dasgupta and Bao [51] and Avdalovic et al. [52] independently reported suppressed conductivity detection in CE, the former group named their arrangement Suppressed Conductometric Capillary Electrophoresis Separation System (SuCCESS). Functionally the suppressor arrangement in both reports were identical (see Figure 2-13 below). Avdalovic et al. demonstrated the separation of anions using a CEM suppressor as well as that of cations using an AEM suppressor (and dilute phosphoric acid as the BGE) while the former authors only illustrated anion separations.

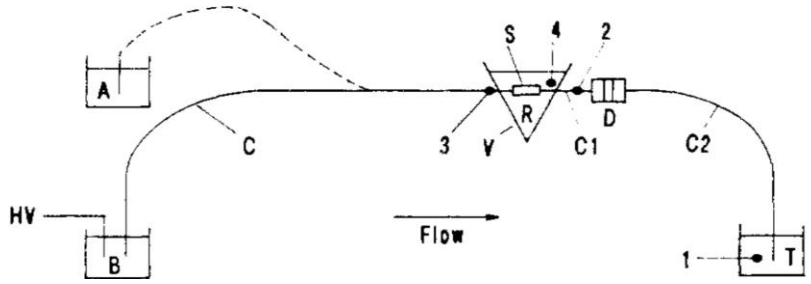

Figure 2- 13 SuCCESS schematic ; A: sample, B: BGE, HV: high-voltage electrode, C: separation capillary, S: membrane suppressor, V: vial

containing regenerant R, C1: capillary connecting suppressor S to detector D, C2: outlet capillary connecting detector D to terminating electrolyte reservoir T, 1-4: potential grounding locations. Reprinted from reference [51] with permission from the American Chemical Society.

The suppressed CE arrangement (Figure 2-13) involves the termination of the separation capillary in a capillary IEM that is surrounded by an electrically grounded regenerant solution. The applied polarity is such that the BGE counterion can travel through the IEM to the surrounding regenerant promoted by the electric field while the chemically induced suppression can also occur. For example, with anions separated by a borax BGE, +HV is used with a CEM suppressor; thus, the ground electrode in the CEM suppressor reservoir is the virtual cathode that provides the motive for the transmembrane transport of the BGE cations. The proton gradient across the IEM helps drive protons from the reservoir to the lumen. The presence of the chemical reagent to provide the proton gradient is important in this case as the electrophoretic current may or may not be enough as suppression current to achieve complete suppression. Experimental findings in [51] showed that suppression was incomplete (causing analyte signals to be lower) if only water was used in the grounding vial instead of dilute acid.

Design of the detector differed in the two publications. In [51], a short capillary at the end of the suppressor IEM terminated in an elastomeric capillary through the walls of which two sensing Pt wires run crosswise, very

close to, but not touching, each other. In the likely superior design in [52], conductivity was measured simply between the ground electrode in the IEM reservoir and a sensing wire inserted into the end of the terminating capillary connected to the IEM. Impressive separations and sensitivity were demonstrated in such systems (Figure 14).

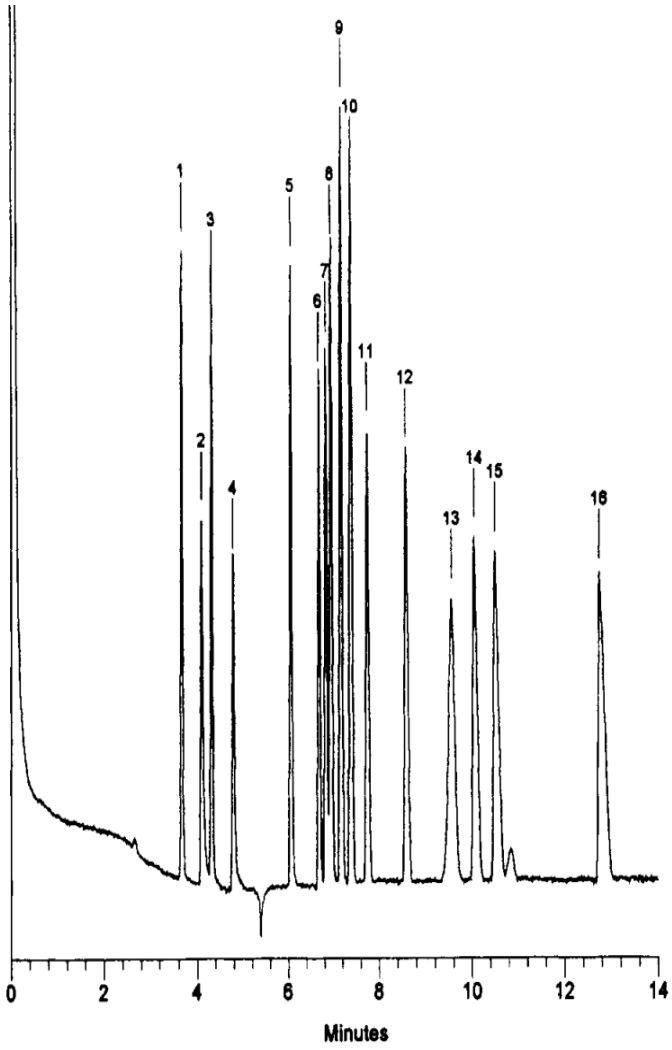

Figure 2- 14 Carboxylic acid separation by capillary electrophoresis with detection by suppressed conductometry , 10 µM each analyte (concentrations in ppm given in parentheses): 1: quinic (1.92), 2: benzoic

(1.44), 3: lactic (0.90), 4: acetic (0.60), 5: phthalic (1.66), 6: formic (0.46), 7: succinic (1.18), 8: malic (1.34), 9: tartaric (1.50), 10: fumaric (1.16), 11: maleic (1.16) 12: malonic (1.04), 13: citric (1.92), 14: isocitric (1.92), 15: cis-aconitic (1.74) (the small peak immediately following is most likely the trans- isomer), 16: oxalic (0.90). Reprinted from reference [52] with permission from the American Chemical Society.

2.5. IEM-based Devices in Suppressor/Suppressor-Like Configurations for Non-Suppressor Applications

2.5.1. Buffer Generators

Membrane suppressors are ion exchange devices. In electrodialytic operation the degree to which ion exchange occurs can be easily controlled by controlling the current. Rather than quantitatively suppressing a NaOH or KOH solution to water for example, one may exchange some controllable amount of the Na^+ in an influent NaX solution to make a NaX-HX buffer where HX is a weak acid. Buffers are widely used in chromatography and in many other areas. Such an electrodialytic buffer generator (EBG) can essentially provide the equivalent of a “Dial-A-Buffer” machine. Control of the applied current and the choice of the IEMs affect the amount and charge type of ions that are transferred. By choosing a proper influent and the applied current (and thus the amount of H^+ or OH^- transferred), different pH level buffers are readily produced. By applying a current gradient, a pH gradient is generated without mechanically mixing multiple chemicals. Chen et al. [53] first used standard, commercially available dual-CEM and dual-AEM

suppressors (Figure 2-15, (a) and (b), respectively below) to generate buffers and pH gradients.

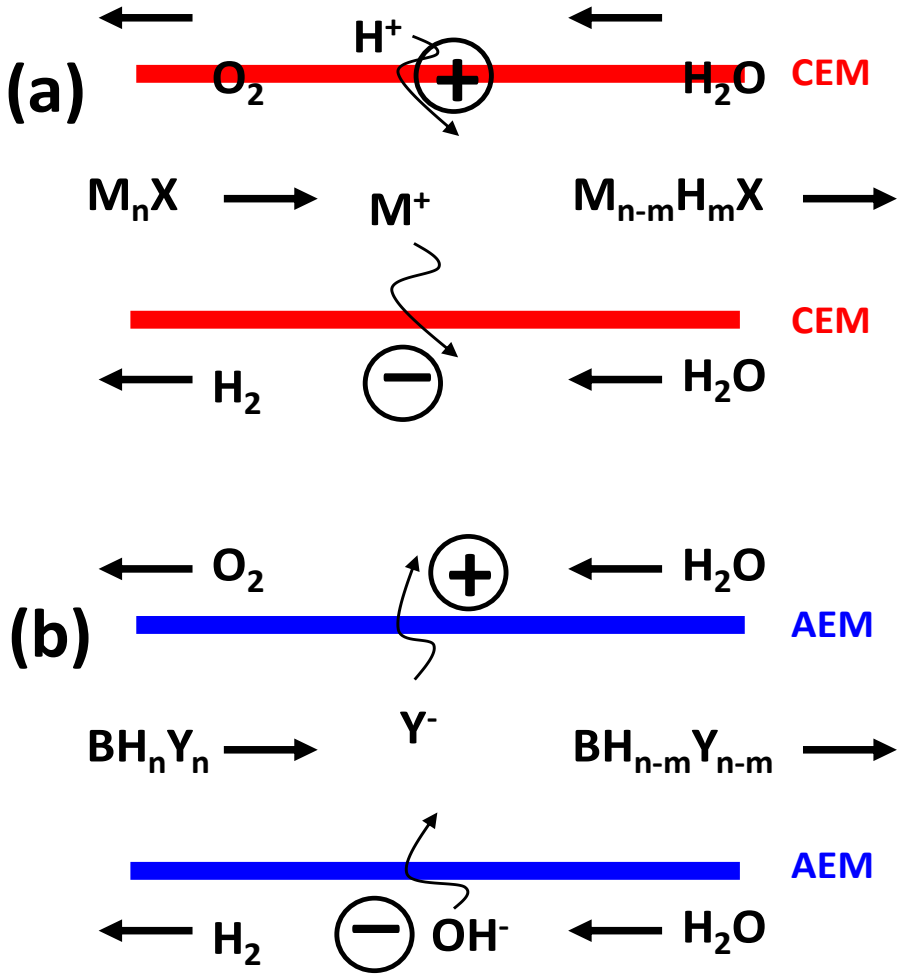

Figure 2- 15 Electrodialytic buffer generator based on (a) a suppressor used in anion chromatography (a dual CEM device) with the strong base salt of a multiprotic acid as the feed solution and (b) a suppressor used in cation chromatography (a dual AEM device) with a strong acid salt of a base as the feed solution. The electrical current controls the removal of the cation and anions in the respective cases to attain the desired pH.

Reprinted from reference [53] with permission from the American Chemical Society.

Using alkali metal salts of multiprotic acids, e.g., phosphoric or citric acid, and a dual CEM suppressor, different amounts of the metal ion was exchanged for H^+ to create a desired pH buffer (Fig. 15a). Similarly, different amounts of OH^- may be brought into an influent containing a strong acid salt of a weak base like ethylenediamine or tris(hydroxymethyl)aminomethane with the strong acid anion correspondingly taken out to create a buffer in the alkaline pH region (Fig. 15b). The authors demonstrated linear pH gradients from pH ~3-12 using multicomponent influent mixtures.

In so far as a metal ion or a strong acid anion is concerned, a suppressor operates only in a subtractive mode, it can only remove the metal cation or a strong acid anion (CEM and AEM-based suppressors respectively). In their more ambitious work [54], the authors designed an EBG that has an AEM and a CEM and three flow channels, otherwise similar in physical configuration to a planar, sheet membrane-based suppressor (Figure 2-16). Further, in addition to an electrode on the far side of each membrane, the center channel contained an electrode that was held at ground potential.

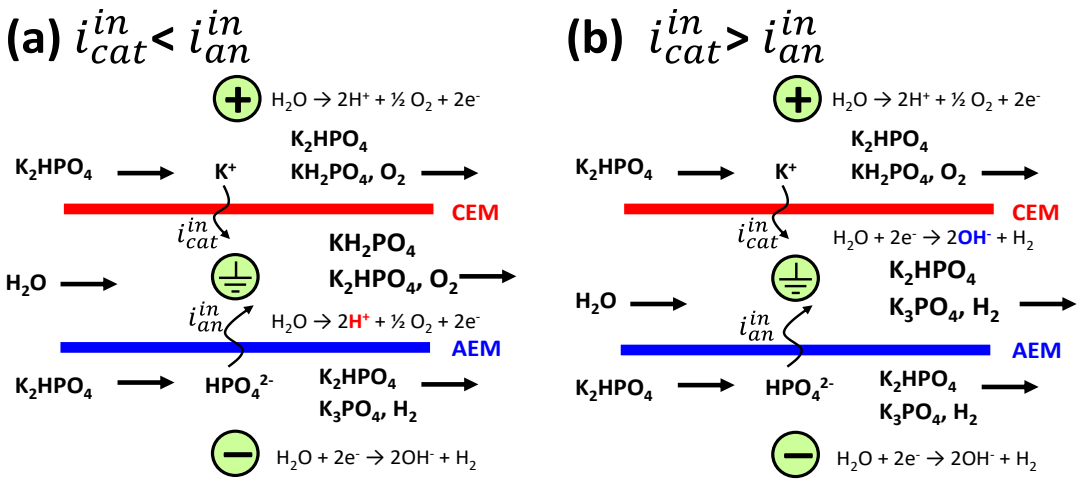

Figure 2- 16 A three-electrode buffer generator consisting of a CEM and an AEM and a grounded central electrode. Although on this illustration the CEM side is held positive and the AEM side is held negative (resulting in cations and anions respectively being added through the CEM/AEM into the central channel), either outer electrode could be held at a positive or negative potential relative to the center ground electrode. When the CEM electrode is held negative and the AEM electrode is held positive the device will be operating in a subtractive mode, it will be removing cations/anions from the central channel respectively through the CEM/AEM into the outer compartment. With K_2HPO_4 as the feed solution on both the outer channels (K^+ is the principal cation and HPO_4^{2-} is the principal anion) and electrode polarities as indicated, when the input current through the CEM (i_{cat}^{in}) is exactly equal to the input current through the AEM (i_{an}^{in}), equivalent amounts of K^+ and HPO_4^{2-} will be transported and K_2HPO_4 will be the central channel effluent. For the case in (a), when $i_{cat}^{in} < i_{an}^{in}$, less equivalents of K^+ are brought in than HPO_4^{2-}. To

compensate, H^+ (and O_2) are generated at the central electrode and K_2HPO_4/KH_2PO_4 (and O_2) exits the central channel. Conversely, for the case in (b), if $i_{cat}^{in}>i_{an}^{in}$, OH^- (and H_2) are generated at the central electrode and K_2HPO_4/K_3PO_4 (and H_2) exits the central channel. Reprinted from reference [54] with permission from the American Chemical Society.

Overall, metal cations could be either brought in or removed through the CEM, depending on the CEM being held positive or negative with respect to the ground. Similarly, anions could be brought in or removed through the AEM. This device could thus operate with considerable latitude over a large range. The penalty paid is that depending on the sign and the magnitude of the independent current levels through each membrane, either H_2 or O_2 may be present in the central channel effluent, in most cases this would need to be removed before further use. The power of the technique is shown in Figure 2-17 where pH and/or concentration gradients are demonstrated.

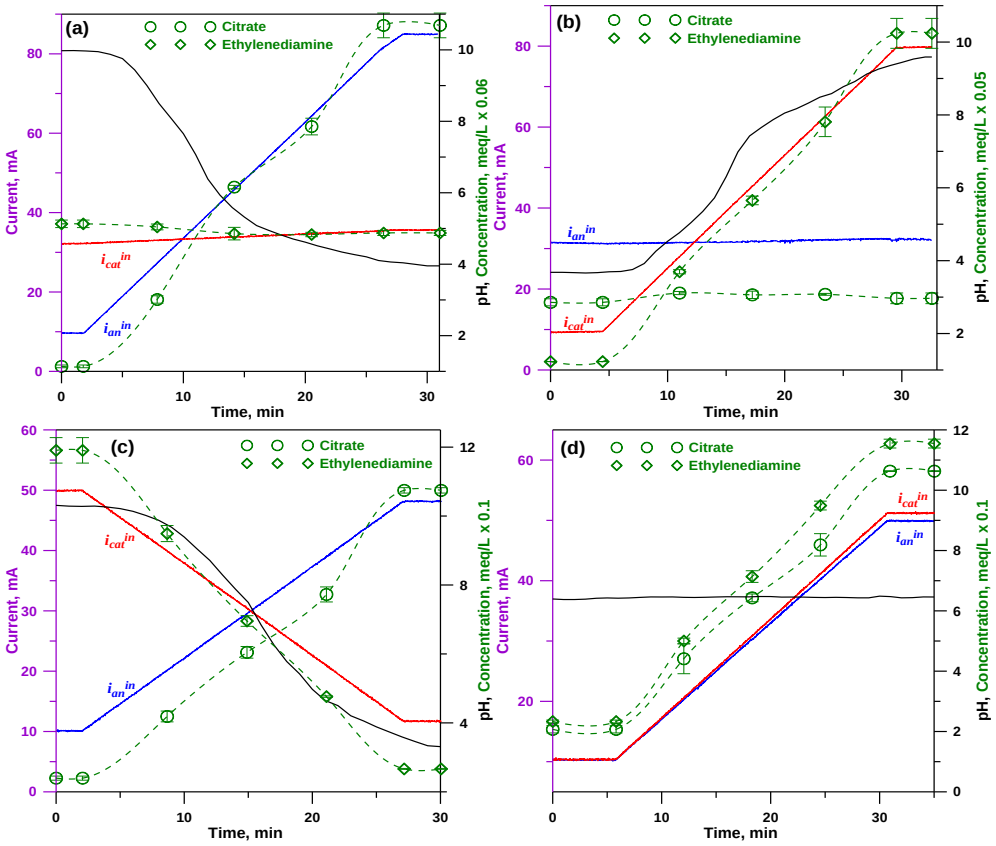

Figure 2- 17 (a) Citrate concentration gradient and descending pH gradient by varying i_{an}^{in} and keeping i_{cat}^{in} constant ; (b) ethylenediamine concentration gradient and ascending pH gradient by varying i_{cat}^{in} and keeping i_{an}^{in} constant; (c) linear pH gradient with a relatively constant buffer concentration when i_{an}^{in} is increased and i_{cat}^{in} is decreased; (d) constant pH with a buffer concentration gradient when $i_{an}^{in}$and $i_{cat}^{in}$are equal and increased at the same rate. Feed in CEM side outer channel: 0.3 M ethylenediamine sulfate; feed in AEM side outer channel: 0.2 M tripotassium citrate; central channel feed: water, 0.25 mL/min. Reprinted from reference [54] with permission from the American Chemical Society.

2.5.2. Water Purifier

A CEM-based suppressor used in anion chromatography removes all cations and replaces them with H^+. An AEM-based suppressor used in cation chromatography removes all anions and replaces them with OH^-. It follows that no matter in what sequence they are placed, a combination of two such suppressors will deionize an influent stream. In water deionization operations using ion exchange resin beds, it is well known that a H^+-form CEX resin bed and an OH^--form AEX resin bed, arranged in any sequence, will deionize a water stream. However, a mixed bed deionizer always provides the best results. Similarly, a device configured like a suppressor, except constructed from a CEM and an AEM (much like the device in Figure 2-16), where the CEM side is held negative and the AEM side is held positive, will simultaneously remove all cations through the CEM and all anions through the AEM. Such a device will be highly current-efficient as the same current is utilized in in transporting both types of ions. Srinivasan and Avdalovic patented such a device [55], shown schematically in Figure 2-18. The device has been commercially available as a “Electrolytic Water Purifier” (EWP), specifically configured for use with commercial IC instrumentation. Others have also observed the production of high-quality deionized water with appropriately polarized CEM/AEM devices [56].

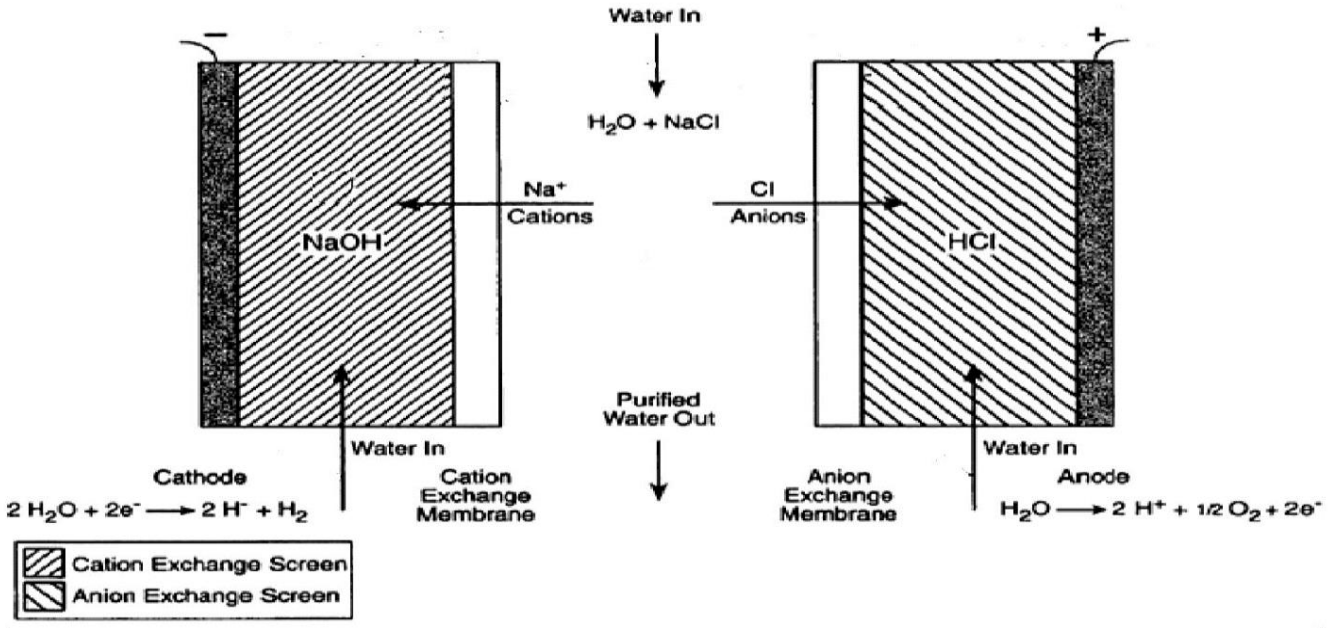

Figure 2- 18 CEM and AEM based water purifier with electrode polarities as indicated. The removal of NaCl is illustrated as an example. Note that the central channel contains no ion exchange material to maximize current efficiency. Adapted from reference [55].

2.6. Electrodialytic Eluent Generators (EEGs)

When IC made its first successful commercial debut with CO_3^{2-}/HCO_3^- eluents in 1977, it was already recognized that an alkali hydroxide eluent would be the best choice for anion chromatography; it is suppressed to water and therefore eluent gradients should have no effect on the background. The reason that actual practice of IC could not begin with hydroxide eluents was twofold. First, available alkali hydroxide reagents invariably contained impurities like chloride and chlorate. Even when very highly purified material was used for eluent preparation, unless extreme care was taken (e.g., all operations conducted inside a purged glove box),

the eluent became contaminated with carbonate over time: we live in an ocean of several hundred ppm CO_2. During gradient elution, the CO_3^{2-} in the eluent results in a far from constant detector background. Importantly, CO_2 continues to be absorbed by the eluent by permeation through polymeric components in the system, increasing carbonate concentration over time and thence the eluting power of the eluent (CO_3^{2-} exhibits much stronger eluting power than OH^-). The second reason that hydroxide was not used in the early practice of IC was the poor selectivity of available ion exchange stationary phases for hydroxide. This meant that large concentrations of hydroxide were needed to make a useful eluent, greatly compromising the usable lifetime of fixed capacity early packed column suppressors. However, it was recognized that if it ever became possible to use pure hydroxide as eluent, this will not only lead to gradient capability but far lower LODs will be possible than those attainable with CO_3^{2-}/HCO_3^- eluents because of the much lower background.

In-line electrodialytic generation of pure hydroxide eluents was first proposed by Strong and Dasgupta [57]. They proposed a very simple concept (Figure 2-19): Separate a donor and a receptor stream with a CEM and provide an electrode in each channel to function respectively as the anode and the cathode. The donor stream contains a source of the desired alkali hydroxide, e.g., if KOH is to be generated, the donor stream may contain KCl or KOH or any other reagent to supply K^+. To prevent impurities from anion leakage when a high donor concentration is used, a solution of KOH

itself will be the most appropriate. Note that while this feed KOH may contain other anionic impurities, the dominant anion will still be hydroxide. The receiver stream consists of high purity water; this flows countercurrent to the donor stream. When a potential above the electrolytic threshold is applied, K^+ is brought into the receiver stream in contact with the negative electrode. The cathode process results in the production of corresponding amounts of OH^- and gaseous H while the anode process results in the production of H^+ and O_2. The cathode effluent thus contains KOH and H_2, the latter can be removed from the stream by a gas permeable membrane. At least two aspects of this device are notable: (a) the purity of the KOH generated is dependent primarily on the purity of the influent water. Both the direction of the electric field and the Donnan barrier towards the passage of anions through a negatively charged CEM prevent the transport of an impurity anion. (b) As long as the cation concentration in the donor stream does not become a limiting factor, the magnitude of the current flowing controls the mass of the KOH generated. Typically, the receiver flow rate is constant and thus the eluent concentration is linearly related to the applied current, following eq. 1 (the C^3 principle: *Current Controls Concentration*). Thus, such a system not only permits generation of very high purity eluents - it enables the generation of eluent gradients through current programming rather than mechanical blending.

2.6.1 Suppressed Product Conductance and Zero Current Penetration. Two Important Parameters for an EEG

To understand and characterize an EEG, aside from current efficiency, two other parameters are of importance. The first is the suppressed product conductance (SPC), this is the conductance value of the generated acid or base eluent, after suppression respectively through an AEM or CEM based suppressor. Ideally this specific conductance (σ) should be the same as that of pure water (55 nS/cm). In practice, because of ever-adventitious CO_2, an SPC value lower than 100 nS/cm is rarely attained. In general values $\leq$500 nS/cm should be considered indicative of a highly pure eluent; there are usually no problems carrying out eluent gradients when at the high concentration end the SPC is <1 μS/cm. The second parameter of interest is the extent of zero current penetration (ZCP). This is the eluent concentration that is produced by an EEG when no current is applied to it. Imagine the device of Figure 2-19 with the feed KX on the CEM side and water on the other. The Donnan potential (arising from the stationary negative charge on the CEM material) that prevents the passage of negatively charge X^- (and hence KX altogether) to the other side. However, if the concentration of KX is high enough, this chemical potential can overcome the Donnan barrier and some KX can leak through. The exact extent of such leakage/penetration will depend on the KX concentration (increasing ZCP with increasing concentration), thickness and degree of functionalization (ZCP decreases with increase in

either) of the IEM. It also depends on the nature of the forbidden ion: a small high diffusivity singly charged ion penetrates much more readily than a large multiply charged ion. A further process that can appear as "leakage" is ion exchange: In Figure 2-19, KOH can form on the receiver side of the membrane without an applied current through exchange of K^+ on the CEM for H^+ in the water. Although H^+ concentration in water is very low, selectivity of an ion exchanger phase for an ion increases with decreasing concentration. ZCP obviously governs the lowest eluent concentration that can be generated and the ZCP value can become significant enough to be of concern if the feed is a concentrated solution. There are few studies of forbidden ion penetration through an IEM in the literature; the only study known to us reports that ZCP is typically a quadratic function of the reagent concentration [58].

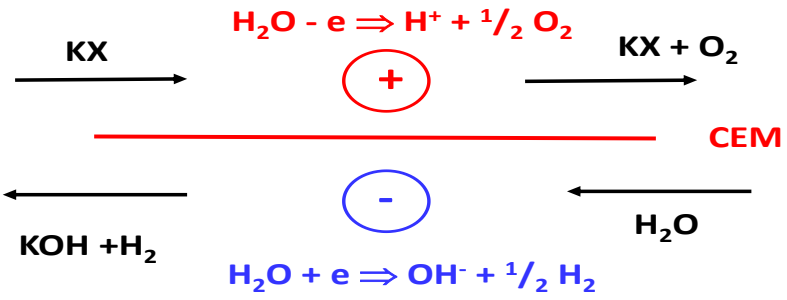

Figure 2- 19 Simplest EEG schematic.

2.6.2. Single Membrane EEGs

Single membrane EEGs of the type depicted in Figure 2-19 were termed Type 1 generators by Strong and Dasgupta [56] and extensively

studied both in planar and tubular configurations using three different CEMs: Flemion, Nafion, and Selemion. (the first is a carboxylic acid type hydrocarbon -skeleton CEM, the others are sulfonated perfluorocarbon material). All showed linear *i-V* behavior with the highest resistance in the conducting voltage regime (208 mA/V) for Selemion, (232-243 mA/V for others). Selemion also exhibited the lowest ZCP. Table 2-2 shows the ZCP and SPC values. In interpreting the SPC data, note that when water of ≤ 63 nS/cm specific conductance (theoretical minimum 55 nS/cm) was pumped through the whole system (all channels and suppressor), its conductance would increase to 100 nS/cm; the latter should therefore be taken as the lowest attainable background value.

Table 2- 2 Type 1 planar generators. Reprinted from reference [57] by permission from the American Chemical Society.

membrane	E, V	i, mA	P_{NaOH}, mM	electrically suppressed conductance (EMS SPC), μS/cm
Nafion	0		4.9	0.37
	2.7	50	33.8	0.36
	3.2	156	99.5	0.40
	3.6	260	176.0	0.34
Flemion	0		2.1	0.16
	2.8	49	32.9	0.30
	3.3	142	95.3	0.31
	3.7	270	176.0	0.34
Selemion	0		0.1	0.16
	3.0	52	33.6	0.36
	3.5	140	91.2	0.47
	4.1	280	181.0	0.80

All the tabulated SPC values are significantly higher than the water background. At least for Nafion and Flemion, the SPC values do not systematically increase with the generated eluent concentration, suggesting contamination by adventitious CO_2 rather than anionic impurities present in the eluent. For Selemion, the SPC increased with the generated eluent concentration, suggesting involvement of membrane breakdown products. Being the most resistive membrane, heat production will be highest with this membrane and decomposition is likely at increased membrane temperatures, especially since it is based on a hydrocarbon rather than a fluorocarbon skeleton. Some CO_2 contamination is inevitable in IC systems that eschew metallic components and uses polymeric components, notably tubing. Some polymers are much more permeable than others: the amount of CO_2 permeated through Tefzel® (a copolymer of ethylene and tetrafluoroethylene) tubing into water as a function of residence time is shown in Figure 2-20, increasing residence time increases the CO_2 contamination.

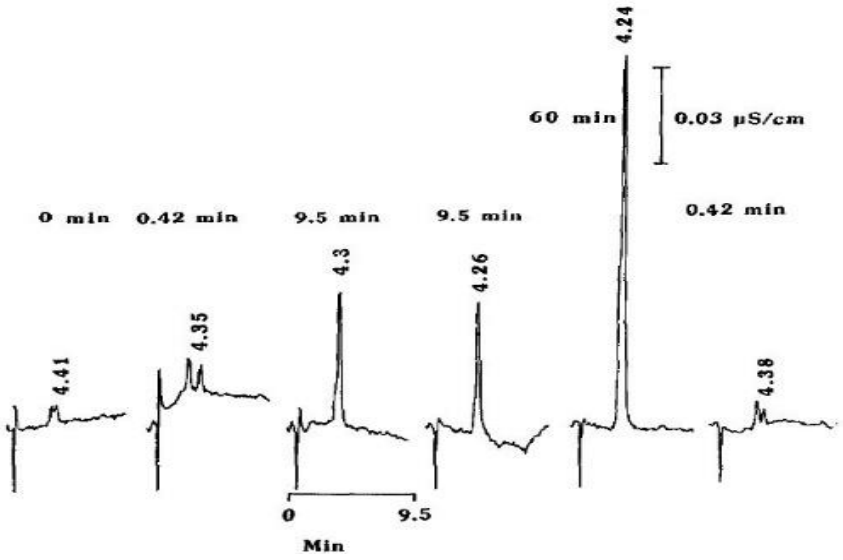

Figure 2- 20 Effect of residence time on permeation of CO_2 through Tefzel tubing (0.5 mm wall thickness) maintained in air into pure water. For short residence times, the authors estimated an intrusion rate of ~0.3 µM/min, emphasizing the magnitude of CO_2 contamination problems. Reprinted from reference [34] by permission from Elsevier.com.

ZCP is generally lower for tubular devices, as they typically utilize a smaller membrane area than comparable planar devices. There are other ways to decrease ZCP, e.g., by decreasing the feed concentration or using thicker membranes.

Single membrane devices are simple both in principle and practice. Such devices are easy to configure if the generated eluent feeds the high-pressure pump. However, a feed system would not be needed if the eluent could be generated on the high-pressure side. This requires that the eluent generator tolerates high pressure (in the case of a hydroxide eluent, on the

cathode side). It is also not essential for the donor solution to be flowing. Instead, it can be a reservoir containing a concentrated donor solution that will work for a substantial period before replacement is needed. In present commercial embodiment, the above is accomplished by having a concentrated donor solution reservoir coupled to a flowing solution of the recipient water stream through a very thick membrane (in reality, a stack of multiple individual CEMs), sometimes termed a “ion exchange connector”. The thickness also minimizes the permeative transport of water under pressure in the receptor channel to the donor reservoir. A pressure-tolerant gas-permeable Teflon AF tube is disposed between the generator cathode effluent and the injector for removal of the gas. The overall configuration is depicted in Figure 2-21. In a similar manner, strong acid eluents for cation chromatography can be generated using a strong acid solution in the donor reservoir, which is separated from a flowing recipient water stream by a stack of AEMs. In this case, the anode is disposed in the receiver channel, H^+ and O_2 is generated therein, the latter being removed thereafter by passage through a gas permeable membrane tube.

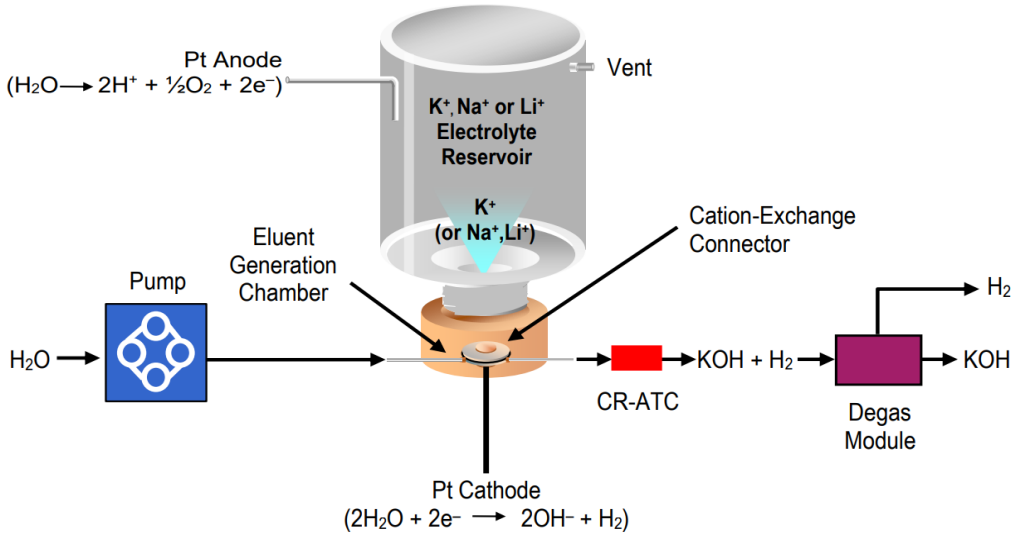

Figure 2- 21 Configuration of present commercially available (hydroxide) eluent generators. See text for details. Courtesy Thermo Fisher Scientific.

2.6.2.1. Single Membrane Capillary Scale EEGs

Most devices are being miniaturized and often there are performance benefits to miniaturization. Ion chromatography is no exception. While much of the earlier work were carried out with 4 mm columns, majority of present users prefer the 2 mm format. Smaller volume electrodialytic eluent generators better suited for the 2-mm columns have been reported [59]. Packed column ion chromatography has long been available in the capillary (0.4 mm i.d.) format. However, among researchers, the typical practice of capillary liquid/ion chromatography utilize columns of even smaller bore. To successfully practice IC in these scales, while the principles remain the same, eluent generators and their internal volumes must also be miniaturized. Sjögren et al. [60] pioneered a new capillary EEG for their high-pressure capillary IC system. The EEG was placed downstream of a high-

pressure pump with and could supply up to 100 mM NaOH eluent with near-Faradaic efficiency; this system did not require pressures in excess of 1000 psi. The EEG design involved two small cylindrical chambers separated by a ~200 µm thick Nafion CEM. The donor (anode) and receptor (cathode) chambers are parts of a male and female block, respectively, the top part being constructed from poly(vinyledene) fluoride (Kynar^{TM}) and the bottom part from stainless steel. These are threaded and fit securely into each other. The device is shown in Figure 2-22 with the two parts disassembled. The bottom terminal end of the top part has a 0.25 mm deep circular recess, 2.5 mm in diameter. A PEEK ring fits tightly over the protrusion of the terminus of the top part and thus provides additional sealing of the membrane disk placed on the flow-through cavity (3.8 µL) of the female part. The top male part contains threaded feed-NaOH inlet/outlet ports. An anode access hole is drilled straight through to the donor cavity. A 100 µm diameter platinum wire is inserted through this hole and sealed therein to function as the anode. The entire metallic bottom functions as the cathode. The EEG was operated in the constant current mode with 25- 50 mM NaOH donor pneumatically pumped through the anode chamber.

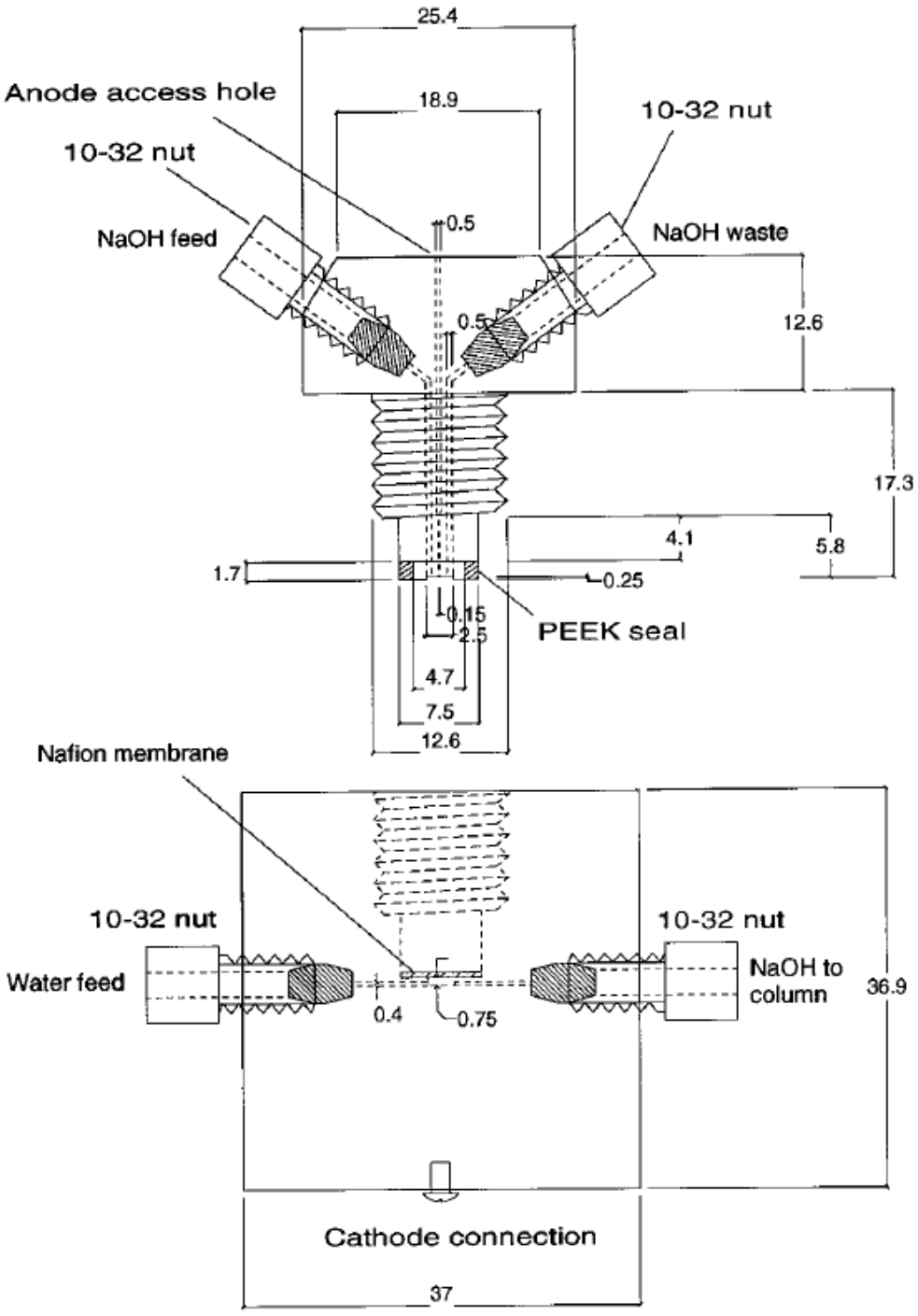

Figure 2- 22 Schematic of the high-pressure EEG. Reprinted from reference [60] by permission from the American Chemical Society.

The generated eluent was degassed through a short length of a PTFE tube, the high pressure facilitates the removal of the concurrently generated H_2 gas to permeate out through the tube wall, the tube is encased in a shell filled with soda lime to prevent the ingress of CO_2. Because the generator membrane was not especially thick, the ZCP values were not negligible despite relatively low concentration feed solutions (0.48 and 0.6 mM for 25 and 50 mM NaOH feed solutions, respectively). The linearity between generated eluent concentration and applied current was excellent (r^2 0.9970 to 0.9990). However, the NaOH generation efficiency based on the measured concentration was slightly super-faradaic, likely because some of the pumped water being lost by permeation through the not-so-thick Nafion CEM. Figure 2-23 shows a gradient separation of 19 analytes. The applied current was increased from 20 to 130 µA @ 10 µA/min, leading to a generated gradient of 2.2-34.2 mM NaOH. This miniature high-pressure EEG was then used to build a fully computer controlled portable capillary IC system [19].

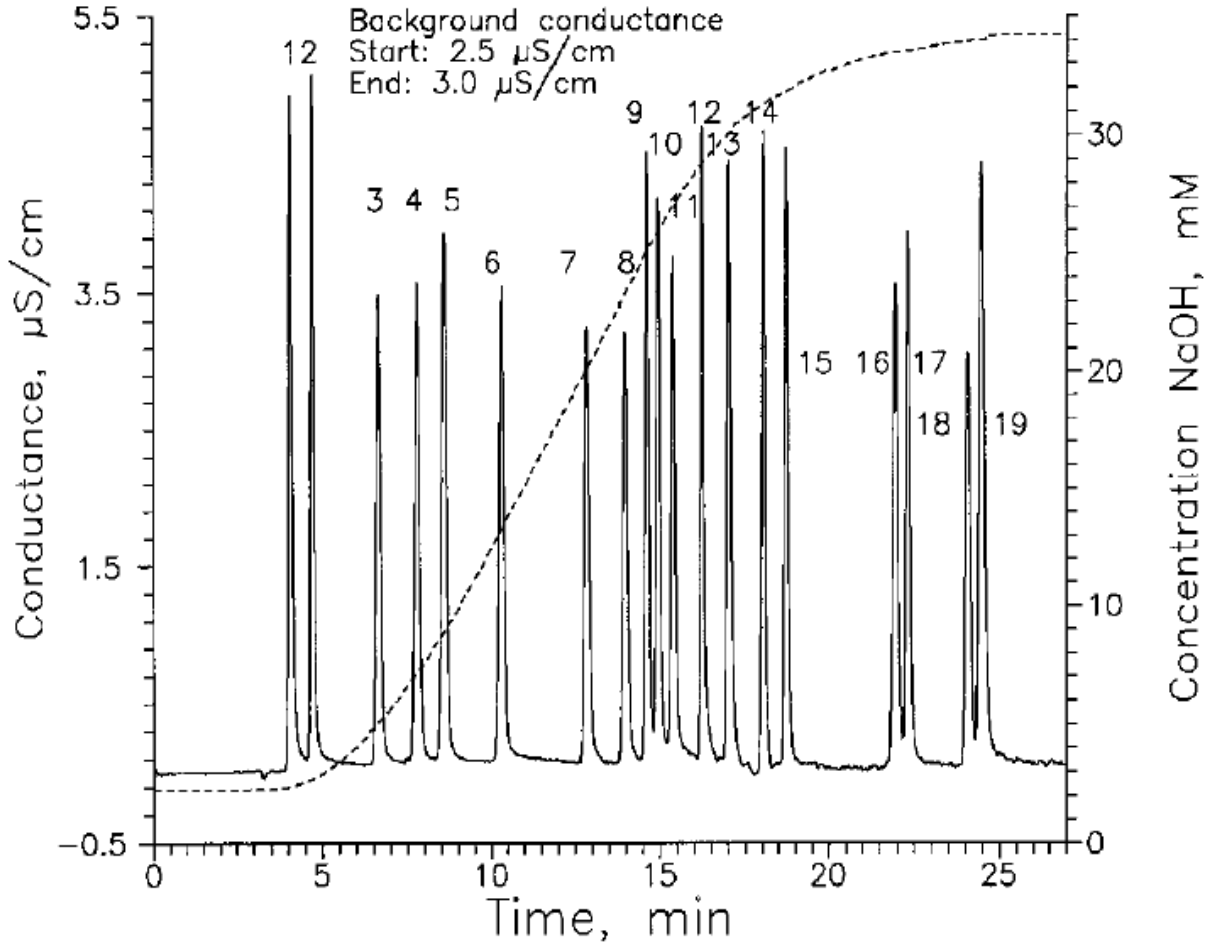

Figure 2- 23 Gradient chromatogram : The right ordinate shows the gradient (dashed trace) in millimolar NaOH. Peak identities: 1, fluoride; 2, formate; 3, monochloroacetate; 4, bromate; 5, chloride; 6, nitrite; 7, trifluoroacetate, 8, dichloroacetate; 9, bromide; 10, nitrate; 11, chlorate; 12, selenite; 13, tartrate; 14, sulfate; 15, selenate; 16, phthalate; 17, phosphate; 18, arsenate; 19, citrate. All compounds injected were 50 µM except selenate and sulfate, which were 25 µM. The baseline increased by ~500 nS/cm during the run, and a baseline subtraction was performed using a blank gradient run. The fluoride peak coelutes with an unidentified

impurity. Reprinted from reference [60] by permission from the American Chemical Society.

2.6.2.1.1. A Single IEX Bead-Based EEG

Much after the initial work of Sjögren et al. [60], the concept of using an IEX resin bead both as a membrane and a high-pressure seal was introduced [61]. Consideration of ZCP in high-pressure EEGs remain important. Effectively beads are thick membranes, permitting more concentrated feed solutions. Yang et al. [62] used a single cation exchange resin bead located in the perpendicular arm of a stainless-steel tee to design a single membrane EEG (Figure 2-24). The device could generate isocratic and gradient KOH eluent (0-100 mM KOH generation was demonstrated) and except at the highest end, the generated concentration was proportional to the applied current with near-Faradaic efficiency. The CEX resin-bead-based EEG is particularly suitable for capillary IC systems due to its low internal volume and mechanical strength (tested to 3200 psi). Hydrogen gas present in the eluent was removed by a short length of PTFE tube as before.

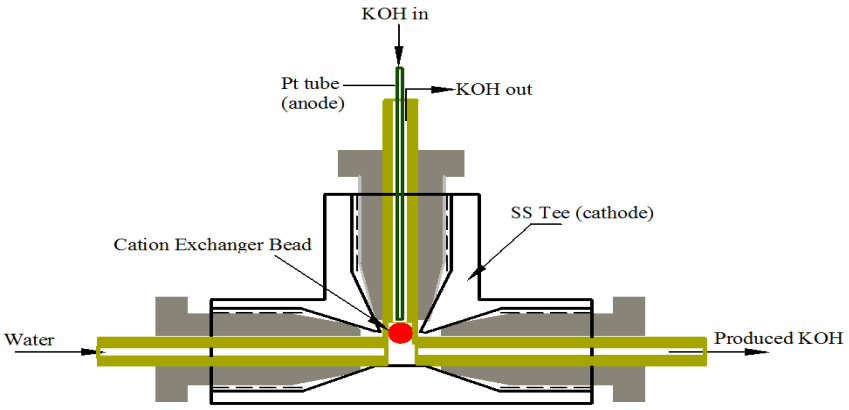

Figure 2- 24 Single resin-bead-based EEG. Reprinted from reference [62] by permission from Elsevier.com.

2.6.3. Gas-Free EEGs

Having to remove generated gases is the principal drawback of single membrane devices. Over the years, efforts have therefore been made towards a gas-free EEG design. Even in the first paper [57] on single membrane EEGs, a gas-free eluent generator comprising of a CEM and an AEM, termed a “Type 2” generator, was explored. Consider the disposition of the two membranes in Figure 2-25; the recipient water flows between a CEM and a second membrane, presently marked “BM”, connoting a barrier membrane.

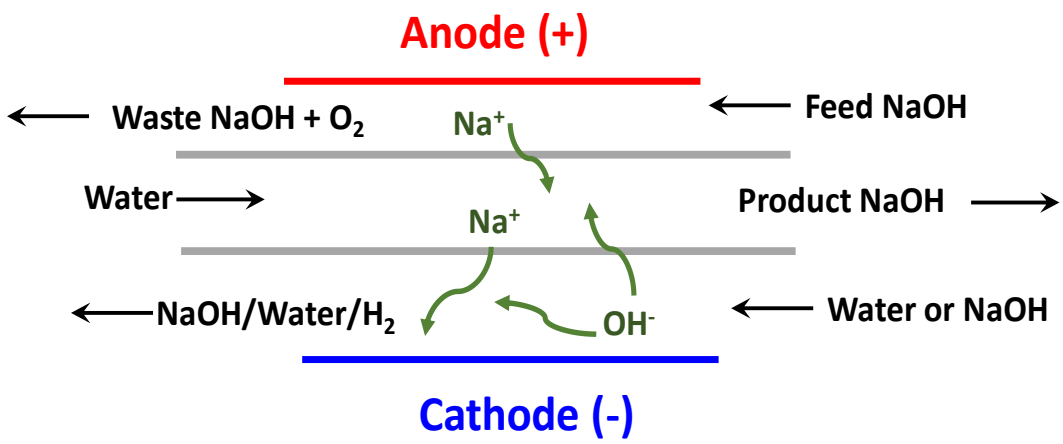

Figure 2- 25 Two-membrane eluent generator schematic. Reprinted from reference [57] by permission from the American Chemical Society.

The function of the barrier membrane is to prevent the passage of the alkali cation (in the present instance, Na^+) to the cathode chamber. An alkali hydroxide solution is fed as the outer solution on both the outer sides of the CEM and the BM. The intention is to transport the metal cation from the anode chamber through the CEM and hydroxide from the cathode chamber into the central stream. Obviously, this scheme cannot work if a CEM is used as the BM, because it does not present a barrier to the passage of Na^+, which will simply pass through it to the cathode. The scheme will work if an AEM is used as the BM, it will prevent the passage of the alkali cation into the cathode chamber and allow the passage of OH^- into the central flow. In this case, gas generated at the electrodes is isolated from the central channel by the membranes and the generated eluent is therefore free of gas. A dialysis or microporous membrane as BM will also

offer some resistance to the passage of the cation while the passage of the anion from the cathode chamber is not completely forbidden.

2.6.3.1. Dialysis Membranes as Barrier Membranes and Donnan-Forbidden Penetration Based EEGs

In one adaptation with a cellulose acetate dialysis membrane as a barrier [57], 150 mA was required to generate 35 mM NaOH @ 1 mL/min, a current efficiency of 37%. The required voltage was 7.1 V, much higher than voltages needed in Table 2-2 at similar currents, leading to unnecessary Joule heating and waste of energy. Perhaps more importantly, if feed hydroxide is put in the cathode compartment to reduce the voltage drop, the passage of impurity anions in the cathode chamber to the central compartment is possible, although not favored over hydroxide. If pure water is put in the cathode channel, this will be at the expense of energy efficiency. Further, with a cellulose acetate type dialysis membrane, hydrolytic degradation of the membrane also produces acetate as an impurity.

Strong et al. [34] investigated alternatives through CEM-CEM devices and relying on stagnant regimes for concentration buildup and Donnan breakdown as shown in Figure 2-26 [63].

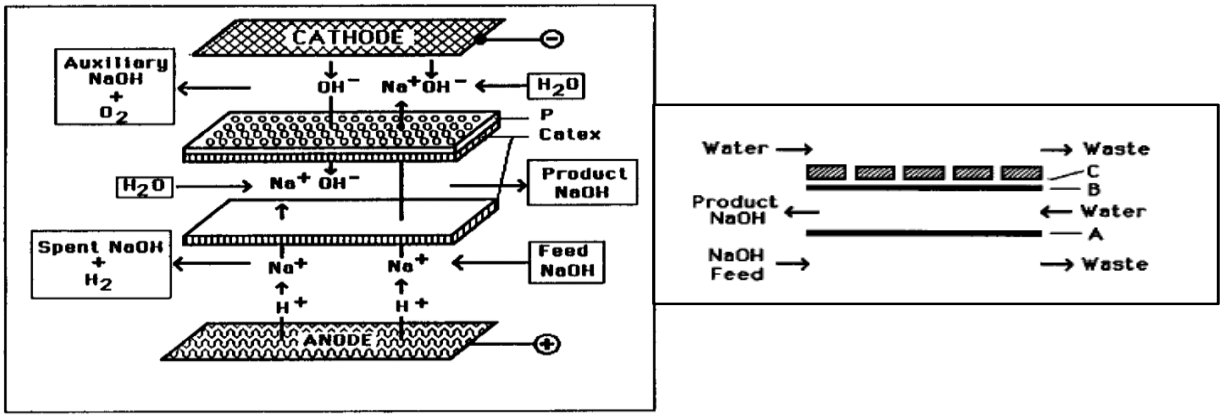

Figure 2- 26 Left: Schematic of a dual CEM planar EEG with a thick perforated barrier to promote stagnant regions and Donnan breakdown. P is a 0.5 mm thick perforated plate of FEP Teflon containing a multitude of small holes (ca. 1 mm dia.). Reprinted from reference [34] by permission from Elsevier.com. Right: Principle of operation, see text for details. Reprinted from reference [63] by permission from Elsevier.com.

In this device, water flows both through the central and the cathode channels while the donor hydroxide (e.g., NaOH) flows as the donor in the anode channel. The operating principle involves transport of Na^+ through the cathode CEM into the perforations where it forms NaOH with cathode-generated OH^- migrating in the opposite direction. The flow in the cathode chamber does not sweep the multitude of the pockets in the perforated plate well, allowing them to accumulate significant concentration of NaOH. The concentration of NaOH in these “accumulators” represents a steady state between the Na^+ transported into the perforations, the NaOH diffusing out

to the cathode flow, and if the accumulated concentration of NaOH is high enough, Donnan-forbidden penetration back into the central flow where it forms the basis of the product NaOH to be used as the eluent. Note that ultimately the donor is the NaOH in the perforations which is highly pure and thus the product NaOH is also much purer than possible to prepare manually. The downside is that the current efficiency is obviously far less than unity. The parameters that govern such eluent generation were studied and the principles examined in detail [63]. Hole diameters <0.5 mm require relatively high voltages to produce significant concentrations of NaOH, increasing the perforation size decreases the required voltage. While the relation between the concentration of the generated NaOH and applied *current* is independent of the hole size, for a certain concentration of NaOH to be generated the required voltage increases with decreasing hole size or increasing plate thickness. Above a certain applied voltage, the potential at the inner surface of the cathode membrane becomes high enough to break down water and the generated eluent is no longer gas-free. More current can be applied with larger hole diameters and for the largest hole diameter (1.55 mm), NaOH is still gas-free at 200 mA, generating 39 mM NaOH. The device responds fast, the 10-90% rise time and the 90-10% fall times for swings between 0 to 20 mM NaOH were 1.1 and 0.84 min, respectively.

2.6.3.2. Dual IEX Resin Bead-Based EEGs

The concept of a resin bead-based EEG was first presented by Yang et al. [64] in a gas-free configuration with a CEX and an AEX bead on the

opposite arms of a cross fitting (Figure 2-27). The ion exchange beads were dried in desiccator and then placed tightly at the tip of the PEEK tubes. After the beads are wetted, they expand and get larger and seal the tubes. In both anode and cathode tubes, KOH flows inside the tubes. While no degassing is required, this design had a lower pressure tolerance (2000 psi) compared to the single CEX bead design in Figure 2-24 because of the mechanical strength limitations of the AEX bead. It also shows higher electrical resistance than a single bead EEG. Lower pressure planar and tubular dual membrane-based gas-free EEGs were also demonstrated in this work [64].

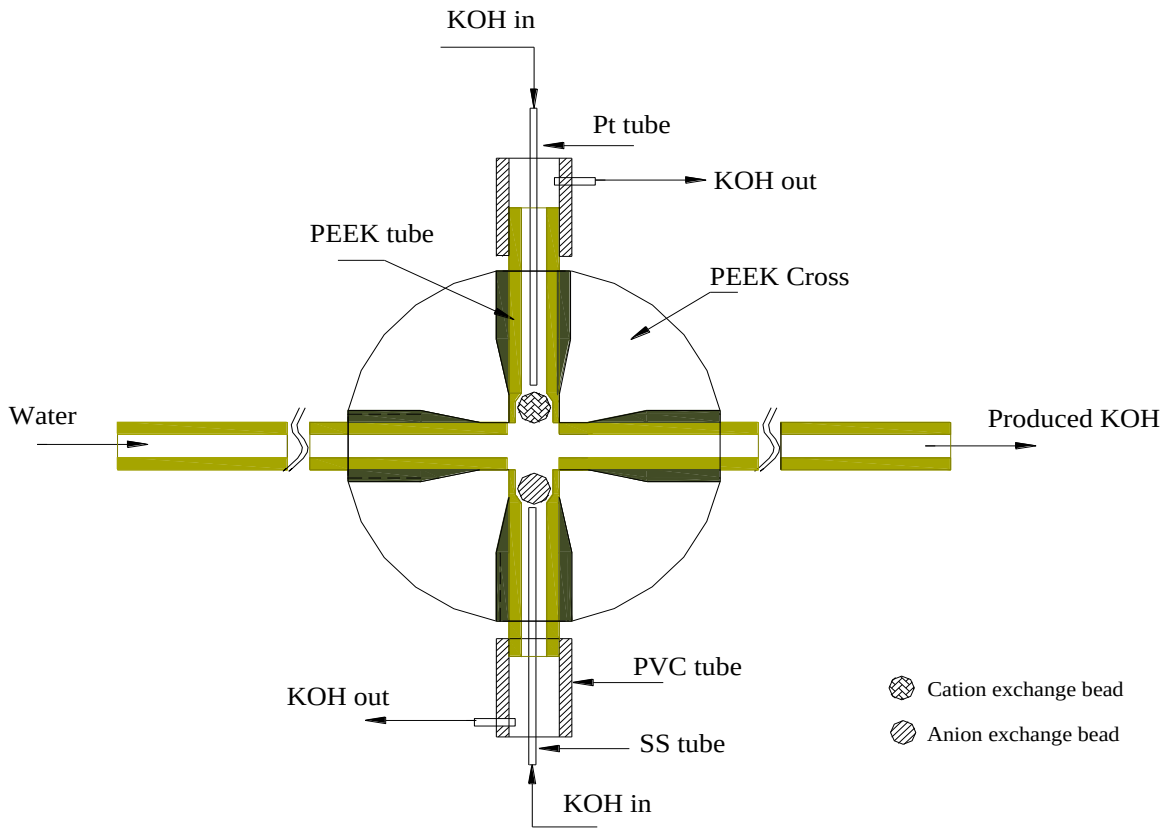

Figure 2- 27 High-pressure bead-based electrodialytic eluent generator. Reprinted from reference [64] by permission from the American Chemical Society.

As with all EEGs, consideration of ZCP in the high-pressure devices remain important. With 4 M KOH feed in both anode and cathode compartments, ZCP for the dual bead device was 1.6 mM KOH for a central flow of 4 µL/min flow (~100 pmol/s). While having KOH in the CEX bead compartment and water in the AEX bead compartment decreased the ZCP, a much greater decrease was observed for the opposite condition (water in the CEX bead compartment and KOH in the AEX bead compartment) - to 3 to 4 pmol of KOH/s, proving the significant role of cation exchange occurring

through the CEX bead in generating ZCP. At the AEX bead, if OH^- ions on the bead are exchanged with the OH^- of the centrally flowing water, there is no net change. This is not the case when K^+ on the CEX bead is exchanged for H^+ in the water stream, leading to KOH production. Hence ion exchange may be the dominant mechanism in ZCP rather than Donnan penetration. Below a feed concentration of 0.2 M, there was no measurable ZCP. The authors also investigated the application of reverse voltage: CEX side negative, AEX side positive) to reduce the ZCP, Figure 2-28 shows the results for a high-pressure dual IEX-bead device.

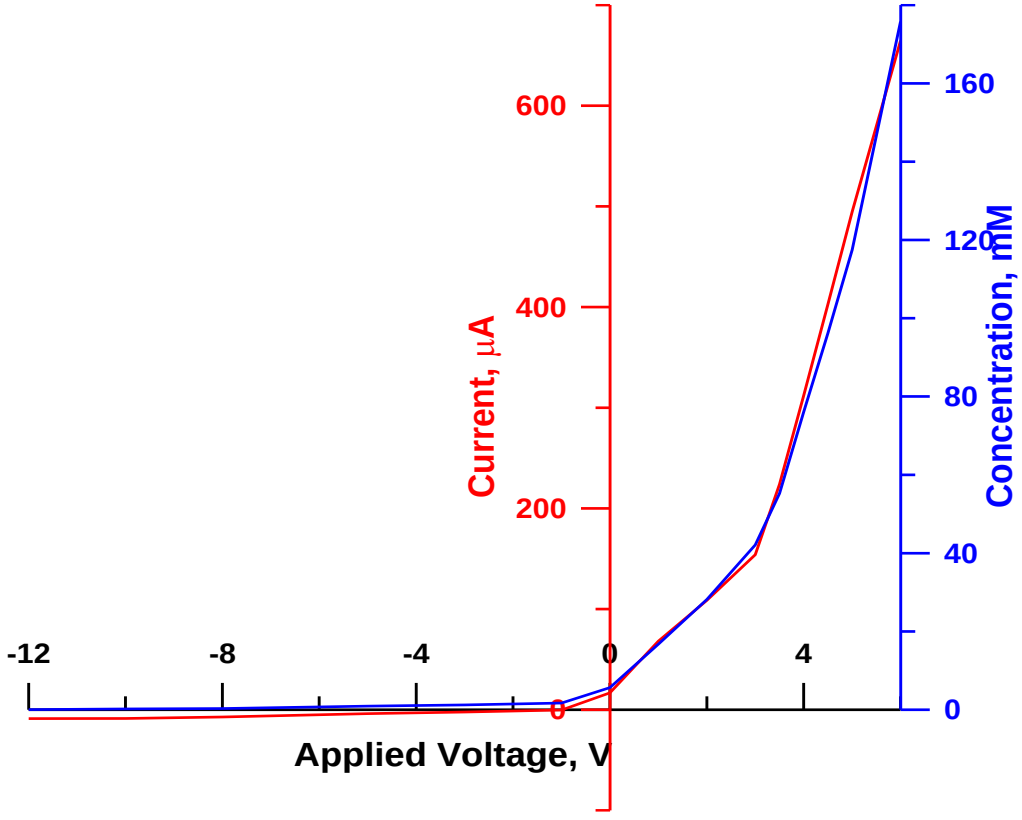

Figure 2- 28 Current-voltage-concentration (i-V-C) behavior of high-pressure bead-based EEG. 4 M KOH in both CEX bead and AEX bead

compartments. Reprinted from reference [64] by permission from the American Chemical Society.

Applying reverse voltage produces a small reverse current with a much smaller slope than the forward i-V slope. A finite positive current flows at zero applied voltage (short circuit) and ~400 pmol/s KOH is generated. An applied voltage of – 1 V is necessary to attain a zero current, which produces ~100 pmol/s KOH. Further reduction in ZCP is possible by applying negative voltages of greater magnitude. these studies later proved to be critical to the invention of the charge detector described in section 10. The high-pressure dual-bead EEG of Figure 2-27 was tested with packed capillary columns (1400 psi @ 7 μL/min) in both isocratic and gradient modes with a hydroxide eluent. For most ions, retention time reproducibility was 0.3-1.5% under gradient elution conditions.

OTIC often requires very little pressure. Eluent generators for such systems can even be based on thin sheet membranes, with the configuration otherwise largely following that of Fig. 26. Both isocratic and gradient elution was demonstrated in OTIC with such low-pressure AEM-CEM EEGs, using a pressure of only 1.6 atm. Later, Yang et al. [65] demonstrated the utility of the dual-bead EEG to generate all three types of eluents: a salt, an acid and a base, depending on the feed electrolyte. Eluents containing KNO_3, MSA and HCO_3^-/CO_3^{2-} eluents were made by feeding 100-200 mM KNO_3, MSA and $NaHCO_3/Na_2CO_3$, respectively. The generation of KNO_3 and MSA are illustrated in Figure 2-29.

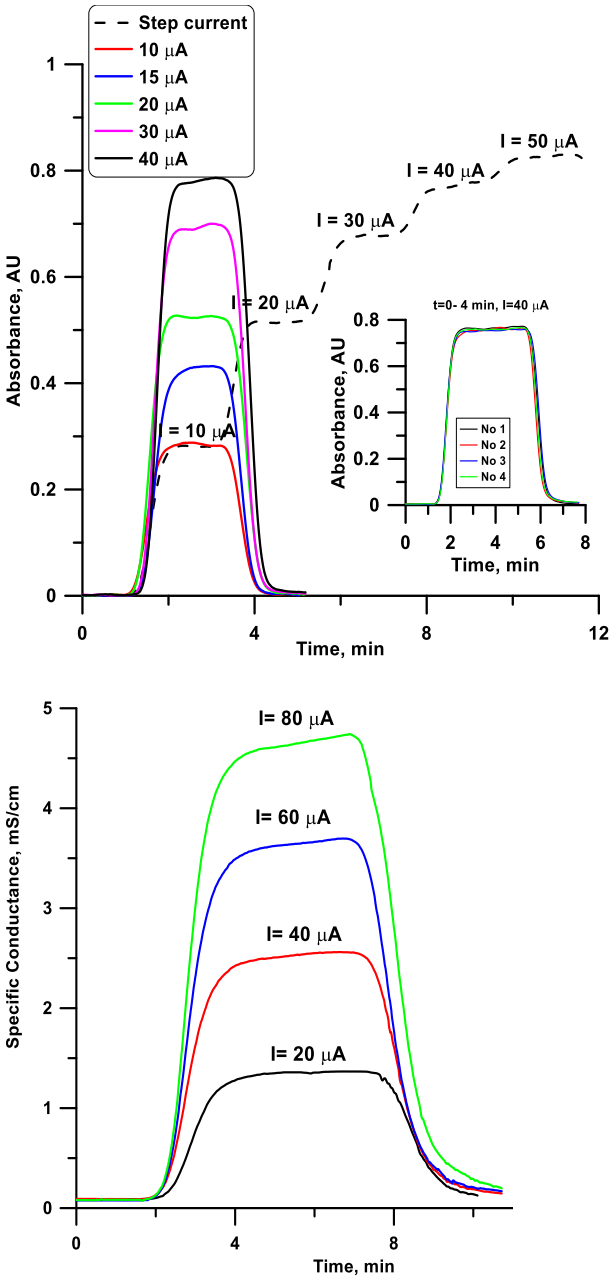

Figure 2- 29 Absorbance profile on the left side shows the KNO_3 generation results with different applied currents. Conductance profile on the right shows the MSA generation results with different applied currents. Reprinted from reference [65] by permission from Elsevier.com.

The same device was used to generate a HCO_3^-/CO_3^{2-} eluent gradient. A solution of 50 mM Na_2CO_3 + 50 mM $NaHCO_3$ was pumped to both electrode channels; a current of 20 μA was applied for the first 4 min and then the current was increased to 60 μA. Retention time standard deviation for fluoride and chloride was respectively 1.3% and 0.7%.

2.6.3.3. BPM Based Gas-Free EEGs

While either an AEM or a dialysis membrane *can* produce gas free eluent, neither is without problems. With an AEM as the barrier membrane on the cathode side, in close proximity to the cathode, reductive deamination of the quaternary ammonium functional groups in the membranes occurs. Although the process may be slow, and it takes a long time before the membrane is unusable, eluent purity is compromised. The use of a dialysis membrane is both current-inefficient and prone to the generation of hydrolytic decomposition products. Presence of impurities in the generated eluent do not permit attainable SPC values to be as low as those with type 1 eluent generators.

A superior approach to solve these problems were recently introduced by Lu et al. [66] where they used a BPM as the BM in the scheme of Figure 2-25 (see Figure 2-9 as to how water is split into H^+ and OH^- at the interface in a BPM). In the actual device shown in Figure 2-30 below, a stack of CEMs (sCEM) is used as the anode membrane, the BPM as the cathode membrane with another stack of CEMs atop it (primarily to provide structural strength and to reduce water transport). The device tolerated

pressures at least up to 21 MPa (3050 psi) generated high purity KOH (SPC 280 nS/cm) up to 100 μeq/min. The authors then followed this up with a methanesulfonic acid generator built along the same principles [67].

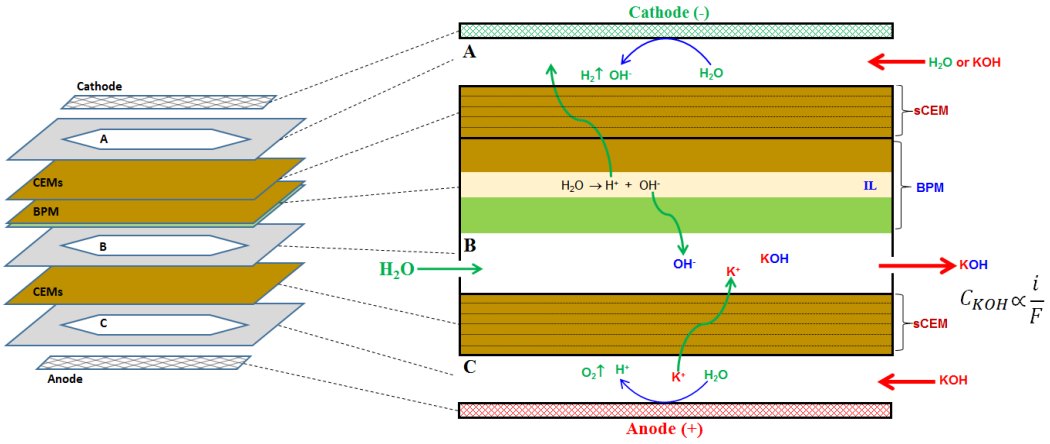

Figure 2- 30 Gas-free high-pressure high purity KOH generator based on a bipolar membrane. Reprinted from reference [66] by permission from the American Chemical Society.

2.7. Eluent Cleanup

The purity of an electrodialytically generated hydroxide eluent is primarily governed by the purity of the input water pumped in as the eluent counterion recipient. If the water contains dissolved CO_2 (this is difficult to avoid if the system is not integrally connected with a freshly deionized water source), it will be converted to carbonate when a hydroxide eluent is produced. To remove any non-hydroxide anions, present in the generated eluent, a secondary purifier called a continuously regenerated anion trap column (CR-ATC) is often used after the eluent generator. The CR-ATC is basically an anion exchange resin bed containing a cathode that is

separated by an AEM from a flowing water receptor (suppressor waste effluent is often used) containing the anode (Figure 2-31)[16]. The impurity anions (as well as some hydroxide ions) are removed by the electrical field to the anode compartment, and fresh electrogenerated hydroxide at the cathode take their place.

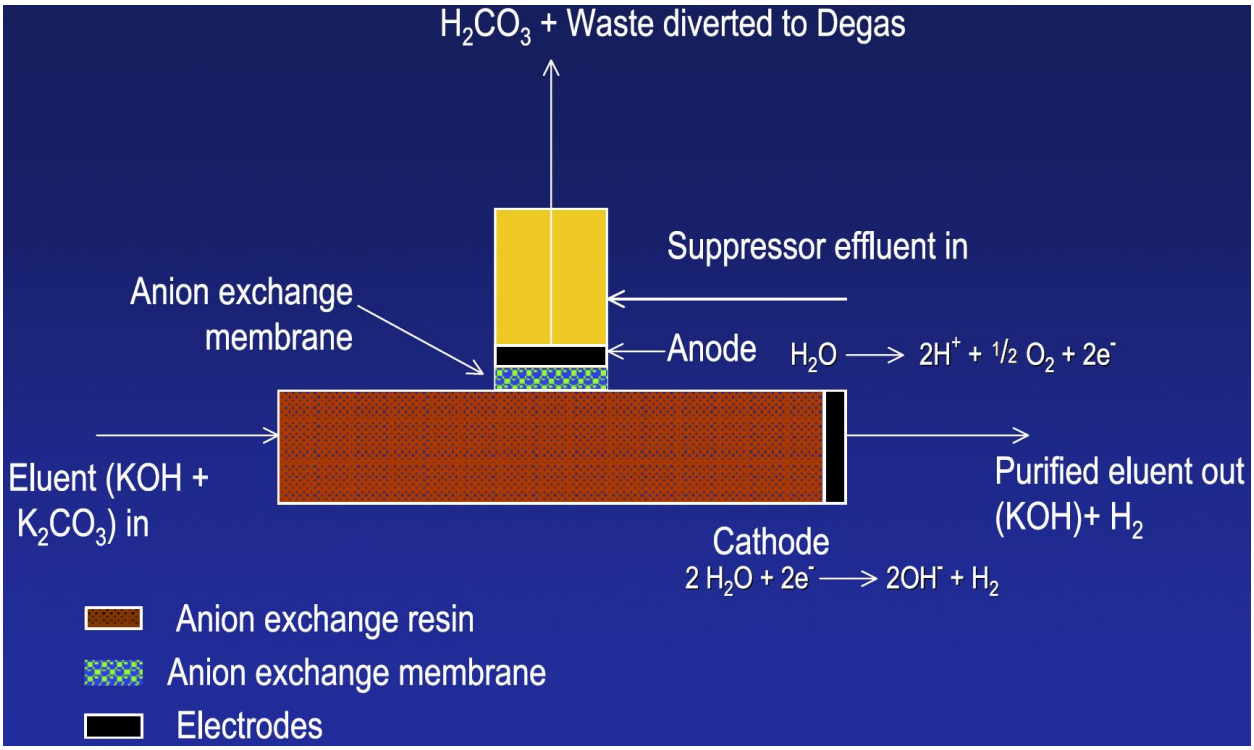

Figure 2- 31 A continuously regenerated anion trap column (CR-ATC). The applied voltage removes any non-hydroxide anion though the AEM into the anode as waste and their place is taken by OH^- generated at the cathode. Reprinted from [16] by permission from Elsevier.com.

2.8. Eluent Generation Strategies to Create Multispecies Eluents

Ion chromatography made its commercial debut with a carbonate/bicarbonate eluent. It is still one of the most popular eluents

used. Except for AEX/CEX EEGs (the results of which are shown in Fig. 30), we have thus far only outlined EEGs that generate only a pure strong acid or a strong base. The design of the commercially available carbonate EEG also uses (a stack each, of) AEMs and CEMs but these are used in a sequential arrangement as shown in Figure 2-32 and not in the simultaneous arrangement as in Figure 2-27. A concentrated solution of K_2CO_3 is used as the common feed, KOH is generated first through the CEM-separated cathode compartment (some reflection will indicate difficulties likely to be encountered if H_2CO_3 were to be generated first) and this is the influent to the AEM-separated anode compartment where CO_3^{2-} is brought in an equivalent amount to make a K_2CO_3 effluent.

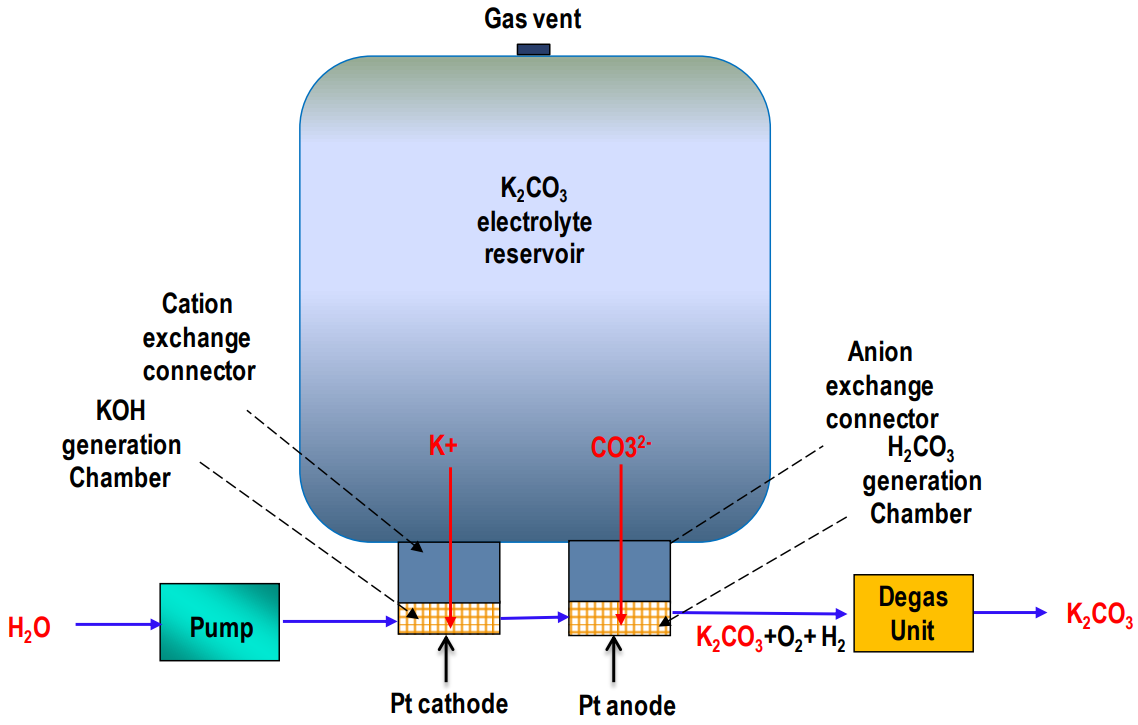

Figure 2- 32 Carbonate eluent generator schematic. See text for details. Courtesy Thermo Fisher Scientific.

Carbonate is most commonly used in conjunction with bicarbonate, however, and not alone by itself. For eluent use, one would like to generate carbonate eluents containing various concentrations of both carbonate and bicarbonate. This is accomplished by converting part of the K^+ into H^+: using the same strategy and principles as outlined in section 5.1, using a CEM-based suppressor to convert influent NaX into a NaX-HX buffer (Figure 2-15a). The only difference here is that this needs to be done here on the high-pressure side and hence carried out in a packed bed format with a stacked-CEM “cation exchange connector”. Although christened somewhat differently, the “electrolytic pH modifier” (Figure 2-33) commercially

marketed for this purpose is simply a high-pressure cation exchange suppressor, albeit with a limited suppression/ion exchange capacity.

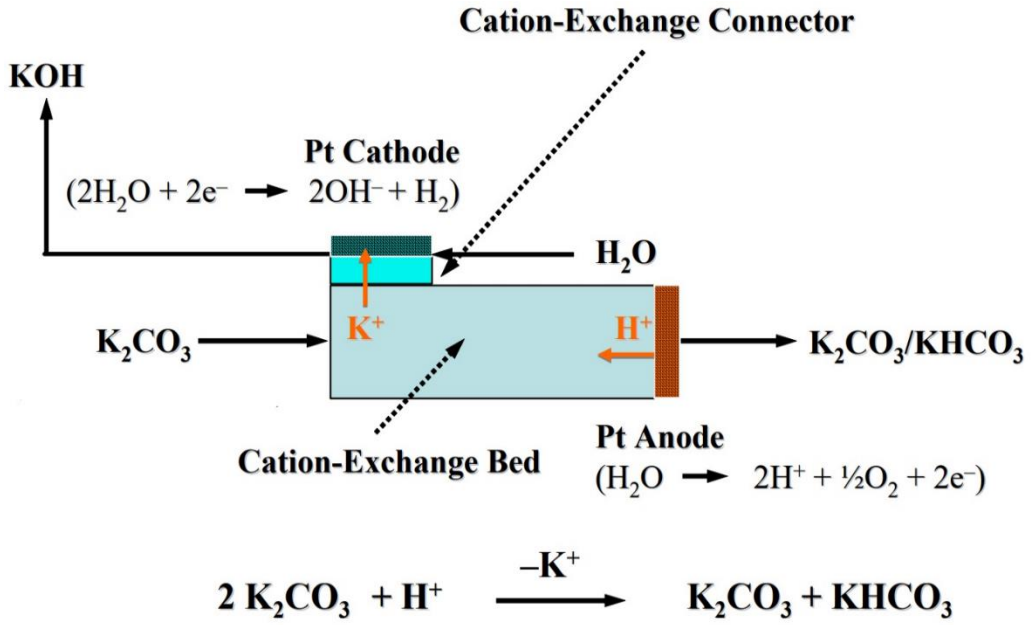

Figure 2- 33 **“**Electrolytic pH modifier” used to convert a carbonate eluent to a carbonate-bicarbonate eluent. See text for details. Courtesy Thermo Fisher Scientific.

More recently Shelor et al. [68] have described a different approach for generating carbonate-bicarbonate eluents. In this approach, a KOH EEG is used. The generated KOH is delivered to a “CO_2 Engasser” where variable amounts of gaseous CO_2 can be introduced. As shown in Figure 2-34, the use of a 10-port valve allows bypassing the KOH EEG to produce pure carbonic acid in several hundred mM concentration if desired – the system can therefore generate eluents of composition anywhere between pure KOH to pure H_2CO_3 with all possible compositions of K_2CO_3 and $KHCO_3$ in-

between. These authors have recently shown pure carbonic acid to be a useful eluent in cation chromatography [69].

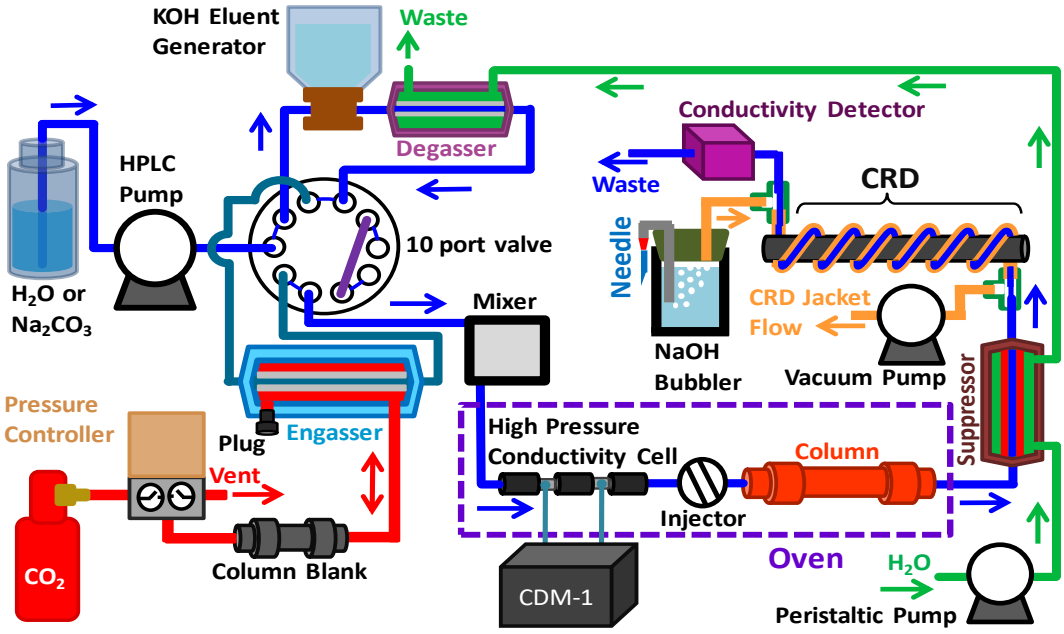

Figure 2- 34 A carbonate-bicarbonate eluent generator based on a KOH EEG and a "CO_2 Engasser". This arrangement can produce eluents ranging in composition from pure KOH to pure H_2CO_3 and those with all intermediate alkalinities. Reprinted from reference [68] by permission from the American Chemical Society.

The analysis of amino acids, peptides and various carbohydrates have often used an eluent gradient that starts with pure hydroxide and eventually ends in addition of some anion of weak eluting power such as acetate. For electrodialytic generation, a strong acid anion of weak eluting power will be preferred. Methanesulfonate (MSA^-) is a convenient choice.

Chen et al [70] have recently described a serial HMSA and KOH EEG that generates the desired gradient from KOH to KOH + KMSA (Figure 2-35).

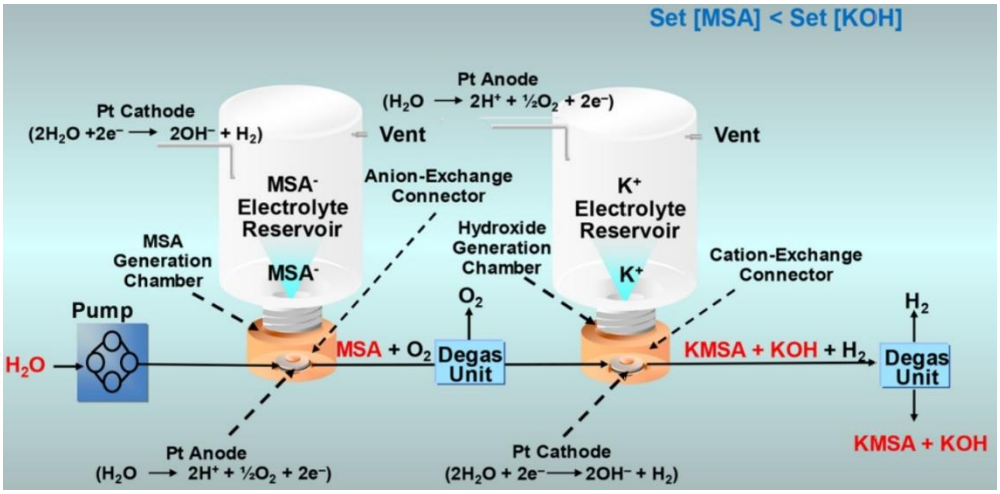

Figure 2- 35 Electrodialytic generation of KOH and KOH+KMSA gradients. Reprinted from reference [70] by permission from the American Chemical Society.

2.9. Combined Electrodialytic Eluent Generation and Electrodialytic Suppression

Most present-day well-equipped ICs routinely use both electrodialytic eluent generation and suppression. In 1991, Strong et al. [34] were the first to demonstrate the power of such a combination. The background SPC was ~300-400 nS/cm independent of the eluent concentration, permitting excellent gradient operation. Such a suppressed IC system provided good linearity and reproducible retention. Strong acid anions could be quantitated over a wide range of concentration, from 0.03 to 100 µM. For the first time it permitted the simplicity of electrodialytically generated eluent gradient IC

along with water-regenerant electrodialytic eluent suppression, a practice that is considered routine today.

We have mostly focused here on the generation of hydroxide eluents (EEGs that produce LiOH, NaOH and KOH are commercially available). The KOH generator is the most commonly used because K^+ has the highest mobility of the alkali metals listed above and thus leads to the lowest voltage drop and least Joule heating across the generator membrane. The greater mobility of K^+ also allows more facile removal in an electrodialytic suppressor, allowing the largest eluent concentration to be suppressed. As outlined in the previous section, K_2CO_3 generators are also available. The present practice for cation chromatography typically uses a strong acid eluent like HMSA using a relatively concentrated solution of it in a reservoir that functions as the cathode chamber. Methanesulfonate is electrodialytically drawn through a stack of AEMs into a flowing water stream containing the anode to generate MSA^-. An electrodialytic suppressor based on two AEMs in a planar configuration then completes the system. A gas-free BPM-based version of the generator has also been introduced [67].

2.10. The Charge Detector

While conductometry has been the principal detection method in IC, “Charge Detection” is a more recently introduced concept that has some unusual merits [71]. A charge detector (ChD) has a configuration identical to the AEM/CEM deionizer (Figure 2-18) or the two-bead AEX/CEX EEG

(Figure 2-27 but with the CEM side held negative). The stream of interest flows between the ion exchangers, while a DC electric field is applied between the distal sides of the two oppositely charged ion exchangers with the electrode polarities the same as that in a deionizing application.

2.10.1. A Charge Detector Is to an EEG What a Light Emitting Diode (LED) Is to a Photodiode

Consider that in an EEG, at least one of the electrode compartments contains an electrolyte and the applied voltage polarity necessarily holds the CEX side positive with respect to the AEX side. If KOH, $NaNO_3$ or CH_3SO_3H is to be generated, the CEX compartment must respectively be a source for K^+, Na^+ and H^+ (the last can be generated from water, as well as from an acid) and the AEX compartment must respectively be a source for OH^- (this can be generated from water, as well as from a base), NO_3^- and $CH_3SO_3^-$. Current is carried by the cation through the CEX and the anion through the AEX to respectively form a base, salt, or acid, in the central channel. Consider now the behavior of a forward-biased LED where holes and electrons are brought forward from the p-doped and n-doped side, respectively. The two then combine to form a photon that proceeds from the junction. The current controls the number of photons (in an EEG the number of molecules of the chemical) thus generated. In an LED, the wavelength of the emitted photon can be changed by changing the semiconductor and hence its band gap. In an EEG, the source ions are changed to make a different product in the central channel. Although we are accustomed to

thinking in terms of salt acid or base generators, an array of EEGs will be ideally suited to generate a combinatorial array of ionic liquids given the choice of appropriate membranes and working media.

Both the EEG and the charge detector represent ionic diodes. Much as in an LED, the diode in an EEG is forward biased; current flows and controls the photon/ion flux. In a charge detector, the diode is reverse-biased (as a photodiode often is): the AEX compartment is held positive with respect to the CEX compartment. These outer compartments may contain water or a compatible dilute electrolyte. Through the central channel, normally just water flows with occasional appearance of the ionic analyte.

To complete the analogy of an EEG/ChD behaving akin to a LED/photodiode, a ChD behaves as a reverse-biased photodiode (PD). In a reverse-biased PD, the applied voltage causes the junction to be depleted of current-carriers, resulting in a very low background current. When photons falling on the junction generate hole-electron pairs, the holes and electrons respectively rush through the p-doped and n-doped semiconductors to the negative and positive electrodes, resulting in the measured photocurrent. All photons that have an energy greater than the band gap of the semiconductor produce the same response. In a ChD, the normal background is that of water, with very low ionic content. The meagre level of H^+ and OH^- in the central channel proceeding respectively through the CEX and AEX membrane results in a relatively low background current.

But when analyte ions enter the zone, cations and anions proceed respectively through CEX and AEX membrane to the electrodes, resulting in a current pulse. Unlike a CD where the response depends on the mobility of the ion (H^+ produces ~5x the response of the same concentration of Na^+), the ChD responds to the total charge the analyte represents and not its mobility – the same amount of H^+ and Na^+ produces the same peak area. It behaves as a pseudocoulometer, effectively acting as a deionizer.

2.10.2. Behavior of the Charge Detector

The fact that the ChD acts as a deionizer gives the ChD an edge over a CD for the detection of weakly dissociated species. While both can only respond to the part of the analyte that is ionized, in the case of a ChD, removal of the ionized part causes the undissociated part to continue to ionize and thus increases the signal beyond what it would otherwise be. As a result, the ChD response for a poorly dissociated analyte is also dependent on the residence time of the analyte in the detector, related inversely to the flow rate. Although it has not yet been explicitly studied, the degree of increase in response with decreasing flow rate is dependent on the rate of dissociation of the analyte and hence its dissociation constant.

Yang et al. [71] introduced the ChD and described several device designs, both IEX resin bead based (hereinafter ChD-B) and IEMs (hereinafter ChD-M). The ChD-B device (internal volume 3 µL) was identical to the EEG in Figure 2-27 except for opposite polarity of the applied voltage.

The response of the ChD-B device to the equivalent amounts of $NaNO_3$, KCl, HNO_3, K_2SO_4, $BaCl_2$ or K_3PO_4 is shown in Figure 2-36.

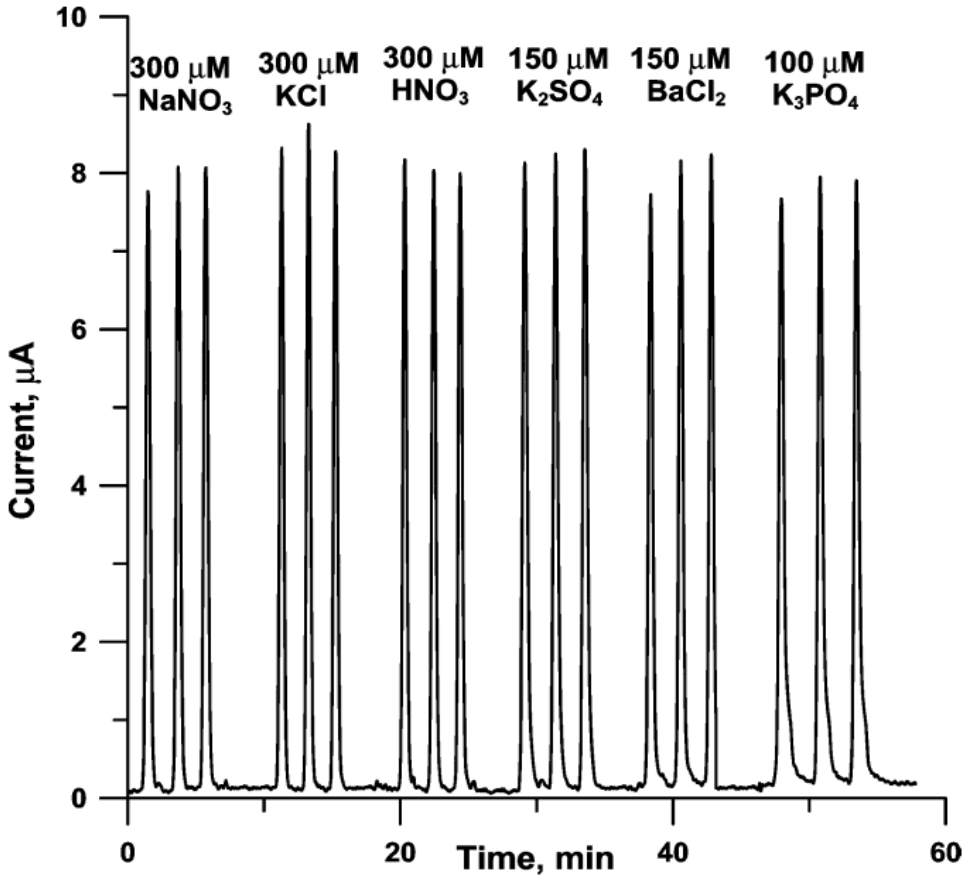

Figure 2- 36 Responses of ChD-B device to 1 μL of different injected analytes of the indicated concentration. Reprinted from reference [71] by permission from the American Chemical Society.

The peak areas are the coulombic signals of the analytes (194 $\pm$ 16 μC) and are the same for all. In conductometry, they will behave very differently: HNO_3 produces 3.5 times the signal of $NaNO_3$. Low concentrations of PO_4^{3-} is not present as such but as HPO_4^{2-} but the production of the latter from PO_4^{3-} by hydrolysis has produced a

corresponding amount of OH^-; together these lead to equal signals in charge detection.

The ChD-M devices were built in two forms: in one the electrodes were in contact with the IEMs to reduce the voltage drop in the exterior compartments and in the other the electrodes were separated by an ion exchange screen. Each of these devices were fabricated in two sizes, with internal volumes of 35 and 125 μL, respectively. The electrode-in-contact design, which generally produced better S/N (and exhibited no performance difference if the electrode compartments were filled with pure water or electrolytes: acid on the CEM side, alkali on the AEM side) is shown in Figure 2-37. The ChD-M data discussed here are from the smaller volume device.

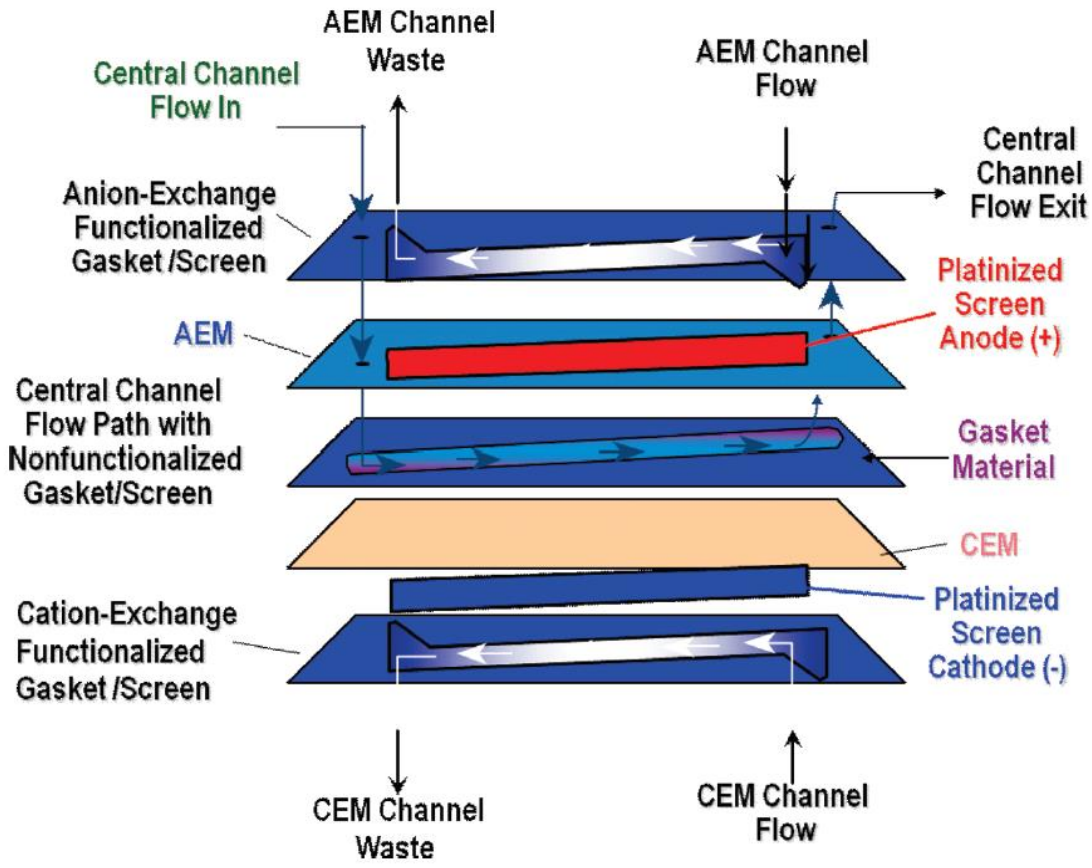

Figure 2- 37 Membrane-based charge detector device with adjacent electrodes. Reprinted from reference [71] by permission from American Chemical Society.

Figure 2-38 shows the superimposed responses of a CD and a ChD-M placed sequentially after in a chromatography system, the sample being 1 μM each of F^-, Cl^-, NO_2^-, CO_3^{2-}, SO_4^{2-} and NO_3^-. Even this “smaller area” ChD-M had an internal volume greater than a typical CD, suggesting further improvements could be made to reduce dispersion. Indeed, the commercial version of the charge detector was introduced with an even smaller internal volume. [72]

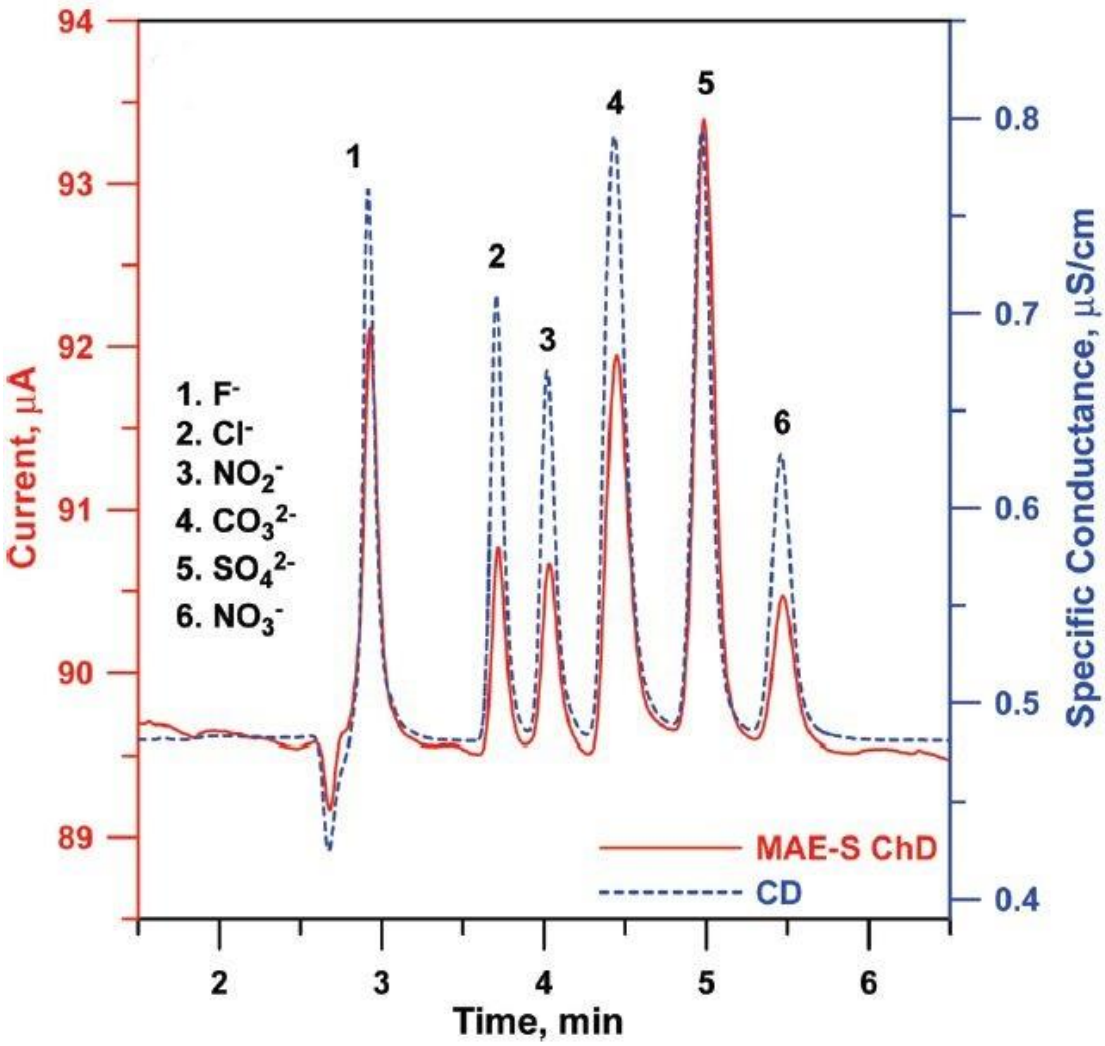

Figure 2- 38 Comparison of conductivity detector and membrane-based charge detector (adjacent electrodes, smaller membrane). Reprinted from reference [71] by permission from the American Chemical Society.

A peak area-based comparison of CD and ChD calibrations for chloride, nitrate and acetate over a 1-25 μM range confirms that the ChD provides statistically identical responses for all three analytes while the CD responses differ between analytes and the differences increase with increasing concentration.

2.10.2.1. A Deeper Look at Charge Detector Operation

The simplistic view of an analyte ions simply carrying their charges to the electrode in a ChD is not accurate. Indeed, if one looks at the electrode compartment effluents, at typical low analyte concentrations, practically no analyte can be detected in the electrode compartment effluent. The capacity of the IEMs (and IEX screens, if used) are so large relative to the analyte amounts injected what goes to the electrodes are the H^+ or OH^- displaced by the analytes from the CEM/AEM respectively. The analyte ions are displaced only very slowly over time by H^+ and OH^- from water dissociation, which is promoted by an electric field, especially at IEM surfaces. The field-induced dissociation of water is much more pronounced at the AEM compared to the CEM surface [73] (the AEM is typically more resistive than a CEM; in a series arrangement, more voltage is also dropped across the AEM than the CEM, leading to a greater electric field across the AEM). The ChD background response comes from the H^+ and OH^- in the background; it can be readily calculated that the background current is much higher than that can be accounted for by H^+ and OH^- concentrations originally present in the influent water flowing through the ChD. The necessary current to remove 10^{-7} M each of H^+ and OH^- with an input flow of 200 μL/min (3.3 μL/s) is only ~30 nA, the actual current observed at almost any applied voltage over 1 V is much higher (of course, water will continue to dissociate as H^+ and OH^- originally present are removed). The field-induced production of H^+ and OH^- affects not only the background

current but the response from a given analyte as well. The applied voltage is distributed across the two IEMs and the central channel. Under background conditions, the central channel contains highly resistive water; as such, the voltage is mostly dropped across the central channel and the field-induced ionization of water at the membrane surfaces is minimized. At constant applied voltage, when a conductive analyte enters the central channel, the potential redistribution applies more voltage across the IEMs, resulting in greater field-induced water dissociation at the IEMs. The overall ChD current response thus comes both from the injected ionic analytes displacing H^+ and OH^- from the corresponding IEMs and their transport to the oppositely charged electrodes as well as the transport of the field-generated H^+ and OH^- at the membranes. When the latter becomes significant, as at higher applied voltages, a superfaradaic response is possible. Increasing the applied voltage increases the field induced dissociation and hence the superfaradaic response, and generally increases the signal to noise ratio (SNR), but up to a certain point. Past a voltage where significant water electrolysis begins at the electrodes (2.5 - 3 V), noise increases greatly, degrading SNR.

2.10.3. A Constant Current ChD

Mori et al. [74] operated a ChD-M device in the constant current mode. In this configuration, the voltage needed to maintain a small constant current is measured; the voltage decreases as the analyte passes through. The constant current charge detector (ChD_i) device used was similar to that

in Figure 2-39, except that the electrodes were separated from the IEMs by an IEX screen of the same type. They signal to noise ratio SNR in the constant current mode was compared with that obtained in the previously used constant voltage mode. The best SNR observed for 50 μM injected KNO_3 (1.3 nmol) was at i_{app} = 1 μA and this was 3.5-fold better than constant voltage operation on the same device (however, with smaller membrane areas, constant voltage operation provides better SNR than the constant current mode). In the ChD_i mode, although the best SNR was observed for $i_{app} \approx$ 1 μA, the SNR was not markedly different for i_{app} in the 0.5 - 20 μA range. In contrast, in the constant voltage mode, there as a pronounced maximum in the SNR near an applied voltage of 2 V. The same amount of each of $NaNO_3$, HNO_3 and $NaClO_4$ were injected into the ChD_i system. As Figure 2-39 shows, although there are considerable differences between the ionic mobilities of the different ions and the affinities of the different ions for the relevant IEMs vary markedly, the ChD_i responses to these analytes are statistically identical.

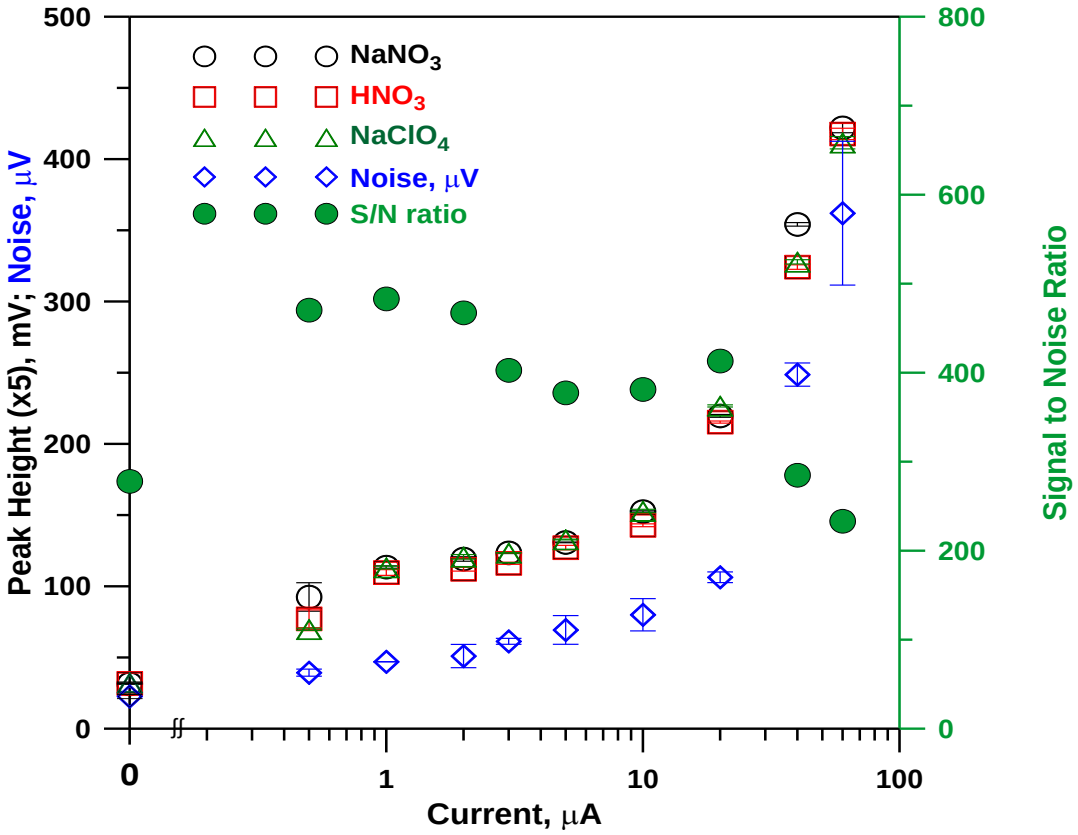

Figure 2- 39 Peak height and noise as a function of applied current. Central channel: water at 0.2 mL/min; outer channels: water at 1.5 mL/min; injected sample: 1.32 nmol of $NaNO_3$, $NaClO_4$, HNO_3 (50 μM concentration). The abscissa is in log scale for clearer depiction of low-current results. The axis is broken before the origin to show i_{app} = 0 results. The SNR values are shown only for $NaNO_3$ (solid green symbols, right ordinate); the data for the other two analytes are very similar. Reprinted from reference [74] by permission from Elsevier.com.

Both residence time (t_R) and i_{app} affect transmembrane analyte transfer. The effect of changing t_R from 4.2 – 35 s was tested at a constant

i_{app} = 25 μA by changing the central channel flowrate. For the same amount of HNO_3, KNO_3, HOAc and $B(OH)_3$ (1.3 neq), the maximum removal achieved was 75%, for HNO_3, for $t_R \geq 20$ s. Both actual ion concentration and ion mobility affect the rate of removal. The total coulombs come from analytes as well as the H^+ and OH^- due to water dissociation. As a result, the area signal does not reflect the contribution of the analytes alone. Both for a ChD operated at constant voltage or the ChD_i, responses increase with increasing t_R and in both cases weak acid responses are much more affected by the residence time than those from strong acids. For strong electrolytes like HNO_3 or KNO_3 and even a moderately weak electrolyte like HOAc, the ChD_i signal increases linearly with residence time. However, for a very weak electrolyte like $B(OH)_3$, the peak area increases exponentially with t_R, either in the constant voltage or current mode.

The electrode reservoir composition does affect the voltage drop across the membrane as well as the SNR. Different solution compositions in the CEM/AEM reservoirs were studied: e.g., water/water (w/w), 1 mM HNO_3 /1 mM KOH (a/b), a/w and w/b. Figure 2-40 shows the results.

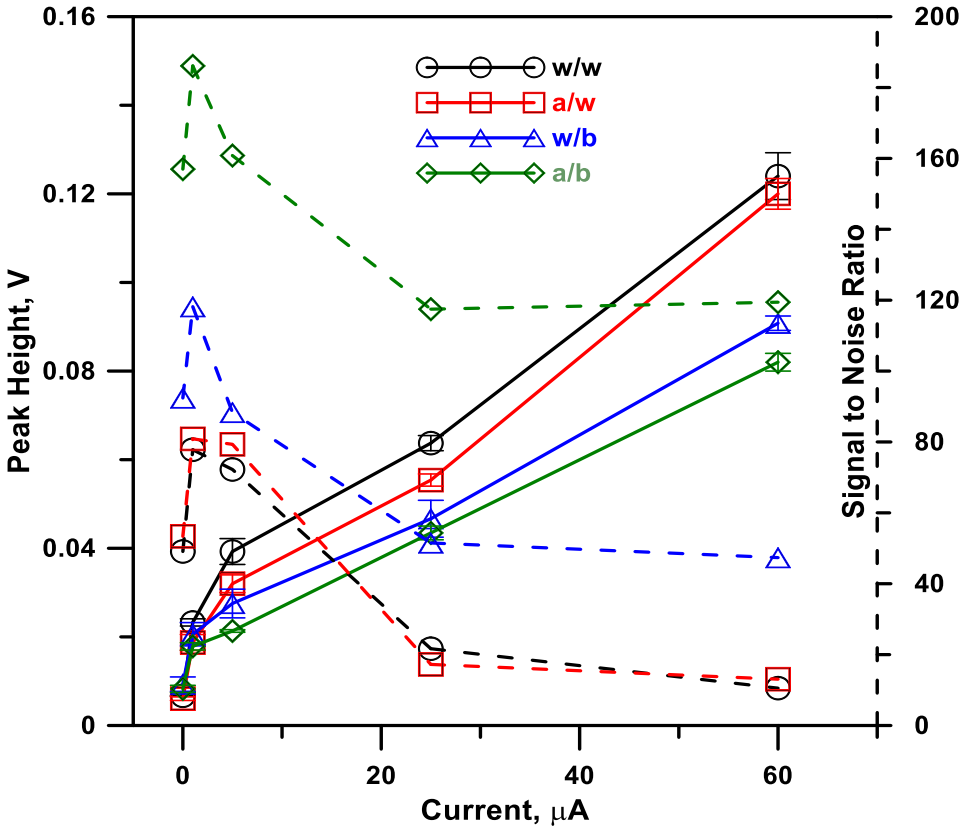

Figure 2- 40 ChD_i peak height (solid lines) and SNR (dashed lines, right ordinate) as a function of current with different electrolyte compositions in the outer channels. Central channel: water at 0.2 mL/min; outer compartment (CEM/AEM) composition: w/w, a/w, w/b and a/b (see text). Outer channel flows are 1.5 mL/min respectively; injected sample: 50 μM KNO_3. Reprinted from reference [74] by permission from Elsevier.com.

As shown in Figure 2-40, the magnitude of the signal and the SNR are not concordant. The highest signals are mostly observed with a/b, but the best SNR is observed with w/w. there is very little difference in either signal magnitude or SNR between w/w or a/w conditions but putting a base

in the AEM compartment increases the signal but increases the noise even more, lowering the SNR.

The dependence of the signal on the nature of the analyte was complex. Bases, whether strong or weak (KOH or NH_4OH for example) elicited a lot lower response than a strong electrolyte acid or salt (e.g., HNO_3 or KNO_3). In this case, analyte OH^- may be taking the place of field-generated OH^- at the AEM, underscoring the particular role of the AEM in the field-induced dissociation of water. Although the responses were not uniform across all electrolytes (especially the bases), all test electrolytes responded linearly and in general, linear calibration curves in ChD_i exhibited y-intercepts closer to zero than those from a CD (Figure 2-41).

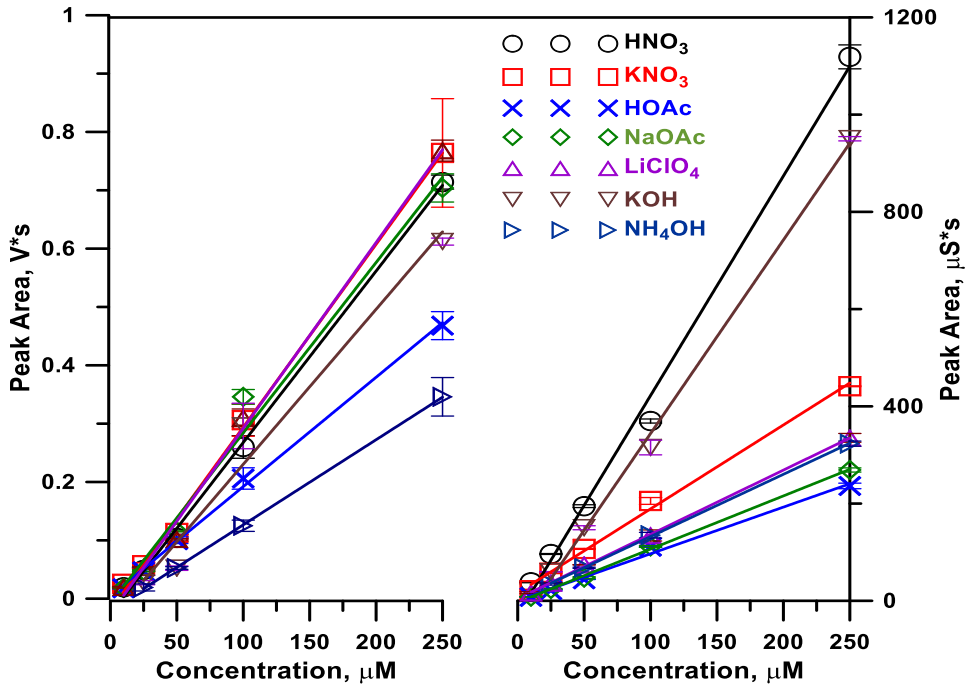

Figure 2- 41 Calibration curves for different electrolytes obtained with a ChD_i (i_{app} = 1 μA) (left) and a CD (right). Error bar indicates standard

deviation (n=3). Reprinted from reference [74] by permission from Elsevier.com.

2.10.4. An Integrated Suppressor-Charge Detector

More recently, Shen et al. [75] integrated a constant current ChD-M with a suppressor. Such an integrated device, dubbed a Sup-ChD, would be expected to reduce dead volume and thus lower dispersion and hence. The ingenious device consists of five stacked flow channels, separated by appropriate gasketed IEMS/screens. Figure 2-42 shows the detailed structure.

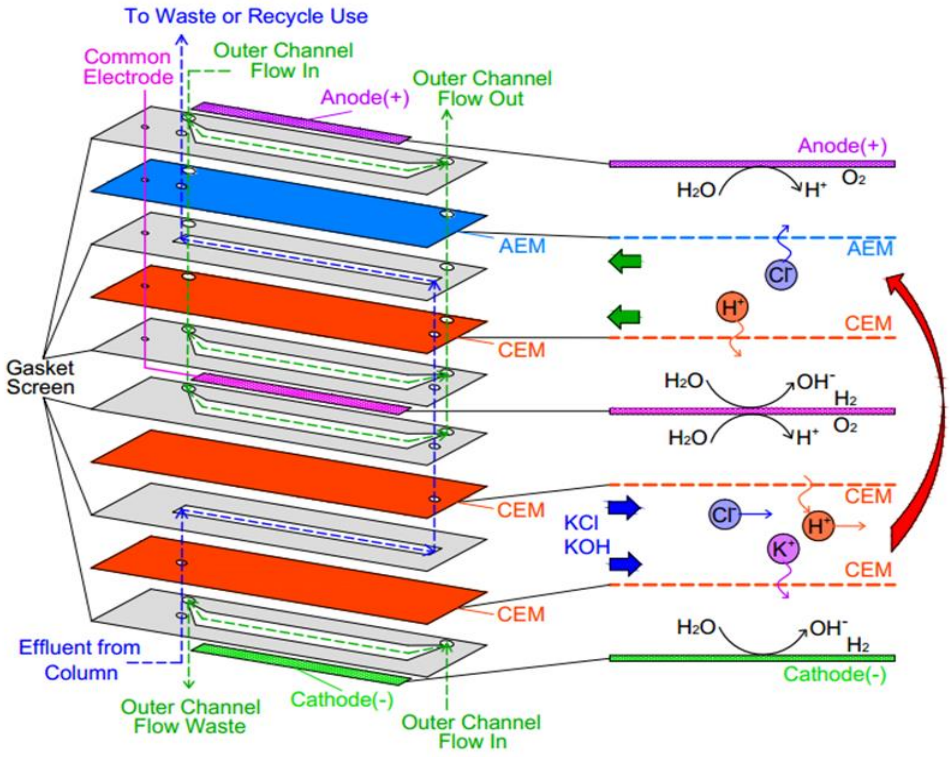

Figure 2- 42 Schematic of Sup-ChD. Reprinted from reference [75] by permission from Elsevier.com.

The three bottom channels constitute a standard double-CEM suppressor. This section has three channels which are separated by two CEMs. The ChD section has three channels which are isolated by an AEM and a CEM. There is one anode electrode at the AEM side of the ChD and a cathode electrode at the CEM side of the suppressor with a common electrode in between which plays the role of the cathode for the ChD and the role of the anode for the suppressor. The Sup-ChD device could suppress up to 80 mM KOH @ 1 mL/min flowrate. The authors found the ChD_i mode to provide better SNR than the constant voltage mode, i_{app} = 6 µA was found to be the optimum. Figure 2-43 shows a comparison of the

Sup-ChD output with that from a separate suppressor and a CD. Overall, the hope for less dispersion was not realized. At least the apparent peak widths in the ChD_i trace in Figure 2-43 can be seen to be larger than a conventional suppressor connected by tubing to a conventional CD. The rate of the removal of ions and hence the peak width is a function of the field strength in a ChD. The operational mode (constant current or voltage), the magnitude of the applied voltage, ChD membrane thickness etc. all may need to be optimized for the detector to least affect the peak width and this optimum may not represent an optimum in the SNR.

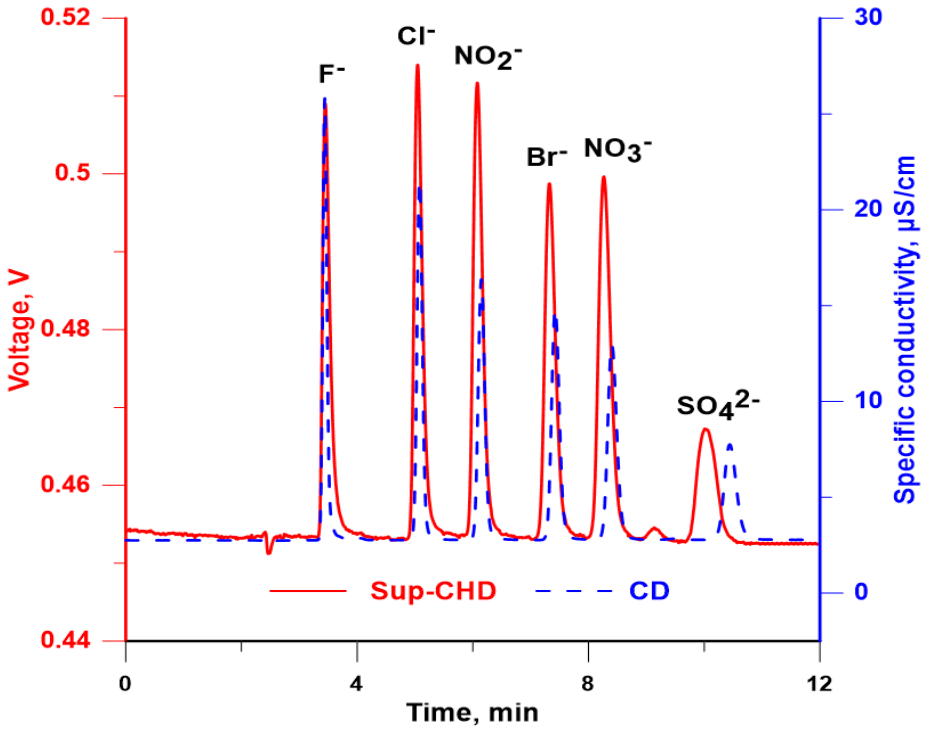

Figure 2- 43 Comparison of chromatograms of injected analytes : 300 µM fluoride, chloride, nitrite, bromide, nitrate; 100 µM sulfate; eluent: 12 mM KOH; flowrate 1.0 mL/min; injection volume: 10.8 µL; column: Dionex

AS20 (4 mm × 250 mm); 30 °C; suppressor current 30 mA; 6 μA applied to ChD. The peak at ~9.5 min is from carbonate, the enhanced sensitivity of the ChD to weak acids allow visualization of this trace contaminant. Reprinted from Reference [77] by permission from Elsevier.com.

2.11. Matrix Isolation and Charge Type Sorting with IEMs

In the deionizer of Figure 2-18, sorting of the sample ions based takes place based on their charge type. The anions end up in the anode compartment and the cations in the cathode compartment while neutrals (along with any particulate matter) exit in the central channel effluent. Collecting the cathode or anode effluent and sending them to cation/anion chromatographs will thus constitute matrix isolation; depending on the relative flow rates of the central vs the peripheral channels, this may also represent some preconcentration.

Although this picture may hold for a deionizer continuously removing a significant flux of ions, as outlined in section 10.2, this does not hold for a charge detector, where analyte ions appear on a transient basis and as they move under the electric field, are basically captured by the oppositely charged IEMs and released only slowly. Sorting ions based on charge in this manner cannot therefore involve passage through an IEM of any significant capacity.

There are other problems in realizing this in a practical manner even if passage through an IEM was rapid. These arise from electrochemical processes the analytes may undergo at the electrode. Even when the analyte is electrochemically inert, chloride is omnipresent and will be converted to chlorine at the anode, which will then attack essentially all system components, at the very least, the AEM. In any case, reproducible volumetric delivery or collection of electrode chamber effluents is a tall order

in the presence of large amounts of electrolytic gases. Through a series of papers, Ohira, Toda and their students have solved these problems and applied these devices in a variety of settings. The first paper [76] explores a number of designs. The simplest was the benchmark control: an annular tubular geometry utilizing a dialysis hollow fiber in a stainless-steel jacket (functioning as the negative electrode) with a Pt wire running through the center and functioning as the anode. If the flow rates were sufficiently slow, even without applied voltage, close to normal dialysis equilibrium (acceptor attaining the same concentration as the donor at the exit) was reached. With 3.5 V applied, the theoretical transfer equilibrium (electrophoretic transfer rate to acceptor equaling diffusive transfer back to donor) was reached with only 5.4 s residence time. However, as previously stated, this benchmark arrangement has problems from electrolytic gases and redox processes at the electrodes.

If only one type of ion is of interest, three flow channels (called a three-layer or 3L device by the authors) are sufficient (Figure 2-44a). This device was used for illustrating the isolation of oxidatively stable cations from a sample, the further requirement being that at the concentrations of interest the analyte cations (e.g., alkali metals and most alkaline earths) form a soluble hydroxide.

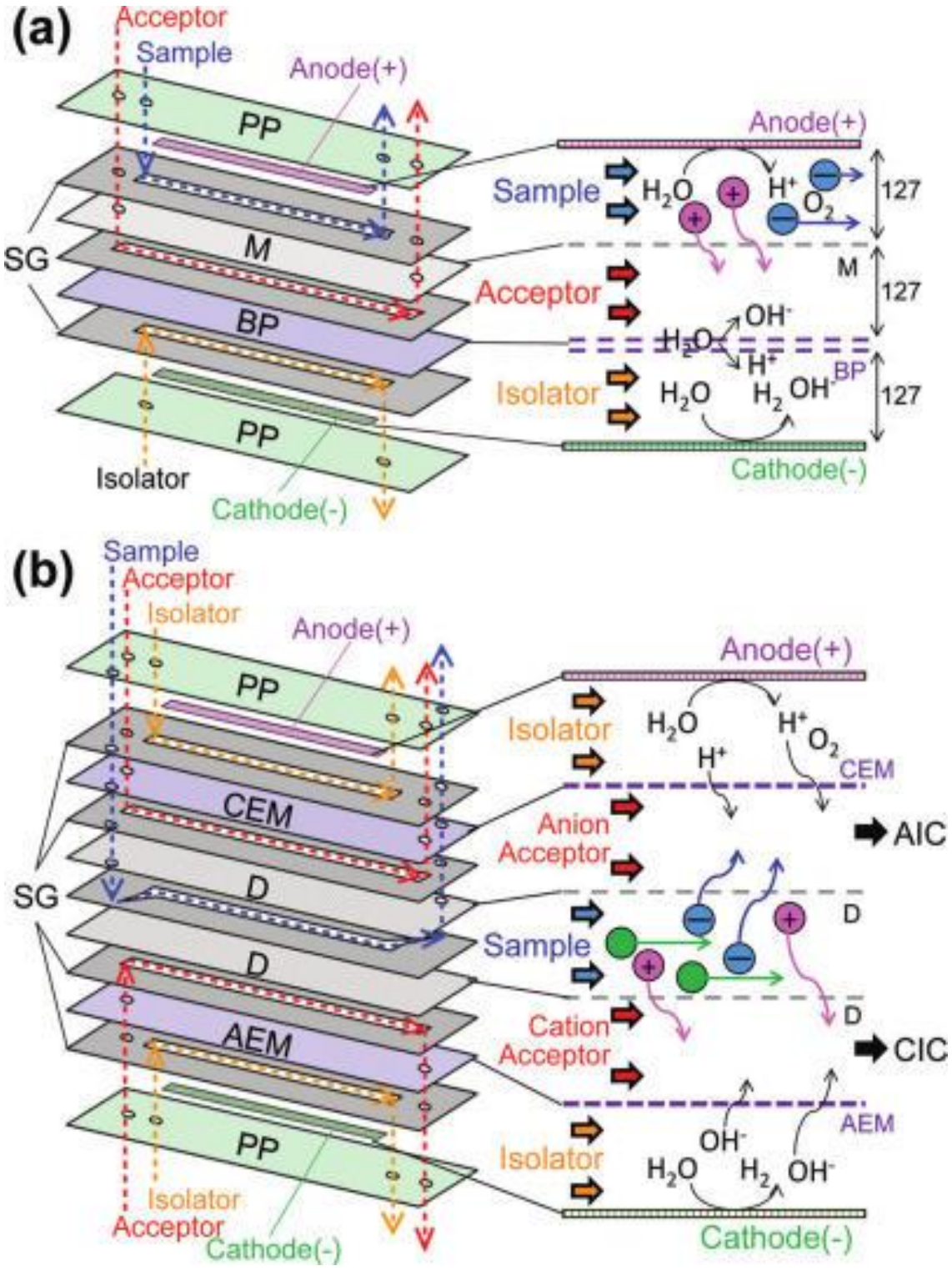

Figure 2- 44 (a) Three-layer device for cation isolation. PP: plastic plates, M: Ion transfer membrane, BP: Bipolar membrane, SG: gasketed screen

for improving mass transfer. (b) Five-layer device for both cation and anion isolation. D connotes dialysis membranes; all other abbreviations as previously used. Reprinted from reference [76] by permission from the American Chemical Society.

In the 3L (active length 80 mm) device, built much like a planar suppressor but intended for cation isolation, the sample is directly introduced into the anode chamber. The sample cations migrate across a dialysis membrane M (molecular weight cutoff 8 kDa, both higher and lower cutoff membranes were tried but this was optimum) but then cannot go across the bipolar membrane BPM whose AEM side is facing inwards towards membrane M. The isolator stream in contact with the cathode can simply be water and when sufficient voltage is applied across the device, water dissociates at the BPM interface allowing the analyte hydroxide to form in the central acceptor channel. The device was set up such that the acceptor effluent directly loaded the loop of a cation chromatography system.

The majority of the work utilized, however, a five-layer (5L) device built with 40-and 120-mm active lengths, and capable of isolating both cations and anions. Referring to Fig. 44(b), the central channel is where the sample is initially introduced and is flanked by two dialysis membranes. The anions migrate up due to the electric field and form the corresponding acids in the anion acceptor channel (the effluent from which is analyzed by an anion chromatograph) and cannot proceed further up to the anode, which

is isolated by a CEM. Meanwhile the cations migrate down and form the corresponding hydroxides in the cation acceptor channel (the effluent from which is analyzed by a cation chromatograph) and cannot proceed further down to the cathode, isolated by an AEM. It would be apparent that a BPM, appropriately oriented, can be used in place of either the AEM or the CEM, much as an AEM could have been used instead of the BPM in the 3L device). However, the voltage drop across a physically thicker BPM is larger and it is more efficient to use a single IEM wherever possible.

In the 5L-120 device, 10/20 V was sufficient to drive more than 99% of the tested cations or anions (Li^+, Na^+, Ca^{2+}, $CH_3SO_3^-$, NO_3^-, SO_4^{2-}) from a sample flowing at 300 μL/min to the intended acceptor solution depending on whether individual IEMs or BPMs were used. Greater voltage is required if the input flow rate is increased. None of the sample cations/anions were found in the unintended acceptors. It is interesting to note that anions required higher voltages than the cations for comparable extent of transfer. This was traced to the cellulose acetate dialysis membranes exhibiting a residual negative charge at all but very acidic pH and additional voltage is required to overcome the Donnan barrier.

How do neutrals behave? Bovine serum albumin (66.5 kDa) was found to remain entirely in the central channel, it obviously cannot pass through a 8 kDa cutoff membrane. Smaller neutral molecules, e.g., dichloromethane, methyl isobutyl ketone, benzene and ethylbenzene, with diffusion coefficients in the same order as the ions studied, diffused to both

acceptor solutions equally in the 5L-40 device with 25 V applied. Under these conditions the test ions were quantitatively transferred to their respective acceptors, while the neutral transfers to each receiver amounted from 0.5 to 10% of the original amount depending on the analyte, as observed by HPLC-UV.

Transfer reproducibility of the six previously listed cation/anion analyte set was tested at concentration levels of 10, 100 and1000 μM of each analyte with the respective precision being 4.2-7.1, 1.3-3.8 and 1.8-3.3%, respectively in relative standard deviation (RSD).

Real samples, including 100-fold diluted urine and milk samples, and bottled water/spring water samples were analyzed after processing by a 5L-120 device. For comparison, urine and water samples were filtered (0.45 μm) and milk was treated three different ways: (a) with Na_2EDTA, for the analysis of calcium, phosphate, and chloride and (b) with HCl for protein precipitation, for all ions other than chloride and (c) filtered (0.45 μm). For water and urine, results for all ions were in excellent agreement between filtered and device-processed samples, except for chloride and bromide which were slightly lower in the filtered samples; it is known that these form anionic complexes that tend to adsorb on particles. In milk it is known that calcium can be bound to phosphate and be protein-bound, in a manner that the calcium is not present in ionic form. The calcium and phosphate results for the device-processed samples agreed well with those for the EDTA or acid-processed samples, and these were higher than just filtration as a

treatment. Results for all other ions were also in good agreement. Matrix isolation was also seen to have other benefits: Direct injection of a filtered bottled spring water sample was found to extend the water dip due to the elution of some poorly retained nonconductive species and this made accurate quantitation of fluoride difficult; this problem was not seen when the sample was processed by the present method.

Chromatographic determination of organic acids is widely performed, but the matrix often calls for lengthy and elaborate sample preparation prior to actual analysis. Matrix components, e.g., proteins, non-ionics, lipids etc. are typically removed by a combination of centrifugation/filtration and solid phase extraction (SPE). Applying the above approach to isolate the desired anions would seem attractive. However, carboxylic acid analytes, especially those of significant chain length, display relatively low mobility. Attempts to transfer them on the previous 5L-40 ion transfer device (ITD) proved to be very inefficient because of their low mobility, compounded by the residual negative charge on the regenerated cellulose dialysis membrane (ζ-potential -6.3±1.0 mV @ pH 9) that represented a barrier to anion transport. There was a substantial difference for voltages required for quantitative transfer for cations vs anions. For example, K^+ (mobility 7.6 $m^2s^{-1}V^{-1}$) and NO_3^- (mobility 7.4 $m^2s^{-1}V^{-1}$) have very similar electrophoretic characteristics but 15 V was required to transfer NO_3^- quantitatively from a solution of 100 μM KNO_3 flowing at 300 μL/min compared to 8 V for K^+. For two smaller carboxylate ions acetate and propionate, even at a lower flow rate of 0.1

mL/min and at the highest practical applied voltage of 25 V (Joule heating sets an upper limit to about 30 V) only ~80 and ~65% was transferred.

Ohira et al. [77] solved this problem by functionalizing the regenerated cellulose membrane with N,N-dimethylaminoethyl methacrylate until the ζ-potential was statistically zero (-0.5±0.8 mV). With this modification, even C6- carboxylic acids could be quantitatively transferred at 30 V (Figure 2-45). The complete analytical system for real samples (various wines, sake, salad dressing, etc.) is shown in Figure 2-46. This comprised of the ITD-based sample processing system, coupled to an ion exclusion chromatography-UV detection system. Sample pH effects were studied. The results were compared with the results of sample pretreatment with conventional SPE.

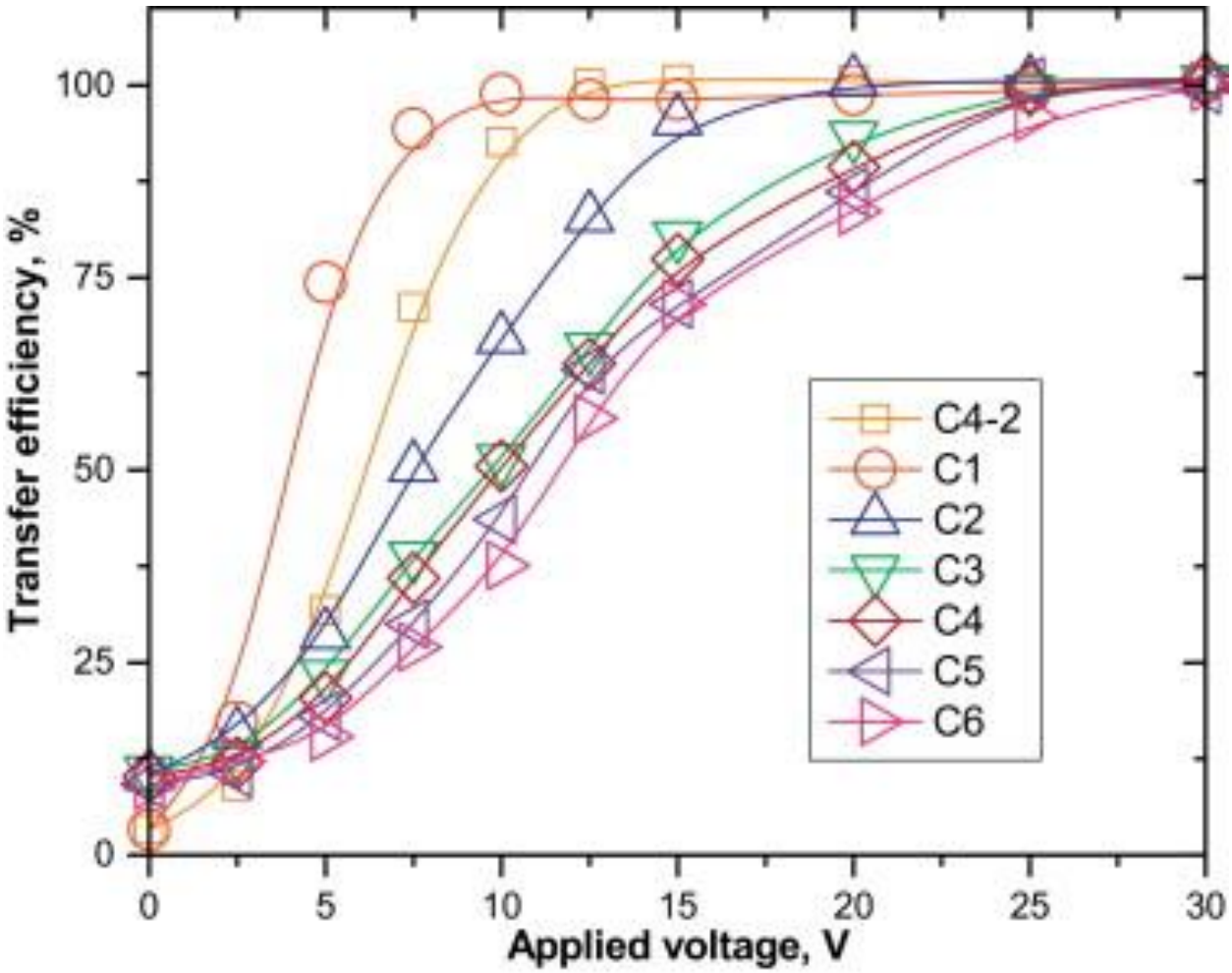

Figure 2- 45 Efficiency of a five-layer 40 mm long ITD with a near-zero zeta potential dialysis membrane for transferring anions as a function of applied voltage. Sample flow rate 0.1 mL/min, test anions: C1-C6 straight chain carboxylic acids, C4-2: succinic acid. Reprinted from reference [78] by permission from Elsevier.com.

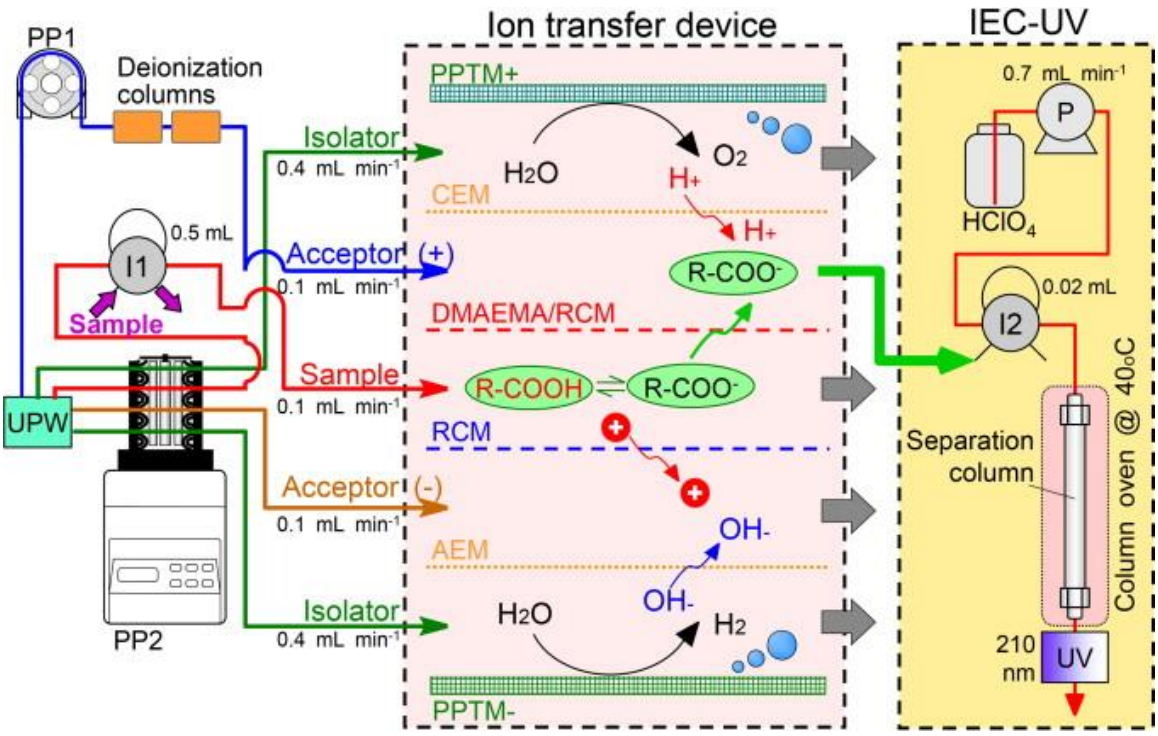

Figure 2- 46 Schematic of the flow diagram of sample pretreatment system with a 5-layer ITD; DMAEMA/RCM connotes dimethylaminoethyl methacrylate (modified) regenerated cellulose membrane. The electrodes used were platinum-plated titanium mesh (PPTM). Reprinted from reference [77] by permission from Elsevier.com.

For an acceptable degree of transfer of the analytes, a central channel flow rate of 0.10 mL min^{-1} and an applied voltage of 30 V were chosen for further work. Ion exclusion separation with UV absorbance detection at 210 nm permitted detection of the various carboxylic acids tested at the single digit µM level. The upper linear response limit ranged from 2 to 50 mM.

A study on the effect of the sample pH (adjusted to 1-8) on recovery revealed that the recovery is affected adversely only when the pH is ≤2.5. A comparison of the current ITD with a benchmark solid phase extraction (SPE)-based method was carried out for organic acids of interest. Recovery being defined as the ratio of the peak area of standard solutions with and without the ITD, the results are shown in Figure 2-47. For many analytes, there was a pronounced pH effect on the SPE method. Even though for a few analytes ITD recovery fell to as low as 75%, the extent of the recovery was highly reproducible.

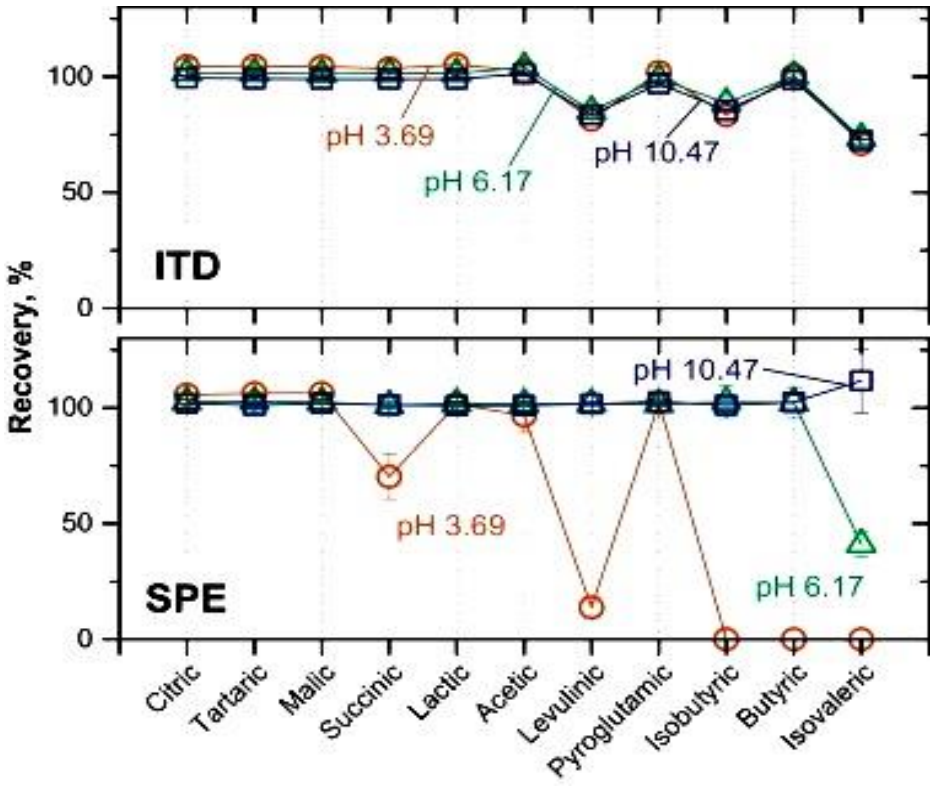

Figure 2- 47 Transfer efficiencies of the present and a benchmark method using a C18 SPE as a function of pH. The sample solution was a mixture of analytes (100 μM each). Solution pH was unadjusted (pH 3.69) and

adjusted with NaOH for pH 6.17 and 10.47. Reprinted from Reference [77] by permission from Elsevier.com.

The effect of the electrodialytic sample pretreatment step compared to only membrane filtration was dramatic for red wine: the huge early eluting peak common to these samples was drastically reduced by the ITD. The concentration of tannins (the dominant polyphenols in red wines) in the ITD-processed sample was <5% of that in the original sample.

The same basic approach was extended to the isolation of trace heavy metal cations from a complex matrix [78]. Unlike previous papers, water could not be used as the receptor liquid, as insoluble heavy metal hydroxides will precipitate. Instead, 50 mM HNO_3 was used. The complete system is shown schematically in Figure 2-48. The rapid replacement of nitrate in the acceptor solution by whatever anion is present in the cathode isolator presented a problem, even when a multivalent ion like phosphate was used as the cathode isolator. Transfer of the phosphate to the acceptor solution also increased the pH of the latter significantly. The authors solved this problem by using a monovalent-selective anion exchange membrane (designated MAEM in Fig. 48), that consists of a very thin layer of a highly crosslinked cation exchanger layer atop an AEM, greatly limiting the passage of multivalent ion. This allowed the use of 10 mM pH 2.1 phosphate buffer as the cathode isolator solution and the rise in pH of the acceptor was not discernible. These results encouraged the authors to also replace the traditional CEM on the anode side with a monovalent selective CEM

(designated MCEM), that is made similarly with a thin layer of a highly crosslinked anion exchanger atop a CEM, designed to prevent any multivalent heavy metal from attaching to the MCEM. The authors studied the behavior of Cd^{2+}, Co^{2+}, Cu^{2+}, Fe^{2+}, Fe^{3+}, Ni^{2+}, Cr^{3+} and Zn^{2+}. Near-quantitative transfer of all ions (except Fe^{3+}, traced to complexation by NO_3^-) could be attained and Fe^{3+} could be transferred quantitatively by using CF_3COOH or $HClO_4$ as the acceptor. The Achilles heel of the technique was intolerance to salt: on a continuous sample introduction setup, recoveries suffered above a NaCl concentration of 1 mM. However, as an injected sample, up to 5 mM NaCl could be tolerated as a transient plug. This would allow the successful use of the technique in many applications after sample dilution. Trace concentrations of Fe, Cu and Zn in bovine and equine serum were measured in the ITD-processed sample and after conventional wet digestion (both time-consuming and error-prone). The results were statistically identical but with much better precision for the ITD-processed sample.

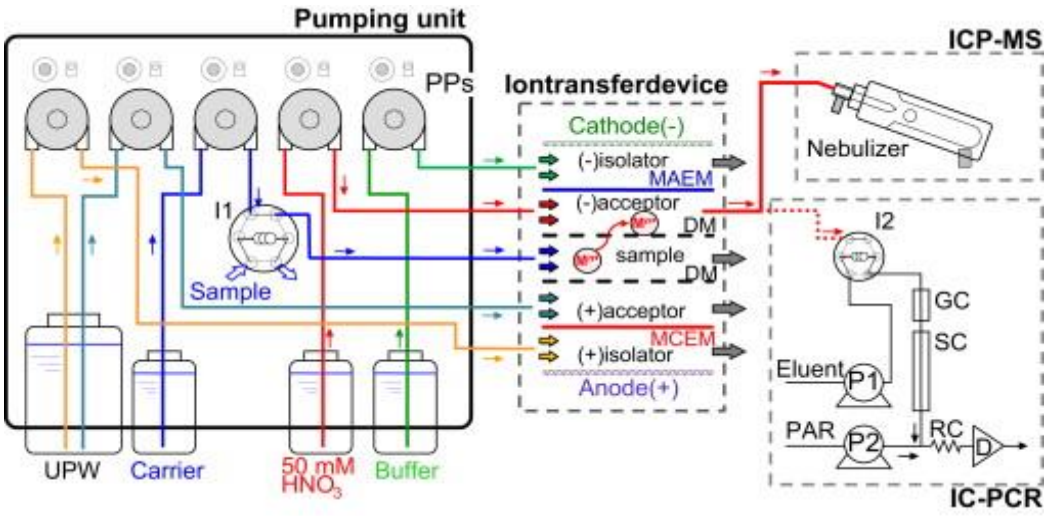

Figure 2- 48 Schematic of the flow diagram , UPW: ultrapure water, PPs: peristaltic pump, MAEM: monovalent selective anion exchange membrane, MCEM: monovalent selective cation exchange membrane, P1, P2: plunger pumps, GC: guard column, SC: separation column, RC: reaction coil, D: absorbance detector, I1, I2: injectors. Reprinted from Reference [78] by permission from Elsevier.com.

An ITD is ideally configured to not only perform matrix isolation but also to concentrate the separated cations or anions. As the analytes of interest are ionic, one obvious way is to pass the effluent through cation or anion exchange preconcentration columns, respectively. In this case, it is desirable to know the acceptor flow rate exactly. A syringe pump would be the device of choice both for a precise delivery rate and to accommodate the backpressure represented by a packed column. Other alternatives are possible: to increase the ratio of the sample flow rate (F_S) to the acceptor flow rate (F_A). Ohira et al. [79] used the ITD to enrich heavy metal ions, other

inorganic cations, and anions (both organic and inorganic), using the same 5-layer device. With F_A fixed at 0.1 mL/min, they studied F_S/F_A ratio from 1 to 100 and found that for all the species tested, quantitative recovery ($C_A/C_S = F_S/F_A$, where C_A and C_S represents the analyte concentration in the sample and the acceptor, respectively) was observed for all ions up to $F_S/F_A = 20$, and for some ions, e.g. K^+, up to $F_S/F_A = 70$ (Figure 2-49). Quantitative recovery does not occur at very high F_S/F_A ratios because the acceptor becomes concentrated enough in the analyte for back diffusion to the donor sample stream to occur. If quantitative recovery is not essential, for heavy metals, an enrichment factor of 100 was attainable with a F_S/F_A ratio of 200. At lower F_S/F_A ratios, e.g., 10 or 50, the LODs for a variety of alkali and heavy metals improve approximately by the same respective factors.

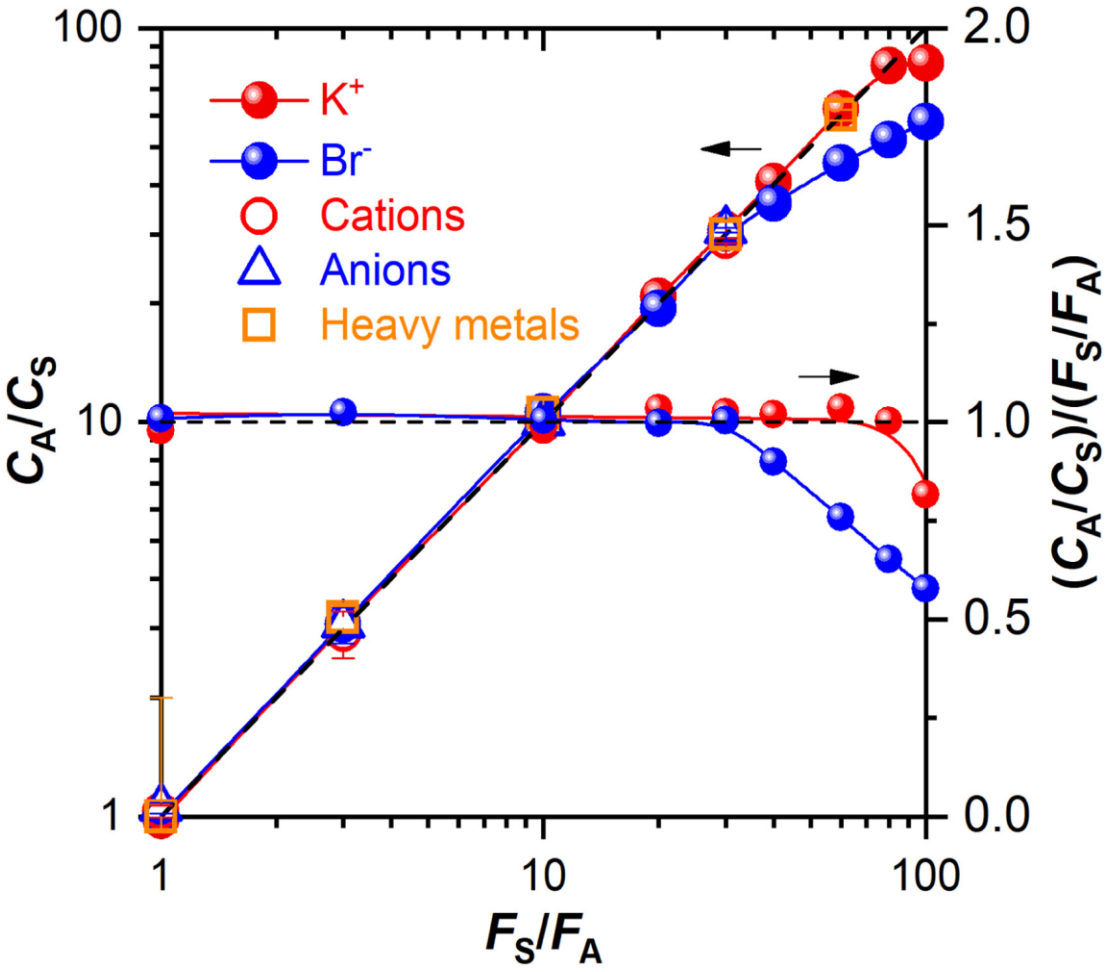

Figure 2- 49 Relationship between the sample and acceptor flowrate ratio and the enrichment factor (C_A/C_S). For the cations and anions, the applied voltage was 35 V, for heavy metals, 15 V. The acceptor and isolator solutions were 30 mM HNO_3, and the acceptor solution flowrate was 0.1 mL/min. Reprinted from reference [79] by permission from Elsevier.com.

A somewhat different and practical application is to preconcentrate haloacetic acids, specifically mono-, di-, and trichloroacetic acid, disinfection by products present at trace levels in chlorinated water. For this application a dimethylaminoethyl methacrylate modified dialysis membrane

as in Figure 2-46 to avoid the negative ζ-potential related issues. Results are presented in Figure 2-50 indicating a ~10x gain is sensitivity for all the analytes; a rather high applied voltage is needed to accomplish this, however.

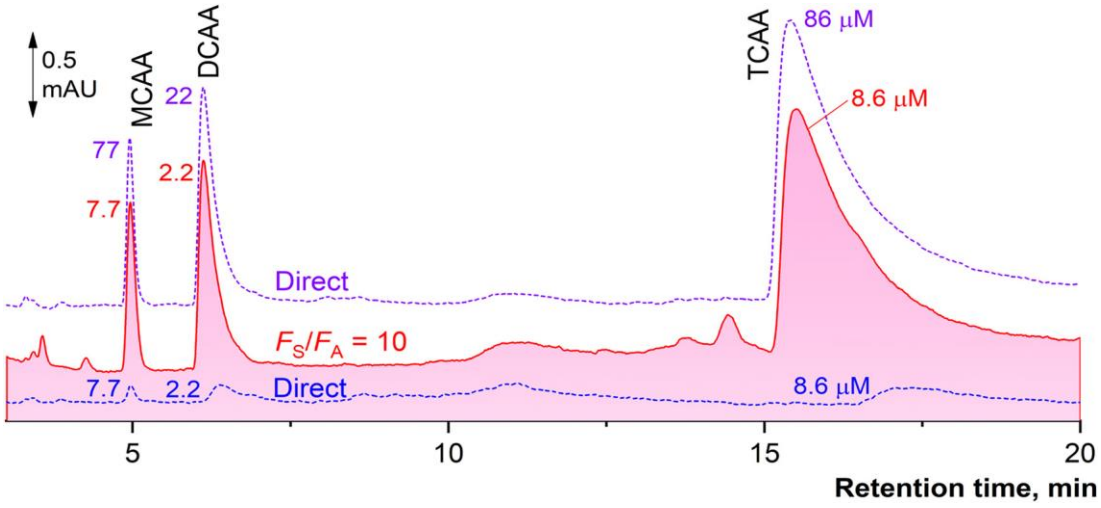

Figure 2- 50 Chromatograms obtained with mono-, di-, and trichloroacetic acid. Solution flow rates were 0.1 and 1.0 mL/min for the acceptor and sample solutions, respectively at an applied voltage of 90 V. Reprinted from reference [79] by permission from Elsevier.com.

An important application carried out with the ITD was the simultaneous determination of Cr (III) and Cr (VI), the two respectively being cationic and anionic [80]. Although cationic Cr (III) is an essential nutritional element, anionic Cr (VI) as $Cr_2O_7^{2-}$ or CrO_4^{2-} (depending on pH) is a class A human carcinogen. In most samples where this measurement is made, the concentrations of concern are low enough such that typically the final

measurement is carried out by an ICP-MS, which cannot innately discriminate between the different forms of Cr.

Even after considerable optimization, conditions could not be achieved in which both Cr^{3+} and $Cr_2O_7^{2-}/CrO_4^{2-}$ were quantitatively transferred to their respective channels in the presence of any significant amount of indifferent spectator electrolytes (e.g., 1 mM NaCl). The authors settled for an optimum compromise in device design and operating conditions in which Cr(VI) is quantitatively transferred and Y^{3+} is used as a tracer. Yttrium has an ionization potential very close to that of Cr. The K_{sp} value of $Y(OH)_3$ is almost identical to that of $Cr(OH)_3$. These characteristics and the rarity of Y make it a perfect tracer to determine the recovery of Cr^{3+} in an ITD-ICP-MS experiment. This approach allowed operation up to at least 10 mM NaCl content (according to the USEPA, 75% of 989 drinking water samples studied had a NaCl content below 2.2 mM).

However, subsequently the researchers discovered that by tuning the surface charge on the dialysis membranes flanking the sample channel and the acceptor/isolator composition, it was possible to get quantitative recovery with samples containing up to 30 mM NaCl; in fact recovery was near-quantitative even at a salinity of 100 mM NaCl. The final optimized device design, with operation at V_{app} = 7.5 V and sample and acceptor flows at 0.2 mL/min was:

+ electrode |30 mM HNO_3 | CEM |10 mM HNO_3 | dialysis membrane(a) | sample | dialysis membrane(c) | 10 mM HNO_3 | AEM | 30 mM HNO_3|- electrode

where dialysis membrane(a) was functionalized with dimethyl aminoethyl methacrylate to render it with a zero to slightly positive surface charge and dialysis membrane (c) was functionalized with vinylsulfonate to render the membrane to have a negative surface charge. ICP-MS detection limits following the ITD for both species were < 0.1 μg/L.

Accurate measurement of Cr(VI) is more important than that of Cr(III). The residence time of the sample in the ITD is ~ 6 s, this limits the interconversion of species. There was no statistical difference in the measured Cr(VI) signal at the 1 μg/L level whether or not 50 μg/L Cr(III) was added to it. No interference was observed from 5 mg/L of other ions such as Mn(II), Co(II), Ni(II), Cu(II), Zn(II), Cd(II), Fe(II) and Fe(III) added to the Cr(VI). In summary, electrodialytic speciation of Cr(III) and Cr(VI) was clearly established as an attractive method.

There is a wide need for the above measurement, but an ICP-MS is not widely available to all. Ohira et al. [81] optimized the ITD with spectrophotometric Cr determination with 1,5-diphenylcarbazide (DPC)-based measurement, the latter being an established well-known and highly specific method for selectively measuring Cr(VI). The ITD was the same as the optimized version in the previous work and operated the same way.

Even with colorimetric detection the authors managed to reach a 0.5 μg/L LOD for either Cr(VI) or Cr(III) in a photometric flow injection analysis (FIA) system coupled to the ITD, with a sample throughput of 30 samples/h. Each acceptor solution aliquot (50 μL) was sequentially injected into a H_2O_2 carrier stream that flowed through the heated reaction coil (60 °C, 400 μL, nominal t_R 30 s). This had no effect on the Cr(VI), but oxidized the Cr(III) to Cr(VI). The stream then merged with an acidic DPC reagent stream and flowed through the second heated reaction coil (60 °C, 350 μL, nominal t_R 13 s) to complete the chromogenic reaction and flowed through an absorbance detector set at 540 nm. Figure 2-51 schematically shows the system. Illustrative output from the system is presented in Figure 2-52.

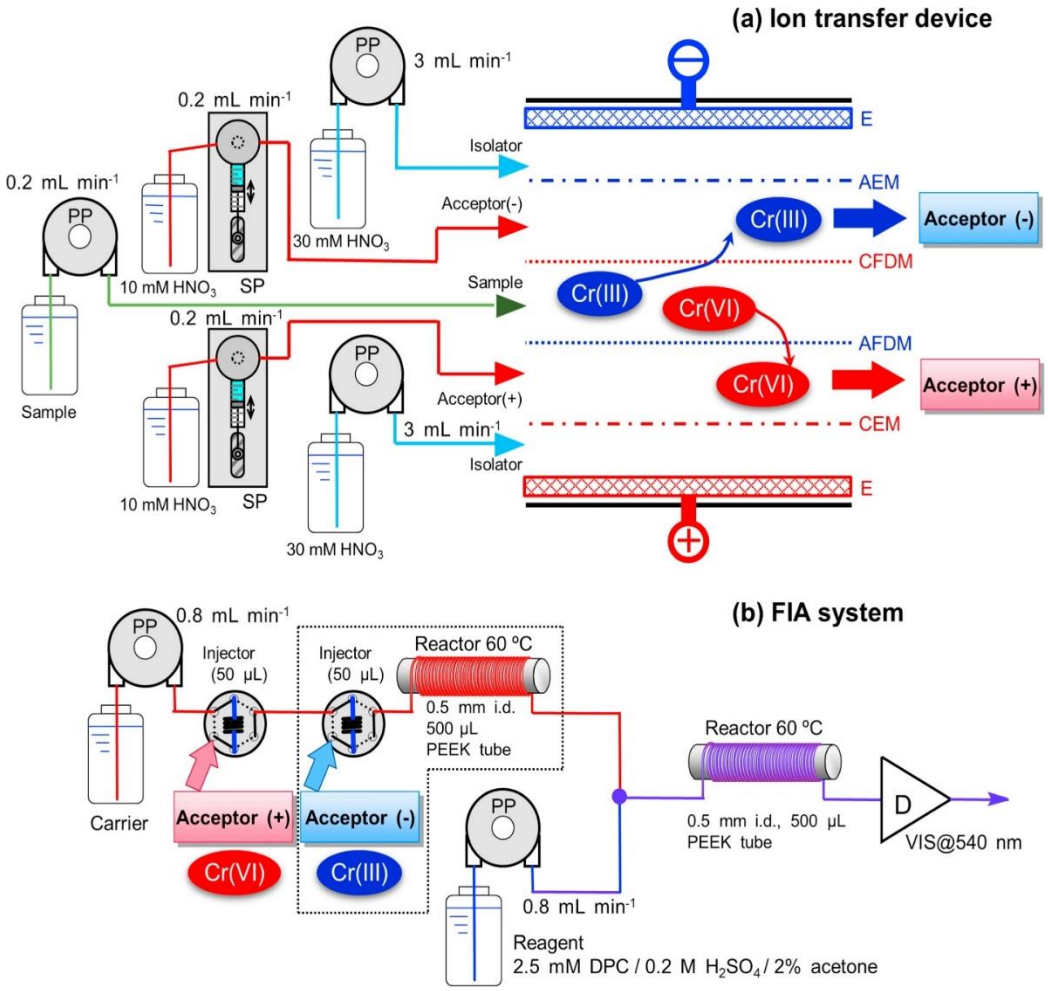

Figure 2- 51 Schematic diagram for the flow system. PP: peristaltic pump. D: Detector. Reprinted from reference [83] by permission from Elsevier.com.

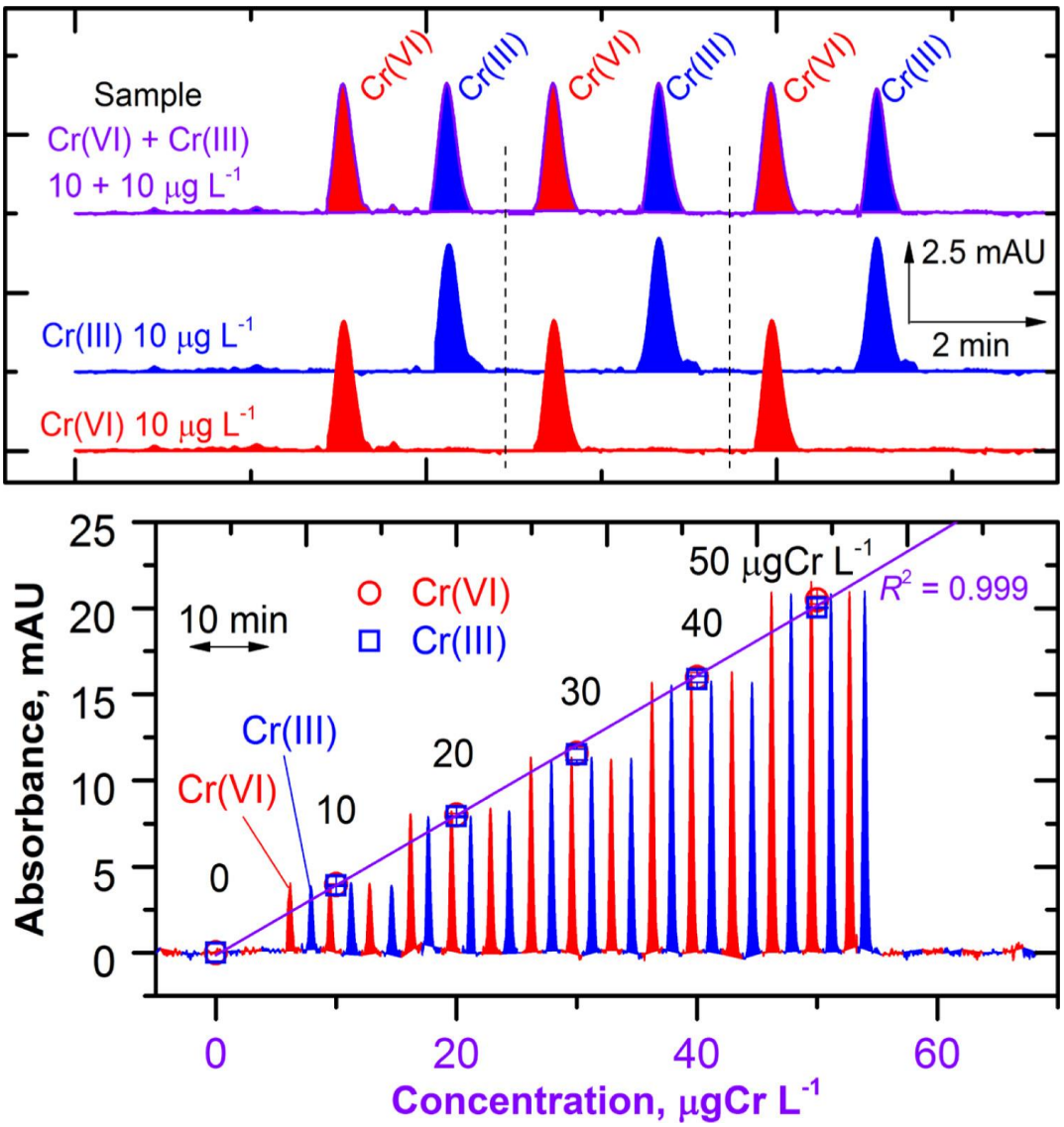

Figure 2- 52 Typical system output of system shown in Figure 2-51 with ITD separation and DPC-colorimetry based flow injection analysis (FIA) system. Reprinted from reference [82] by permission from Elsevier.com.

Interferences of several metal cations and oxometal anions were studied by adding Fe^{3+}, Cu^{2+}, Mn^{2+}, Co^{2+}, Ni^{2+}, Zn^{2+} and Pb^{2+} to the 10 μg L^{-1} Cr(VI) test standard; there was no discernible effect. The metal cations are transferred to the Cr(III) acceptor stream since they are positively

charged. However, without the ITD, very small concentrations (in the single digit mg/L level) of Cu^{2+} or Fe^{3+} interfered with the Cr(VI) measurement. Not only did the ITD provide a robust affordable method for measuring the Cr(III) and Cr(VI), but it also provided essential matrix isolation for an interference-free measurement.

2.12. Use of IEMs for Reagent Introduction

2.12.1. Postsuppressor Ion Exchange for Detection of Weak Acids

In suppressed anion chromatography, the suppressor converts the anions to the corresponding acids. For strong acids, this is beneficial because they are fully ionized and thus the analyte detection sensitivity is improved. However, weak acids with $pK_a \geq 4$ are poorly ionized, leading to highly nonlinear response as a function of concentration. Very weak acids with $pK_a \geq 7$ are essentially unionized in the suppressed effluent, leading to no response at all. Karu et al. have reviewed in detail the efforts in this area [82]. All methods thus far devised to detect weak and very weak acids have centered on converting the weak acid into some other chemical that is more ionized. Tanaka and Fritz first described the detection of weak carbonic acid (H_2CO_3) to fully ionized KOH. They passed the H_2CO_3 through a packed K^+-form cation exchanger to convert it to $KHCO_3$. They then passed this through a OH^--form AEX column to render the $KHCO_3$ to KOH [83]. Berglund and Dasgupta [84] adopted the same principle. But they used a two-stage tubular IEM device to first convert the acid HX to NaX by cation exchange

and then converted the NaX to NaOH by anion exchange. Referring to Figure 2-53, they proposed the use of two independent conductivity detectors: A suppressed hydroxide eluent IC system with its terminal detector (Detector 1) is followed by the two-stage converter and a second detector (Detector 2). Simultaneous consideration of the two signals not only provided information about the pK_a of the analyte but also the possibility of quantitation without calibrating for a specific analyte. The two-dimensional data thus aided the identification of the analyte as well.

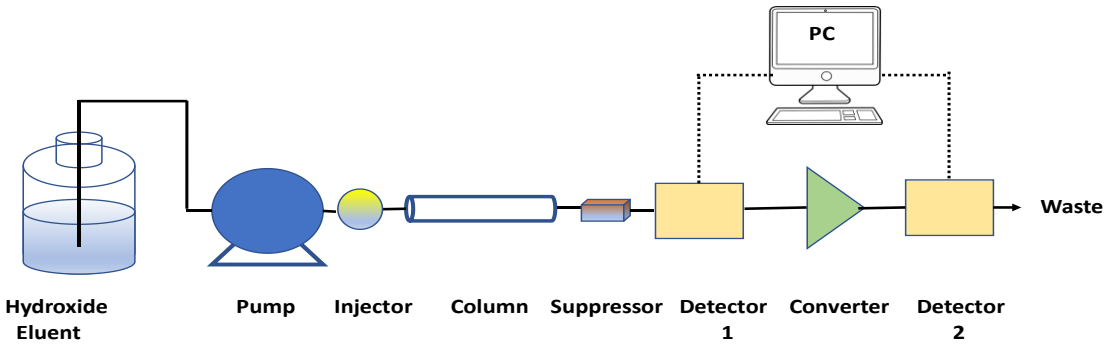

Figure 2- 53 Two-dimensional Conductometric IC system schematic. Adapted with modifications from reference [84].

Unfortunately, such a system is of limited value in truly improving the detectability of weak and very weak acids. To convert HX into NaX by cation exchange, it is imperative that significant concentrations of H^+ derived from HX are present for the desired exchange process to occur. For very weak acids, this is not the case. Overmore, once any exchange takes place forming NaX, one essentially has a NaX-HX buffer system with very little free H^+ available for exchange.

To overcome the limitation of low conversion efficiencies with higher pK_a analytes, Berglund and Dasgupta [85] subsequently attempted to *simultaneously* exchange both the available H^+ and X^- ions for M^+ and Y^- (where MY is a near-neutral salt) such that buffer formation would not occur as in the previous case, thus allowing the exchange process to continue. Simultaneous cation and anion exchange were accomplished by using a flow configuration bounded on one side by a cation exchange membrane (CEM) and on the other by an anion exchange membrane (AEM). A tubular design, similar to the dual tube annular design in Figure 2-2, was used except that the inner tube was a radiation grafted poly(ethylvinylacetate) AEM tube and the outer tube was a Nafion CEM tube. Unlike Figure 2-2, an inserted filament or a helical configuration was not possible due to the poor structural strength of the AEM tube. Individual electrolytes consisting of NaF, LiF, LiCl or NaCl, 25-75 mM in concentration, were tested as the cation/anion replacement reagent. Higher ion replacement regenerant concentrations favor the desired ion exchange process but high concentrations also result in increasing reagent ion penetration and thus a higher background conductance. The lowest background was observed with LiF because Li^+ and F^- each respectively exhibits lower equivalent conductance compared to Na^+ and Cl^-. With a LiF replacement reagent, 80-100% of strong acid analytes were converted to LiF. Signals for monoprotic carboxylic acids improved >10x compared to conventional suppressed results. Moreover, anions such as arsenite and silicate that were not

detected by conventional suppressed IC system at all, could be detected by the LiF conversion system. In retrospect, instead of using the same reagent for both cation and anion replacement, the background conductance from ion penetration would have been better optimized if the cation replacement reagent consisted of the traditional small cation (Li^+ or Na^+) and a large multivalent anion (e.g., polystyrenesulfonate) which would have greatly inhibited reagent leakage through the membrane. Similarly, an anion replacement reagent that would have shown much less leakage is a polycation (e.g. poly(diallyldimethylammonium) in combination with a small anion (Cl^- or F^-).

Instead of weak acid anions, similar conversion of a weak base cation, e.g., NH_4^+ to a corresponding strong acid salt in a specially designed electrodialytic suppressor and thence to a strong acid have been reported but only in the patent literature [86,87]. As described, this will be difficult to operate these under gradient elution conditions.

In a series of papers, Caliamanis et al. [88-90] studied the conversion of HX to NaX precisely exploiting the strategy outlined above: As a counterion for Na^+ they used EDTA, at the optimized pH (9-11), this would be present as the tri- or tetraanion. They were able to use a commercial planar sheet-based CEX IEM ("micromembrane suppressor" [15]) as the HX→NaX converter device before conductivity detection, using 10-100 mM Na-EDTA as the sodium source, a slightly alkaline pH (optimized for a given analyte)

improved the observed conversion permitting the measurement of borate and cyanide at the 50 μM level, not possible in conventional suppressed IC.

2.12.2. Postsuppressor Donnan-Forbidden Base Introduction for Detection of Weak Acids

Interestingly, while reagent leakage has been portrayed in much of the above as undesirable, precisely this property was used by Al-Horr et al. [91] for weak acid detection. If an alkali hydroxide, e.g., KOH, NaOH, LiOH, etc. is located on one side of a CEM while water flows on the other, the leakage of the base into the water can be negligible at low reagent concentrations. However, with increasing concentration, the Donnan barrier will eventually be overcome, and reagent leakage will occur. The leakage flux depends on the charge density on the IEM, the IEM thickness, and the concentration differential. If a low and *constant* concentration of the leaked base (e.g. 0.1 mM) is established in the effluent, any eluting acid HX, essentially regardless of its pK_a, will react with this background OH^- forming X^-, the net reaction being

$$OH^- + HX \rightarrow X^- + H_2O \quad ...(2)$$

the net process thus being the replacement of the highly mobile OH^- (equivalent conductance ~200 μS/(cm.mM) compared to most other ions (20-80 μS/(cm.mM)). The emergence of an analyte HX will thus result in a negative excursion from the baseline conductance. Near-universal response to most anions is the result of the base introduction; very weak

acids anions such as arsenite, silicate, borate, cyanide, etc. can be very sensitively detected. Figure 2-54 shows the detection of such ions at low levels, along with other ions in a dual detection system where a conventional suppressed hydroxide eluent IC system is followed by IEM-based KOH introduction and a second detector. The KOH introduction can also be conducted electrodialytically, this is considered in the next section along with its advantages and disadvantages. Al-Horr et al. examined three different CEM-based KOH introduction systems: planar, tubular and filament-filled annular helical, the latter being the same as that used as suppressors [9,10] except being much shorter in length. Passive KOH introduction is the desired process here, exchange of H^+ for K^+ at the membrane surface is not. As such, decreasing the available membrane area is beneficial. Of the three designs tested, the FFH design performed the best (background noise level of $\leq$ 7 nS/cm and a band dispersion value $\leq$ 82 µL).

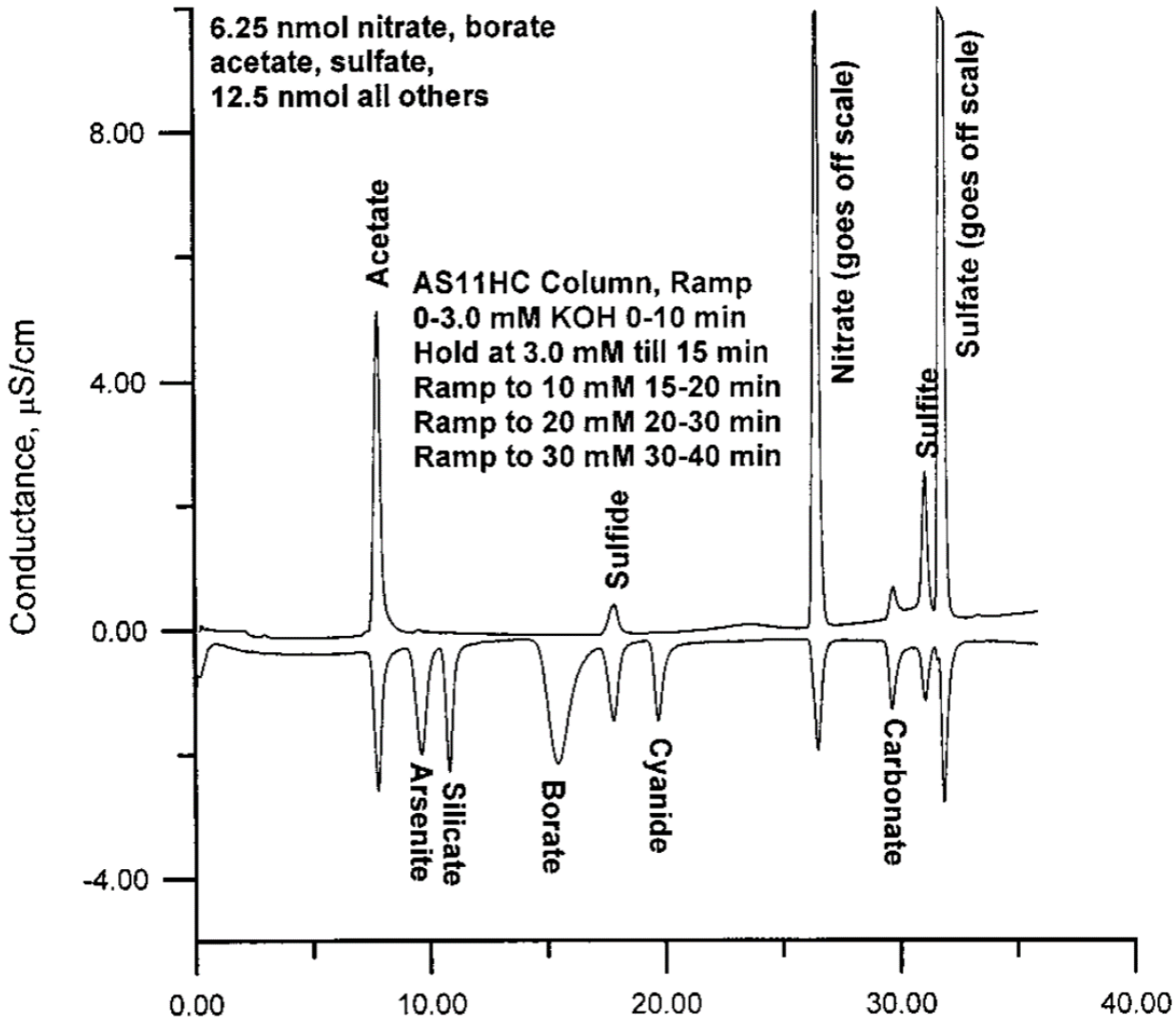

Figure 2- 54 2D ion chromatogram obtained using gradient elution, 25-µL injection volume. The abscissa is time in minutes. Reprinted from reference [91] with permission from the American Chemical Society.

2.12.3. Electrodialytic Reagent Introduction. Detection of Weak and Very Weak Acids

The detection of very weak acids by introducing a very small amount of a base after IC separation and suppression was discussed in the foregoing section. Instead of introducing a base by a mechanical pump or

through Donnan breakdown, current-controlled electrodialytic reagent introduction could potentially be advantageous because of facile control. As in the previous case, the amount of base introduced is very small and thus even with a hydroxide generator that is not gas-free, the amount of electrodialytic gas generated can be very small and can mostly dissolve in the solution. With only a modest amount of backpressure applied, no degassing is needed. Berglund et al. [92] first examined this in the same configuration as Figure 2-53: After the usual CD following suppression (D_1) and then detecting conductivity again (D_2) after electrodialytic NaOH introduction; LODs down to µg/L levels were possible with analyte acids of pK_a values as high as 9.5.

The microelectrodialytic NaOH generator (MNG) depicted in Figure 2-55 contained a 0.5 mm i.d. Nafion tubing as the CEM and two 100-µm diameter Pt wires as electrodes. One is put inside the Nafion tube as the cathode and the anode is wrapped around the tube. An adjustable constant current source introduces the NaOH. The feed electrolyte (10 mM NaOH) flows outside the membrane while the suppressed column effluent (essentially water) is flowing inside the ~1-cm long Nafion tube and exits as a very dilute NaOH solution whose exact concentration is governed by the applied current. The system can function continuously with repeatable background conductivities. Reproducible chromatography is possible without appreciable dispersion. An illustrative chromatogram is shown in Figure 2-56 with the two detector outputs shifted corresponding to the transit

time between the two detectors to align the analyte signals. The chromatogram is divided into five regions. In (a), Fluoride and borate are unresolved and an unresolved impurity present in the sample is largely responsible for the 2nd peak in the D1 response.

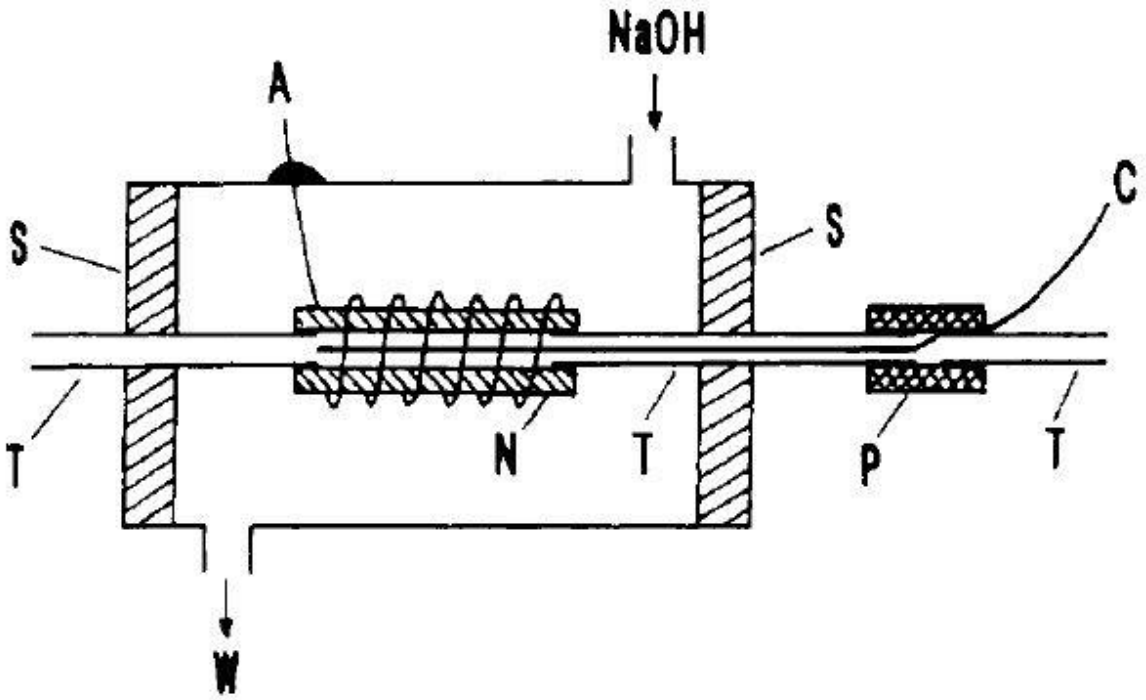

Figure 2- 55 Microelectrodialytic NaOH generator (MNG) : T, connecting Teflon tubes, 0.3-mm i.d.; A and C, anode and cathode platinum wires; N, Nafion tube (0.5 mm i.d.); P, poly(vinyl chloride) pump tubing; W, waste; S, jacket sealant. Reprinted from reference [92] with permission from the American Chemical Society.

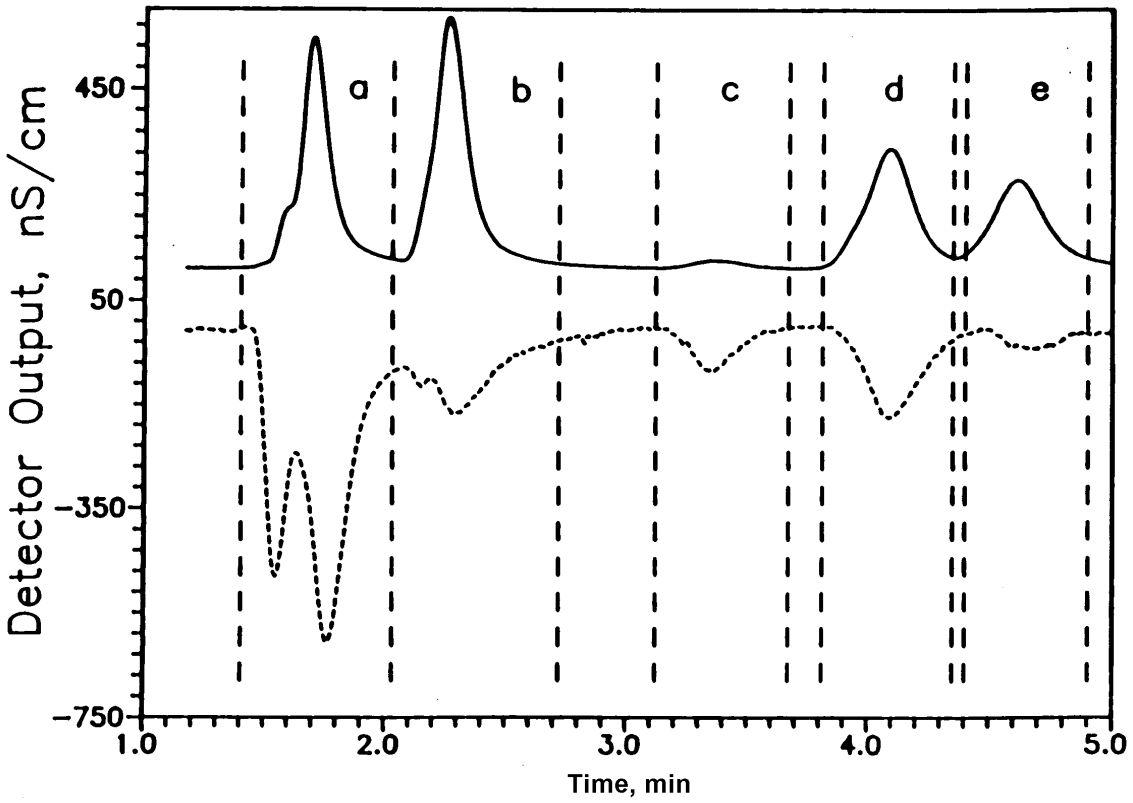

Figure 2- 56 Dual Channel system output for a sample containing 25 µM each of (a) fluoride, borate and an unknown impurity, (b) chloride and glyoxalate (c) an indeterminate amount of dissolved CO_2, (d) arsenate, and (e) malonate and nitrate, and. Solid and dashed lines D_1 and D_2 outputs respectively. The peaks have been synchronized in time Reprinted from reference [92] by permission from the American Chemical Society.

Once it is recognized that boric acid has practically no response in D_1, the dual channel output clearly confirms the presence of an unidentified impurity in segment (a). In segment (b), chloride and glyoxylate were unresolved in the D_1 response, it is in fact not possible to conclude that there

are two coeluting components. In contrast, D_2 response clearly show two separate components. Segment (c) shows the response from dissolved CO_2, prominent in D_2 but barely visible in D_1. For segment (d), the peak is very similar in shape in both detectors - this would not be possible unless the peak is due to a pure analyte. First, from the significant D_1 response it can be concluded that the analyte has a low pK_a. For a monoprotic strong acid, let us say with an anion equivalent conductance of 50 µS/(cm.mM), the D_1 response would be ~4x the D_2 response. Here the D_2 response is almost comparable to the D_1 response. This suggests that that the analyte may be multiprotic and the second proton may be much less ionized than the first proton; while only the first proton responds in D_1, both show up in D_2. The analyte cannot be S^{2-} whose pK_1 and pK_2 are both too high. The behavior does fit that of an anion like arsenate (or phosphate) with a pK_1 of 2.22 and a pK_2 of 6.98 (pK_3 is too high to register in either detector). Finally, segment (e) shows that the analyte here is possibly that of a strong acid anion: since it has a much larger peak in D_1 than in D_2; the response is actually from a mixture of malonate and nitrate. The method provides good detectability for strong, weak and very weak acid anions simultaneously and simplifies data analysis because of negligible dispersion.

Sjögren and Dasgupta [93] later utilized a setup similar to that used in [92] except that a water-regenerant electrodialytic suppressor and an optimized MNG device were used. The suppressed effluent conductance of the 3-50 mM NaOH eluent flowing at 1 mL/min was near that of pure water

and was raised to 23-27 µS/cm (~100 µM NaOH introduced) with an applied current of 160 µA. The electrode lengths and positions were adjusted so to minimize the needed voltage at any given current. Experiments showed that the noise is minimized when the cathode length equals most of the active membrane length in the MNG without significantly exceeding it: cathode lengths of 10-16 mm were optimum for the 15 mm MNG tube. Interestingly, band dispersion caused by the MNG depended on whether voltage was applied. For chloride (an early eluting ion for which changes in dispersion is more easily discerned) the induced dispersion values were 94 $\pm$ 6 vs. 67 $\pm$ 4 µL, respectively with and without voltage applied. The applied potential likely causes the anions to migrate radially outward in the lumen and thus get into a lower flow velocity regimen.

With a detector background of 100 µM NaOH, the D_2 peak response amplitude will increase up to a maximum peak apex concentration of 100 µeq/L of the analyte acid where the NaOH has been completely neutralized by the analyte acid. Beyond this concentration, the behavior depends on the pK_a of the analyte acids. For strong acids or those with relatively low pK_a, past the “titration end point” of 100 µeq/L, excess acid will appear and it will still be ionized (e.g., for chloride we now have NaCl + HCl). With increasing analyte concentration then, a W-shaped peak results, the apex conductance may be higher than the original baseline if the analyte concentration is high enough. The situation is different when the analyte acid has a higher pK_a. As the pK_a increases to $\geq$5, the apex of the peak

increasingly becomes a flat plateau and loses the W-excursion. An NaX/HX buffer system is formed past the neutralization point and any weak acid HX further added does not much ionize; the conductance thus becomes constant. Much can be concluded therefore about the pK_a of an unknown analyte by observing the D_2 response behavior at different dilutions (or different introduced base concentrations) and comparing the D_1 vs. D_2 responses. Figure 2-57 illustrates this behavior.

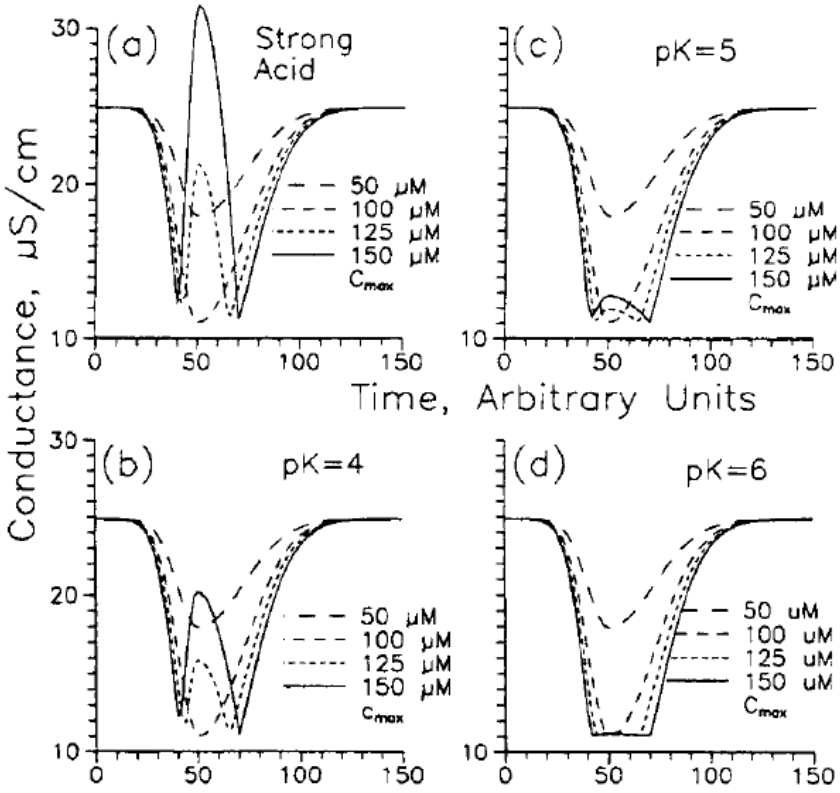

Figure 2- 57 Responses for different concentrations (50-150 µM at the peak apex, D_2 background 100 µM NaOH) of a monoprotic eluite acid ranging from (a) strong acid to (d) pK = 6. The simulated peak profile is

modified Gaussian and is assumed to be 60. Reprinted from reference [93] by permission from the American Chemical Society.

On the second detector (D_2), LODs of some 14 anions tested ranged from 1.2 µM for phthalate to 8.6 µM for borate. Response linearity for some 9 anions tested over a 0-500 µeq/L injected concentration range exhibited a linear r^2 value of 0.9998 to 1.0000. Originally, it was suggested that W-shaped or flat-plateaued peaks are best quantitated after dilution to a point where normal behavior has been restored. More recently, it has been shown that both normal and oddly shaped peaks like the above can be quantitated based on their width at a fixed height [94].

MNG designs thus far discussed were all tubular devices. Sjögren and Dasgupta [95] developed a planar device (Figure 2-58) with superior performance. As Figure 2-58 indicates, the suppressed effluent from D_1 enters into the microfluidic cathode channel. Na^+ is electrodialytically transferred from the anode channel to the cathode and the effluent from the cathode chamber, now with a background of ~0.1 mM NaOH, proceeds to the second detector D_2. Several operational problems with previous devices were solved by the planar design. The current efficiency in generating NaOH was quantitative, the devices permitted greater current density than tubular devices and provided lower noise and dispersion. A study of 2, 4 and 8 cm long devices indicated an optimum channel length of 4-cm. A 2-channel ion chromatogram for a mixture of both strong and weak acid analytes is shown in Figure 2-59.

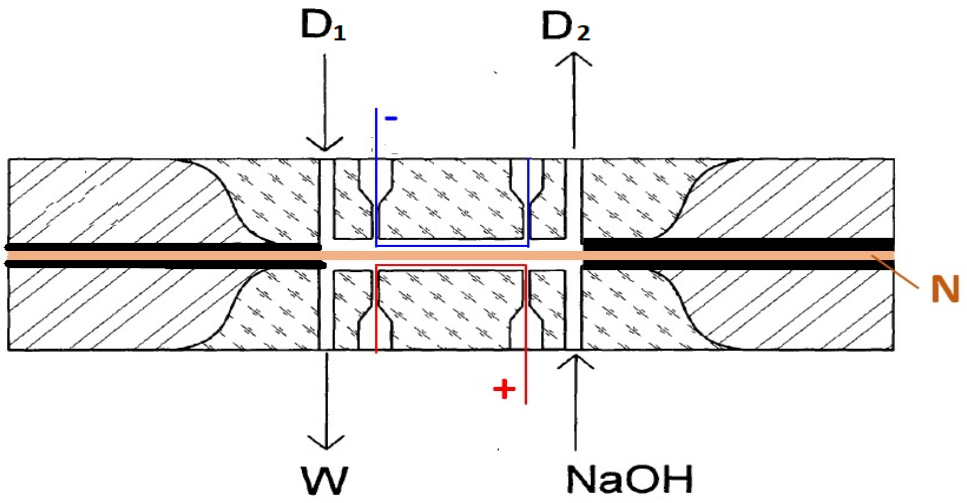

Figure 2- 58 Schematic of planar MNG. Adapted with modifications from reference [95]. A thin Nafion sheet (N) is sandwiched between two Plexiglas plates; the sheets contain a machined square cross section (0.25 x 0.25 mm) channel, typically 4 cm long. Four access holes were drilled in each plate. Pt electrode wires were passed through the inner holes and these apertures then sealed. The two outer holes permitted liquid I/O to the MNG, the top cathode channel being the NaOH receiver channel where the D_1 effluent is brought in as the input and the channel effluent is directed to D_2. The bottom, anode compartment, simply provides a flow channel for the donor NaOH stream. Reprinted from reference [95] by permission from Elsevier.com.

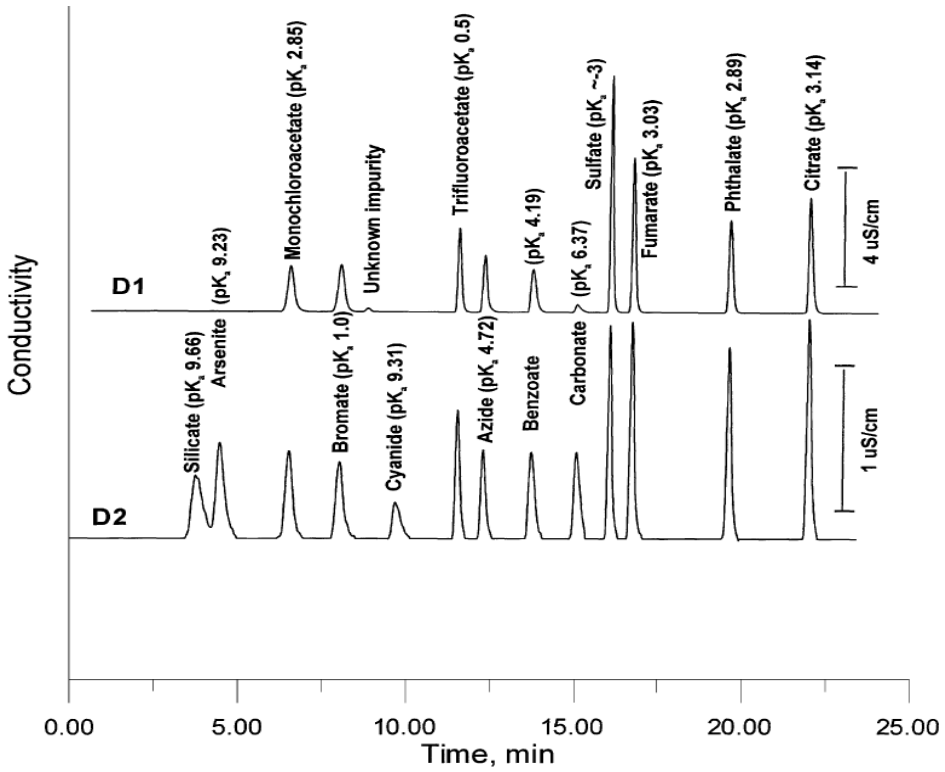

Figure 2- 59 Two-dimensional detection in gradient IC. The eluent concentration was increased from 2 mM to 30 mM KOH over the first 16 min and then held constant at 30 mM. The concentration of all analytes was 25 μM except for silicate, arsenite and cyanide, which were 50 μM. Carbonate was not deliberately added; it is from adventitious CO_2 contamination. D_2 responses are inverted to show positive signals; both detector outputs are background subtracted and the D_2 time was advanced by the inter-detector transit time to synchronize the eluite responses. Reprinted from reference [95] by permission from Elsevier.com.

As shown in Figure 2-59, the responses of weak and very weak acids with $pK_a \geq 6$ are vastly improved in the second detector after NaOH

introduction. Additionally, detailed consideration of D_1 and D_2 outputs for analytes of different pK_a reveals much about their nature. For example, for analyte $pK_a > 5.8$, at D_1 the analyte is <50% ionized and a sudden decrease in D_1/D_2 signal ratio occurs at just about this pK_a value. The authors also showed that for pK_a >5, the S_1^2/S_2 ratio (S_1 and S_2 being the D_1 and D2 signals, respectively) is linearly related to the pK_a and thus permits its determination.

2.12.4. Electrodialytic Introduction of a Postcolumn Reagent

The chromatographic analysis of transition metal ions or lanthanides most commonly involves an ion exchange or ion-interaction separation [96] followed by postcolumn introduction of a chromogenic reagent, e.g., 4-(2-pyridyl(azo) resorcinol) (PAR), 2,2′-(1,8-Dihydroxy-3,6-disulfonaphthylene-2,7-bisazo)bisbenzenearsonic acid (Arsenazo III), etc. Similar processes are also carried out in flow injection determination of these metals. The introduction of the reagent, whether by pneumatic or mechanical pumping, causes unavoidable and undesirable volumetric dilution. While the introduction of a concentrated reagent at a very small flow rate may avoid significant volumetric dilution, when the flow ratio of two streams vary greatly, good mixing is more difficult to accomplish, and greater mixing noise deteriorate LODs. The problem can become particularly an issue in the capillary scale as robust pumping options are limited.

Mishra and Dasgupta [97] designed the device in Figure 2-60 as a capillary scale electrodialytic reagent introduction device. It is a miniature

CEM-AEM device built on a ¼-28 chromatographic union much the same as the planar devices used previously for low pressure capillary scale eluent generation [64].

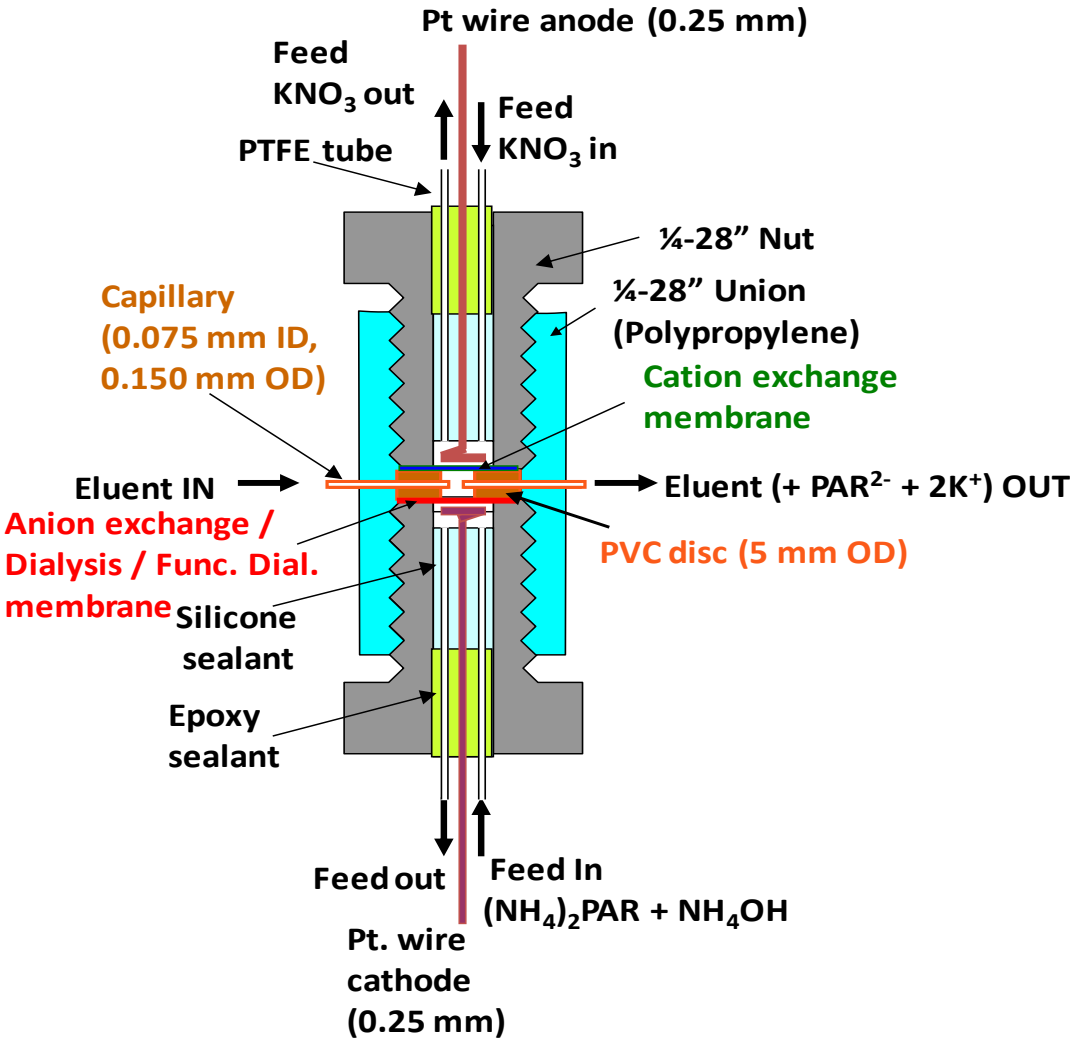

Figure 2- 60 IEM-based capillary electrodialytic reagent introduction system schematic. Reprinted from reference [97] by permission from the American Chemical Society.

It was discovered that the very large and very hydrophobic PAR anion simply could not be introduced through an anion exchange membrane

typically used in suppressors (vinylbenzyl chloride radiation grafted on 75-125 μm thick PTFE, ~10% crosslinked and then quaternized). Similar membranes, even custom made with only 25 μm thick PTFE did not permit the introduction of PAR. Cellulose acetate dialysis membranes (wet thickness 30 μm, 12-14 kDa molecular weight cutoff) used instead of the AEM permitted current controlled introduction. The same membrane was also tested after an aliphatic anion exchanger was incorporated – the membrane was sprayed with a mixture containing glycidyl methacrylate and ethylene dimethacrylate (75:25 v/v) and a small amount of 2,2'-azobis-isobutyronitrile as initiator and allowed to polymerize in a nitrogen atmosphere for 24 h at 60 °C. This was then functionalized by treating it with 50% (v/v) N-methyldiethanolamine at 75º C for 12 h, resulting in an anex capacity of 0.11 mequiv/g. A greater amount and an overall higher range of PAR introduction was possible with the unfunctionalized dialysis membrane, but the anex-functionalized membrane permitted more stable introduction with lower noise. Figure 2-61 shows illustrative data for PAR introduction in the FIA mode with Zn^{2+} as the analyte.

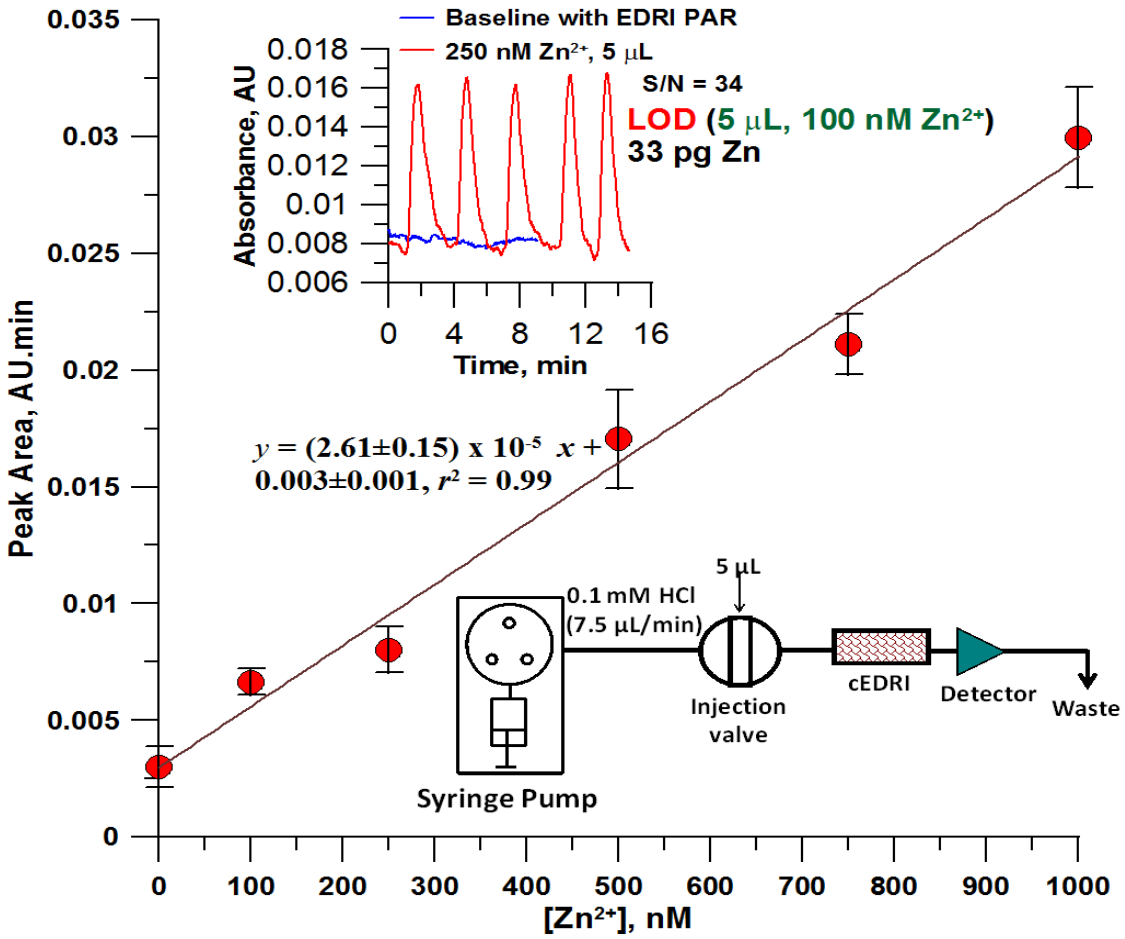

Figure 2- 61 PAR introduction system utilized in the FIA mode. Error bars indicate ±1 standard deviation. Reprinted from reference [97] by permission from the American Chemical Society.

2.12.5. Introduction of Reagents Through an IEM

Reagent introduction is a necessary step in most flow-based liquid phase methods. This does not have to be electrodialytic as in the foregoing section but can be concentration gradient driven with an ion exchange mechanism or the concentration difference can be high enough such that the Donnan barrier is overcome. In common with electrodialytic introduction, this type of reagent introduction process has the advantage

that no volumetric dilution occurs. Pankratova et al. [98] acidified their sample prior to potentiometric sensing of nitrite to improve sensitivity by flow-through cation exchange device. The design was much like that of a planar suppressor except containing a single CEM; an acid donor flowed on one side and the sample on the other. The authors suggested that the desired degree of acidity be attained by varying the sample flow rate (as sample salinity may vary). In a more recent paper the same group has offered a new approach to the phosphomolybdate-based trace phosphate determination in seawater, taking particular advantage of the highly saline matrix [99]. Measurement conditions in this approach involve highly acidic conditions (pH $\leq$1) as well as several mM levels of molybdate. This was accomplished with the serial system shown in Figure 2-62.

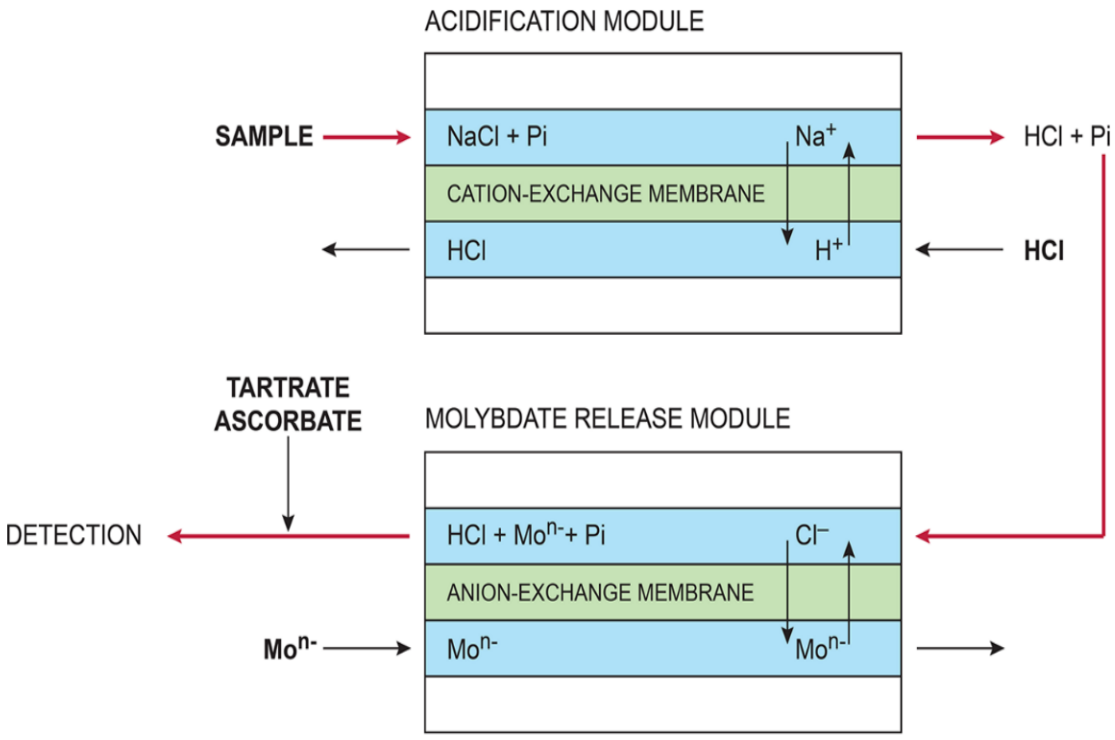

Figure 2- 62 Reagent introduction scheme for seawater phosphate (denoted by Pi in the figure) determination. The residence time, device dimensions and HCl concentrations are adjusted (optimum 5 M) to reach the optimum level of acidity. The acidic sample then flows through an AEM device and chloride in the sample is partially exchanged (6 mM molybdate donor) for the requisite concentration of molybdate. Other necessary reagents are then introduced. Reprinted from reference [99] by permission from the American Chemical Society.

For future adopters, the process in Figure 2-62 can be accomplished by a single AEM/CEM device. Although the symbolism in Figure 2-62 suggests that only ion exchange is involved, with several molar HCl on one side of the CEM, Donnan-forbidden penetration of HCl almost certainly

contributes to the acidification. An acid other than HCl may have been better for use with peristaltic pumps. In our experience, regardless of the type of pump tubing, HCl vapor can permeate and corrode metallic system components.

While both of the above more recent applications utilize acidification, adding base has been practiced for a long time. Adding ammonia through a CEM is facile and is particularly convenient when the pH does not need to be raised much beyond 10. Because of significant vapor phase concentration over a solution of concentrated NH_3, in many cases it is even possible to introduce sufficient ammonia while the flow stream travels through a small segment of a CEM suspended over concentrated NH_3 in a closed container. Davis and Peterson [100] described the introduction of ammonia through a 20 cm long bundle of 5 sulfonated polyethylene hollow fibers postcolumn so they could detect several nitrophenols in the visible instead of at 280 nm where multiple other compounds interfered. These authors also earlier patented the general strategy of the use of hollow fibers (both IEM-based and other types) for postcolumn reagent introduction in HPLC.

Sulfonated polyethylene hollow fibers make relatively poor CEMs, however. Dasgupta and Gupta [101] used only a 3 cm length of a Nafion tube immersed in a stirred 50% NaOH solution to introduce sufficient base through Donnan breakdown to hydrolytically decompose injected hydroxymethanesulfonate to formaldehyde and sulfite; this requires

strongly alkaline conditions. The amount of NaOH introduced had to be sufficient to overcome the buffer capacity of the buffered carrier stream as well. The hydrolysis product then reacted with acidic pararosaniline to form the detected colored product.

Hydrogen peroxide is an important analyte that is determined by a variety of methods in a variety of applications. One particularly sensitive fluorometric approach uses the peroxidase-catalyzed oxidation of *p*-hydroxyphenylacetic acid to its dimer that is fluorescent. However, the fluorescence is maximized at pH ≥10 (sufficient to ionize the phenolic protons) while the enzymatic oxidation step best proceeds at a pH of 5.5. An approach where the enzymatic oxidation is first carried out in a pH 5.5 buffer and then the stream is passed through a short CEM-based reactor immersed in NH_4OH has been used with both an immobilized enzyme system [102] and the enzyme in solution [103]. In such systems, base introduction occurs primarily by passage of unionized NH_3 through the membrane. Note that ion exchange for NH_4^+ would not be a desired process here; keeping the membrane short helps minimize the contact of the flow stream with the membrane. Similar systems for ammonia introduction have been utilized in many other publications since.

2.13. Donnan Dialysis Separation and Preconcentration

Donnan dialysis utilizes counterdiffusion of two or more ions through an IEM, most commonly a CEM, to achieve separation etc. There are many reviews available, a short and succinct review is by Davis [104]. Donnan

dialysis involves permitted ion transport to provide the continuous countercurrent diffusion of allowed ions. The process exploited is often the passage of the trace concentration of the analyte ion from a very dilute donor solution to a much higher ionic strength solution (acceptor) where the analyte ion concentration is low or nonexistent but contains high concentration of another ion that counterdiffuses to the donor side to compensate. The process is fundamentally driven by the activity gradient and the fact that forbidden ion transport can be negligible in comparison. Imagine a high concentration of a salt AX separated by a CEM from a trace concentration of a salt BY (where A and B are cations; X and Y are anions and are not transported). Exchange of A and B takes place in equivalent amounts rapidly. But the transfer of B continues well past the point that *concentration* of B is equal on both sides as the *activity* of B on the acceptor side is still much lower than that on the donor side because of the much lower *activity coefficient* of B in the presence of a large AX concentration. Additional chemical manipulations, e.g., putting a complexing agent in the acceptor side to render B into a negatively charged complex ion that can no longer cross the CEM, gives yet another incentive for B to continue to transfer to the donor side. In addition, using a large donor/acceptor volume ratio provides concentration enrichment relatively quickly. Blaedel and Haupert [105] first pointed out the manifold possibilities of these type of manipulations prior to analysis. In the intervening years, the availability of alternative techniques including various types of SPE has reduced the

actual use of Donnan dialysis by the practicing analyst. The account here is therefore necessarily abbreviated.

2.13.1. Preconcentration of Cations by Donnan Dialysis

Cox and DiNanzio [106] performed selective enrichment of 1-100 μM Cu^{2+} into a receptor, a receptor composition of 200 mM $MgSO_4$ and 0.5 mM $Al_2(SO_4)_3$ provided the best enrichment factor (EF), 12. An increase in temperature, membrane area, and stirring rate, all increased the rate of ion transfer. Specifically, the ratio of the volume contained to the membrane surface area governs the short-time EF; lower this ratio, higher the EF. IEM tubes are thus much better suited than IEM sheets; Cox and Twardowski [107] used a 0.7 mm i.d. 2.45 m long Nafion CEM tube (internal volume 0.77 mL) through which the same optimized $MgSO_4$-$Al_2(SO_4)_3$ receiver liquid was pumped or recirculated while it was immersed in a large volume (1000 mL) of the stirred sample. The enrichment of Cu, Cd, and Zn was investigated. In single-pass experiments, the EF increased with decreasing receiver flow rate, reaching ≥15 at flow rates of ~0.2 mL/min. At flow rates greater than ~3 mL/min, the EF becomes almost independent of the flow rate, a condition favored by the authors. They observed single-pass EF values of 2.2-2.4 for all three metals at a flow rate of 3.5 mL/min. When a 5 mL volume of the receiver was recirculated @8 mL/min for 10, 20, 30, 40 min, the EFs for Cu were 17, 38, 48, and 49, respectively; those for Zn was essentially the same and those for Cd only marginally smaller.

If a complexing agent is used in the receiver to chelate the analyte of interest, a high concentration of receiver electrolyte becomes unnecessary. By tuning the pH of the receiver electrolyte enables selective enrichment of one metal ion over others when several are present in the donor. Cox et al. [108] observed that the pH control of iminiodiacetic acid used as receiver and its pH control can very much affect the relative selectivity of transfer (Figure 2-63), albeit this experiment was conducted singly, not from a mixture.

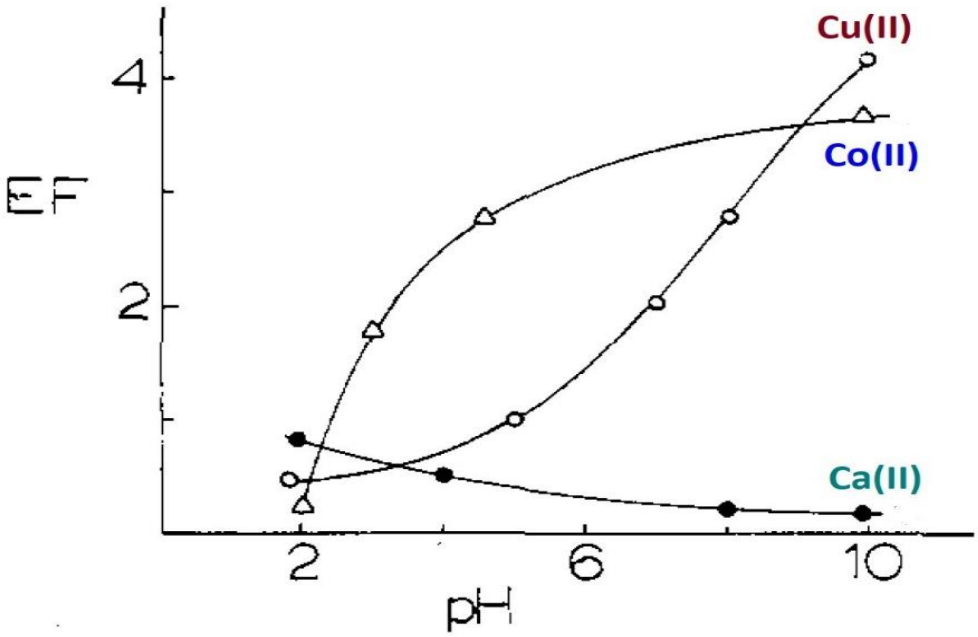

Figure 2- 63 Donnan dialysis of cations into a chelating medium. Receiver: 0.02 M LiCl, 2 mM IDA at stated pH; samples, 10^{-5} M single component solutions of the metal at pH 4. Adapted with modifications from reference [108].

2.13.2. Donnan Dialysis Preconcentration and Manipulation of Anions

Donnan dialysis of anions has been less studied but a particularly interesting question is how anions from weak acids and multiprotic acids behave since their ionization is pH dependent. Cox and Cheng [109] studied the relevant factors for Donnan dialytic preconcentration of several probe analytes (chloroacetate, pyruvate, arsenate, phosphate, etc.) across an AEM into a 0.1 M KNO_3 receiver (pH adjusted with KOH/HNO_3). Their critical finding was that when the receiver pH is much less than the pK of the most acidic species, the transfer rate was independent of sample pH over a wide range. Interestingly, variation of receiver pH does not affect the transfer of strong acid anions. On the other hand, presence of strong acid anions may affect the attainable EF of weak acid anions, limiting the value of the technique.

Cyanides are involved in ore-processing operations. The metallocyanide complexes involved are anionic and the importance of this chemistry in gold extraction is well known. Akretche and Kerdjoudj [110] studied the utility of 5 different anion-exchange membranes on Donnan dialytic separation, preconcentration and recycling of metallocyanides of Au, Ag, and Cu in the presence of excess free cyanide and also explored the utility of multiple stages. One conclusion was metals that form a single complex cyanide species, e.g. Au, transfer faster than a metal such as Cu for which three different cyano species form under the experimental

conditions; however, this may depend on the choice of a specific membrane. The use of a third compartment can improve the separation between the metals.

The presence of an excess of fluoride in potable water arising from its presence in the source water is a concern in several parts of the world. Removal based on Donnan dialysis through an AEM has been repeatedly studied for this purpose [111-113]. The use of different AEMs, and effects of pH, concentration, and nature of exchanged counterions, have all been studied in detail.

2.13.3. Donnan Dialysis Preconcentration and IEM Treatment Prior to IC Analysis

DiNunzio and Jubara [114] investigated Donnan dialysis as the preconcentration method for the determination of trace transition metals by postcolumn reaction detection ion chromatography using PAR, the detection chemistry was discussed earlier [97]. The major problem in applying Donnan dialysis here is the incompatibility of the receiver composition with typical IC conditions. High concentrations of a multivalent electrolyte like $MgSO_4$ or $Al_2(SO4)_3$ as the receiver rapidly exhausts the capacity of a typical IC column when this is injected as the sample matrix. The authors reasoned the only way to make such preconcentration feasible is to design the receiver electrolyte and the separation column/eluent composition in a concerted manner to assure compatibility. The receiver electrolyte chosen was 0.1 M $Al_2(SO_4)_3$ adjusted to pH 0.5 with H_2SO_4. A relatively high

capacity strong acid type sulfonate functionality cation exchange column was used for separation with a tartrate eluent at pH 4.0. A gradient was run to separate Cu, Ni, Co, Cd, and Mn in under 30 min. Much of the ionic strength in the receiver comes from the acid. The small injection volume and the buffer capacity of the eluent rapidly takes care of this acidity. Aluminum is so well complexed by tartrate, the Al is essentially all converted to the tartrate complex form and is not significantly captured by the column. Donnan dialytic preconcentration was carried out for an hour with 200 mL sample and 0.5 mL receiver electrolyte using a planar CEM cell. Attainable LODs for the studied metals ranged from 1 μg/L Ni to 25 μg/L Cd. Compared to standards (not processed through Donnan preconcentration), the analytical precision decreased from 5% to ~12% in RSD. While this was a remarkably clever chemical design, current practice permits better and faster separations on column-eluent combinations that will be incompatible with this approach.

Cox and Tanaka [115] studied Donnan dialytic preconcentration of anions prior to ion chromatography. Their strategy involved a dual step procedure to ensure compatibility with IC analysis. The idea is to use a carbonate-bicarbonate receiver electrolyte in the first Donnan dialysis step, this electrolyte is similar to the eluent used in IC in composition but has a much higher concentration (0.04 M Na_2CO_3, 0.16 M $NaHCO_3$). This amount of carbonate-bicarbonate if directly injected would cause problems in chromatographic separation. The additional second step was then to use

cation exchange for H^+ by passage through a Nafion CEM tube (with a stirred CEX slurry in H^+ form outside the CEM tube for regeneration) whence the receiver matrix, once collected, largely goes off as CO_2. There is no loss of typical analyte acid ions. A planar AEM was first custom-synthesized [116] and a Donnan dialysis cell was built around it. Using 100 mL stirred sample and 5 mL receiver electrolyte, dialysis was conducted for 30 min. The receiver was then diluted to 10 mL in a volumetric flask (in case any osmotic flux from the sample diluted the receiver; within experimental precision, ca. 4%, no evidence for this was found) and then subjected to H^+-exchange as outlined above. For Cl^-, NO_3^-, PO_4^{3-} and SO_4^{2-}, the respective EF values attained under the above conditions were 16, 14, 15, and 14 and variation of the sample pH in the range 3.8-9.4 had no effect. The authors became sufficiently enamored with their Nafion CEM-tube suspended in a CEX resin slurry as a H^+-exchanger (curiously, they called this process a dual ion exchange method) that they found multiple other uses for it. The determination of trace anionic impurities by IC in NaOH by first passing the sample through a H^+-exchanger is obvious and well known but the same process can also be applied to remove any matrix anion that forms a volatile acid. Thus, determination of trace nonvolatile anions in Na_2CO_3, $NaHCO_3$, NaCl etc. were accomplished [117]. They also carried out controlled H^+-exchange for (partial) neutralization [118] in much the same way that electrodialytic suppressors have been used later [53].

Determination of trace ionic impurities is the forte of IC, but this is difficult when these are to be measured in a similarly charged polyelectrolyte, for example when chloride or sulfate present in poly(styrenesulfonate) (PSS) are to be measured. If any of the matrix polyelectrolyte is injected into an oppositely charged IC column, the polyelectrolyte will essentially poison whatever IEX sites on the column it binds to. Because of simultaneous multiple site binding, this binding is essentially irreversible. Cox and Dabek-Zlotorzynska [119] found Donnan dialysis ideally suited to both isolate and concentrate various trace anions in a PSS sample which was subjected to Donnan Dialysis across an AEM into a carbonate receiver. The attained EF for chloride was slightly (ca. 12%) higher from a PSS solution matrix compared to a dilute chloride standard. If more accurate results are needed, multiple analyses with incremental standard addition of the desired analyte were recommended. For chloride as analyte, the use of added nitrate, which did not indigenously occur in the sample, as an internal standard was also successful. The authors also applied the technique to polyacrylic acid as the sample; however, the enrichment factors were much lower than in the case of PSS.

2.14. IEMs for Gas Collection

2.14.1. Diffusion Scrubbers for Gas Collection

In atmospheric analysis it is often necessary to discriminate between gas-phase and particulate species when it is not possible to chemically discriminate between them. For example, IC analysis for nitrate cannot

discriminate between whether the nitrate originated as gas phase HNO_3 or particulate NH_4NO_3. The placement of a filter does neither guarantee passage of the HNO_3 gas through it nor the integrity of collected NH_4NO_3. Atmospheric samples are spatially, and temporally heterogeneous and low concentrations require prolonged sampling. Gaseous HNO_3 can be removed by the filter substrate or by an alkaline crustal particle collected by the filter. Particulate NH_4NO_3 already collected on the filter may be lost by evaporation when the air temperature rises. These problems can be solved by a diffusion-based collection approach, which discriminates between gases and particles based on their vastly different diffusion coefficients. When a gas-particle mixture flows through a tube and the tube walls behave as a good sink for the gas, under appropriate flow conditions, the gas molecules will have ample opportunity to collide with the wall and thus be collected on the wall while the particles will travel through the tube essentially without loss. There are several extant reviews on the diffusion-based sampling and analysis of atmospheric trace gases [120-122].

The first example of diffusion-based gas collection was a glass tube that was coated with oxalic acid inside. Air was sampled through it in the field to immobilize gaseous ammonia on the wall. After bringing the tube back to the laboratory, the tube washings were analyzed for NH_4^+ [123]. This was called a *diffusion denuder*. Obviously, such a tube needs to undergo thorough washing and recoating before it can be used again. Dasgupta [124] recognized that a jacketed Nafion CEM tube can be used as a continuous

collector for ammonia. A 0.9 mm o.d. Nafion CEM tube was jacketed by a 1 mm i.d. thick wall glass capillary, 30 cm long and holes drilled into the glass wall at each end (on opposite sides) to act as I/O ports to the annular space. The space between the CEM tube and the jacket was sealed with silicone adhesive at each end. Sulfuric acid (0.5 M) was pumped at 50 μL/min as the collector liquid. The device provided essentially quantitative collection (99.6-99.9+%) for gas flow rates up to 1.54 L/min and gaseous NH_3 concentrations from 15 ng/m^3 to 2.2 mg/m^3. The device was termed a "diffusion scrubber" (DS). A similar IEM-based DS based on a radiation-grafted thin-walled (100 μm) PTFE AEM tube was next described for collecting gaseous HNO_3 [125]. In this case, 0.1 M K_2SO_4 was used as the scrubber liquid with 5% sulfamic acid added to eliminate interference from gaseous NO_2. Real-time response to HNO_3 was demonstrated with a UV absorbance detector.

There are problems with using membrane tube-based DS devices in the above geometry (later termed gas-inside scrubber, GIS). The tubes must be thin-walled for reasonably rapid transport of the collected ion. Such tubes are generally available only in relatively small diameters, which makes it difficult to sample at a significant flow rate and still maintain laminar flow conditions (necessary for diffusion-based collection). Even if a thin-walled tube is custom made with a larger i.d. (as was the case for the AEM tube above at 3 mm i.d.), structural integrity then becomes a problem. The pressure of the annular liquid as it flows pushes the thin walls of the

membrane inward, distortion from a cylindrical shape may occur. A more convenient geometry is to suspend the membrane tube within a concentric jacket tube with inert inner walls. This geometry was later termed a gas-outside scrubber, GOS. The sampled gas flows through the annular space – collision of the gas molecule with the outer wall has no effect but contact with the centrally placed IEM tube may result in uptake. The collector liquid flows through the IEM tube and may be coupled to a continuous analyzer. The IEM tube is often filled with a filament to reduce the response volume inside and thus the response time. GIS-type scrubber collection efficiencies can be computed from the Gormley-Kennedy Equation [121]. Calculators are available to estimate collection efficiencies for the GOS type scrubbers, given DS dimensions and the analyte diffusion coefficient [126].

Even for the above GOS devices, porous hydrophobic membrane tubes have generally become preferred over IEMs for ionogenic analytes. While IEMs are ideally suited to capture ionogenic gases, rather high concentrations of the displacing ion must be present to rapidly transport the captured ion [127]. The use of a scrubber liquid that has a significant displacing ion concentration raises the bar on how pure it must be to reduce the baseline/blank value. If an acid is used to collect NH_3 on a CEM, the residual ammonium in the acid (in use, the acid reservoir invariably absorbs ammonia) controls the system blank. A CEM tube, however, is still preferred over a porous membrane tube in collecting certain analytes of importance, none of which are transported in ionic form, as detailed below.

2.14.2. CEM Tube Diffusion Scrubber Based Analysis Systems for Atmospheric Gases

2.14.2.1. Formaldehyde

The efficiency of collection of an analyte gas molecule is not only determined by its diffusion coefficient and the DS dimensions but also the Henry's law constant for the gas. The Henry's law constant is a measure of the affinity of the molecule to be in solution. Even when the Henry's law solubility is not very favorable, the uptake can be made efficient by some fast reaction that results in uptake: Ideally, every collision of the gas molecule with the IEM should result in uptake; in other parlance, the *sticking coefficient* should be unity. As an analyte gas, Henry's law constant for NH_3 in water is quite modest and if one were to use a CEM in Cs^+-form, with CsOH as the collector liquid, the uptake would not be nearly as efficient compared to an H^+-form CEM with an acid as the collector liquid where the primary uptake mechanism is the conversion of NH_3 to NH_4^+, a fast proton transfer process. Formaldehyde as HCHO has a Henry's law solubility that is even lower than that of ammonia. It is not scrubbed very well by contacting with water at all. However, at equilibrium, water dissolves a substantial amount of HCHO. This occurs through the hydration of formaldehyde as methylene glycol, $CH_2(OH)_2$, a process that takes substantial time in pure water. It is, however, subject to both acid- and base-catalysis. Even with a porous (hydrophobic) membrane diffusion scrubber (PMDS), considerable difference in collection efficiency is observed as with

pure water vs a dilute H_2SO_4 solution as the scrubber. But a Nafion membrane diffusion scrubber (NMDS) with a dilute acid flowing as scrubber liquid is far more efficient. The internal acid solution keeps the exposed CEM exterior in H^+-form and the high functional group density makes the membrane surface behave as a *superacid.* This helps the reactive uptake of HCHO. Moreover, when a PMDS is used, only a fraction of the surface is porous. A gas molecule must collide with the solid polymer surface but arrive at, and diffuse through, the pore to collide with the collector liquid at the pore interface. Finally, a PMDS is subject to changing collection efficiencies as solids may form through evaporation and block the pores over time; in general, a PMDS is very intolerant of any dissolved solid in the collector liquid.

An NMDS for the measurement of HCHO and H_2O_2 was first described in [127] with different inlet designs and particle deposition characterized. The basic design of the NMDS is shown in Figure 2-64.

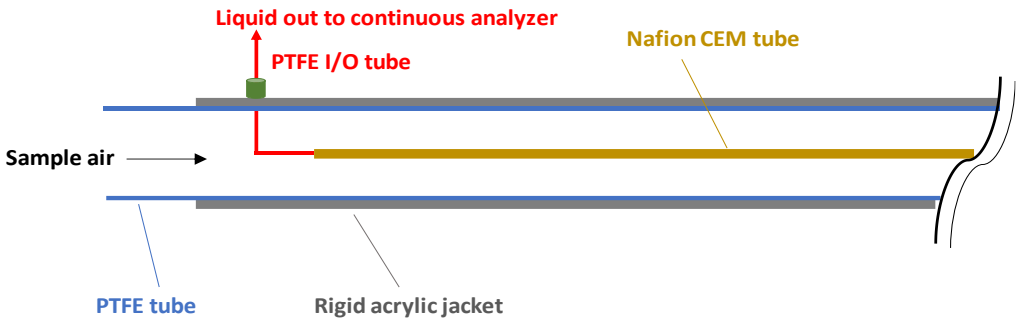

Figure 2- 64 A Nafion membrane diffusion scrubber (NMDS) , one half is schematically shown; air and liquid flows countercurrent. The typical active membrane length is 40 cm, the Nafion IEM is ~0.9 mm o.d. when wet and

used with a thermally shaped right-angled PTFE tube for liquid I/O. The acrylic jacket is lined with a 5 mm i.d. PTFE tubing to provide inertness. In practice, the CEM tube is typically filled with a filament to reduce liquid residence time and thus improve response time.

A sensitive way to measure formaldehyde is the Hantzsch reaction, which involves the cyclization of an amine, an aldehyde and a β-diketone, to form a fluorescent dihydropyridine derivative. 2,4-pentanedione is most commonly used as the β-diketone. Zhang et al. used it with a NMDS achieving an LOD of 75 parts per trillion by volume (pptrv) HCHO [127]. Fan and Dasgupta [128] used cyclohexanedione instead of pentanedione because it forms a more intensely fluorescent product and achieved a gas phase LOD of 9 pptrv. Figure 2-65 shows the response of this system to 80 pptrv HCHO. Li et al. [129] simplified the detector relying on a liquid core waveguide with a LED light source and used it in a major field study. At 30 pptrv, this version did not quite attain the previous LOD but was more than adequate to measure diurnal variations in urban HCHO levels as illustrated in Figure 2-66.

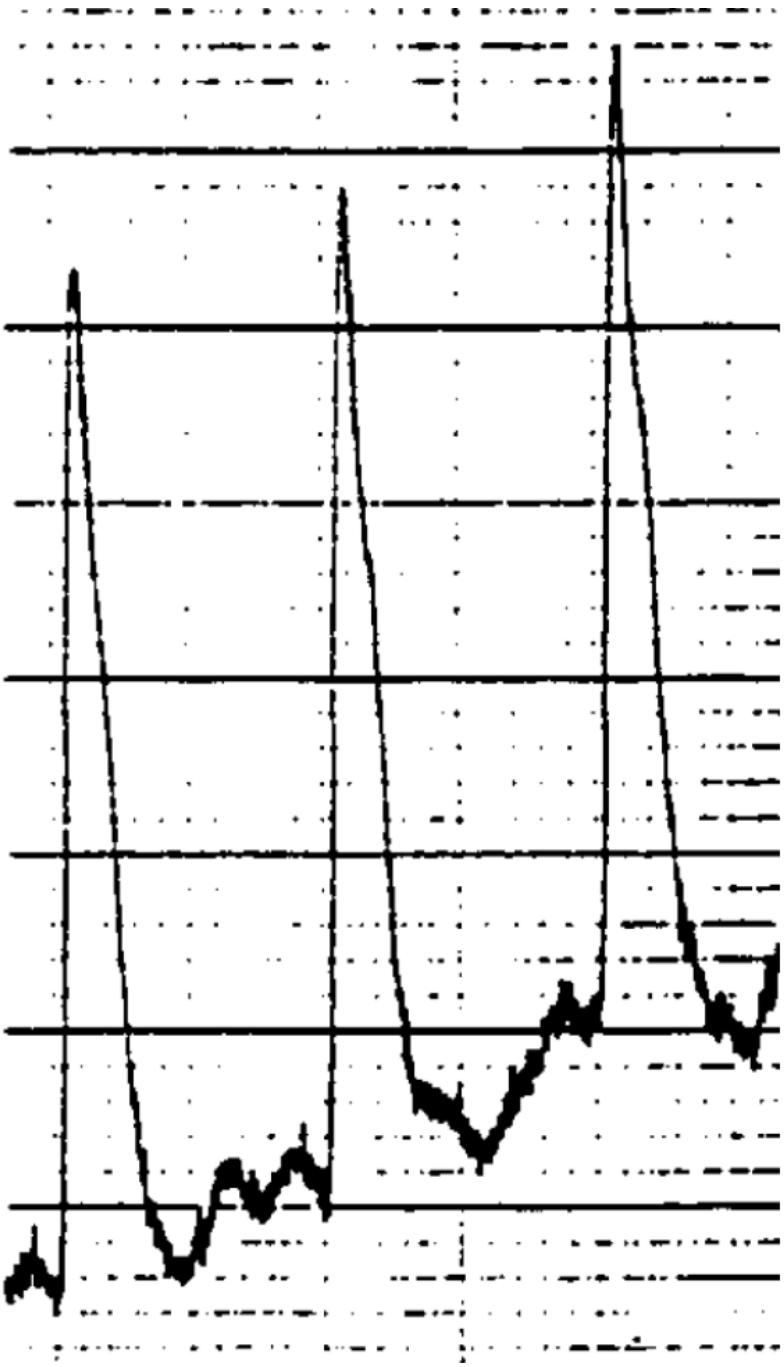

Figure 2- 65 Response to 80 pptrv HCHO in a NMDS-cyclohexanedione Hantzsch reaction fluorometric detection system. The air sample inlet is modulated so that the it alternates between 3 min sample air and 20 min

of zero air. The peaks are thus 23 min apart. Reprinted from reference [128] by permission from the American Chemical Society.

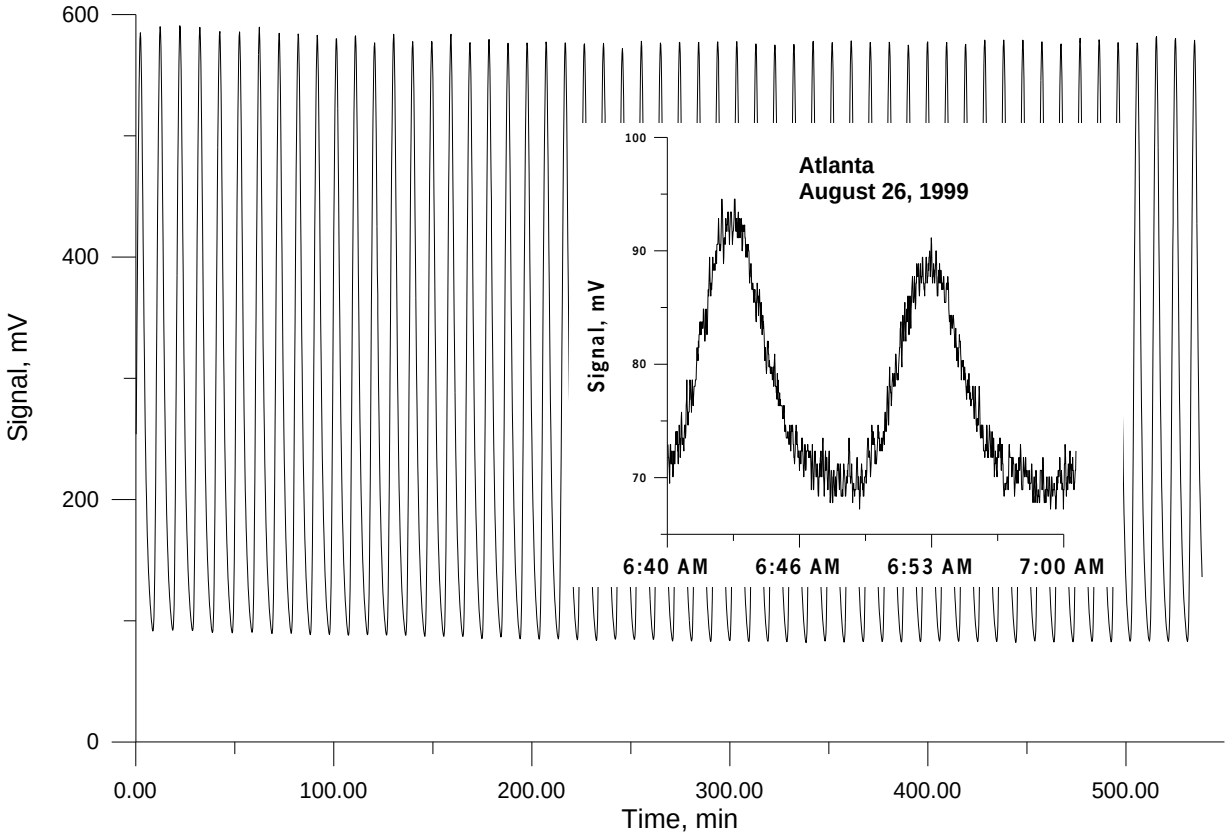

Figure 2- 66 Typical instrument stability of the NMDS-LED-LCW Fluorescence detector. Overnight run, sample 4.6 ppbv HCHO (3 min sample, 7 min zero). The inset shows the lowest concentrations encountered during the Atlanta supersite campaign; heavy rainfall occurred during the previous evening resulting in relatively clean air; these peaks represent 420 and 500 pptrv, respectively. Reprinted from reference [129] by permission from the American Chemical Society.

Formaldehyde is one of the key species for understanding atmospheric chemistry and is one of the principal products of

photochemistry in a polluted atmosphere. It is a key player both in the generation of ozone as well as being the primary product of the ozonolysis of terminal olefins. Although the cyclohexanedione reaction is more sensitive, almost all later studies have used pentanedione, which can be purified easier and does not suffer from positive interference from high levels of H_2O_2 if present. The NMDS – pentanedione-Hantzsch reaction-based instruments have been used in numerous ground- and aircraft-based studies, in the US and during the Paralympic games in China and have been shown to compare well with different direct spectroscopic instruments [130,131,132,133,134].

2.14.2.2. Hydrogen Peroxide

Hydrogen peroxide (H_2O_2) is also a key species in atmospheric chemistry. Along with its organic congeners, methyl hydroperoxide (MHP, CH_3HO_2) and hydroxymethyl hydroperoxide (HMHP, $OHCH_2HO_2$), H_2O_2 is a key indicator of atmospheric photochemistry. H_2O_2 has a very high Henry's law constant and is one of the principal agents involved in the oxidation of atmospheric SO_2 dissolved in cloud water to H_2SO_4. HMHP is an adduct of HCHO and H_2O_2 and exists in a reversible equilibrium; it cannot be distinguished from H_2O_2 in a reaction-based assay. As previously stated, a highly sensitive procedure to measure hydrogen peroxide is the oxidation of nonfluorescent PHPA to its fluorescent dimer, mediated by the enzyme *peroxidase* [103]; both H_2O_2 and MHP can perform this oxidation.

Other chemistries have also been developed for measuring H_2O_2. Bovine hematin not only can act as a *peroxidase* mimic for determining H_2O_2, for the same activity it is far less expensive than a real enzyme e.g., *horseradish peroxidase* preparation. Oxidation by MHP is very poorly mediated by hematin; only 5-10% of the sensitivity obtained by a *peroxidase*-mediated system is observed. Whereas the peroxidase-mediated oxidation proceeds best at a pH far removed from where the product is optimally fluorescent, hematin catalysis proceeds well in an ammoniacal medium at a pH where the product is fluorescent. In addition to PHPA, a multitude of nonfluorescent substrates that are oxidized to intensely fluorescent products are suitable; inexpensive p-cresol is particularly attractive [135]. Another attractive inexpensive substrate is thiamine (Vitamin B1) that is oxidized to fluorescent thiochrome [136]; the latter is optimally excited by an inexpensive but high intensity 375 nm LED. Another very well-known chemistry is the transition metal ion catalyzed oxidation of luminol by H_2O_2 that is accompanied by intense chemiluminescence. Whether MHP can oxidize luminol is not known. However, oxidants such as NO_2 or O_3 elicits chemiluminescence from luminol when these gases directly contact a luminol solution. Yet another highly specific (no reaction with MHP etc.) chromogenic chemistry for H_2O_2 is based on the uptake of H_2O_2 by a titanium (IV)- porphyrin complex, oxo[5,10,15,20-tetra(4-pyridyl)porphyrinato]titanium(IV) [$TiO(TpypH_4)^{4+}$],

(TiTPyP), to form the H_2O_2 adduct which results in a shift of the absorption spectrum to a higher wavelength [137].

Aside from chemical discrimination, H_2O_2 can be collected selectively over MHP based on the choice of the membrane. Whereas a PMDS collects both H_2O_2 and MHP, an NMDS collects H_2O_2 with very high efficiency, but not the more hydrophobic MHP. All the above reactions have been used with an NMDS to selectively measure H_2O_2. Zhang et al. [138] described the first NMDS based gaseous H_2O_2 determination system (Figure 2-67) that uniquely has a single flow line; the authors were able to achieve am LOD of 5 pptrv.

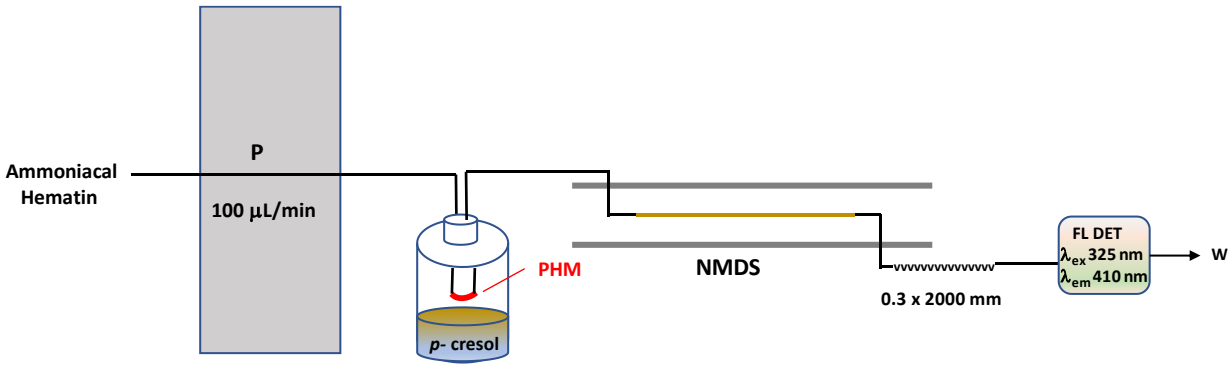

Figure 2- 67 Single flow-channel NMDS-based gaseous H_2O_2 measurement system. Ammoniacal hematin flows through a short segment of a porous hydrophobic membrane (PHM) suspended over pure *p*-cresol. The vapor permeates through the membrane and introduces *p*-cresol into the flow stream which then travels through the NMDS. The collected H_2O_2 then reacts (t_R 1.4 min) and the fluorescence is detected by a filter fluorometer. Adapted from reference [138].

Li and Dasgupta [139] designed a fully automated instrument, shown in Figure 2-68, relying on the NMDS and the hematin-thiamine chemistry. The DS liquid effluent is aspirated by a pump and flows through injector I (which provides for liquid phase calibration, analysis of rainwater, etc. Thiamine is mixed with the DS effluent in coil L1 followed by introduction of hematin and mixing coil L2 (thermostated at 30 °C). The fluorescence is then detected by the transversely placed near UV LED-illuminated liquid core waveguide (LCW)-based detector. Liquid enters through inlet LI in the tee T and the emitted light travels through a collection fiber optic FO to a PT through a pair of blue optical filters OF. The Teflon AF fluorescence detection cell is based on the tube AF jacketed from external light by stainless steel jacket tube SSJ and irradiated transversely by the LED which is monitored by the photodiode PD placed radially across.

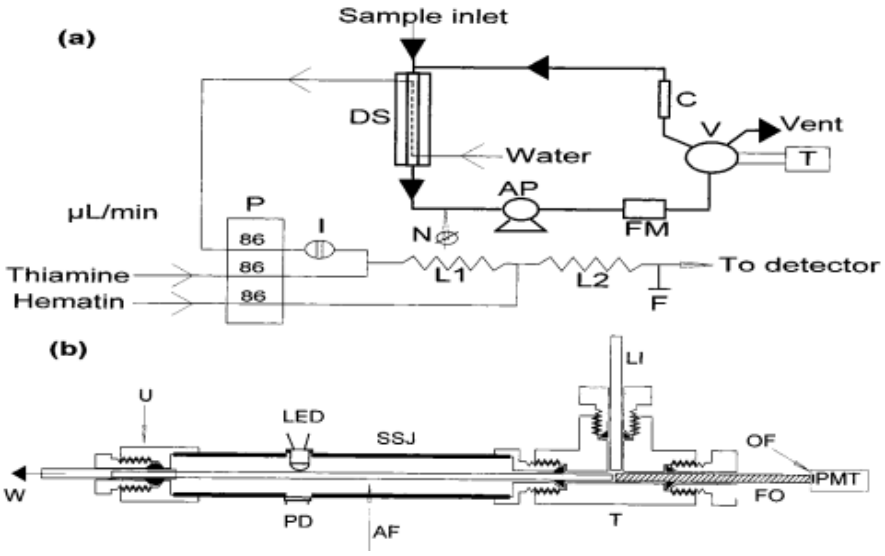

Figure 2- 68 (a) Instrument schematic. P, peristaltic pump; DS, diffusion scrubber; L1, thiamine mixing coil; L2, main reaction coil (thermostated at 30 °C); F, flush port (normally closed); AP, air aspiration pump; FM, flowmeter; N, 23-ga. hypodermic needle (supplementary flow); V, three-way solenoid valve controller by timer T; C, activated carbon column. (b) Detector schematic. Transversely illuminated fluorescence detector schematic. T: Entrance PEEK tee; LI: Liquid inlet; FO: Silica fiber optic; OF: Colored plastic optical filter; PMT: Miniature photomultiplier tube; AF: Teflon AF 2400 liquid core waveguide; SSJ: Stainless steel jacket, LED: 375 nm light source; PD: Photodiode for monitoring source light intensity; U: outlet union; W: waste. Reprinted from reference [139] by permission from the American Chemical Society.

In almost all DS-based instruments, the air inlet is modulated between the actual sample and zero (in the illustrated case, sample air from

which the analyte has been removed) except for airborne deployment where continuous response is essential. In the present case, the exhaust of the air pump AP is directed by timer(T) controlled 3-way valve V. During the sampling period, valve V directs the pump exhaust to vent. Note that needle N allows a small amount of ballast flow that the pump aspirates in addition to the flow through the DS inlet. When V switches to the other position the pump exhaust passes through purifier cartridge C that removes all analyte and this is fed to the DS inlet. As this flow is slightly larger than what the pump aspirates through the DS, the balance (equal to the ballast flow drawn through N) flows out through the inlet port. The detailed design of the thermostated NMDS is shown in Figure 2-69. DS is able to collect near-quantitative H_2O_2 for significant range of flowrates. The collection efficiency *f* varied from 98 to 88% from a flow rate (Q) of 0.78 to 2.94 L/min; ln (1- *f*) varies with 1/Q. The instrument was tested thoroughly for interference from SO_2, O_3, etc.

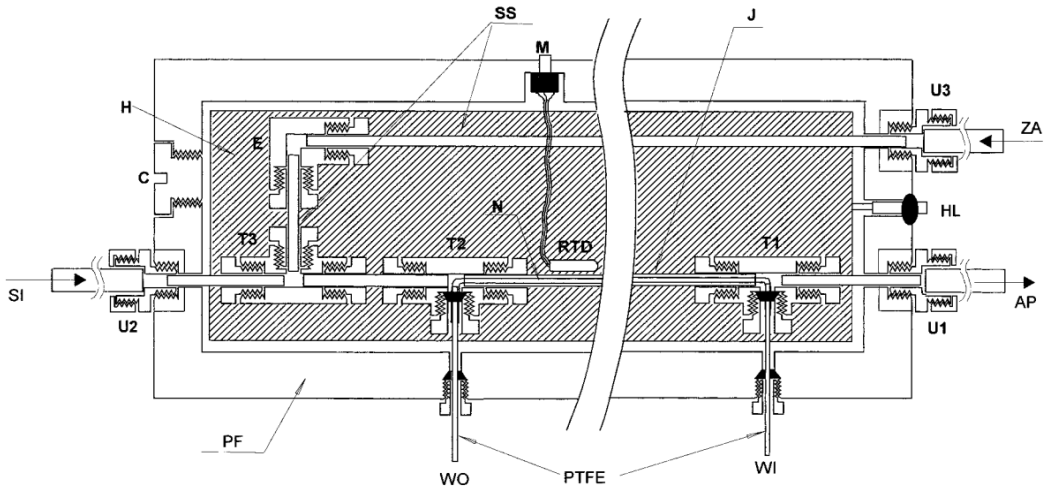

Figure 2- 69 Diffusion scrubber and housing. Key: U1, U2, U3, PVDF $^{1}/_{4}$-$^{1}/_{8}$-in. tubing union fittings; SI, sample inlet; ZA, zero air inlet; AP, to air pump; T1, T2, T3, PVDF tees; E, PVDF elbow; N, Nafion tube; J, PTFE jacket; SS, stainless steel tubes; WI/WO, water inlet/outlet (PTFE capillaries); RTD, platinum resistance thermometer connected to miniature three-wire jack M; PF, Plexiglas frame; C, filler cap; H, heater (top and bottom); HL, heater leads. Reprinted from reference [139] by permission from the American Chemical Society.

Li and Dasgupta [140] mixed the NMDS effluent with a solution of Co(II) and luminol, mixed in-line, inside a LCW chemiluminescence detector to achieve an LOD of 25 pptrv H_2O_2. Ozone interference was 0.5% on an equimolar basis; there was no interference from SO_2 and NO_2. The same authors explored visible absorbance detection based on the TiTPyP reaction [141]; the NMDS effluent was mixed with the strongly acidic TiTPyP reagent and allowed to react for 2.9 min before detection in a 50 mm path

LCW-based absorbance detection cell, using a 450 nm narrow bandpass filtered LED, the authors achieved an LOD of 26 pptrv H_2O_2.

Li et al. [142] described a novel automated continuous instrument for the simultaneous measurement of atmospheric hydrogen peroxide and MHP. A Nafion membrane diffusion scrubber (DS) was used with the hematin-thiamine reaction system was used to collect H_2O_2. An expanded PTFE based PMDS was used to collect both H_2O_2 and MHP but the collected H_2O_2 was catalytically destroyed before the MHP was measured by the peroxidase-thiamine chemistry. The respective limits of detection were 25 pptrv H_2O_2 and 15 pptrv MHP. A particularly innovative aspect of this work was the use of two independent LED source LCW based fluorescence detectors where both output fiber optics led to the same detector PMT. The LEDs were alternately pulsed on for 5 s and the baseline signals were deliberately offset – the software algorithm picked out the individual analytes (Figure 2-70).

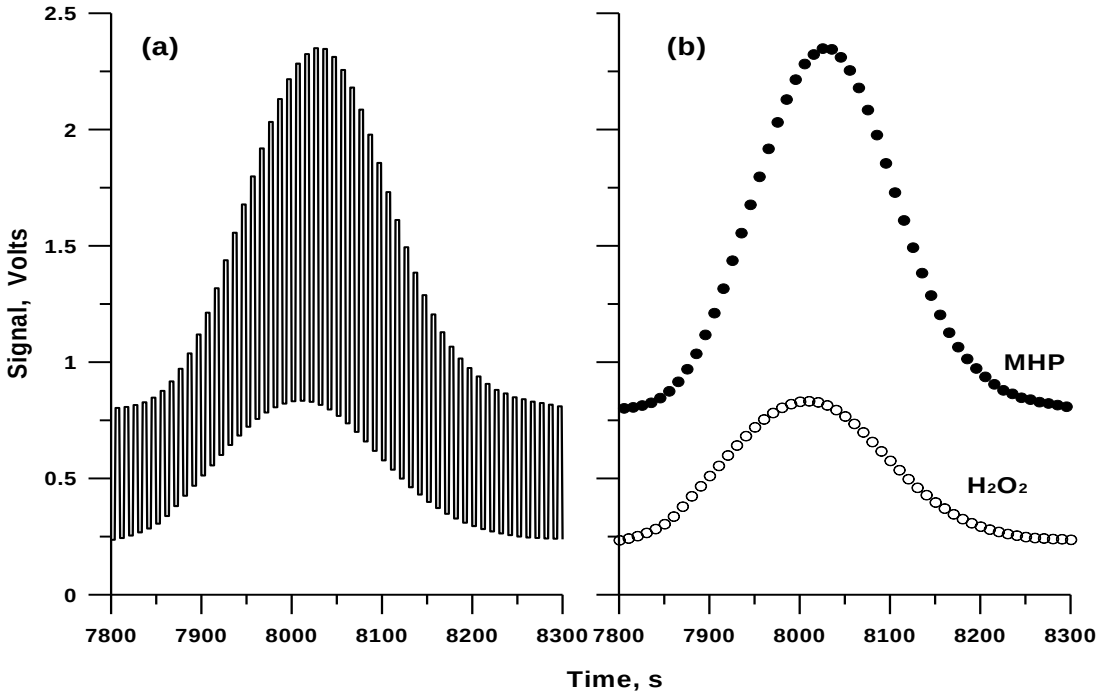

Figure 2- 70 Instrument response. (a) Raw composite PMT response. The sample contained 2.0 ppbv H_2O_2 and 3.4 ppbv MHP. The lower and upper envelopes of the composite trace constitute the individual signals for H_2O_2 and MHP, respectively. (b) Software-isolated signal for the two channels. Reprinted from reference [142] by permission from the American Chemical Society.

2.14.2.3. Hydrogen Sulfide

A sensitive method for the measurement of either hydrogen sulfide or mercaptans is the reaction with fluorescein mercuric acetate (FMA); the fluorescent reagent forms nonfluorescent products upon reaction with H_2S or thiols. The method is attractive also because facile excitation of FMA by a blue LED. Toda et al. [143] have shown that selective determination of gaseous H_2S over CH_3SH (or other mercaptans) is made possible because

H_2S can be collected by a NMDS but CH_3SH (and presumably other mercaptans) cannot, because of their greater hydrophobic nature. Measuring CH_3SH by difference is possible using a PMDS, which collects both analytes. Such a difference approach has obvious limitations if the H_2S concentration is much larger.

2.15. CEM-Based Evaporators/Concentrators

The proton loves to be hydrated; CEMs in the H^+-form have very high affinities for water. If the water activity outside is lower (as may be induced by dry/hot gas flow), the water in a solution flowing through the lumen of a CEM tube will also evaporate. This can be used for either preconcentration or postconcentration, but some caveats are in order. First, the water transport rate is very dependent on the ionic form of the CEM, conversion of the CEM into forms other than H^+ will reduce the rate of water transport. For this reason, such a device can only be used where all the analytes are in the acid form, e.g., between the suppressor and the detector in a suppressed anion chromatography system. Alternatively, if a sample is to be preconcentrated prior to injection, it must be converted to the acid form by running it through a suppressor first. The second caveat is that an anion may not pass through a CEM, but an un-ionized acid molecule may do so. Thus, there may be loss of some weak acids in molecular form, especially those with high vapor pressures at the operating temperature.

Takeuchi et al. [144] experimented with hollow and filament-filled CEM-tubes in various forms: a maze, as a filament filled helix, and in the filament-

filled serpentine-II configuration, in all cases a dry gas flow proceeding countercurrent on the outside with the entire device kept at an elevated temperature. The filament-filled helical and maze devices performed the best; the design of the maze device is shown in Figure 2-71. Figure 2-72 shows how the detector output changes as the column effluent is fed through an FFH type concentrator at different temperatures, plotted both in the conventional format with time as the abscissa or in terms of volumetric output. Many aspects of flow through a tubular concentrator are not intuitive. In laminar flow through a cylindrical tube, the radial velocity profile is parabolic, the velocity at the wall is zero. In the present case, there is a continuous net mass flux to the wall and the flow rate as well as the velocity continuously decreases along the tube axis. As such, a theoretical understanding of how the dispersion of an injected band (how is that defined here? Temporal? Volumetric?), resolution between adjacent bands (because the volume between them decreases as well) is affected by evaporation is not yet available. It is possible that a hybrid system, where the column effluent is gas-segmented prior to evaporation but degassed prior to detection can be advantageously used. Presently it is clear that simple evaporation can improve detection sensitivity, but temporal resolution may be adversely affected. Nevertheless, there are many situations where postcolumn concentrations can be of great value, especially for late-eluting broad peaks as shown in Figure 73(a) for the determination of environmental perchlorate [145].

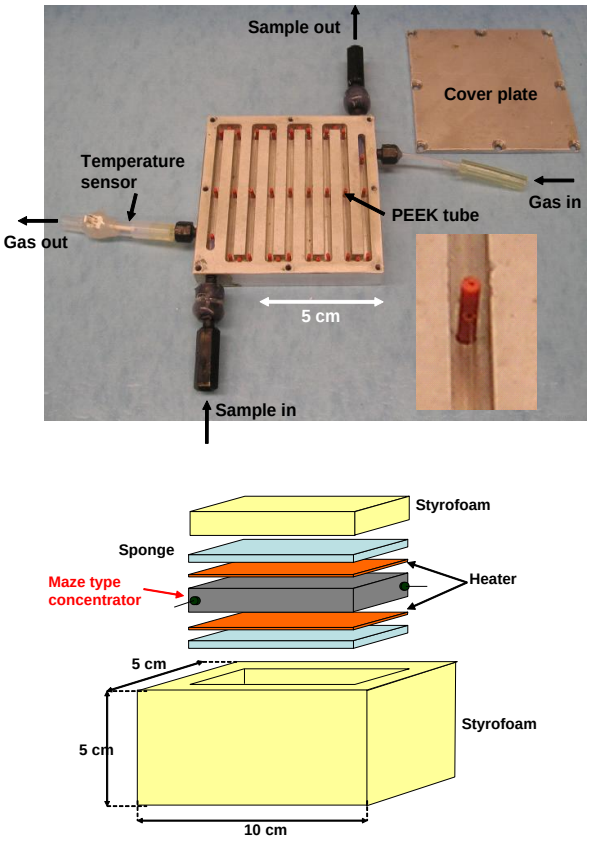

Figure 2- 71 Maze type device. PEEK tubing segments (red) are used as posts, cemented to appropriately drilled holes in the copper maze housing. The inset at the bottom right shows a Nafion tube threaded through a hole in the post. The assembly is sandwiched by siliconized flat heaters and placed inside an insulated enclosure.

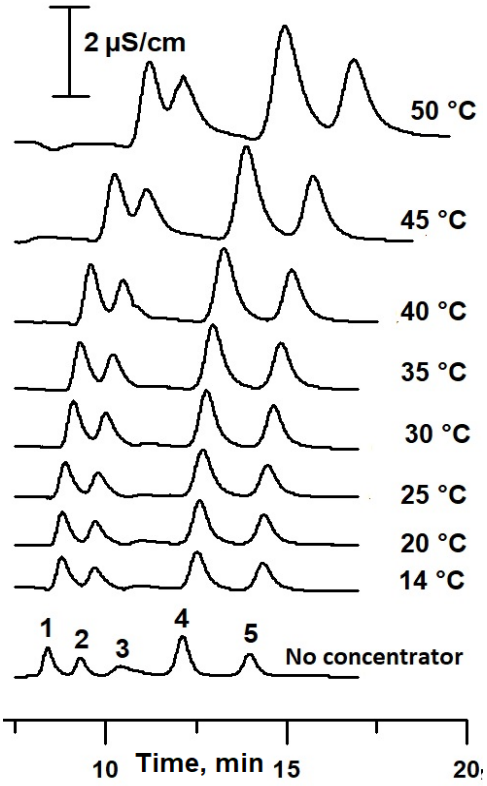
2 µS/cm
50 °C
45 °C
40 °C
35 °C
30 °C
25 °C
20 °C
14 °C
1
2
3
4
5
No concentrator
10
Time, min
15
20

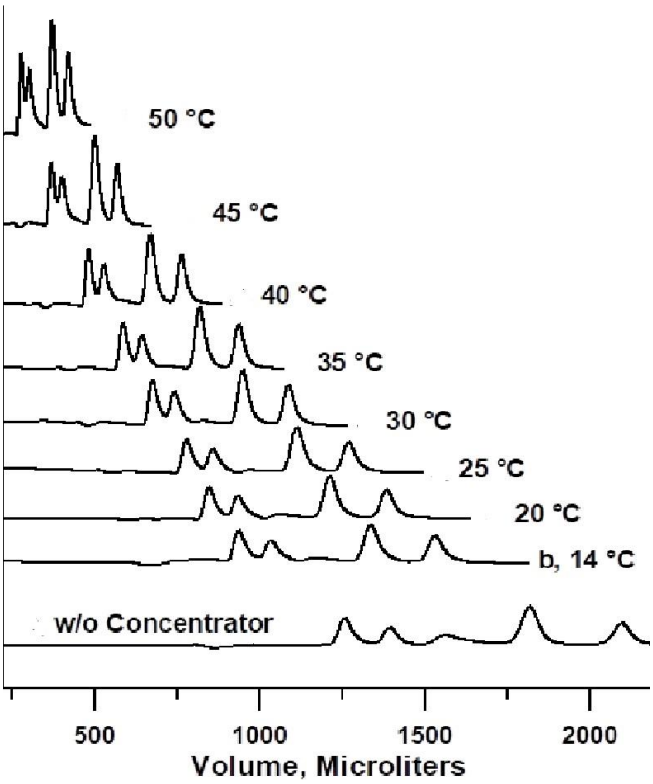
50 °C
45 °C
40 °C
35 °C
30 °C
25 °C
20 °C
b, 14 °C
w/o Concentrator
500
1000
1500
2000
Volume, Microliters

Figure 2- 72 Left: Chromatogram (conventional depiction with time as the X-axis) for postcolumn concentration with nylon filament-filled Nafion helix concentrator (229 μm i.d., 330 μm o.d., 127 μm dia. Filament, 62 cm long), chromatographic flow rate 150 μL/min, 5 SLPM N_2 drying gas at different exit temperatures. Peak identities: (1) chloride, (2) nitrite, (3) carbonate, (4) sulfate, (5) nitrate. Note disappearance of the carbonate peak with increasing temperature. Right: the same chromatogram is plotted with the liquid volume exiting the detector as the abscissa.

The problem of reduced resolution etc. does not appear in pre-injection evaporative concentration as demonstrated in Figure 2-73(b). The viability of the technique for practical determination of trace environmental perchlorate has been demonstrated by Takeuchi in unpublished work.

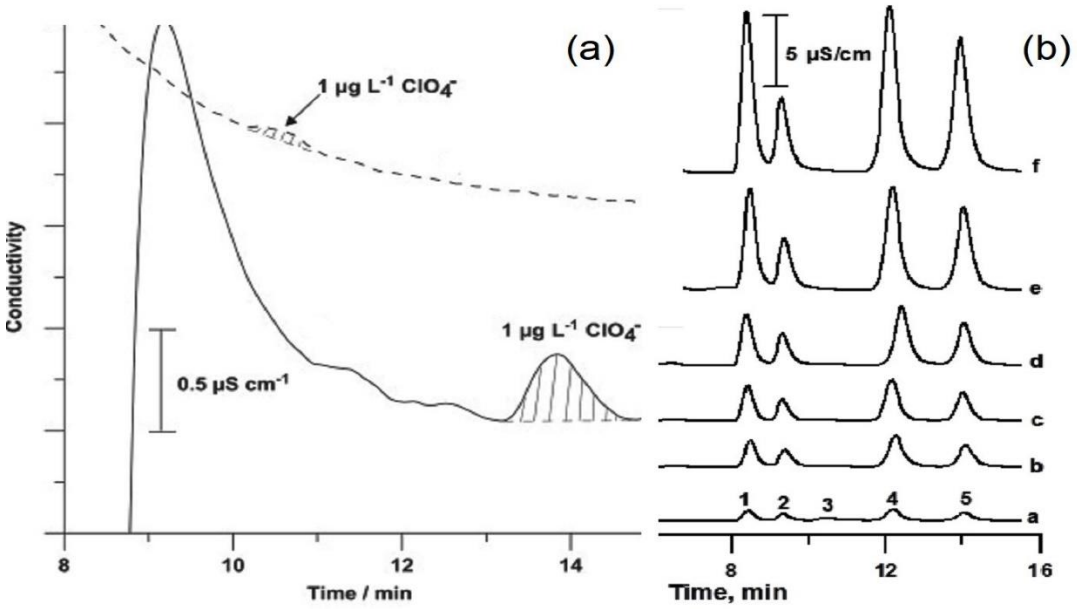

Figure 2- 73 (a) Chromatograms of 1 µg/L perchlorate sample with/without the post-column concentrator (solid line and dashed line, respectively). (b) Chromatogram of precolumn concentration with tubular Nafion IEM-based maze type concentrator at 5 SLPM of nitrogen, 60 °C. a) without concentrator, and with fixed volume loop injection, flow rates into the preconcentrator: b) 200 µL/min, c) 170 µL/min, d) 150 µL/min, e) 140 µL/min, f) 135 µL/min. 1) chloride, 2) nitrite, 3) carbonate, 4) sulfate, 5) nitrate.

2.16. CEM-Based Gas Dryers

Evaporation through the membrane is basically water transport along a water activity gradient. This can not only take place from a stream of liquid, water can be removed from a gas stream to dry it partially or completely for a variety of purposes. Dryers based on Nafion tubes (a parallel bundle of

tubes is often used) constitute a major commercial product [146]. A search for the keyword “Nafion Dryers” will elicit more than 5000 citations, a thorough review of this topic is beyond the scope of this article. Sadly, a review that explicitly covers this topic is not available albeit articles characterizing such dryers are available [147,148]. We can only cite a few specific papers and mention applications. Although there are many applications of these CEM-based dryers that have nothing to do with analytical chemistry (e.g., in space flight humidity control [149]), majority of applications are indeed in the analytical sciences. In many spectroscopic or even chromatographic measurements, variable amounts of water or just water in the sample, poses a problem.

Some illustrative applications include reduction of water loading effects is plasma-based analytical systems [150]; an IEM-based dryer usually performs much better than a chilled condenser desolvation system. The membrane dryer also acts as a pulse dampener for the plasma and thus improve the analytical performance of an ICP-MS system [151]. Similar gains are seen a microwave plasma torch atomic emission spectrometry [152]. It is of utility in removing moisture in cold vapor atomic absorption spectroscopy [153], in the sampling of various organosulfur compounds [154], for continuous use in spectroscopic monitoring of CO_2 and CH_4, etc. [155]. Some recent applications include fast drying for peroxy/hrdroperoxy radical determination using a large diameter Nafion dryer [156] or using it as the

amplification reactor itself [157], removing water and N-methyl-2-pyrrolidone from ionic liquids (ILs) [158], etc.

In this context it is useful to note that many IL-Nafion composites have been extensively investigated in the last 10 years [159,160], incorporation of organic cations dramatically changes the transport properties of Nafion [161] and these Nafion-IL cation composites, in combination with graphene, carbon nanotubes, etc. have become the basis for a whole class of new electrochemical sensors [162]. However, this is quite beyond the scope of this review.

The use of Nafion dryers need to be approached with some thought. It is sometimes forgotten that that small polar molecules (much as we have seen in the NMDS examples) will be transported readily though Nafion (the dryers represent nothing more than one or more GIS devices in parallel). That during the drying process through a Nafion dryer, di- and tri-methylarsines are completely lost after hydride generation and prior to measurement by atomic spectroscopy [163], or losses of certain hydrocarbons occur prior to gas chromatography [164] should not appear as surprises. It is also a strongly acidic surface, often the agent causing acid-catalyzed rearrangement of certain analyte molecules during passage through a Nafion dryer [164,165]

2.17. Water/Humidity Sensors Based On High Water Affinity of CEMs

The affinity of CEMs for water has been harnessed in many ways. Perfluorocarbon-based CEMs are much more stable than hydrocarbons. The fluorescence behavior of many fluorophores depends on the water activity surrounding them. The first humidity sensor to exploit this was reported in 1987; it monitored the change in the fluorescence lifetime of Rhodamine 6G (R6G) in Nafion, with a detailed account appearing in 1989 where the change in fluorescence intensity was the measurand [166]. Almost two decades later, the same measurement system was used to monitor the water content of CEMs in fuel cells [167]; these authors used the ratio of fluorescence intensity at two wavelengths. Several dyes with N-phenyl groups sorbed on Nafion were investigated by Sadaoka et al. [168] using the absorbance change as a measure of relative humidity (RH). One of these dyes, crystal violet, was further studied in detail by Raimundo and Narayanaswamy [169]; a methanol-treated, 5 μm thickness film with a Nafion:crystal violet molar ratio of 10:1 showed a linear response range from 30 to 70% relative humidity, with good stability and reversibility. The plasmon resonance wavelength change was the measurand in a surface plasmon waveguide sensor that was studied over a humidity range of 20-50% RH [170].

For most sensors, a direct electrical transducer is preferred. Huang [171] at the National Bureau of Standards was the first to examine fluorinated

CEMs as RH sensors. Specifically, he used a sensing film that contained a mixture of both perfluorocarboxylate and perfluorosulfonate polymers with approximately equal amounts of each types of functional groups present on the film. His work also provided a comprehensive survey of RH sensors based on organic films until then and their shortcomings. Huang measured the conductance of the sensors (film thickness 100 μm) at 10 kHz and his specific domain of interest was high RH levels (~>40%) at high temperatures (up to 90 °C). as shown in Figure 2-74. The results show low hysteresis (2%) and high sensitivity for the sensor; a similar humidity span elicited an order of magnitude lower response span for non-fluorinated CEM sensors. Another relatively early paper [172] also proposed Nafion on porous glass as a conductometric RH sensor.

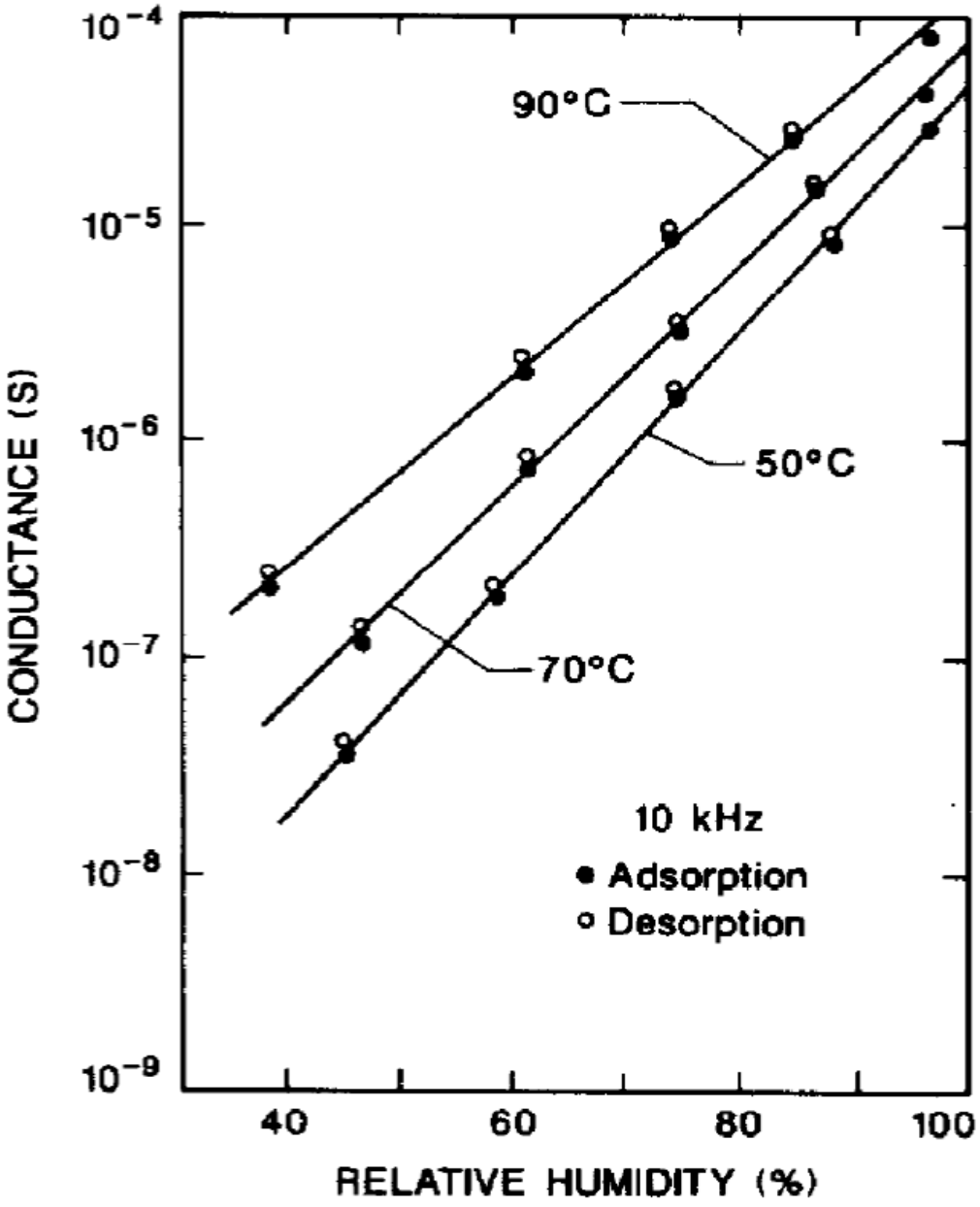

Figure 2- 74 Adsorption and desorption isotherms for response of the sensor. Reprinted from reference [171] by permission from Elsevier.com. Each experimental point is an average value of four adsorption or desorption cycles. Note logarithmic ordinate.

CEM-based humidity sensor behavior has mostly been studied with the IEM in the H^+-form. Wang et al [173] studied the conductometric behavior of H^+-, Li^+- and Na^+- form Nafion to variations in RH, casting thin films on interdigitated electrodes on an alumina substrate (Figure 2-75). The impedance changes of the sensing films as a function of RH are shown in Figure 2-76. In Li^+-form, the film showed the lowest impedance. In the Li^+-form, it also had enough resolution down to 10% RH, that for the other forms were lost at a higher RH, making them of limited value to perform low RH measurements. The authors explained their results on the basis that the hydration status of the Li^+ ion in the polymer matrix most affected the film conductance. The same group examined impedance response of Nafion and sol-gel derived SiO_2 – Nafion composite films *(approximate mass ratio 3:1) on similar interdigitated electrode platforms for RH measurement [174].* This paper was mostly focused on understanding the complex impedance behavior of the different sensors. In terms of performance, the SiO_2-Nafion composite films are an order of magnitude less sensitive than an equivalent Nafion IEM-based sensor but exhibits much better linearity.

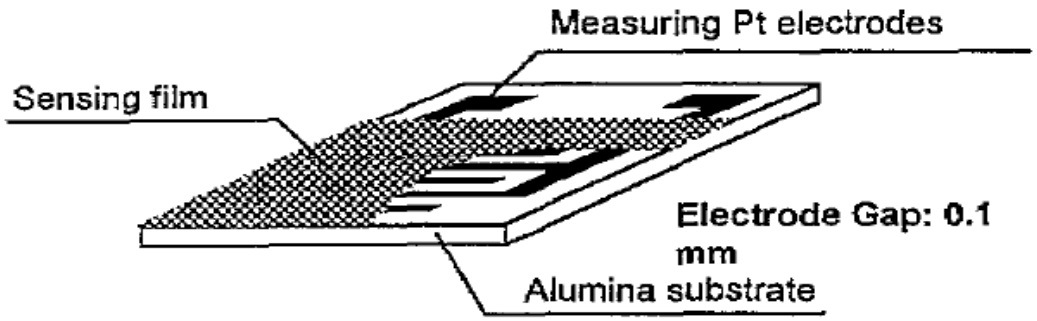

Figure 2- 75 Schematic view of sensor construction. Reprinted from Reference [173] by permission from Elsevier.com.

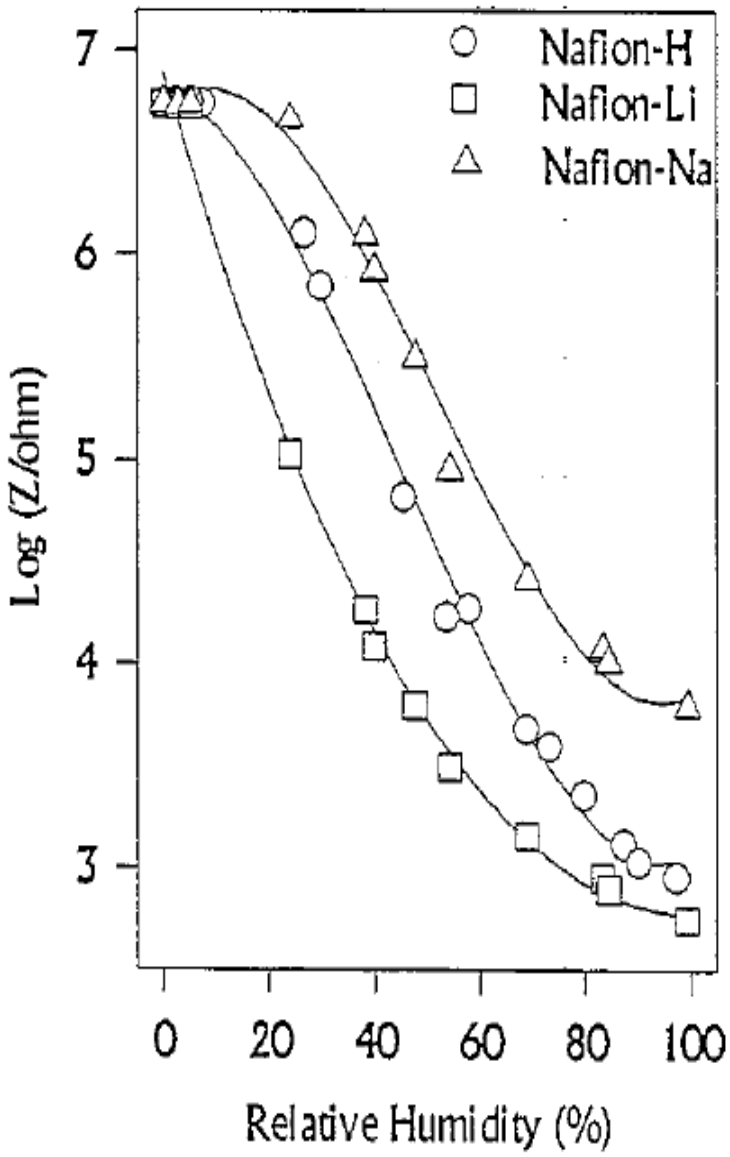

Figure 2- 76 Impedance responses (1 V, 1 kHz) of different ionic forms of Nafion to varying RH. Reprinted from Reference [173] by permission from Elsevier.com.

Amperometric or coulometric sensors for water relying on its electrolytic decomposition was introduced by Keidel some 6 decades ago [175]. These are still in commercial use for measurement of trace water in the gas phase. Platinum or rhodium wires are wound on closely spaced twin

threads on an inert substrate and serve as electrodes, as much as 45 VDC is applied across them. The sensor is dipped in concentrated phosphoric acid and put inside a flow cell. While being flushed with a dry gas, the full DC voltage is applied. The applied voltage is capable of extracting water from H_3PO_4, electrolyzing it and converting the H_3PO_4 to HPO_3 and thence partly to P_2O_5 (hence the name P_2O_5 sensor, although it is likely the ultimate state reached is somewhere between HPO_3 and P_2O_5). Long as gas sample flow rate over the sensor is not excessive, it will capture all the water present in the gas stream, and this will be electrolyzed to H_2 and O_2. Under these conditions, the sensor behaves as an absolute coulometric sensor for water. At high water levels (≥1000 ppm), it is better not to attempt to electrolyze all the water but apply a lower potential and use it as an amperometric sensor and calibrate it for such use. Huang and Dasgupta [176] used this principle to construct their Nafion-based amperometric sensor, where a DC potential is applied and the sorbed water is electrolyzed. They described a probe-type and a flow-through type sensor (Figure 2-77). In the former, A platinum wire, insulated by a tubular PTFE sleeve, is inserted inside a blunt-ended hypodermic needle, each snugly fitting into the other. A small amount (~3 μL) of an alcoholic colloidal solution of Nafion or a structurally similar perfluorosulfonate ionomer (both generically called PFSI) is deposited at the tip of the needle and allowed to cure 4-12h @ 70-100 °C. The flow-through configuration utilizes a 3 mm i.d. flexible wall polymer tube. Two platinum wires (25-50 μm dia.), very close to, but not touching each other,

are placed in the lumen of the tube, radially passing through the tube (inserted through a fine hypodermic needle, which is then removed). A small amount (2-5 μL) of the PFSI solution is put on the pair of wires, allow to dry into a film and then thermally cured. Two other sensors, briefly reported on, used interdigitated rhodium film electrodes on alumina, similar to Figure 2-75 and twin rhodium wires wound on a ceramic substrate (similar to the Keidel geometry [175]), both dip-coated with PFSI solution and thermally cured.

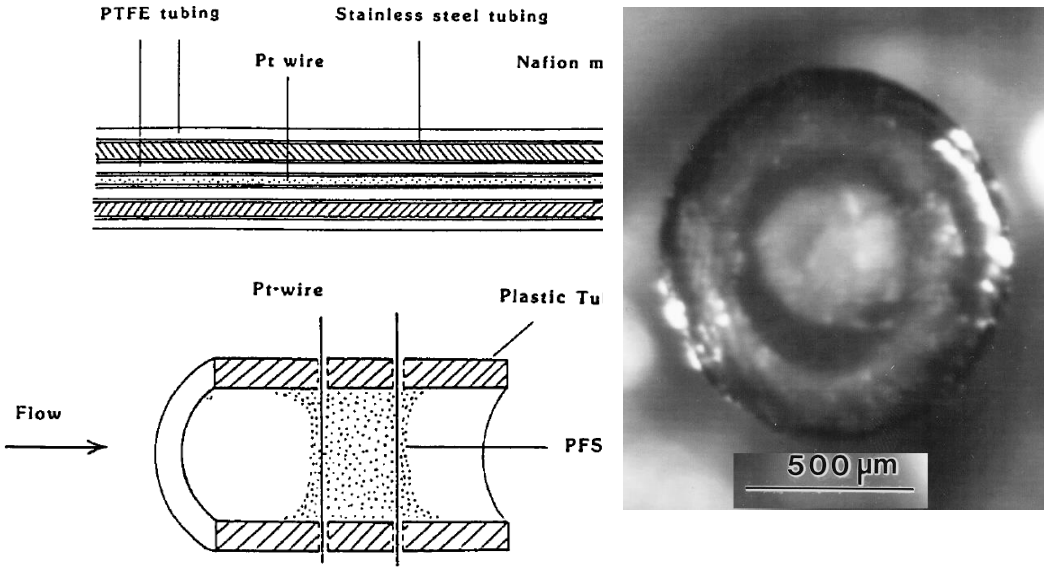

Figure 2- 77 Needle-based probe type sensori) (left top). Flow-through sensor (left bottom). Reprinted from Reference [176] by permission from the American Chemical Society. Right: microphotograph of tip of probe-type sensor.

Predictably the sensor response increased with the amount of polymer deposited on the sensor electrodes but at the expense of sensor response time (especially the rise time). The Dow PFSI was available in a variety of equivalent weights, for the same mass of the sensing film, response increased with decreasing equivalent weight, but higher equivalent weight sensors showed better long-term stability. Some sensors were made with multiple layers of the different PFSI; it was generally found that the lower measurement limit was controlled by the component with the highest affinity for water. Very low moisture levels are typically specified as ppm water or the corresponding dew point temperature rather than in terms of % RH. As a reference point, 0 to 5% RH at 25 °C corresponds approximately to gas-phase concentrations of 0-1500 parts per million by volume (ppmv). Based on a preliminary assessment of reproducibility data the authors estimated the lower measurement limit of the needle sensor to be ~130 ppmv H_2O (dew point of ~-40 °C) and that for the interdigitated microsensor to be ~20 ppmv H_2O (dew point of ~-55 °C). These sensors had significant film thickness; the best case 90-10% response time was of the order of 5 s, the 10-90% rise time was much more dependent on the applied voltage and approached the best case fall time values. As a benchmark, these were much better than leading commercial sensors as demonstrated in Figure 2-78.

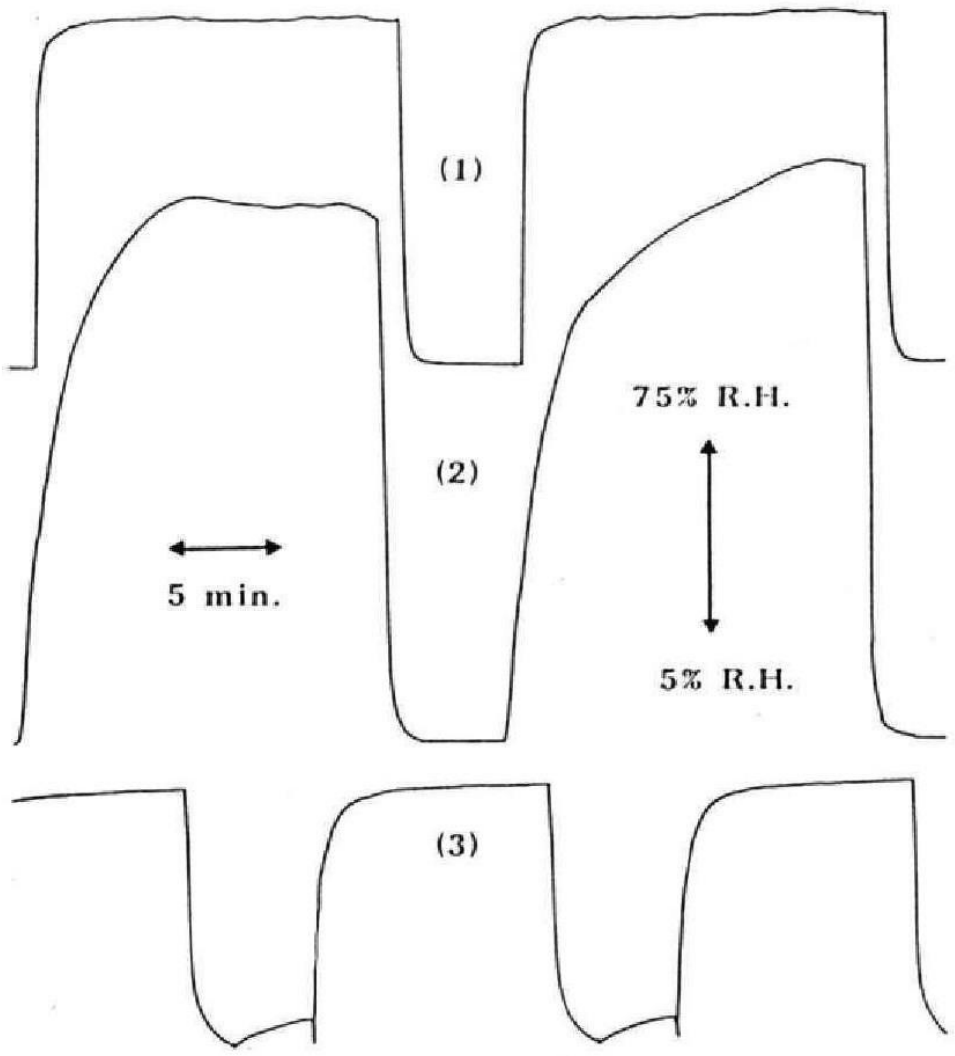

Figure 2- 78 Response behavior of (1) the needle type CEM-based amperometric sensor compared to (2) an ac impedance type sensor based on a quaternary ammonium functionalized polymer and (3) a capacitive sensor based on a hydrophilic polymer film, over a 5-75% RH test swing. Both comparison sensors were commercial. Reprinted from reference [176] by permission from the American Chemical Society.

Sensor 2 had a rise time ≥ 5 min and although sensor 3 was somewhat better at 1.5 min, that for the CEM-based amperometric sensor (sensor 1) was <20 s. Moreover, the sensor 2 exhibited poor long-term precision and sensor 3 exhibited significant hysteresis. The amperometric sensor responds to compounds that both (a) partition to the PFSI film *and* (b) are electroactive. Polar compounds like diethyl ether, dichloromethane or acids such as acetic acid or formic acids produces very little amperometric response because either they do not significantly partition to the PFSI film or are not electroactive (the sensor is 2700, 3100, and 8800x more selective for water than formic acid, acetic acid, and acetone). However, electroactive polar neutrals such as alcohols and other compounds such as formaldehyde etc. show significant response. For the homologous alcohols, e.g., methanol, ethanol, 2-propanol, 1-propanol and 1-butanol, the area response ratios relative to water were 0.096, 0.11, 0.04, 0.08 and 0.07, respectively. Lower methanol response compared to ethanol comes from a lower partition coefficient. Otherwise, the response decreases with increasing chain length of n-alcohols; making the sensor an effective detector of water or lower alcohols. Gas chromatographic detection application was shown. Water in nonresponding matrices like benzene can be determined at low ppm (w/w) levels readily by direct injection. The concern of ammonia or volatile amines poisoning the cation exchange sites proved unfounded: the protonated species migrate to the cathode and are eliminated as the free base by the water-generated

hydroxide. As a gas chromatographic sensor, the LOD of the sensor was estimated to be $\leq$ 10 ng H_2O /s.

Su et al [177] took the amperometric moisture sensor one significant step forward by microfabricating multiple sensors on a single 0.75 mm thick silicon wafer. Each individual sensor was contained within a 3x5 mm area and contained 50 μm wide, 2 mm long metal electrodes with varied spacing of 50-200 μm. The metal electrodes were gold with a Ti underlayer. After covering the intended bonding pad region, the wafer was spin-coated with PFSI solution @4000 rpm and flash-cured at 120 °C for 60 s. The resulting film thickness, measured by two independent techniques, ranged between 170 and 200 nm. After removal of tape and dicing, individual sensors were put in TO-5 packages and wire-bonded. The effort to make very thin film sensors was inspired by a desire to make fast responding sensors. Water shows sorption-desorption behavior on most surfaces and any measurement of response time of a fast-responding sensor may actually reflect the time for water sorption/desorption on the line leading to the sensor. To avoid this situation, the test arrangement had dry N_2 and controlled RH streams arriving at the sensor through independent valved conduits. The switchable valves (on/off) have response times of 10-15 ms. Sensor response under these conditions is shown in Figure 2-79. The two leftmost traces show the rise and fall profiles (0–75% RH swing at ambient temperature) on an expanded time scale, while the central panel shows repeated response cycles (reproducibility 0.36% RSD, n=5), all foregoing at

room temperature. The rightmost trace shows the sensor temporal fall profile in an expanded time scale at 66 °C. The rise time for the sensors is typically 50–100 ms while the fall time is as little as 20–30 ms, the latter being even lower at an elevated temperature. As may be expected, increased film thickness increases response time while increased temperature decreases response time. Doubling the film thickness from ~200 to ~400 nm results in a ~25% increase in both the rise and fall times. Fall times are always substantially shorter than rise times for this type of sensor than the rise times. During the sorption event (signal rising) both mass transfer at the air-film interface and diffusion through the film is involved whereas only the diffusion through the film is involved in determining the fall time.

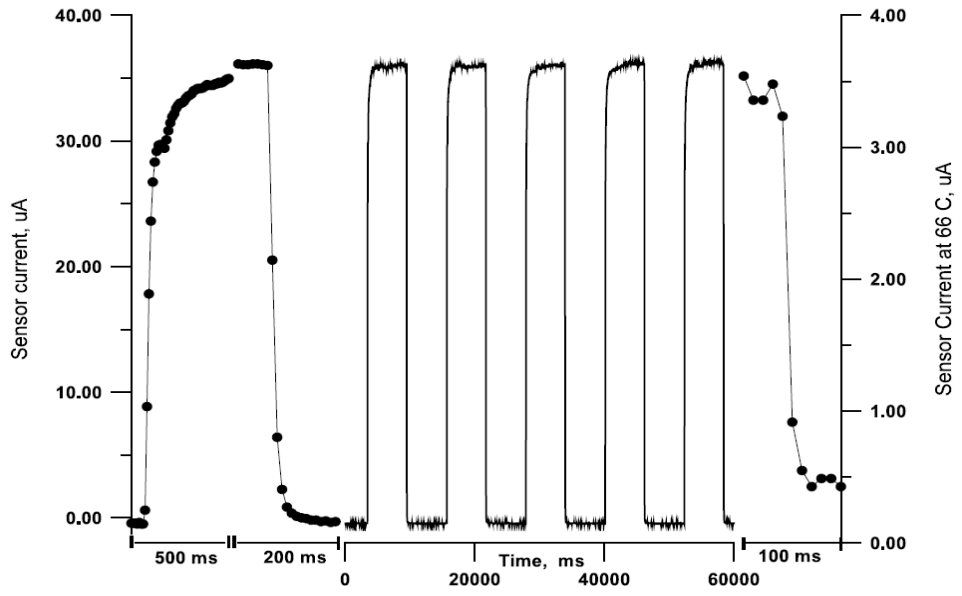

Figure 2- 79 Sensor response time : see text for details. Reprinted from Reference [177] by permission from Elsevier.com.

If we consider the fall time only for the moment, from the known diffusion coefficient of water in Nafion, one can compute the characteristic time for diffusion through a 200 nm thickness to be 150 μs, far less than the observed response times. This suggests that electrode processes and kinetics (double layer charging etc.) and capacitive effects probably play a highly significant role in determining response time: further significant gains in response speed are not likely to be realized with incrementally thinner films. Additional proof of this is provided by response profiles at elevated temperatures. The rise time is only marginally affected by an increase in the temperature (the constraints of interfacial mass transfer at the film/air interface remains the limiting factor) while the fall time drops to less than 10 ms at 66 °C, too great a decrease than can be expected on the basis of the known temperature dependence of the diffusion coefficient of water in Nafion, suggesting that a major drop in capacitive effects occur (note that total water retained in the film and which contributes to the capacitance, decreases exponentially with temperature).

This remains the fastest responding sensor reported for water and thereby provides some interesting applications. Breathing monitors in critical care applications typically involve inserting a cannula into each nostril and sampling a small flow of air through these into a spectrometric CO_2 monitor (via a CEM-based dryer!). Figure 2-80 shows the response of one of the microfabricated moisture sensors above, connected in series with a resistor and a 9 V battery, the voltage drop across the resistor was

monitored. It is obvious that the sensor faithfully responds to the greater humidity of the exhaled air and even the structure of a single exhalation event can be monitored.

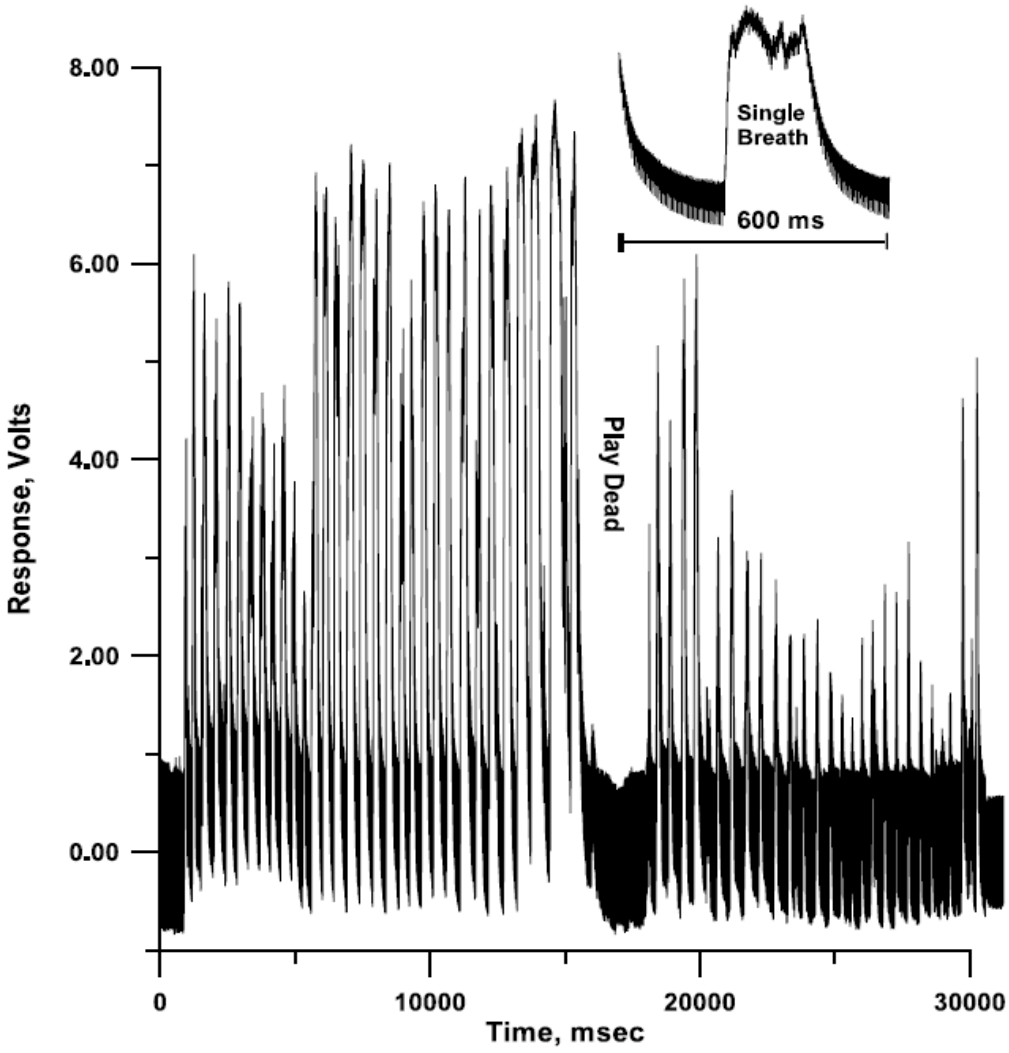

Figure 2- 80 Response of sensor placed near a nostril. See text for details. Reprinted from Reference [177] by permission from Elsevier.com.

Electrode material choice for the microfabricated sensors above was not ideal, however. Gold is not inert at the voltages used and is oxidized. It

is possible to operate the gold electrode-based sensors with low amplitude (±1 V) square wave excitation over long periods but the response speed is sacrificed. Of noble metals, rhodium is the most resistant to electroinduced oxidation but crack-free rhodium plating is difficult. Kuban et al. [178] made similar microfabricated electrodes but made a crack-free 1 μm thick Rh coating on the gold underlay with pulsed plating techniques. These sensors tolerated significant applied voltage and even 2-2.5 V DC applied voltages provided 30-50 ms 10↔90% rise and fall times; these sensors were tested to be stable over 3 months and may well be stable indefinitely.

Another sensor that was described about the same time as the above Rh-electrode based amperometric sensors used Na^+-, K^+-, and Ca^{2+}- form Nafion as the sensing film in a field effect transistor [179]. In the abstract, the authors stated the sensor response was “RH dependent over the range of 12 ±93% RH with msec response time”; but no actual data or discussion on response time appeared further.

Many efforts have been made to put additives to the Nafion film, particularly with a view to extend the range of Nafion-based sensors to lower humidities, to measure moisture at low ppmv levels. Huang and Dasgupta [180] combined H_3PO_4 with PFSI; it was possible to form a stable film at PFSI:H_3PO_4 ratios of ≥5:1. Both needle and interdigitated electrodes-on-wafer type sensors were studied; results here pertain to the needle type sensor based on a 100 μm dia. central Pt wire electrode. The 18 ga. Needle tip was coated with 2-μL aliquot of the PFSI-H_3PO_4 solution (in 50% ethanol)

and dried for 2 h at 70 °C, this process was repeated twice more. Being exposed to constant humidity for 2-3 h while subjected to the operational voltage was sufficient for the sensor to reach a stable steady state and provide reproducible response to varying RH. This contrasts with a standard "P_2O_5" sensor that takes days to come to an operational state, sometimes weeks. Study of the sensor in very low humidity such as 0-100 ppmv moisture (0-0.3% RH at 25 °C) showed that incorporating the H_3PO_4/P_2O_5 in the PFSI makes the sensor much more sensitive at low RH levels: a 10:1 PFSI: H_3PO_4 film produces almost 100x more current at V_{app} = 15 V at these moisture levels compared to a pure PFSI film. The authors tested a wafer-type sensor continuously for 3 months to evaluate performance at low moisture levels (0-1200 ppm) with special emphasis on the 2-150 ppm range (approximately -70 to -40 °C in dew point) with V_{app} = 15 V. the results are shown in Figure 2-81. The moisture levels reported on the abscissa comes from a chilled mirror hygrometer as benchmark. The moisture input variations were carried out in a random order and no corrections were made for laboratory temperature variations. For the results shown in Figure 2-81, the uncertainty of the reference instrument need also be considered. In this moisture regime, the measured current levels show a log-log relationship with the moisture content. Although the authors experimented only down to 2 ppm moisture, given that the current steeply increased with applied voltage, it was believed that sub-ppm moisture levels should be measurable with a higher V_{app}.

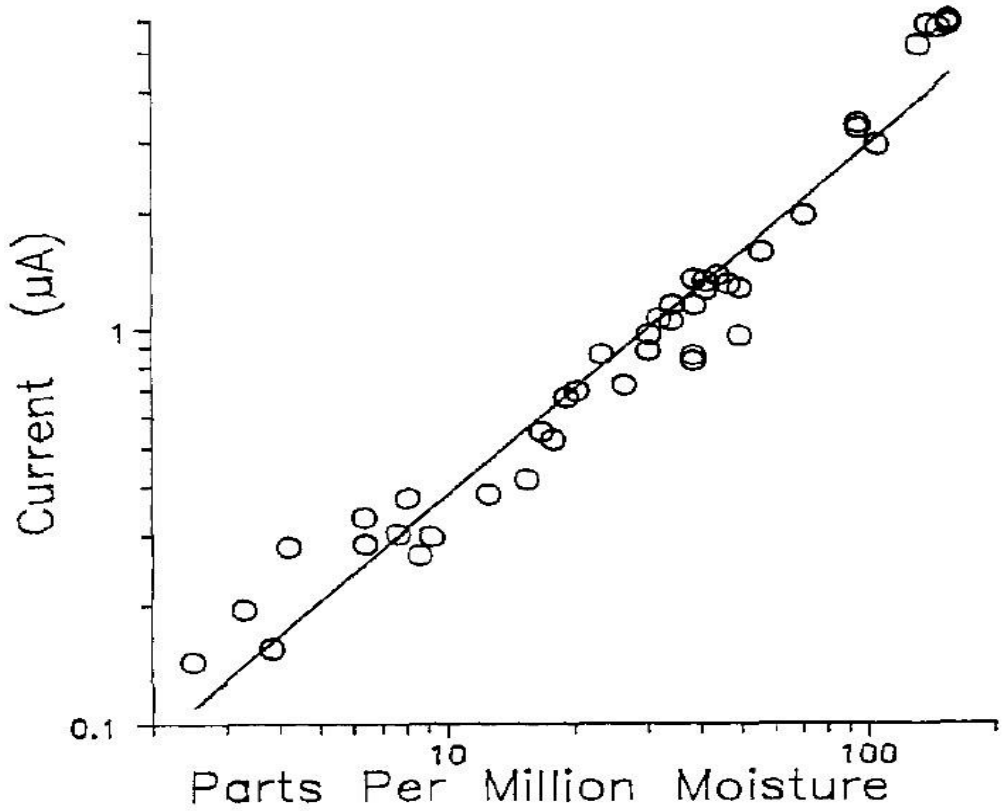

Figure 2- 81 Logarithmic plot of low-level moisture content vs sensor current for a 5:1 PFSI:H_3PO_4 film wafer sensor. Reprinted from reference [180] by permission from the American Chemical Society.

A "P_2O_5" sensor cannot tolerate high moisture surges: a large surge of water for any significant period makes the moisture-sensitive coating into liquid H_3PO_4 which can take on water beyond the 85% H_3PO_4 composition because the speed of electrolysis cannot keep up. Liquid can then drop off the sensor. In remarkable contrast, a PFSI:H_3PO_4 composite sensor can undergo prolonged exposure to very high humidity without any adverse effects. A 5:1 film sensor was placed in a $Mg(ClO_4)_2$-dried N_2 stream flowing through a pair of three-way valves. By activating the valves for very short

periods (0-5 s), it was possible to admit a flow stream containing 3400 ppm moisture. At the operative flow rate (20 mL/min), ~0.8 µg of water was introduced per s valve on-time. The response of the sensor (100-V DC applied) is shown in Figure 2-82. The sensor was then exposed to an atmosphere of 95% RH (~30,000 ppm) and the above experiment repeated immediately thereafter. It is obvious from the data in Figure 2-82 that not only is there no irreversible effect from prolonged exposure to a highly humid atmosphere, but the response also remains unaltered.

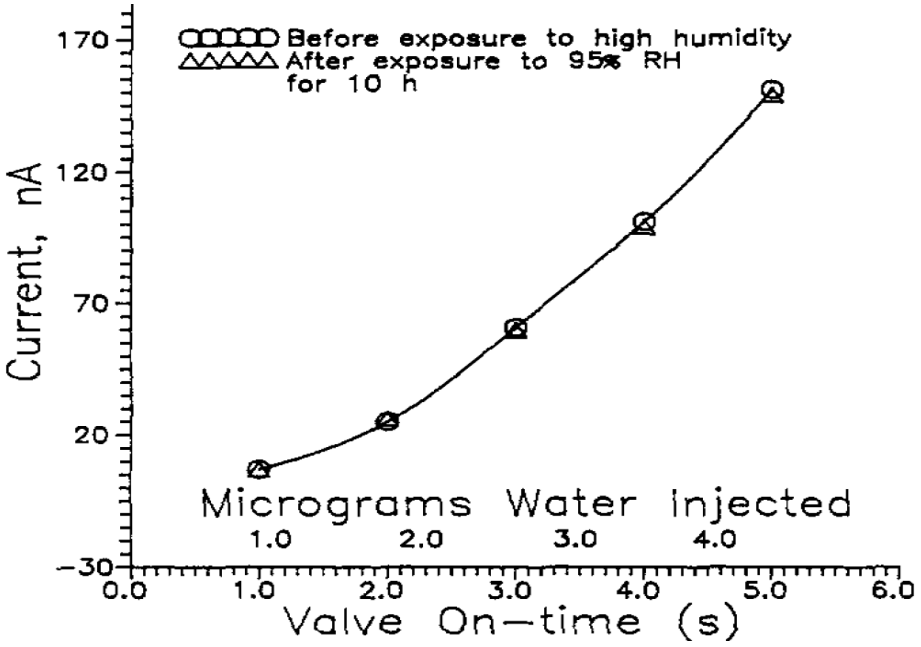

Figure 2- 82 Immunity of hybrid film sensor response to exposures to very high moisture levels over extended period. Reprinted from reference [180] by permission from the American Chemical Society.

In 2005, Chen at al. [181] incorporated 0.5-4% carbon nanotubes (CNT) in Nafion to make films on a quartz crystal microbalance (QCMM). A

composition containing 4% CNT provided optimum response and using a chilled mirror hygrometer as a reference sensor, an LOD of ~16 ppm H_2O was established. The resonant frequency of a QCMM decreases as the film sorbs water and thus gathers more mass; the marked improvement upon incorporating CNT in Nafion can be seen in Figure 2-83.

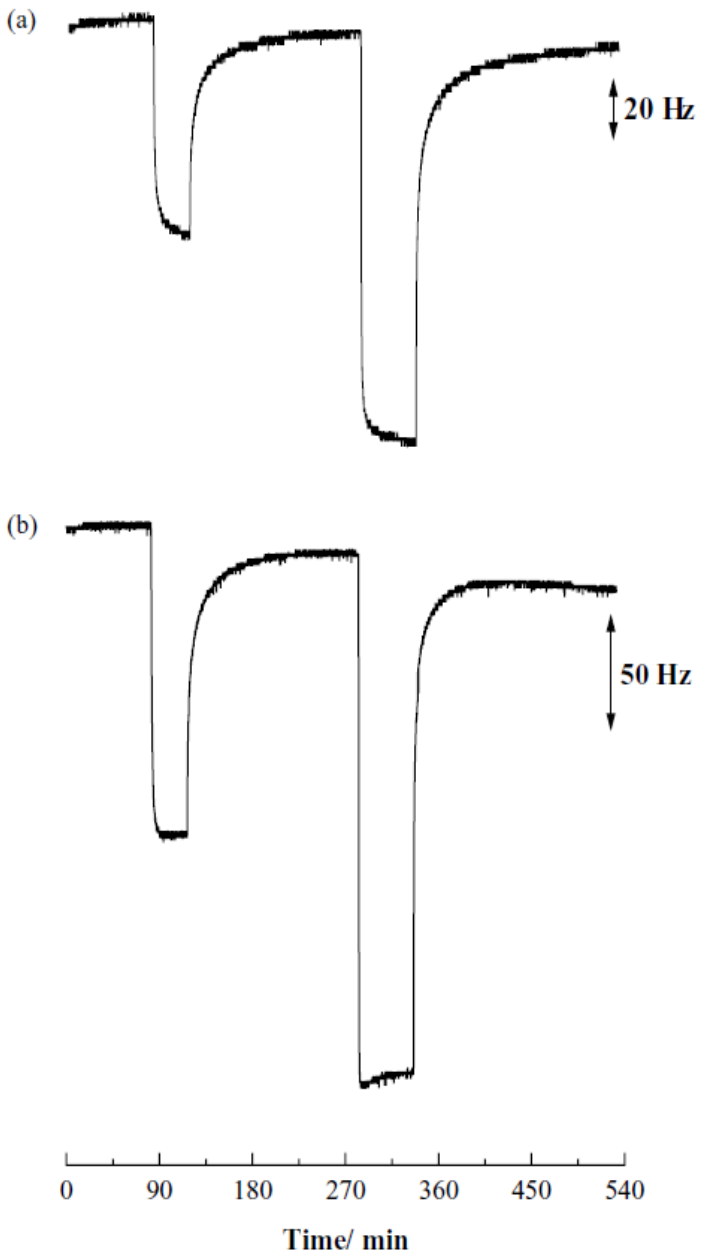

Figure 2- 83 Effect of adding CNT on the sensitivity of humidity sensing for water vapor content of 178 and 308 ppmv (a) without CNT and (b) with 4 wt.% CNT.

The same group later compared the behavior of single-walled CNTs vs. multiwalled CNTs using the same QCMM platform [182]. There was a

significant increase in the sensitivity in going from single-walled to multiwalled CNTs but the LOD improved only marginally from ~16 to ~14 ppm H_2O; the response time increased significantly in the process (5 s to 23 s) as well. About the same time, Wu et al. [183] reported the behavior of TiO_2-Nafion composites as impedance-based sensors for RH. It is not clear that this composite has any benefits over unmodified Nafion. The multiwalled CNT-Nafion composite has since been deposited on a surface acoustic wave resonator as an electrospun film, the authors did not conduct low humidity experiments (<10% RH) [184]. The linearity above 10% RH was good ($r^2 \geq 0.98$) with a reasonable response time (3 s).

2.17.1. CEM-Based Moisture Sensors for Use in Liquids

Water sensors for use in liquids are mostly capacitive, typically based on a nanoporous hydrophilic substrate like alumina with an affinity for water. Selectivity is made possible by controlled ingress: if the pores are small enough, water is the only relevant molecule that can enter. PFSI thin-film sensors of the type used in the gas phase cannot usually be used in solution because of solvent swelling, electrode poisoning by adventitious impurities, etc. In addition, in many solvents, voltages that would be applied to the gas phase moisture sensors are high enough to cause problems with high background currents, even in the absence of moisture. Huang and Dasgupta [185] explored hydrophilic cross-linked polymers, polyvinyl alcohol (PVA)-H_3PO_4 or PVA-PFSI-H_3PO_4 with pulsed applied voltage so that the consumption of water at the electrodes during the pulses will be mitigated

by diffusive transfer from the bulk to improve the sensor sensitivity. The authors reported on two basic sensor geometries, one was a direct adaptation of the Keidel P_2O_5 sensor where closely spaced Rh or Pt-wires are twin-threaded on an inert substrate and the other involved a stainless steel rod covered with a Nafion tube and then having a Pt-wire tightly wound on it as a coil. In both cases, the sensing polymer was formed by dip-coating and thermally curing at 120 °C. In some cases, e.g., with acetone, a protective overcoat of a cellulose triacetate film of controlled porosity was used as well. The sensor geometries are referred to as cylinder and coil, respectively. all experiments were conducted in a glove box with a gas phase moisture content well below 100 ppmv. The PVA-H_3PO_4-PFSI was applicable to a wide variety of solvents, ranging from a highly nonpolar solvent such as hexane to polar solvents like acetone or acetonitrile. For the same mass concentration of water, water activity is higher in less polar solvents, leading to higher sensor response as shown in Figure 2-84. Many solvents cannot be dried to a zero-moisture level; standard addition is therefore the only viable way to measure water content of the original solvent as the response to the solvent matrix may not be zero. This would be most evident for diethyl ether in Figure 2-84.

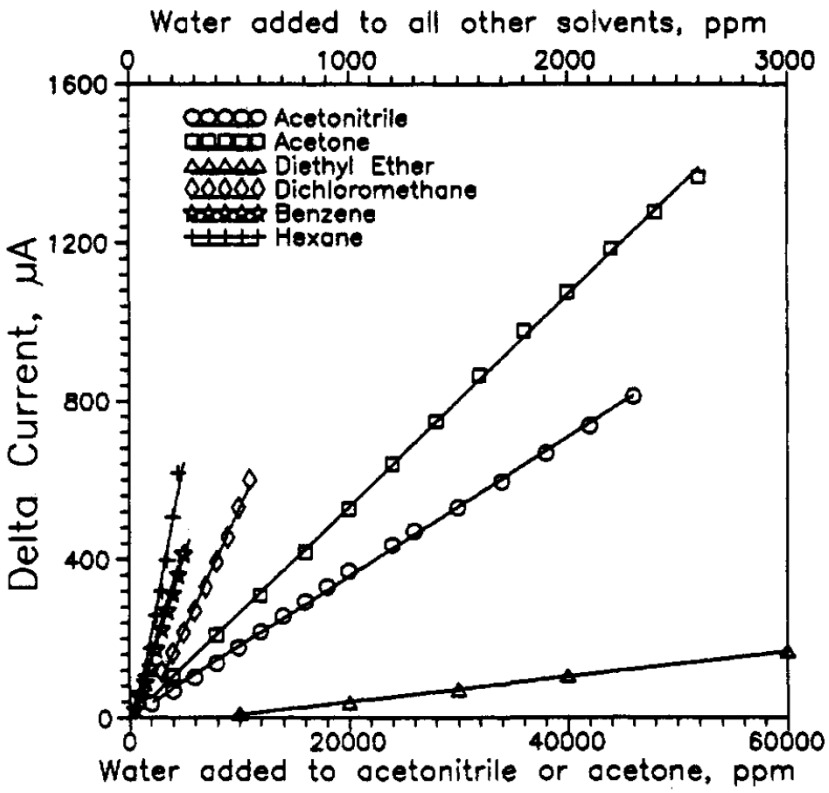

Figure 2- 84 Response of a PVA-H_3PO_4-PFSI sensor to water in various solvents. Scan -0.5 to 4.0 V at 3 V/s. The cylindrical sensor used in this work utilized 50-µm Pt electrodes with 400-µm spacing, an 8-µm film of Nafion overcoated with the PVA-H_3PO_4-PFSI composite membrane. Reprinted from reference [185] by permission from the American Chemical Society.

2.18. Miscellaneous Uses.

Even when we confine ourselves to just analytical utility, IEMs have too many and too diverse analytical applications to be adequately covered by a review like this. To pick a few, their roles as isolators/separators in

electrochemical cells [186,187,188] or as grounding elements in electroosmotic pumps [189,190,191] are often critical.

The use of IEMs or membranes doped with ionophores/specialized ion exchangers in ion-sensing applications represents a vast area that deserves its own dedicated reviews and has several classic ones [192,193], including recent updates [194-196].

Bipolar membranes (BPM) were briefly discussed before and have many industrial applications [197], their analytical applications have thus far been few. But they seem to hold much promise in that area. A review of this nature is inherently incomplete by nature, we are sure there are omissions. Patents were not cited if the information was available in the peer-reviewed scientific literature. Still, some important work remains only in the patent literature. One can only hope the we have not made important omissions; we merelyish to assure the reader that this was not a deliberate act of commission.

Chapter 3

MOLDABLE STRONG CATION EXCHANGE POLYMER AND MICROCHANNEL FABRICATION

3.1. Introduction

Ion exchange membranes (IEMs) comprise fixed ionic groups attached to the polymer backbone. They permit transport of oppositely charged counter-ions; these travel via the immobile charged sites on the polymer matrix. The same charged sites act as a barrier to the uptake or passage of like-charged ions.[198] For a cation-exchange membrane (CEM), cations can migrate across the membrane matrix while anions are not taken up or transported. The obverse is true for an anion exchange membrane (AEM) that has positively charged fixed sites. This selective transport property of IEMs is utilized in manifold applications, in water/wastewater treatment, food and beverage industries, fuel- and chlor-alkali cells, production of semiconductors, pharmaceuticals, and power generation, to name a few.

The first synthetic organic ion exchanger, based on a polyhydric phenol-formaldehyde skeleton, was introduced in 1935.[199] Since that time, they have evolved from laboratory curiosities to components in everyday consumer products. Perfluorinated versions were developed for use in chlor-alkali cells, they provide long-term physical and chemical and stability even at elevated temperatures, a highly caustic chemical environment as well as very high current densities. Nafion® is often considered the

benchmark perfluorosulfonate cation exchanger. Perfluorinated ion exchangers are expensive, however, and few applications use chlor-alkali cell-like conditions. Growing demand for cost-effective materials have led to the development of a variety of IEMs based on polystyrene, poly(arylene ether sulfone), poly(arylene ether ketone), polybenzimidazole, poly(vinyl chloride) backbones, discussed at some length in a review.[200] Surface fluorination of otherwise nonfluorinated membranes is occasionally used to bring about desirable properties.[201]

3.1.1. Special Needs in Miniature Analytical Applications**.**

Our interest lies in analytical applications of IEMs, often in a miniature scale. Liquids flow through small tubular conduits; ion exchange / transport is typically accomplished using a chemically or electrically induced ion gradient.[202] The only tubular IEM commercially available is based on Nafion. Sulfonated polymers do not survive thermal extrusion. The route to Nafion involves the sulfonyl fluoride as the intermediate. In this covalent form it can be extruded. This is then subjected to alkaline hydrolysis to make the sulfonate and then converted to the H^+-form. The smallest commercial Nafion tube has a dry i.d. of 0.35 mm.[203] Distinguishing dry vs wet dimensions are important as all H^+-form CEMs expand considerably upon wetting. In early use of Nafion tubes as flow-through ion exchangers, we reduced internal volume by inserting an inert filament.[204] Hydrodynamic dispersion therein was further reduced by coiling it to a small diameter: forcing the flow through the annulus generates a centrifugal flow component

that flattens the parabolic flow profile. A more recent electrodialytic version of a similar device operating in the sub-μL/min flow regime has three parallel flow channels within a single IEM block with the central channel having an equivalent diameter of 40 μm.[205] Creating microchannels in IEMs by laser machining/drilling is not possible as thermal decomposition destroys the functionality. The availability of a (pre)polymer that can be solution cast around a mandrel (e.g., one or more fine wires that upon removal will form correspondingly sized channels) will permit small-volume flow-through designs. Nafion is available as a colloidal solution. Casting around a wire mandrel to make a microbore IEM conduit is possible.[206] However, at ~$50/g, this is an expensive proposition. The solutions are relatively dilute: many rounds of solution application, drying, curing and repeating these steps are needed. Not only does Nafion adhere poorly to most surfaces, due to dimensional change upon wetting, soon as it is wetted during use, the film swells and detaches from the substrate.

To make a sheet membrane, solution casting of a (pre)polymer on a flat plate is common. One frequent ingredient of such solution-cast membranes is polyvinyl alcohol (PVA); it is inexpensive, even compared to styrene-divinylbenzene based polymers most commonly used to make ion exchangers.[207] PVA itself is very hydrophilic; simple solution-cast PVA films dissolve in water. However, thermally annealed or chemically crosslinked PVA films are not water soluble; such treatment also reduces swelling/water affinity and improves mechanical strength.[208,209] PVA can be cross-linked

by one or more difunctional agents (such as glutaraldehyde,[208,210] maleic acid,[201,211-213,214] succinic acid, etc. An agent such as sulfosuccinic acid[215-218] can provide both crosslinking and a strong acid functionality. To incorporate ion exchange functionalities into PVA, one early strategy was sulfation of PVA itself.[219] A multitude of ionomers have been blended with PVA, including Nafion,[220-222] carboxylic acids including alginic acid223 and acrylates.[215,224] Sulfonated (poly)sulfones,[225-227] phenol-formaldehyde[228] and graphene oxide,[229] and various other sulfonic acids[207,230] have also been used. Not surprisingly, by far the most common ionomer put into PVA has been the same functional unit common to most commercial strong cation exchangers, poly(styrene sulfonic acid, PSSA).[211-218,232-234] With the possible exception of a very early study,[232] all of these membranes have been chemically crosslinked with an external agent, most commonly glutaraldehyde. Such crosslinking is known, however, to make the polymer rigid, limit water absorption. This reduces ion mobility in an IEM and thus adversely affects energy efficiency and performance, especially in electrodialytic applications.

It is not known if IEMs made without bifunctional crosslinkers are sufficiently stable long-term to be suitable for analytical applications. It is well known that solution-cast PVA films become water-insoluble upon thermal annealing; it has been reported that the same can be accomplished by UV irradiation; marked spectral changes in the film occur at the same time.[235] With regard to PVA-ionomer composite IEMs, specifically when the

latter is styrene sulfonic acid, all such composite monomers have thus far only been made beginning with both components already in polymeric form.

A material derived from PVA and monomeric styrenesulfonate (SS) with the latter is polymerized *in-situ*, has not been characterized. Properties of interest include specific conductance, water absorption, etc. as a function of the ionomer content. Of particular interest to us is the moldability of such polymers. We made a series of PVA-SS composite of varying ionomer content. The use of Fenton's reagent (FR) as an initiator led both to crosslinking of the PVA itself and polymerization of the SS in-situ. A PVA-polystyrenesulfonate (PVA-PSS) polymer is also studied.

3.2. Experimental

Materials. Polyvinyl alcohol (PVA): partially hydrolyzed (PH, 86-89%): Molecular Weight (MW) range (10-26 kD, hereinafter LMW; 57 – 66 kD, hereinafter MMW; 88 – 97 kD, hereinafter HMW) and fully hydrolyzed (FH, 98-99%) same MW ranges except the LMW grade had a MW range of 11-31 kD) were from www.alfa.com; sodium p-styrenesulfonate hydrate (SSNa, 93.0%, www.tciamerica.com.) sodium poly(styrenesulfonate) (PSSNa, MW 70,000, www.alfa.com, ferrous ammonium sulfate heptahydrate and potassium persulfate (www.avantorsciences.com), hydrogen peroxide (30%, www.fishersci.com) were obtained as indicated.

3.2.1. Synthesis

PVA solution (10% w/v) was made by adding the necessary amount of PVA to room temperature water in a beaker with a stir-bar. The beaker is

then immersed in water in a larger beaker acting as a water bath. The latter is brought to boiling with the inner solution continuously stirred. After a clear solution was obtained without any undissolved residue remaining, the requisite amount of SSNa solution was immediately added to the hot PVA solution with stirring. Stock aqueous SSNa solution (50% w/v, based on anhydrous SSNa) was prepared from the as supplied solid, containing 7% water. The stock SSNa solution was added to PVA solution in different volume ratios to have SSNa: PVA nominal mass ratios ranging from 1:19 to 1:1.5 (5-40 wt% SSNa in final polymer, see Table A-S1 in the Supporting Information (SI)). To initiate the polymerization, 100 µL 1 mM $Fe(NH_4)_2(SO_4)_2$ was added to each aliquot containing 4 g by combined weight of PVA + SSNa (ranging in solution volume from 27.2 to 38.4 mL for the mixed solution), mixed briefly and followed by 100 µL 3% H_2O_2 (making FR *in-situ*) The mixture was then stirred (room temperature, 1 h) and poured on to 35 mm dia. petri dishes and left undisturbed at room temperature for 5 - 7 days. The resulting membranes were then annealed at 120 ℃ for 24 h. The membranes were then converted to the H^+-form by submerging in stirred 0.1 M H_2SO_4, with frequent reagent replacement (at least 10x at $\geq$ 2h intervals) to affect quantitative conversion. In most cases, the membranes were annealed at 120 ℃ overnight again before further characterization. The series of membranes synthesized above are hereinafter referred to as PVA-SS5 to PVA-SS40, the numerals reflecting nominal wt% SSNa in the final polymer. Note that the material is tested and

used in the H^+-form, the wt% styrenesulfonic acid content ranges respectively from 4.5 to 37.3% on an anhydrous basis. Unless Na is explicitly mentioned, the H^+-form was tested.

A PVA-PSS25 polymer was made by mixing 15 mL 10% PVA and 10 mL 5% PSSNa (MW 70 kDa) solutions with the same FR initiator as above. Both the PVA-SS25 and PVA-PSS25 polymers were also made with 100 μL 0.75 mM $K_2S_2O_8$ used as the initiator; various incubation conditions discussed in the results section were used; all above polymers were annealed as before at 120 °C overnight.

3.2.2. Boiling Water Test (BWT)

To simulate electrodialytic use conditions where joule heating affects a membrane, and to check for dissolution, a rectangular PVA-SS25 membrane segment was oven-dried overnight at 85°C, allowed to cool in a closed vial, weighed by difference and dimensions measured (high resolution digital microscopy, VHX-5000, www.keyence.com), minimizing ambient exposure. It was then boiled in water for ≥ 1h, dried (overnight, 85°C), reweighed, remeasured and the whole process repeated once more.

3.2.3. Water sorption measurements

The sorbed water content (SWC) was gravimetrically determined. Membrane samples were first dried in a vacuum oven (50 °C, 635 mm Hg, 24 h) and weighed. Following water immersion (room temperature, 24 h), excess water was drained and blotted off before weighing the wet membrane. The SWC is expressed as a fraction of the dry polymer mass.

3.2.4. Specific conductance measurements

The basic circuit arrangement (see Figure A-S1 in the SI) consisted of an adjustable frequency sine-wave excitation source (operated at 1 kHz except as stated, Model 4011, www.bkprecision.com), a precision reference resistor R_r (1 kΩ, unless specifically stated otherwise) placed in series with the membrane under test. Similar arrangements have been often used.[236] The resistance of the membrane R_m is computed as:

$$R_m = R_r V_m / V_R \qquad \ldots(1)$$

where V_m and V_R are the voltages across the membrane and R_r.

The conductance across the thickness of the membrane ("normal conductance") was measured using two disk-shaped neodymium magnets (3.13 mm dia.) as electrodes. The membrane, slightly larger than the disk diameter and wetted with deionized water, was placed between N-face of one disk and the S-face of the other, thus held by the magnets and assuring intimate electrode contact and even and constant pressure; the measured conductance may depend on the exerted pressure.[237] The effective electrode area A was thus taken to be 7.69 mm^2. Electrical connection to each magnet was made with cables terminating in plated ferrous metal leads placed on the outer face of the magnets. The effective membrane thickness (δ) was obtained by a micrometer measurement of the distance between the outer faces of the magnetic disks with and without the membrane in place. During measurement, the membrane, initially wetted with deionized water, was placed in a sealed bag (with the leads exiting the

bag through an otherwise sealed port) with a pool of deionized water at the bottom of the bag to ensure a 100% RH environment. There was no measurable current in the circuit with an inert plastic spacer (about the same thickness as the membranes) between the magnets. The normal specific conductance κ_n is given by:

$$\kappa_n = \frac{\delta}{R_M A} \qquad \ldots(2)$$

The resistance of the membrane along one of the longer dimensions of the membrane ("tangential conductance") was measured by using a pair of rectangular magnets at each end of a piece of rectangular membrane (see Figure A-S2 in SI) in a 100% RH enclosure as before. In all cases, the height of each magnet (51 mm) exceeded the height (*h*) of the membrane studied. The membrane thickness δ is directly measured with a micrometer, given that the distance between the pair of magnetic electrodes is *L,* the measured resistance of the membrane being R_M, the specific conductance in the tangential direction (κ_t, along the plane of the membrane) is then given by

$$\kappa_t = \frac{L}{R_M h \delta} \qquad \ldots(3)$$

3.2.5. Ion-exchange Capacities (IEC)

Based on the composition of the prepolymer mixture, the theoretical IEC/unit mass can be directly computed. The actual IEC was titrimetrically determined for all polymers: a given sample of a H^+-form membrane was stirred overnight in a calculated 50% excess of ~0.1 M NaOH (standardized

with primary standard 0.1 M KHP). The excess NaOH was then back-titrated with the standard KHP.

3.2.6. Fabrication of IEM Microconduits

The fabrication of a single ~30 μm bore microchannel with 365 μm o.d. connecting tubing is described below as an illustrative example (Figure A-S3). A 25 μm ϕ tungsten wire is threaded through two short lengths of 100 μm i.d., 365 μm o.d., silica capillaries. Two drops of hot-melt adhesive, ~35 mm apart, are applied to the outer surface of the 35 mm dia. petri dish wall and allowed to harden. These are used as supports for the silica tubes which are put on the respective glue drops, the tips ca. 0.5-1 mm apart and two more drops of glue are used to hold them in place. The prepolymer solution is then poured over the assembly to a height of 2+ mm above the tubes. One wire end is now affixed with tape, the other end is then similarly fixed after stretching the wire taut. During room temperature polymerization over several days, the dish and its container are maintained in a vibration-free, dust-free environment. After a solid polymer is formed, the hot glue is removed before the assembly is annealed (120 °C overnight).

3.3. Results and Discussion

3.3.1. Choice of PVA and Form of Ionomer

Sodium vinylsulfonate (VSNa), rather than SSNa, was initially chosen because of its lower equivalent weight (EW) and mixed with various types of PVA. All of the resulting material failed the BWT (dissolved or became soft and sticky), however. With the inclusion of 6% glutaraldehyde

(GA) the FH HMW PVA-based polymers survived the BWT. The FH MMW polymers also survived the BWT provided ≥ 8% GA was added. Under the same conditions, the corresponding PH polymers did not pass the BWT. Based on the BWT, GA was better as a cross linker than either ethylene glycol dimethacrylate or ethylene glycol diglycidyl ether added in similar amounts. Regardless, these VSNa-based polymers were not further pursued. Although mechanically stable,the ionomer was found to slowly leach from the membranes as seen in repeated regeneration-IEC measurement cycles. We henceforth also tested for mass loss in BWT, beyond loss of mechanical integrity, as measured by drying and weighing (and repeating this process, if the first BWT showed no significant loss). In some cases, we also repeatedly measured the dry dimensions of rectangular polymer samples after a BWT, re-drying, and repeating the process. Results for a sample of a PVA-SS25 polymer are presented in Figure A-S4.

We chose to synthesize the polymers in the sodium form and convert to the H^+-form after annealing rather than directly making the polymer with the H^+-form SS monomer because of some initial difficulties encountered in the latter process. Subsequent experiments, not discussed here, however, have shown that this is also possible and may be preferred as it obviates post-polymerization H^+-conversion. No difference between the polymers made in the two different routes could be seen. We noted that if SSCa was substituted for SSNa, the volumetric swelling upon wetting of the annealed

polymer (in salt form) was substantially lower. The initial sodium form of the membrane was nearly colorless to white whereas the thermally annealed H^+-form membranes get increasingly darker in color with increasing ionomer content (Figure A-S5) and increasing annealing time; spectral information appears in Figures A-S6 and A-S7.

3.3.2. Polymer Stability and Need for Crosslinker

With VSNa, the HMW FH PVA required the least amount of GA to provide a polymer stable in boiling water. PVA-SS membranes were hence made solely with FH HMW PVA. One trial composition (PVA-SS15) was initially made both with and without various amounts of GA. To our surprise, polymers without any GA, survived the BWT/mass loss test just as well once the polymer was converted to the H^+-form and further annealed. No cross linker was henceforth used.

Given the ability to pass the BWT, we also studied the effect of boiling PVA-SS(5-40) polymers in methanol and ethanol. Not only all of the polymers remained mechanically intact in boiling alcohols, it was apparent that they absorb less methanol and ethanol and swell less than with water, in marked contrast to how Nafion behaves in water vs. methanol. This is consistent with observations that addition of PVA to proton exchange ionomers reduces methanol permeability and thus improves their utility in methanol fuel cells.[217] The tolerance to alcohols (and acetonitrile) with minimal swelling may enable applications of these membranes in hydroorganic solvents.

3.3.3. Choice of the Initiator and Polymerization Conditions

Fenton's reagent has particular merits as an initiator in polymerization of vinylic moieties.[238] The graft copolymerization of poly (vinyl acetate) on to wool is particularly notable.[239] In grafting poly(ethylacrylate) on cellulose, a polyol like PVA, FR was far more effective than a Fe(II) – $K_2S_2O_8$ initiator. The FR system does not require added heat. Our default procedure lets the polymerization continue at laboratory temperature (ca. 20 °C) until a dry solid polymer layer remains (5-7 days). After the initial hour of incubation, the FR-initiated polymerization was also allowed to continue in a covered (not sealed) dish at 50 °C. However, is resulted in a polymer that was less clear and with more bubbles. PVA hydrogels are often made by repeated freeze-thaw cycles;[240] it is known that phase separation occurs, and regional crystallinity develops (see Fig. A-S8). If polymerization is conducted at an elevated temperature, given the high water-affinity of the very polar sulfonate group, perhaps some of the surrounding PVA region is effectively dehydrated, thus developing some phase separation and microcrystallinity in the PVA phase. However, after H^+-conversion and overnight annealing (120 °C), both polymers pass the BWT and show no ionomer leaching.

Multiple factors are at work for the stability of these polymers. The PVA-PSS25(Na) polymers were made also with no initiator (separately at 20 and 50 °C) and also with $K_2S_2O_8$ initiator (at 20, 50 and 80°C). Even after annealing, none of these survived the BWT. In contrast, a water-insoluble

polymer resulted if the process was started with PSS25 in the H^+-form. Similarly, the annealed PVA-SS25(Na) polymer (made at 20 or 50 °C) with the FR initiator passed the BWT. None of the PVA-SSNa formulations passed the BWT when made without initiator or with $K_2S_2O_8$ (20° C, 50° C, 80° C). Note that the polymers made with FR were always softer and less brittle than without FR. PVA solutions itself when allowed to sit and re-solidify with and without FR added, respectively result in water-insoluble and water-soluble products. We conclude that FR helps cross liking in PVA as well as interpolymerization with styrenic chains. Further, annealing the PVA in the presence of strong acid is known to result in polyene formation,[241] which is also evidenced from the darkening of color, clearly promoted by greater acid content (Figures A-S5- A-S7). Some credit an interpenetrating polymer network[217] towards an insoluble polymer that exhibits no mass or IEC loss in prolonged use and regeneration cycles (Figure A-S9); the solubility of PVA-PSS(Na) does not support such a conclusion.

3.3.4. Ion Exchange Capacity

Figure 3-1 shows the IEC values of one batch of PVA-SS (5-40) polymers; a second batch showed essentially the same results, namely that the measured IECs closely correspond to the nominal composition of the polymer. It is clearly possible to make polymers with greater functional group density than Nafion, the benchmark CEM, which has an EW of 1100-1200. Careful optimization of temperature and duration of annealing of the

H^+-form will be needed to make usable PVA-SS polymers with SSNa contents of 50% and above. The high acidic content leads to excessive polyene formation during annealing that makes the polymer rigid and brittle, but too little leads to excessive water absorption, also weakening it.

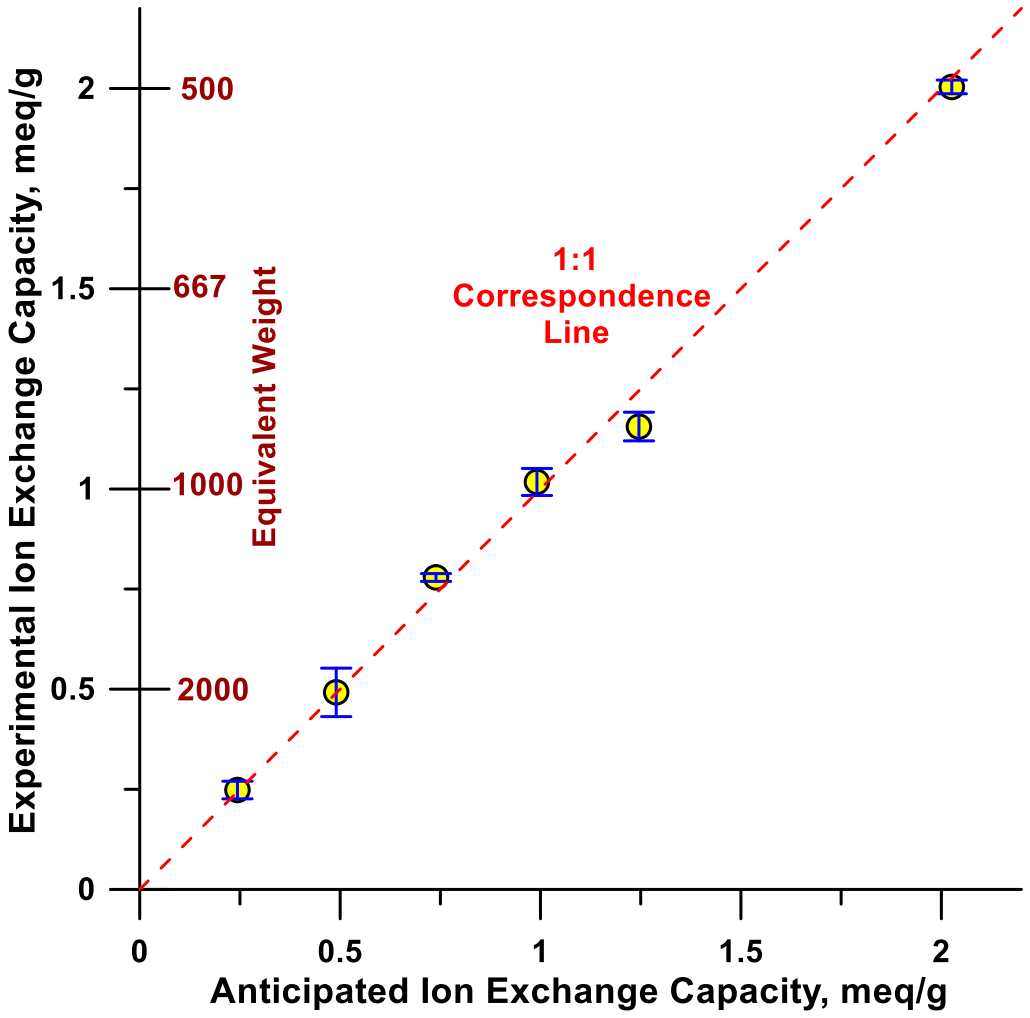

Figure 3- 1 Titrimetrically measured (n=3, ±1 sd error bars shown) IECs in meq/g (corresponding equivalent weight is given by 1000/IEC) as a function of the capacities computed from the initial reactant composition. A near-ideal correspondence is observed.

3.3.5. Water Uptake

Figure 3-2 shows the water sorption data for the PVA-SS series of polymers. As both the x and y data are experimental quantities, error bars (n = 3 each) are present in both directions. Gravimetric water uptake (blue circles) seemingly increases exponentially with the IEC. A plot of the gross water uptake per mole H^+ (yellow diamonds) appears at first sight to be anomalous as there is a minimum at intermediate IECs. In reality, the values are exaggerated at low IECs as the PVA matrix itself, without any sulfonic acid, can take up water. The gravimetric water uptake for the three lowest-IEC samples are nearly as well interpreted by a linear curve as an exponential fit (r^2 0.997 vs. 0.973, respectively) and lead to respective extrapolated value of 0.357 and 0.561 g water absorption for zero-IEC PVA. A more appropriate way to plot the water uptake per mole of H^+ would be to correct for this matrix water absorption. This is what is done in the red bars, with the higher and lower end of each bar representing extrapolation to zero-IEC PVA water content, assuming a linear fit (LE) or an exponential fit (EE). It is seen that for all but the highest IEC polymer (PVA-SS40), the average($\pm$SD) water absorption per mole of H^+ is essentially constant at 81$\pm$9 mol water/mol H^+, albeit it dramatically increases to twice this value for PVA-SS40. For Nafion 115[242] and 117,[243] the values are 23 and 14-19 mol water/mol H^+ respectively. The near-doubling of water uptake per mole sulfonic acid between PVA-SS25 and PVA-SS40 compositions is remarkable. The thermally annealed PVA matrix, with polyenes formed,

absorbs relatively little water. Whether through FR-induced crosslinking/hydrogen bonding/polyene formation, the polymer chains adhere to each other sufficiently to provide mechanical rigidity and lack of solubility. Incorporation of styrenesulfonate, the latter polymerizing to the extent it can, should improve mechanical robustness. In the acid form, the estimated pKa values of protonated PVA and 2-styrenesulfonic acid are -1.87 and -2.11, respectively (www.chemicalize.com). Some proton transfer from the $-SO_3H$ to the alcohol group would occur, a form of H-bonding. Availability of water results in water uptake by the strong acid group, homogeneously present in the polymer. For an ionomer content corresponding to PVA-SS25 and below, this water uptake apparently does not disrupt the skeletal structure sufficiently to affect an increase in mol water absorption per mol H^+ present. With PVA-SS40, the ionomer content is high enough for water absorption to cause sufficient skeletal expansion to allow more water to be absorbed. Indeed, although PVA-SS50 can be made in the sodium form, H^+-conversion results in a membrane of poor wet strength.

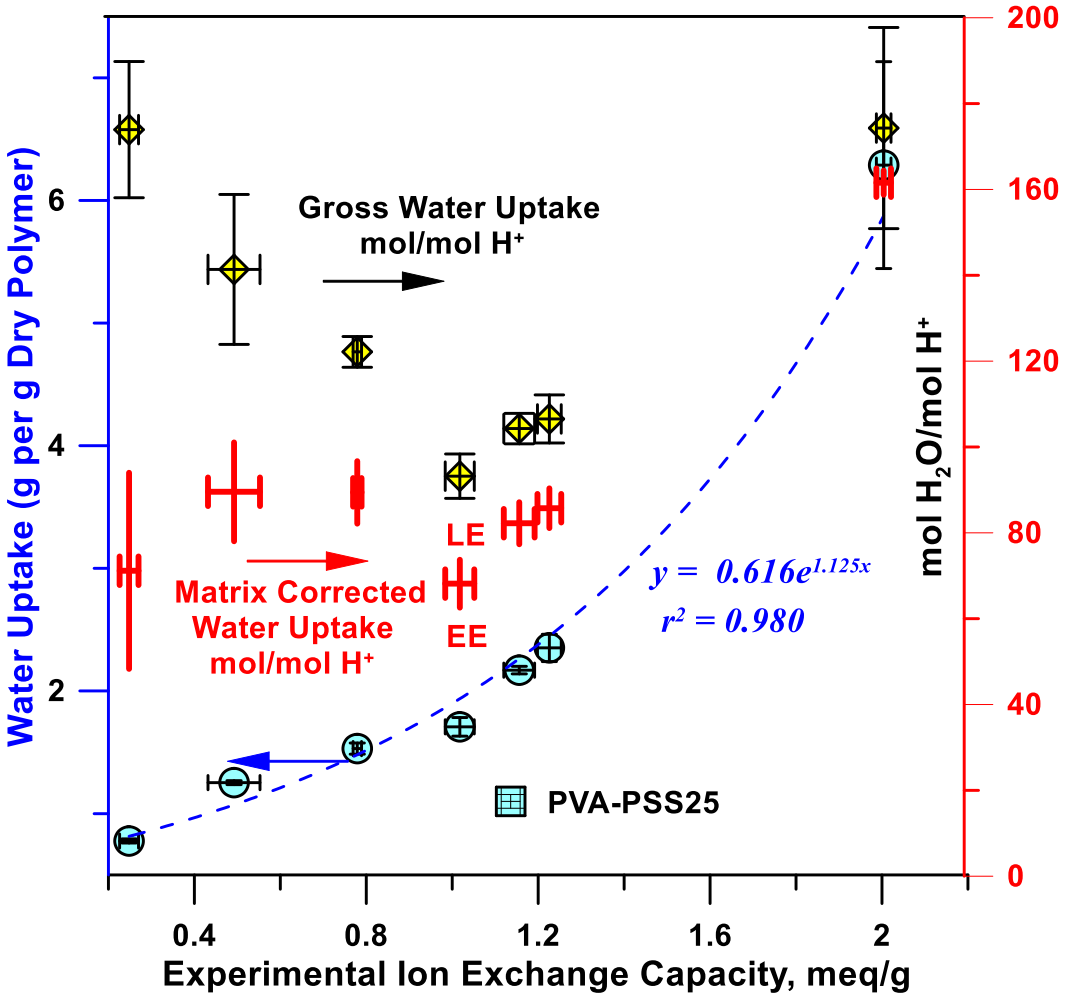

Figure 3-2 Water uptake of the experimental polymers. The blue circles (left ordinate) present gravimetric water uptake per unit dry polymer mass, the single square shows the datum for PVA-PSS25; the yellow diamonds (right ordinate) represent the same water absorption as mol water/mol H^+ and the red bars (right ordinate) presents the latter data after correction for absorption by the PVA matrix; the top and bottom end of each red bar represents matrix corrections made by linear (LE) or exponential (EE) fit extrapolation (see text for details).

The more rigid nature of the PVA-PSS25 polymer compared to the PVA-SS25 polymer persists post-conversion to H^+-form and hydration. The water uptake is essentially half of that of the PVA-SS25 counterpart (see Figure 3-2).

3.3.6. Specific Conductance (κ)

The literature on the κ values of IEMs and their measurement is extensive; most of it, however, relates to Nafion and/or its composites.[39,40,46-49] Often when there is much information, a lot is contradictory as in the present case. This makes comparison with literature data or following literature procedures difficult. First, almost axiomatic with the definition of a membrane, most IEMs have one dimension (the thickness) much smaller than the other two. The cognoscenti have long been aware about the considerable anisotropy in IEM κ values: according to one set of measurements, for hydrated Nafion 117, the tangential specific conductance (κ_t), that along the plane of the membrane, is ~4x higher than that normal to the plane of the membrane (κ_n, i.e., that across the membrane).[237] Others assume that when the membrane is fully hydrated, there is no anisotropy.[243] Yet others have chosen to argue that there should be no anisotropy:[244] *In Nafion, protons migrate via water molecules absorbed in the micropores. Since Nafion has an amorphous structure with micropores, it is reasonable to expect an isotropic proton movement which is independent of the direction of the measurement.* The biggest irony is that typically only a single value of κ is stated, even by manufacturers. Invariably

it is the κ_t value (because it is always higher?) even though the κ_n value would be the more relevant parameter in most IEM applications.

Second, there is no universally agreed on environmental conditions (membrane form, surrounding solution, humidity) and electrical measurement strategy (full impedance analysis to determine the real component of the impedance to simple Ohm's law-based measurement) for the measurement of κ. While a full impedance analysis may be ideal, when, as presently, the primary intention is to compare the relative performance of a number of newly made membranes compared to a benchmark, this ideal approach isnot practical, especially when the membranes are used only under DC conditions. Some even state that the κ_n value increases with IEM thickness.[245] The variation in reported κ values of Nafion is so extensive, a statistical analysis exists on 3539 records compiled from 310 original publications.[246]

We have used here serial measurement in comparison with a reference resistor,[236,243] with a low-voltage sine-wave excitation at 1 kHz, to pay homage to Kohlrausch's original choice for ac conductance measurement.[247] While we have made no exhaustive studies, our experience does not necessarily support the beliefs that κ is current-independent or frequency-independent at $f \geq 10$ Hz.[236]

3.3.6.1. Specific Conductance Upper Limit for a Hypothetical Isotropic IEM

In this section we consider if the specific conductance of a hypothetically isotropic IEM or at least its upper limit, can be predicted

based on its IEC. While the functional group /charge carrier density may be linearly related to 1/EW, the relationship with κ is complicated by water uptake and volumetric swelling that increases with 1/EW, effectively diluting the carrier density. Even for a given polymer, the relationship between κ and the membrane water activity is complex. The sorbed water essentially surrounds the protons and eventually builds charge conduction channels in the hydrophobic matrix. Yang et al.[242] show data for Nafion 115 over a broad range of water activities and temperatures (80-140 °C). Remarkably, κ rises exponentially 3+ orders of magnitude in the range of 0-5% of saturation water activity. Thereafter to saturation water activity, it rises barely an order of magnitude more in an approximately linear fashion.

The “dry” density of Nafion 115 or117 is 1.98 g/cm^3 and the linear coefficient of expansion either in thickness or length in going from 50% RH to liquid water immersion at room temperature is 10%, with a corresponding water uptake of 38% w/w.[248] At 2.05 g/cm^3, the wet density is not all that different; the same value has been reported by direct density measurement of wet H^+-form Nafion membranes.[249] For 1100 EW Nafion, 1 equivalent of H^+ is contained in 1.1 kg of the dry polymer which weighs 1.52 kg fully wet and will occupy a volume of 0.740 L. The equivalent solution H^+ concentration would thus be 1.35 M.

From solution conductance of polymeric sulfonates, we attempt to estimate what the maximum isotropic specific conductance of a polymer having the same physical properties as 1100 EW Nafion should be. Early

literature contains equivalent conductance data for poly(vinylsulfonic acid), PVSA,[250] as well as both isotactic and atactic forms of poly(styrene sulfonic acid), $PSSA_i$ and $PSSA_a$.[251] These values are remarkably constant as a function of concentration. For 0.2-8.0 meq/L PVSA of MW ~35 kDa, the equivalent conductance Λ (in S m^{-1} eq^{-1} L) varied from 13.6 to 13.0. For 0.01-1.1 meq/L 267 kDa $PSSA_a$ and 0.2-1.5 meq/L 175 kDa $PSSA_i$, Λ respectively ranged from 12.9-13.4 and 12.6-13.0. We use the PVSA data for further musings as it goes to higher concentrations. Unlike the case for Nafion where the polyion is solid and immobile, this is not the case for PVSA, the polyanion will contribute to the observed conductance. The mobility of the anion, however, should be independent of the degree of polymerization, as the mass to charge ratio remains constant, much as with DNA.[252] Although the equivalent conductance value for vinylsulfonate has not been reported, the Λ_0 value for ethanesulfonate, the actual monomeric unit, has been reported to be 3.96 S m^{-1} eq^{-1} L.253 The corresponding value for H^+ is an order of magnitude greater at 34.98 S m^{-1} eq^{-1} L. If we thus assume that of the total observed Λ for PVSA of 13.0, the conductivity contribution of the proton is 90%, the Λ attributed to H^+ would be 11.7 S m^{-1} eq^{-1} L. Admittedly, applying the Λ_{H+} for 8 meq/L PVSA to 1.35 eq/L H^+ (representing 1100 EW Nafion) may be a stretch. But Λ values only decrease with increasing concentration; this can be considered the possible upper limit. It provides an isotropic homogeneous solution κ value for Nafion as 15.8 S/m. The above, however, does not account for the vast difference

in diffusivity that must be present between a dilute aqueous solution and a well-hydrated Nafion matrix. At 25 °C, the self-diffusion coefficient of H_2O in liquid water is 2.30 x 10^{-5} cm^2/s,254 while that in Nafion 117 has been reported to range from 0.16-0.56 x 10^{-5} cm^2/s with a recent radiotracer measured value being 0.387 x 10^{-5} cm^2/s.255 Hence the mobility should be 5.9x lower, an isotropic κ of 1100 EW Nafion should be <2.7 S/m.

Of course, unlike a solution, Nafion is not an isotropic conductor. The reported values vary over a very large range.[246] Manufacturer and US Department of Energy specifications both call for a specific conductance of 10 S/m; ironically this refers to κ_t, not relevant in the vast majority of cases in the manner an IEM is actually used.

3.3.6.2. Specific Conductance Values of Presently Synthesized and Some Commercial Membranes

Figure 3-3 shows the relevant κ_n data for two batches for PVA-SS polymers as a function of the IEC; the data for the two batches agree closely. The κ_t values therefore were measured only for batch 2. The change in the κ_t/κ_n ratio (the anisotropy index) with the IEC or water content is explored later (Figure 3-4); however, κ_t/κ_n is always >1. The κ_n value increases monotonically to ~0.8 S/m up to an IEC of ~1.25 meq/g then decreases by the time an IEC of 2 meq/g is reached to ~0.6 S/m. A less pronounced but statistically discernible decrease (1.29 to 1.28 S/m) happens for the κ_t value between the ~1.2 and 2 meq/g IEC samples. The κ_n value, even for our lowest IEC polymer, is significantly higher than a

hydrocarbon based CEM like Fumasep FKE-50 or a low EW (950) perfluorosulfonate CEM with long side chains as in Fumapem FKE-930, both of which are touted for their low resistance (which may be more of a consequence of their thickness (50 and 30 μm, respectively), rather than a high κ (not specified by the manufacturer).

Comparing the κ_n value of the PVA-PSS25 with its PVA-SS counterpart is difficult because the ionomer content differs slightly from nominal polymer composition and the IEC of this particular composition is in a region where the κ_n of the PVA-SS polymers rises steeply with the IEC. The datum for the sole PVA-PSS composition tested can easily fall on this PVA-SS curve. On the other hand, as the κ_n values increase significantly with water absorption in the intermediate IEC region, and as PVA-PSS25 has a significantly lower water affinity than PVA-SS25 (Figure 3-2), κ_n for PVA-PSS25 may be intrinsically higher than PVA-SS25 because the orientation of the poly(styrenesulfonate) chains are more random. Indeed κ_t value for PVA-PSS25 is significantly lower than PVA-SS25, indicating that PVA-PSS polymers may be more isotropic than PVA-SS polymers.

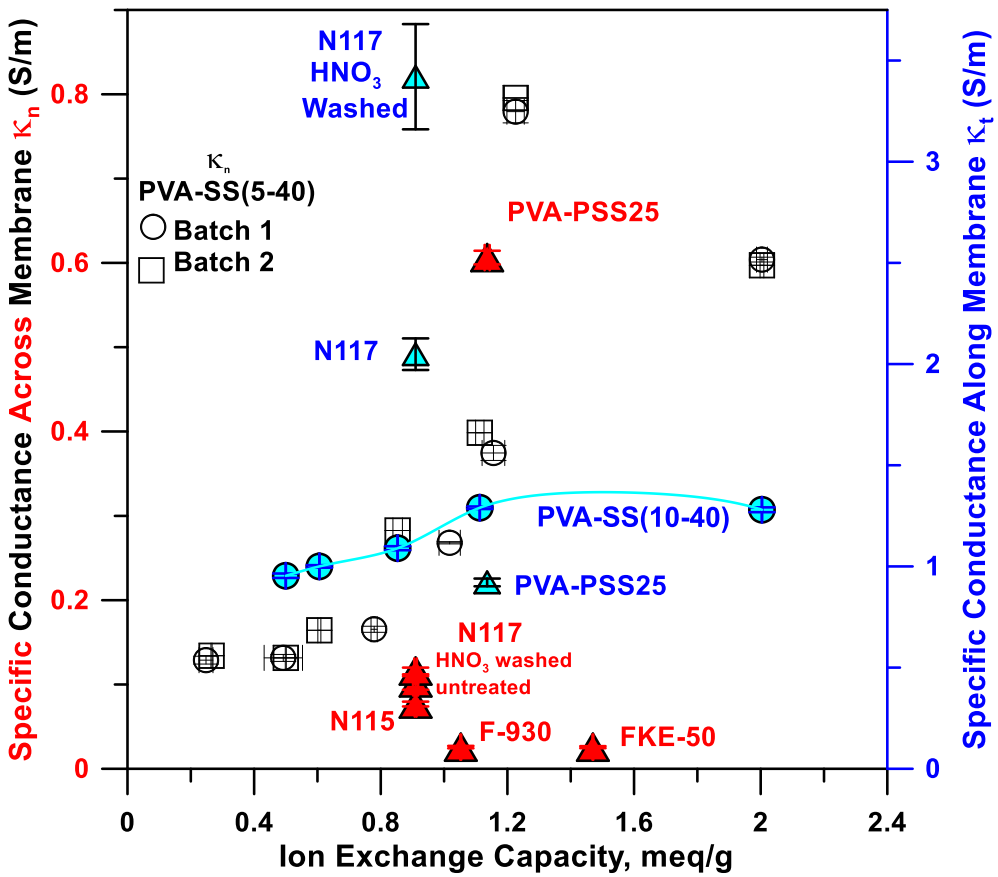

Figure 3-3 Normal (across the membrane) specific conductance κ_n plotted with the left ordinate, in red and black; black squares and circles for two separate batches of PVA-SS(5-40) polymers and red triangles for PVA-PSS25 and several commercial polymers (Nafion 115 and 117 and Fumapem F-930 and Fumasep FKE-50). The right ordinate (in blue), depicting the tangential specific conductance κ_t, is scaled with a 4.5x greater span than the left and the corresponding data for PVA-SS(10-40) and Nafion 117 are depicted by filled blue symbols. In all cases κ_t exceeds κ_n, typically by a significant factor.

We measured both Nafion 115 and 117 to have greater κ_n values than the two Fumatech membranes mentioned above. Nafion 117 is likely the most characterized IEM; we measured both its κ_n and more commonly reported κ_t value. While one may assume that the membrane, already supplied in H^+-form, would be readily hydrated when wetted with water, there are multiple reports, spanning decades, as to how procedures of boiling in various acids and water, etc. get the membrane fully hydrated and increase the measured κ value.[237,243] With some skepticism, we followed the procedure of boiling in 30% HNO_3 followed by washing and boiling in deionized water.[237] To our surprise, κ_t, which was already nearly twice the value of a PVA-SS polymer of comparable IEC, increased by another 70%; however, κ_n increased by only 14%. The fact that the treatment Results in effects of such different magnitudes on the two different directional κ values suggests that a realignment of the polymer chains, rather than simply better hydration, may be involved.

3.3.6.3. Conductance Anisotropy

For an isotropic conductor, the anisotropy index (κ_t/κ_n) has a value of 1; higher values of this ratio indicate increasingly greater anisotropy. In Figure 3-4, the anisotropy index for PVA-SS polymers is plotted both as a function of the IEC and the reciprocal water absorption. In both cases an exponential dependence with a finite intercept reasonably describes observed behavior. κ_t/κ_n for the PVA-SS polymers ranged from 2.14 to 7.25, decreasing with increasing IEC, the best-fit equation predicting that at high

IEC it will reach a limiting value of 2.1. It is also interesting that the extrapolation of κ_t/κ_n to zero polymer content per unit mass of sorbed water (i.e., pure water), correctly predicts that the conductivity will be isotropic ($\kappa_t = \kappa_n$), as would be expected in a solution.

The κ_t/κ_n value for PVA-SS25 is 3.24±0.11; that for PVA-PSS25 is 1.52±0.04, less than half. The ionomer chain in the latter already exists in a polymeric form when it is put into a polymer matrix and likely has less freedom for directional orientation. Our value for the anisotropy index of Nafion 117 (κ_t and κ_n data present in Figure 3-3; κ_t/κ_n are 26.7±1.4 and 33.6±3.7 for the untreated and acid-boiled membrane; the values are not statistically different) is much higher than any of the polymers made here (maximum κ_t/κ_n value 7.25). The very high hydrophobicity of the perfluorocarbon matrix may result in greater directional alignment of the charge carrier groups.

3.3.7. A Molded IEM Microchannel.

A principal goal behind making these polymers is to fabricate IEM-based microstructures for monolithic microsuppressors,[205] eluent generators,[256] etc. for open tubular ion chromatography. While the polymer is cast around a 25 μm mandrel, after thermal annealing and conversion to the H^+-form, the polymer expands. The best estimate for the channel size is around ~30 μm. While microscopic measurements indicate a channel size of 25-29 μm, optical measurements of such a small radius of curvature channel through a far thicker polymer layer underestimates the diameter, based on

micrometer measurements of the wire or the capillary imbedded in the polymer. Figure 3-5 shows a ~1.5 mm x ~30 μm dia. channel.

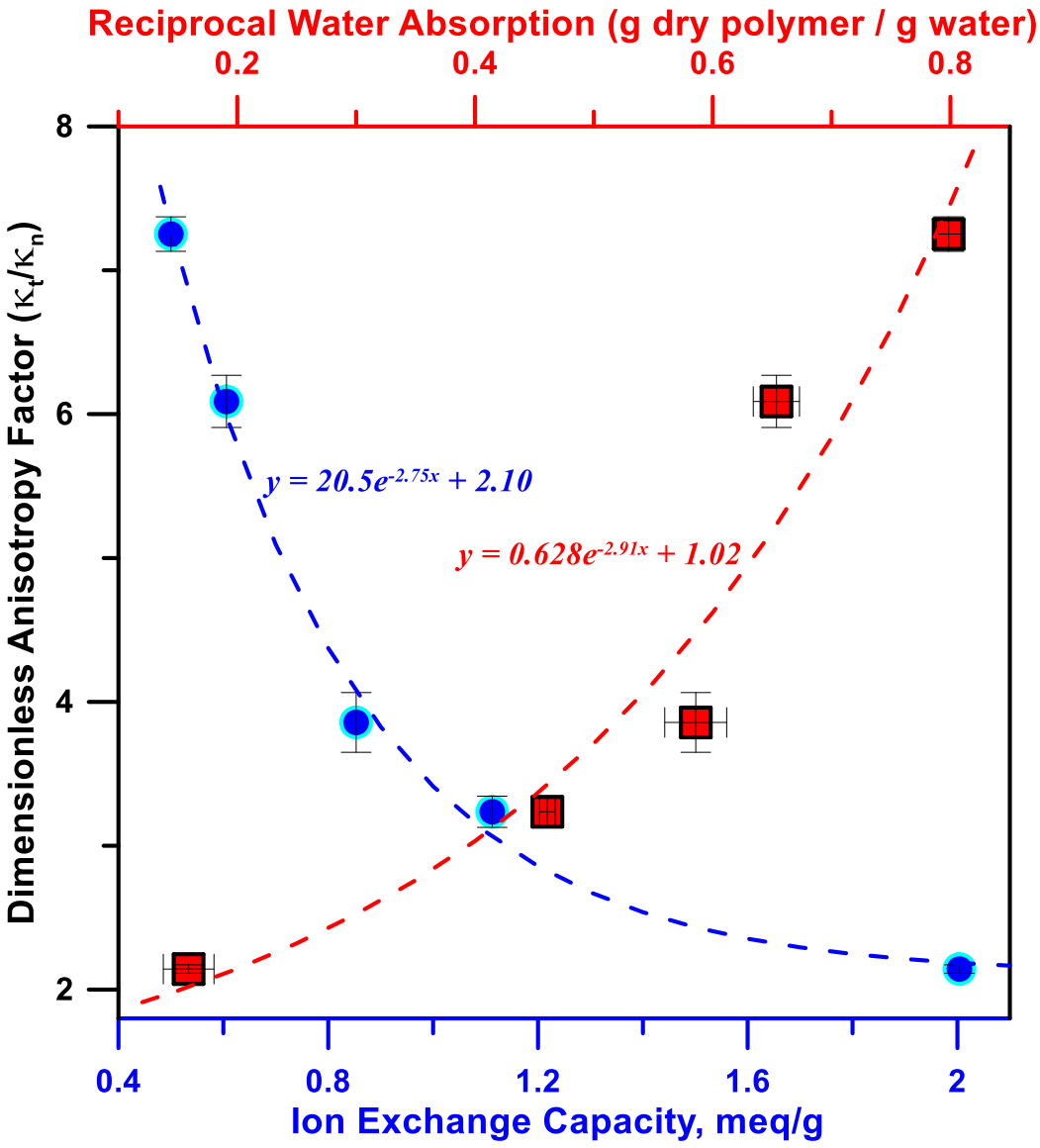

Figure 3-4 Conductance anisotropy, represented by κ_t/κ_n , is plotted both as a function of the IEC (bottom abscissa) and gravimetric water absorption (top abscissa). Best fit equations for are also shown.

Figure 3-5 Prepolymer solution (PVA-SS25) cast microchannel , ca. 1500 μm long, 30 μm in diameter. The larger connecting channels, originating from 360 μm o.d. guide capillaries, are ~400 μm in i.d.

While most of our channels were made based on a 25 μm mandrel, we have successfully tested larger diameter wires up to 100 μm. Tungsten wire is commercially available down to 15 μm and can be etched to smaller diameters with H_2O_2,[257] perhaps most conveniently after the wire has already been fixed in the molding structure. Making smaller channels should thus be possible, especially as the polymer expands in the latter stage, releasing the wire. It has no adhesion to the wet hydrated IEM: one does not have to pull a fragile microwire stuck to a polymer.

A much smaller length microchannel, of ~0.5 mm length and the same ~30 μm i.d., is shown in Figure A-S10. The ~400+ μm outer channels are too large to tightly fit 360-375 μm o.d. tubes. Commonly available 635 μm (0.025 in.) o.d. PEEK tubing (available in various i.d.'s, including 390 μm that tightly sleeves ~360 μm o.d. tubes) fit tightly in the elastomeric polymer. We serendipitously discovered that such connections and the channel will withstand at least ~300 psi. Flow of water through a transparent channel of nearly the same refractive index is not readily visible. Any

injected dye bolus requires too high a concentration with so little optical depth and risks penetration into and permanent staining of the polymer. So, we injected air bubbles (see the videoclip airbubbles.mp4 in the SI), but also looked for alternatives that would not exhibit the compression and expansion characteristic of gas bubbles. In this vein, a suspension of particles, nominally of a size that would pass through a 25 μm channel, was put in while water was pumped at 1 μL/min. Of course, the particles formed multiple clumps, blocking the channel. As the pressure built up to 280 psi, the clumps began to exit the system and the pressure dropped to 5.2 psi. The pressure theoretically needed to pump water at 22 °C through a 500 μm long 30 μm channel is 5.8 psi. See the videoclip particles.mp4 in the SI. A few sequential frames of the passage of the particles are presented as Figure A-S9.

3.4. Conclusion

In conclusion, we have described an attractive way to make a moldable cation exchange polymer and to fabricate microchannels therein. We hope to soon describe actual utility as IC suppressors and other microanalytical ion exchange applications.

Chapter 4

MOLDABLE CAPILLARY SUPPRESSOR FOR OPEN TUBULAR ION CHROMATOGRAPHY BASED ON POLYMERIC ION EXCHANGER

4.1. INTRODUCTION

Conductivity is a universal trait of ions in solution. As such, it is the detection mode of choice in ion chromatography (IC). In IC, the mobile phase is obligatorily an ionic eluent, typically of orders of magnitude greater concentration than those of the analytes of interest. Detecting trace ionic analytes in such a highly conductive background would be impossible; this problem was solved by eluent *suppression*.[258] In anion chromatography, the *suppressor* is a proton exchange device that exchanges all influent cations for H^+. Placed before a conductivity detector, it converts an alkali hydroxide or the salt of a weak acid (e.g., Na-borate) used as eluent to pure water or weakly conducting boric acid, respectively while analytes like Cl^-, NO_3^-, SO_4^{2-} etc. enter the detector as highly conductive corresponding acids. From their original packed resin bed incarnation, suppressors have long adopted continuously regenerated membrane-based forms. A recent review covers this, along with other analytical uses of ion exchange membranes,[259] but of course they will continue to evolve.[260]

From reduced sample and eluent consumption to a smaller footprint, miniaturization has many benefits, IC is no exception. The first micro-scale suppressed IC utilized a 0.19 mm i.d. packed column coupled to a thermally stretched Nafion® perfluorosulfonate tube with active dimensions of 200 μm

i.d. and10 mm length.[261] Others later used a 11 mm long ~100 μm i.d. (estimated, dry i.d. given as 80 μm) tubular Nafion suppressor[262] or a 19 mm long 50 μm i.d. radiation-grafted sulfonated PTFE tube[263] with 180 μm i.d. packed columns. Capillary IC was reviewed some time ago.[264] In between, alternate use of packed capillary suppressors was advocated for use with larger (320 μm i.d.) capillary columns[265] but contemporary interest has been on open tubular (OT) IC, which has been recently reviewed.[266,267] Because of much smaller band volumes making a small enough suppressor is a much greater challenge than with packed columns. The first OTIC suppressor was fabricated by repeated coating of a 50 μm Pt-wire mandrel placed between two 75 μm i.d. capillaries with a colloidal solution of Nafion.[265,268] The suppressor suffered from poor adhesion of the membrane to the column

The mandrel approach was continued by this group by forming a polymer around the mandrel and functionalizing the polymer further as needed to be an ion exchanger.[269,270] However, these columns were too large to be practical. The first practical OTIC suppressor was electrodialytic and was used successfully with 20-30 μm i.d. columns.[271] This device contained two 0.45 mm φ drilled parallel regenerant channels for electrode placement bracketing an eluent channel in a block of Nafion. The eluent channel was made by puncturing the solvent-swollen polymer with a 0.3 mm φ needle; the polymer is not physically removed but a *crack* is made. The honed end of a capillary column and a similar tapered exit tube were

inserted into this channel from opposite sides leaving a suppression gap of 400-1100 μm. The close placement prevents the crack from sealing itself. With an applied electric field, such a device can provide more than adequate suppression capacity, up to 100 mM KOH @ 100 nL/min and excellent signal-to-noise (S/N) ratio for both isocratic and gradient elution modes. The design has several disadvantages, however: (a) The *cracks* do not translate to reproducible channels from one device to another, (b) When flow is stopped, especially for an extended period and then restarted, the crack does not necessarily regain the original dimension, in a constant pressure flow system this change in restriction undesirably affects the overall flow rate, and (c) Nafion blocks of necessary dimensions are not commercially available.

Such a device can also be used with chemical regeneration, where only the eluent channel is needed.[272] While the suppression gap is ~< 1 mm, the overall depth of the channel must be several mm to securely hold the column and the exit tube. Thermal decomposition of ion exchange polymers (IEPs) precludes laser drilling, and because of limited flute lengths of mechanical drills at these dimensions, drilling a ~ 5 mm long hole through a polymer block is not possible with drill diameters <150-200 μm. These drilled apertures do not change backpressure over time but even over sub-mm lengths, the dispersion of bands from a 20-25 μm i.d. column is perceptible. We have recently described a high-capacity IEP with attractive properties, including the ability to be molded around/on existing

structures.[273] Such a material can allow the concepts of (a) having a column and an exit tube with a wire mandrel inserted between them and casting an IEP around the mandrel and (b) having a predrilled IEP block and inserting the column and the exit tube into it, to be combined. As mentioned, the former has problems of a cast IEP adhering to a capillary exterior upon wetting and the second has the difficulty of drilling a long enough hole small enough in diameter. If an IEP block is preformed around a microwire mandrel, which can then be removed, honed column and exit tube ends can be forcibly inserted into the premade channel making leakproof connections and leaving a suppression gap of desired length. The fabrication and characterization of such a device is described in this paper, along with a tubular metal capillary functioning both as the suppressor exit, as well as the first conductivity detection electrode in contact with the suppressed effluent. The terminal electrode, of a similar metal capillary, is placed only ~100 μm from the first, joined by an insulating sleeve.

4.2. EXPERIMENTAL SECTION

4.2.1. Reagents and Materials.

Poly(vinyl alcohol) (PVA, 98-99% hydrolyzed, 88-97 kDa, alfa.com); sodium p-styrenesulfonate hydrate (SSNa, 93.0%, tciamerica.com), ferrous ammonium sulfate heptahydrate (avantorsciences.com), hydrogen peroxide (30%, fishersci.com), and acetic acid (ACS grade, us.VWR.com) were obtained as indicated.

4.2.2. Capillary Suppressor. IEP Synthesis.

Details of making this class of polymers were previously given.[273] To make the specific composition used here, Fenton's reagent (100 μL 3% w/v H_2O_2 freshly added to 100 μL 1 mM $Fe(NH_4)_2(SO_4)_2$) as initiator was added to 32 mL of a mixture of 75% by weight PVA and 25% by weight sodium styrenesulfonate (SS) and mixed well. Note that the (pre)polymer solution was prepared in the sodium (Na^+) form.

4.2.3. IEP Microchannel Fabrication.

The procedure for casting the (pre)polymer solution around a tungsten wire mandrel was previously described.[273] In the present work, up to three parallel microchannels, each 30-35 mm long, were simultaneously prepared in a single IEP block. As actual suppressors require only ≲ 8 mm lengths, multiple usable units could be sliced and diced from each batch. A 35 mm diameter plastic petri dish is used as the mold. Three diametrically opposed small holes, 5 mm apart, were drilled on the walls of the dish, ~2 mm from the bottom, and 3 strands of tungsten wire, 15-50 μm in dia., were strung across and fixed taut in place with a drop of hot-melt adhesive each at the entry and exit points (See Figure B-S1 in Supplementary Information (SI)). The prepolymer solution was poured over the assembly to a height of 2+ mm above the wires; and allowed to polymerize at room temperature for 5-7 days in a vibration/dust-free environment. After the dry polymer was formed, the hot glue was removed, and the assembly annealed for 24 h at 120 °C. Next, the polymer disks with the wires still imbedded were

repeatedly treated with 0.1 M H_2SO_4 ($\geq$ 2 h each time, at least 10 times) to convert the material to the proton form. After washing thoroughly with water, the disk was annealed again at 120 ℃ but only for 3 hours. In the presence of the strongly acid sulfonic acid, the PVA dehydrates and crosslinks, forming poly(ene)s and turning dark brown. Overannealing will make the polymer brittle while underannealing may lead to leaching of styrenesulfonate. Next, the polymer disks were submerged in DI water for 4-7 days; upon hydration the polymer expands sufficiently to detach from the wires, which could now be removed. Removing the wires mechanically by simply pulling on them does become the more difficult with smaller diameter wires but it is possible for entire range of wire diameters stated. Except as stated, data reported here rely on devices made with 35 μm wires.

4.2.4. Post-Fabrication Steps.

Each suppressor block is cut to a size of ~2 mm thick 4 mm wide and 8 mm long. High-resolution digital microscopy (VHX-5000, www.keyence.com) was used for dimensional characterization. Initial examination however showed a thin layer of black particles in the channel, possibly originating from the oxide exterior of the tungsten wires used. Use without further cleaning led to discernible noise in the conductivity signal, likely due to sporadic dissolution or dislodgement of such particles. Each device was therefore washed (using 365 μm silica capillaries forcibly inserted into the channels for liquid I/O) for a prolonged period (4 days, 2

μL/min) with a micropump capable of high pressures. The initial registered pressure of 115 psi decreased to ~30 psi after washing. A clear and clean channel was microscopically observed after washing it further with1 M H_2SO_4 pneumatically @ ~200 nL/min for 3 h.

4.2.5. Leaching Studies. Suppressed Background Conductance and Mass Spectrometry (MS).

The background conductance of the suppressor effluent is an indication of any ionic monomer/oligomer leaching from the suppressor. Rather than pure water, we used electrogenerated KOH as the influent; contamination of stored water with CO_2 impossible to avoid. Electrogenerated KOH produces a lower suppressed conductance than a water influent and also reflects more realistic in-use suppressor conditions. The test arrangement is shown in Figure B-S2. An ICS-2000 pump delivers water @ 100-400 μL/min through a KOH eluent generator, and a 2x250 mm AS-19 IC column. The flow was split after the column by a tee between the μsuppressor and the macrosuppressor (2-mm ERS-500, all above from www.thermofisher.com). A PEEK restrictor tube (25/360 μm i.d./o.d., 1.52 m long) preceded the μsuppressor. The flow split ratio between the macrosuppressor and μsuppressor was measured to be 227:1. The macrosuppressor effluent conductivity was measured by the ICS-2000 conductivity detector, calibrated with standard KCl.

4.2.6. μSuppressor and μConductivity Cell.

The μsuppressor was followed by a μconductivity cell, constructed from custom stainless-steel (SS) tubes, 38/150 μm in i.d./o.d. (www.k-tube.com), similar to hypodermic needle-based cells.[274] The first tubular electrode (~ 8 mm long) was inserted into one end of the IEP microchannel. The free end of the SS tube was then inserted into a short segment of a 150/360 μm i.d./o.d. PEEK tube. The second electrode tube was then inserted into the open end of the PEEK tube until it touched the first electrode (monitored ohmically). The second electrode was then retracted with a rotatory motion until the electrical contact was broken. The honed end of a separation column or other connecting tube was then inserted into the entrance of the suppressor channel leaving a gap of 2.2, 0.7, or 0.4 mm (this is the active suppressor length, microscopically measured, respectively designated μsuppressor A, B, and C), between the column/tube end and the first electrode. See the inset of Figure 4-1 for the μsuppressor-detector arrangement. The cell constant, as measured with a standard KCl solution for a number of the μconductivity cells constructed in the above fashion ranged from 60-110 cm^{-1}. Given the area of the metallic annular face of each electrode is calculated to be 1.65×10^{-2} mm^2, these cell constants imply the gap between the electrodes is of the order of 99-182 μm; however, this can be correspondingly larger if the inner surfaces of the tubes play any role.

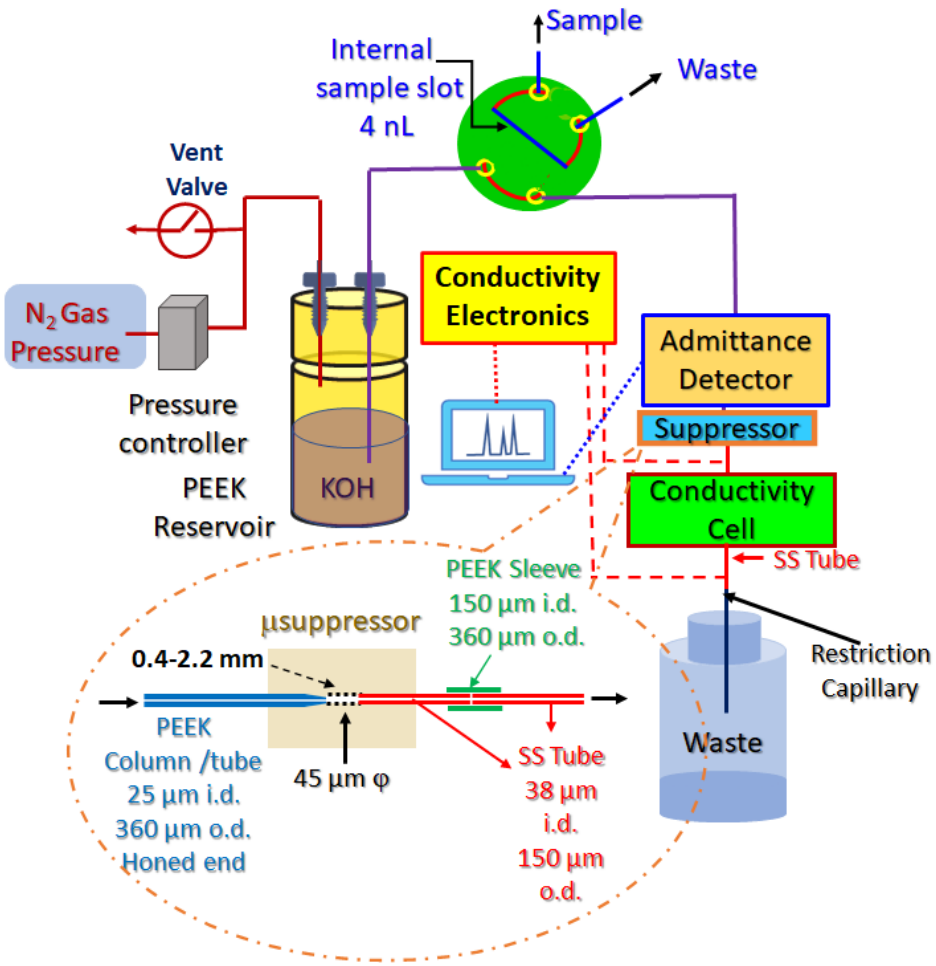

Figure 4- 1 System set up for testing the PVA-SS microchannel suppressor. Chromatograms were also obtained using this arrangement.

4.2.7. Suppression Capacities.

The suppression ability of µsuppressor A was tested for 1-16 mM KOH; at flow rates between~440 - 1700 nL/min as preparatory studies for the MS-based leaching experiments (see below). However, both the active length of µsuppressor A and the flow rates used are much larger than those used in actual OTIC, so suppression capacity was further conducted with µsuppressor B (active length 0.7 mm), operated at a more typical OTIC flow

rate of 168 nL/min (linear velocity 5.7 mm/s) using electrogenerated KOH eluent from a capillary ICS-5000 system and a split flow arrangement. All μsuppressor experiments were conducted with 10-20 mM polystyrene sulfonic acid (Av. MW 75 kDa, purified by dialysis (courtesy Diduco AB, Umeå, Sweden) as a stationary regenerant surrounding the μsuppressor.

4.2.8. MS Experiments.

Prior to MS experiments, water was pumped through μsuppressor A and the macrosuppressor continuously for two weeks to simulate use. Experiments were conducted with both water and 0.01% v/v acetic acid as the influent in both suppressor cases at respective flow rates of 5 and 250 μL/min using the built-in pump of the MS instrument (Thermo TSQ Quantum Discovery Max). Water and HOAc respectively simulated background conditions, and that of an acidic analyte elution. In all cases, 60 30-s long scans with a FWHM resolution of 0.7, spanning the full 30-1500 m/z range of the instrument, were acquired, averaged, and exported. MS operating conditions are in the SI.

4.2.9. Chromatographic System.

The chromatographic system is illustrated in Figure 4-1. A digital pressure controller (P/N 990-005103-100, https://ph.parker.com/us/12051/en/ oem-ep-miniature-pressure-controller) provided pneumatic pressure to drive manually prepared KOH as eluent. A solenoid vent valve (skinner valve, New Britain, CT) allowed for quick release of pressure when desired. An electrically actuated 4-nL internal loop

injector (C74MPKH-4574-.004EH, www.vici.com) was used to inject the sample. PEEK capillaries (25/360 μm i.d./o.d., P/N 1574, www.idex-hs.com) were sulfonated and then coated with AS18 latex (Courtesy Thermo Fisher Scientific) to make an OT anion exchange column.[267] A variable-frequency admittance detector (TraceDec, www.istech.at) was placed on the column immediately before it entered the μsuppressor, which was followed by the μconductivity cell. The system was controlled by a desktop computer with software written in LabView™ in-house.[267] All data were acquired using a programmable system on chip, PSoC5LP (CY8CKIT-059, www.cypress.com) @ 183 Hz.

4.3. RESULTS AND DISCUSION

4.3.1. Leaching from Suppressor Membranes.

Degradation of IEPs occurring over time leading to loss of ionic functional groups.[275-278] Only significant loss of such groups will be registered by an elevated conductance background; given the low conductance background attained in routine IC, such major leaching does not occur in commercial suppressors. However, larger molecular weight ions that do not necessarily have high mobility in solution may not contribute much to background conductance and still present a significant and undesirable background in mass spectrometry. We have previously reported ESI-MS data for several commercial suppressors for anion chromatography,[279] albeit presently available suppressors contain such a great variety of ion exchange membranes and screens, it was not possible

to test all of them. However, the devices tested uniformly showed most of the ion current is due to peaks present in 400-800 m/z range and not surprisingly, by far the greater amount of signal was seen in the negative ion mode; anion suppressors contain negatively charged cation exchange material. The nature of leaching from the new μsuppressors is therefore of interest both qualitatively and quantitatively, although the latter is difficult to compare with macrosuppressors because dimensions and use conditions are so different. Presently described μsuppressor A has a residence volume of 3.5×10^{-3} mm^3, and the typical OT IC flow rate is 0.15 μL/min; the 2 mm ERS500 has an estimated internal volume of 15 μL and the typical flow rate is 250 μL/min. Unfortunately, MS examination of the effluent under these operational conditions is not possible; the present instrument will reliably operate only at flow rates $\geq$ 5 μL/min. As a first approximation, the mass of the leachate in the effluent should be independent of the flow rate. If the MS would behave as a strictly mass-sensitive detector, then the MS output should not markedly differ if a given suppressor is operated at two different flow rates and the entire effluent is seen by the MS, within the limitation that nebulization and ionization efficiency decreases some with increasing flow rates. On the other hand, if the impurity ions originate not in the suppressor but the influent fluid itself, the signal will increase with increasing flow rate. Raw ion chromatograms for pumping (a) DI water and (b) 0.01% HOAc pumped into the MS at 5 and 250 μL/min (i) directly (ii) through the ERS-500 suppressor with 0 and 20 mA drive currents are shown in Figure B-S3

and B-S4. It will be readily seen that the impurities in the influent water blank are essentially confined to the m/z ≤200 range. Figure B-S5 is more instructive in that it plots the ratios of the cumulative ion counts at the two different flow rates in 7 different mass ranges for pure water as influent (the data are available in Table B-S1) as a function of blank water counts. Except for the m/z ≤200 range, in all other cases the ion counts a for the suppressor effluent at the 50x different flow rates are quite comparable, including the m/z 200-800 range, where much of the non-blank signal originates. The same is observed for the HOAc influent, notably that the total ion counts in the m/z 200-800 region are comparable at the two flow rates (Figure B-S6, Table B-S2).

With the above in mind we compared the MS response to the μsuppressor A and ERS-500 effluents, both at 5 μL/min. The results are shown in Figure 4-2 and Figure B-S7 for water and HOAc influents, respectively; the difference is notable. Indeed, Figure B-S8 shows that the overwhelming majority of the peaks observed for μsuppressor A are also present in the blank water.

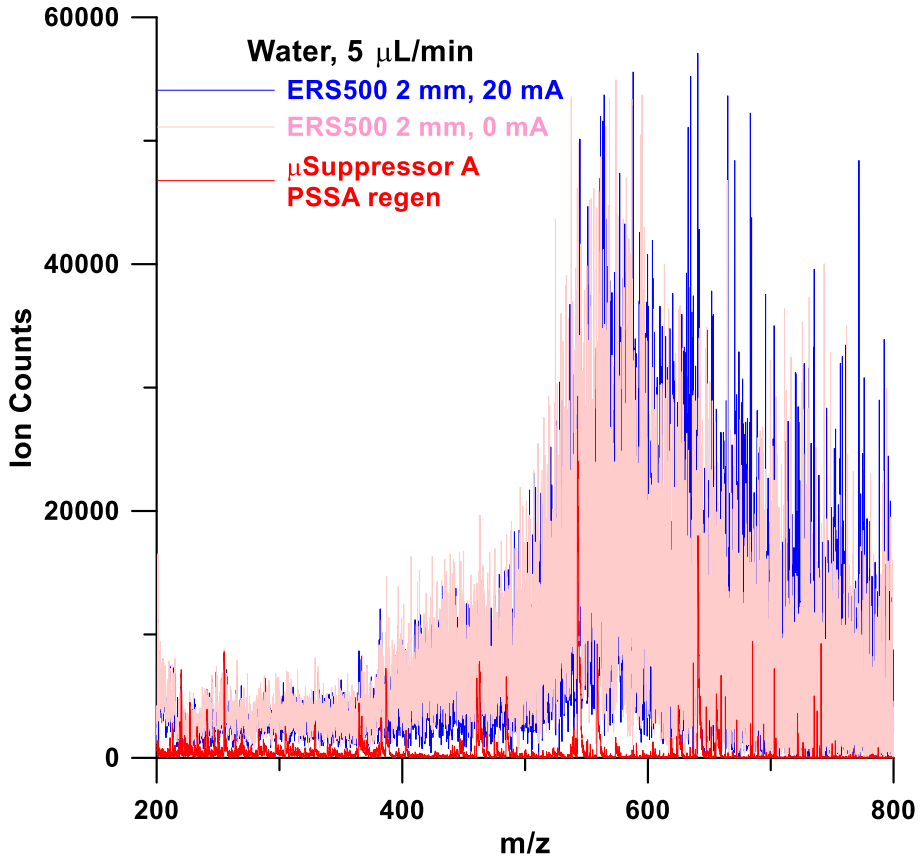

Figure 4- 2 Suppressor MS background counts , water influent. See Figure B-S7 for data for 0.01% HOAc influent.

4.3.2. Background Conductance Measurements.

The suppressed background conductance (SBC) from μSuppressor A remained between 1.2-2.0 μS/cm for 1-16 mM KOH concentrations @ 440 nL/min, with a linear r^2 value of 0.9890 and an intercept of 1.25 μS/cm, suggesting complete suppression (Figure B-S9). At 845 nL/min, also suppression appear to be complete, albeit the SBC was slightly higher at 1.7-4.7 μS/cm. However, at 1300 and 1700 μL/min, suppression capacity was clearly exhausted at some point between 8 - 12 mM and 4 – 8 mM, respectively. The maximum mass flux with demonstrated complete

suppression would thus be 13.5 neq/min, corresponding to 43.4 neq/(mm^2.min) for the 0.311 mm^2 available membrane area. The macrosuppressor, with a total membrane area of ~740 mm^2 (K. Srinivasan, Thermo Fisher Scientific, personal communication, June, 2021) specifies a maximum suppression capacity of 200 mM KOH @ 0.25 mL/min, that translates to a comparable 67.6 neq/(mm^2.min), which, however, is accomplished in the presence of an electric field. Also notable in the data in Figure B-S9, is that at low eluent concentrations (≤2 mM), where the eluent is completely suppressed regardless of the flow rate, the SBC actually increases with increasing flow rate, opposite of what will be expected if conductive monomers were significantly leaching from the suppressor at a constant rate.

As previously stated, μsuppressor A has too large an active length and tested flow rates were larger than presently used OTIC systems. μsuppressor B (0.7 mm gap) was therefore tested at a fixed flow rate of 168 nL/min, typical of present OTIC use, while the KOH concentration was stepped through 0, 3, 5, 7, 9, 11, 13, 15, 17, 20, 25, 30, and 40 mM, with 10 min dwell time at each finite concentration. Figure 4-3 shows the SBC data as a function of time. The data indicates that the device can suppress up to 30 mM KOH at this flow rate. Although this observed capacity may be regenerant concentration/flow limited, we did not presently explore this further as OTIC columns require a much lower eluent concentration to get the same retention factor. It has been shown that packed and OT columns

based on the same latex particle not only have the same selectivity but the exact retention factors at the same eluent concentration are proportional to the stationary phase capacity per unit eluent volume in the column, termed γ_{iex}.[280] The γ_{iex} values for an AS18 packed column and an AS18 coated 19 μm φ OT column were 118 and 8.6 μeq/mL, respectively, clearly indicating that much lower eluent concentrations are required to obtain essentially the same separation (bearing in mind that the linear relationship is between log k and -log [E] and not k and [E], [E] being the eluent concentration.

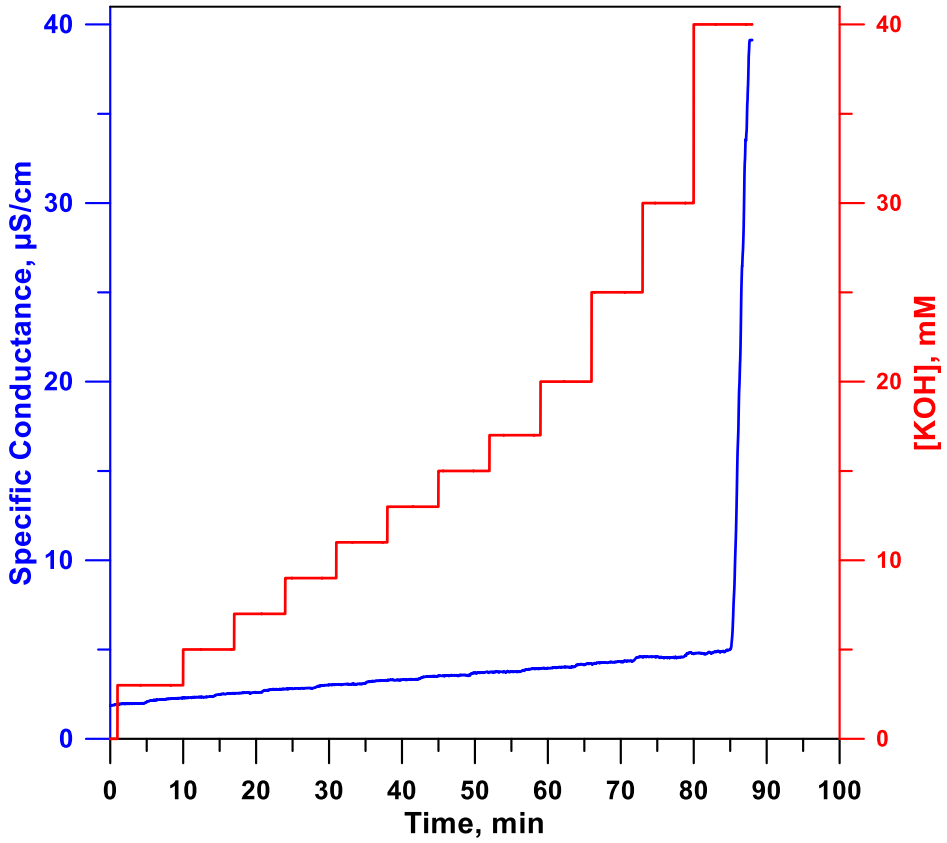

Figure 4- 3 Suppressed background conductance exhibited by μsuppressor B (0.7 mm active length) at a flow rate of 168 nL/min as KOH concentration is changed stepwise.

4.3.3. Mass Transfer in the Microsuppressors. Is there Laminar Flow?

In any membrane-based ion exchange device, either mass transport *to* or *through* the membrane can ultimately limit the suppression capacity limiting step. However, whenever “quantitative” exchange is desired, as in a suppressor, and the device is operated to approach its maximum capacity, mass transport *to* the membrane must become the limiting process towards the end. Except for one early simulation,[281] mass transport in suppressors have not been much studied. In Figure 4-3, the SBC does increase from ~2 to 4.6 μS/cm linearly, with a slope of 94±6 nS/cm/mM KOH. Those familiar with suppressor behavior will recognize that this is not due to incomplete suppression; a very small amount of impurity, e.g., ~0.02% chloride relative to the KOH is sufficient to account for this degree of increase. At an SBC of <5 μS/cm, even as little as a change of 0.1 μS/cm is detectable. This conductance is equivalent to that due to 0.36 μM KOH. If this is the maximum unsuppressed amount in a 30 mM KOH eluent, the eluent is 99.999% suppressed. Mass transport to the wall for flow through a cylindrical conduit can be described by the first term approximation of the Gormley-Kennedy equation[282]:

$$1 - f = 0.819 \exp(-3.657\ \mu) \qquad (1)$$

where, f is the fraction removed and μ is a dimensionless parameter equal to $\pi DL/Q$, D being the diffusion coefficient of the transported species,

L being the length of the tube and *Q* the flow rate. Using the diffusion coefficient of K^+ (1.94×10^{-5} cm^2/s), and a flow rate of 2.80×10^{-6} cm^3/s (168 nL/min), only 99.7% removal is predicted for a 0.07 cm suppressor length according to eq 1. However, eq 1 pertains strictly to laminar flow conditions, which are the *least* conducive to efficient mass transfer to the wall. While the very small absolute flow rates in these μsuppressors may favor attainment of laminar flow, the abrupt diametric transitions at the entrance and exit of the device hinder the same. Standard texts suggest a length of 0.05 dN_{Re} where *d* is the diameter of the tube and N_{Re} is Reynold's number ($4Q\rho/(\pi d\eta)$, ρ and η being the density and viscosity of the fluid) is needed to attain 98% of the fully developed laminar flow pattern;[283] with present numerical values put in, this amounts to only 0.2 μm. However, given that mandrel-cast channels will have perfectly smooth walls; this is also likely to inhibit development of perfectly laminar flow.

4.3.4. Chemical vs. Electrodialytic Suppression. Choice of Regenerant.

One of our motivating reason to pursue OTIC is facile field application, perhaps even in extraterrestrial exploration. In any field use, especially in space applications, simplicity, small footprint, and low power consumption are paramount. An electrodialytic suppressor can provide more capacity but is more complex in design with a necessarily larger power requirement and footprint, albeit admittedly not by a large margin. However, there are less things to fail in a chemically regenerated suppressor, which

is also known to stabilize more rapidly. Since limited number of samples are to be analyzed at a time, and in OTIC, the absolute amounts involved are very small (for 10 mM KOH eluent flowing at 150 nL/min, an 8-hour work day will consume < 1 μeq of eluent, requiring a proportionate amount of regenerant. To prolong the period before regenerant replacement is needed, obviously it will be preferable to use a higher regenerant concentration, assuming only a finite volume of regenerant can be carried on-board. The downside of a higher regenerant concentration is that Donnan-forbidden ion (or regenerant) penetration increases, increasing the background conductance and noise, and deteriorating sensitivity. To our knowledge, details of such regenerant penetration has been studied only once before, more than 3 decades ago.[284] These authors used an electrostatic model to predict that the forbidden regenerant flux through the membrane should increase as a quadratic function of the regenerant concentration; this was observed. In addition, as may be predicted, such penetration decreased dramatically with increasing size and charge of the regenerant counterion. In so far as membrane properties are concerned, the ionic site density (reciprocally related to the equivalent weight, EW) was considered the only factor, a higher charge density predictably decreases the penetration of a similarly charged ions. Like other transmembrane fluxes, for a given concentration difference across the membrane, the flux is assumed to be linearly proportional to the membrane area and inversely as its thickness. With water flowing inside and 25 meq/L H_2SO_4 (a

regenerant commonly used since the early days of membrane suppressors[285,286])on the outside, different samples of Nafion (EW 1100, a polymer with a perfluoroether matrix) was found to exhibit a flux of 8-10 pequiv/(cm.min). A radiation grafted PTFE tube with an EW of 520 showed a flux of 3.0 pequiv/(cm.min); however, a radiation grafted poly(ethylvinyl acetate) tube of EW 570, showed a flux of 23.3 pequiv/(cm.min), which could not be explained.[284] In comparison, the present polyvinyl alcohol-polystyrenesulfonate membrane, with a MW of ~800, exhibited a forbidden ion flux of ~400 pequiv/(cm.min) under the same test conditions! Although the quadratic dependence on the regenerant concentration is observed as well (Figure 4-4), these results indicate that the nature of the matrix polymer profoundly affects the overall transport and is particularly high for the very hydrophilic poly(vinyl alcohol) based present polymer that exhibits extremely high water absorption.[273] Sulfuric acid at significant concentrations cannot be used as regenerant with this membrane.

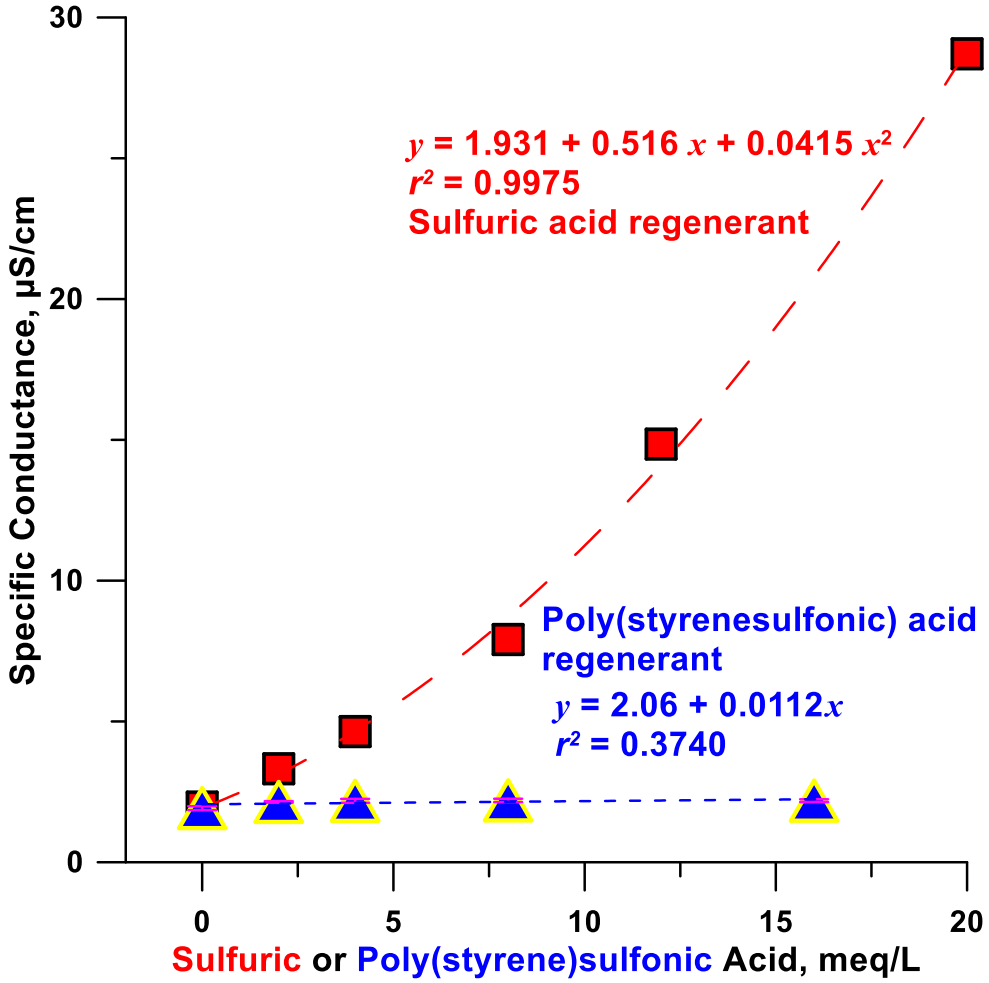

Figure 4- 4 Regenerant penetration , Sulfuric vs. poly(styrenesulfonic) acid. µSuppressor made on 50 µm wire mandrel (channel φ ~77 µm, active length 1.5 mm). DI water influent, 195 nL/min.

Acids with anions that are multiply charged like naphthalenetrisulfonate or large like dodecylbenzenesulfonate exhibit dramatically less penetration but it was also observed early that a polymeric multiply charged ion like poly(styrenesulfonate) shows essentially zero detectable penetration.[284] Fortunately, this material is commercially

available for this particular purpose in highly purified form and provides excellent results (Figure 4-4).

4.3.5. Two-Dimensional Detection in the OT Format.

The Achilles heel of suppressed IC is poor and nonlinear response to weak acids and essentially no response to very weak acids. In a review of the various approaches developed to measure all acids regardless of their K_a, Karu et al.[287] concluded that demonstrably the best approach is to introduce a small amount of strong base and measure the conductivity again.[288] A methodically simpler variation of this technique, involving vapor phase introduction of the base through a nonionic membrane, was recently introduced. Such two-dimensional conductometric detection can not only provide detection across the K_a horizon, it can provide K_a and ionic mobility values and identify presence of impurities. However, a potential pitfall common to all these techniques is the possible loss of neutrals (including un-ionized (very)weak acids) through the suppressor membrane. Shortly after the initial invention of IC[258] and the introduction of nonsuppressed conductometric technique,[289] Okada and Kuwamoto[290] pointed out that low concentrations of KOH provide excellent conditions for detection of very weak acids. Because of the low γ_{iex} values, OT columns provide a unique opportunity to nonsuppressed admittance detection first, followed by a suppressor and suppressed detection.

Normally, connecting any external detector leads to an unacceptable amount of dispersion, however, admittance (often inappropriately called

contactless conductance[291]) detection is possible on-column and is widely used in capillary electrophoresis. On the other hand, it produces poor and nonlinear response in very small capillaries when the background conductance is low, as in suppressed OTIC. Operating at low probe frequencies may ameliorate the problem,[292] but does not eliminate it.[293] A sequential on-column nonsuppressed admittance detector followed by a suppressor with an integrated true conductivity detection cell following it thus provides a uniquely applicable arrangement. In Figure 4-5, we show the results of an arrangement that is far from optimized. Given the much higher background conductance of the nonsuppressed detector and the fact that no thermostating was used; column and detector were both in ambient air, baseline noise is much higher. One may justifiably question whether new analytes that were not detectable in the suppressed detector can be detected under these circumstances at all. This question is clearly answered by the asterisked peaks in the nonsuppressed trace that are not visible in the suppressed trace. The second asterisked peak can be identified as CO_2 but the first peak, completely unanticipated may in fact be due to sodium present in the analytes: recall that in all surface agglomerated columns, the underlying cation exchange sites are also accessible, in principle allowing for simultaneous cation-anion analysis. Further, possibly minor analyte peaks, are denoted by question marks (and showed in amplified form in the red trace) and quite possibly the shoulder on the nitrate peak may be other weak acid analytes whose presence can only be

confirmed with certainty only after further improvement in S/N. Note that in Figure 4-5, not only the time scale has an offset between the top and bottom abscissae to account for the passage through the suppressor and the detector, the span is also longer in the suppressed chromatogram time scale to account for the additional column length.

Prima Facie, the two-dimensional detection approach, specifically the nonsuppressed detection, will not work with gradient elution. However, baseline rise in a gradient run occurs much more slowly (lower slope) than analyte peak excursion; given the progresses that has been made in Fourier analysis of chromatographic data,[294] or simply numerical baseline interpolation between peak valleys, should be straightforward to implement.

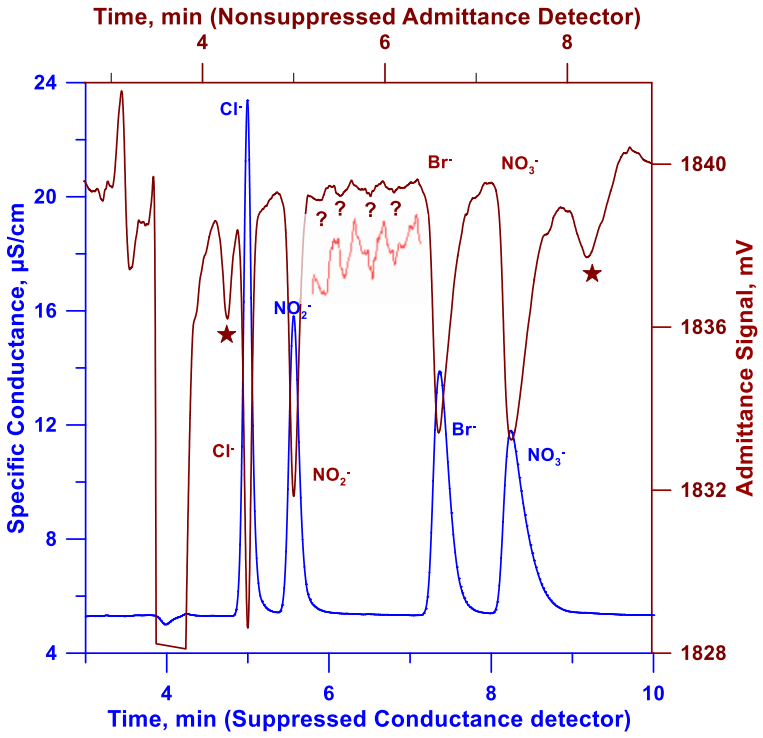

Figure 4- 5 Nonsuppressed admittance detection (dark red trace) before μsuppressor C and suppressed conductivity trace (blue). Note time axis

origin Abscissa span: bottom axis 3.00-10.00 min, top axis 2.70-8.925 min. PEEK column, 25 /360 μm, i.d./o.d.; Total length: 517 mm; Flow rate: 115 nL/min; 100 μM each analyte; Eluent: 4 mM KOH. Admittance excitation 650 kHz, conductivity excitation: 3 kHz; Sampling rate: 187 Hz.

4.3.6. Suppressor-Induced Dispersion and Column Efficiency.

The data currently presented all obtained with an automated commercial internal slot injector for convenience, the minimum injection volume was 4 nL. In a 25 μm φ column, this amounts to a length of ≳ 3 cm, ~6% of the length of the 51 cm column, much greater than what would provide optimum efficiency. But even under these conditions, it is possible to conclude that suppressor induced dispersion is still perceptible: peak efficiencies decrease from the nonsuppressed to the suppressed detector, there is even a perceptible difference between the efficiencies observed with the 0.4 mm vs. the 0.7 mm suppressor (see Table 4-1). There is thus still a continued incentive to develop smaller bore suppressors, especially if the column bore is to be reduced further.

It is worth comparing the efficiencies reported in Table 4-1 with those calculated from the relevant form of the Golay equation[295,296] which does not have any stationary phase mass transfer limitations (unlikely in a monolayer latex-based stationary phase, where individual latex particles are only 65 nm in diameter):

$$H = \frac{2D_m}{u} + \frac{1+6k+11k^2}{24(1+k)^2}\frac{r^2}{D_m}u \qquad \ldots(2)$$

Table 4- 1 Theoretical and Experimental Efficiencies

Analyte	Ret Factor k	Efficiency kPlates/m (sd)			
		Theoretical	Non-Suppressed	Suppressor 0.4 mm	Suppressor 0.7 mm
Chloride	0.31	32.4	29.0 (2.4)	22.1 (0.5)	20.7 (0.7_5)
Nitrite	0.46	24.7	23.4 (3.1)	17.0 (0.5)	15.2 (0.4)
Bromide	0.92	17.9	13.3 (3.0)	12.6 (0.3_5)	11.6 (0.3)
Nitrate	1.15	14.6	8.3 (0.3)	8.3 (0.5)	7.1 (0.2)

where H, D_m, u, k, and r respectively connotes plate height, diffusion coefficient of the analyte in the mobile phase, eluent liner velocity (0.404 cm/s for the data in Table 4-1), analyte retention factor and the radius of the capillary, respectively. D_m was computed from the tabulated equivalent conductance data and the Nernst-Einstein equation and in cm^2/s ranged from 1.89×10^{-5} for NO_3^- to 2.07×10^{-5} for Br^-.[297] It will be observed that except for nitrate, the experimental values for the nonsuppressed detection are not vastly different especially considering the large injection volume is adversely affecting the early eluting peaks in particular. The experimental plate counts were computed based on $5.54\ (t_R/W_{0.5})^2$ which implicitly assumes a Gaussian peak; this is clearly not the case for nitrate. In addition, the difference from theoretically expected values seems to increase with increasing *k.* While we have neglected resistance to mass transfer in the stationary phase, this is inversely related to the diffusion coefficient in the stationary phase; this is expected to be smaller for high *k* analytes. Finally, the difference in efficiency for nitrite in the nonsuppressed and the

suppressed mode is not only due to dispersion in the suppressor but also the dependence of ionization and hence the conductivity signal on the concentration.

From eq 1 it can be readily computed that if operated at the optimum flow rates, the maximum efficiencies that should be attainable will range from ~62,800 plates/m for NO_3^- to ~91500 for Cl^-, but those efficiencies will require corresponding flow rates of 0.01 – 0.04 cm/s, 40 - 10x lower than that used, resulting in impractically long separation times.

4.3.7. Low Level Performance. Limit of Detection.

Figure 4-6 shows the system response at sub-ppm levels (40 fmol, 1.4-3.2 pg injected) with two segments (2.0-3.0 min, 5.2 – 6.2 min) of the baseline are shown magnified (right ordinate) as the blue traces. The drift corrected baseline standard deviations are 1.2 and 1.1 nS/cm, respectively. One would appreciate that these values are respectable by commercial benchtop standards and especially remarkable in the absence of thermostating. The Signal/baseline standard deviation of the chloride peak is ~900. On a S/N = 3 basis, the LODs for Cl^-, NO_2^-, Br^-, NO_3^- are estimated to be 1.2, 3.8, 7.6, and 6.8 μg/L, respectively.

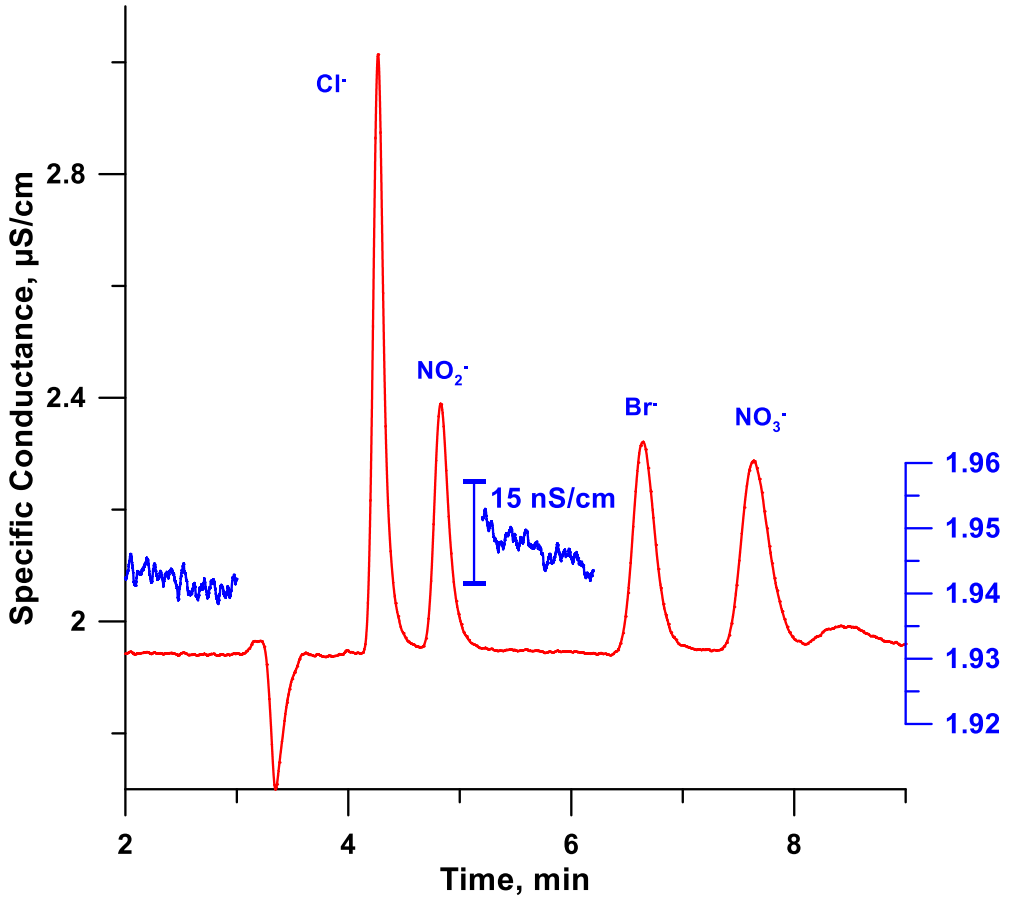

Figure 4- 6 Chromatogram at 10 μM analyte level. Suppressor length 0.7 mm; conditions same as Figure 4-5 except flow rate is 126 nl/min.

4.4. CONCLUSION

We established a method to fabricate microsuppressors by casting a novel ion exchange polymer around a wire mandrel, crosslinking the material by thermal annealing, and subsequently removing the microwire. Despite a highly hydrophilic ion exchanger matrix, low background conductance chemical suppression and excellent detection performance was shown possible with an integrated tubular microconductivity cell, with LODs for common ions in the single digit μg/L or single to double digit

femtogram amounts injected on-column. The suppressor used in this work was ~45 μm in bore; although sub-mm in active length, the induced dispersion is perceptible. The next step will be to couple smaller bore columns and suppressors of matched bore

Chapter 5

SUMMARY AND FUTURE WORK

5.1 Summary

In this dissertation, a novel moldable high-capacity ion exchange membrane was formulated, developed, and characterized. The synthesis utilized environmentally friendly chemicals. The fact that the new IEP can be cast into any mold from the prepolymer solution gives it unique capabilities as no other IEP has been described. The IEP can be made with PVA:SS ratios over a wide range and the experimental IEC values closely match those theoretically expected from the ratio of the starting ingredients. Very high IEC values can be realized. The IECs of the polymer are stable over many repeated regeneration and utilization cycles. It absorbs more water compared to available IEMs in the market.

This dissertation demonstrated that a cylindrical microchannel can only be made by using a fine wire as a mandrel, that such cahnnel can be used successfully as a microsuppressor in the current practice of OTIC. A low conductivity background (approaching pure water) is obtained and a significant range of eluent concentration can be suppressed. The suppression capacity was measured for a 45 μm bore 700 μ, long suppressor and peak efficiencies were measured for both 400 and 700 μm lengths of the suppression channel. The IEP material, in the form of the

microsuppressor was characterized for leaching of ionic and neutral materials from the polymer matrix. Similar results were obtained on a commercial suppressor based on a radiation grafted PTFE membrane. much greater leaching was observed from the later membrane, creating an undesirably high MS background.

5.2 Future Work

The actual column size that is currently used in our OTIC system is 19-25 μm. This suggests that a 45 μm bore of the capillary suppressor is still too large. Indeed, suppressor-induced dispersion was measurable. An obvious step will be to miniaturize the capillary suppressor to $<$ 25 μm channels by casting the (pre)polymer solution around smaller wires like 15 μm resulting in $<$ 25 μm channel in the hydrated form of the polymer. Such efforts are already being made in the laboratory.

This novel IEP is mechanically strong for intended applications without adding any cross-linker. However, fabricating the chemically regenerated μsuppressor from it requires regenerants with large counterion rather than sulfuric acid which is a typical regenerant in this field to avoid any regenerant leaking due to broken Donna forbidden barrier. I suggest adding very a few percentages dose of cross-linker such as glutaraldehyde may resolve this limitation.

The IEM containing the microchannels can also serve as the capillary size electrodialytic eluent generator (EDG) for IC applications. Chapter 2 of

this dissertation discusses the necessity of EDGs in IC and their vital role to generate an online ultrapure eluent to protect the columns and perform a very robust IC.

Appendix A

SUPPORTING INFORMATION FOR CHAPTER 3

Table A-S 1 Preparation of PVA-SSNa polymers

10% w/v PVA, mL	PVA Taken, g	50% w/v SSNa, mL	SSNa Taken, g	Total weight PVA + SS Taken, g	Total Solution volume mL	Anticipated wt %SSNa dry polymer
38	3.8	0.4	0.2	4.0	38.4	5.0
36	3.6	0.8	0.4	4.0	36.8	10
34	3.4	1.2	0.6	4.0	35.2	15
32	3.2	1.6	0.8	4.0	33.6	20
30	3.0	2.0	1.0	4.0	32.0	25
28	2.8	2.4	1.2	4.0	30.4	30
24	2.4	3.2	1.6	4.0	27.2	40

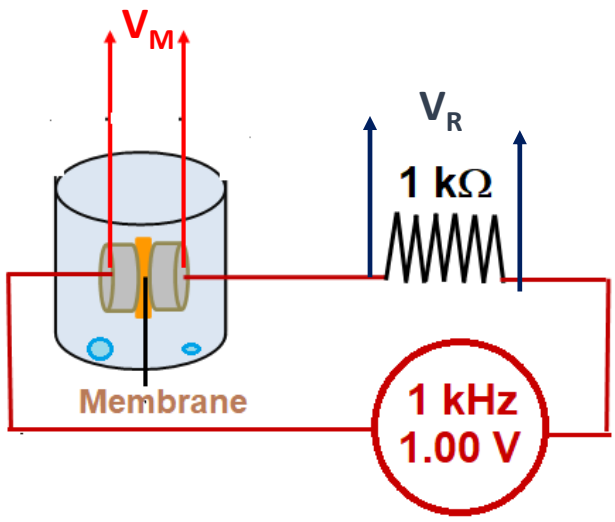

Figure A-S 1 Measurement arrangement for across the membrane specific conductance (κ_n). The test membrane, just larger than a pair of 3 mm dia. Neodymium magnets that contact it from either side, is initially wetted with deionized water and then put in a air-filled ziploc® bag with some liquid water at the bottom. The membrane is excited with 1 kHz sine wave, 1.00-1.20 V in amplitude with a 1 kΩ precision resistor in series. The voltage

across the membrane (V_M) and that across the resistor (V_R) are measured by independent high input impedance voltmeters.

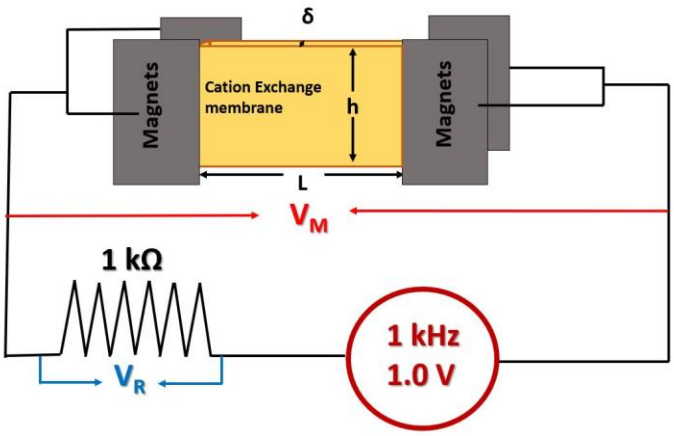

Figure A-S 2 Arrangement to measure tangential specific conductance (κ_t).

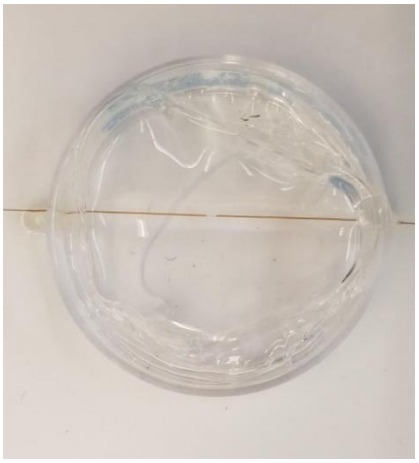

Figure A-S 3 Photomicrograph of a microchannel under construction. The silica capillaries (100 μm i.d., 365 μm o.d.) are affixed on the petri-dish with a drop each of hot-melt adhesive. The 25 μm tungsten wire insert can be seen between the two capillaries. The clear prepolymer solution has already been poured and is largely polymerized

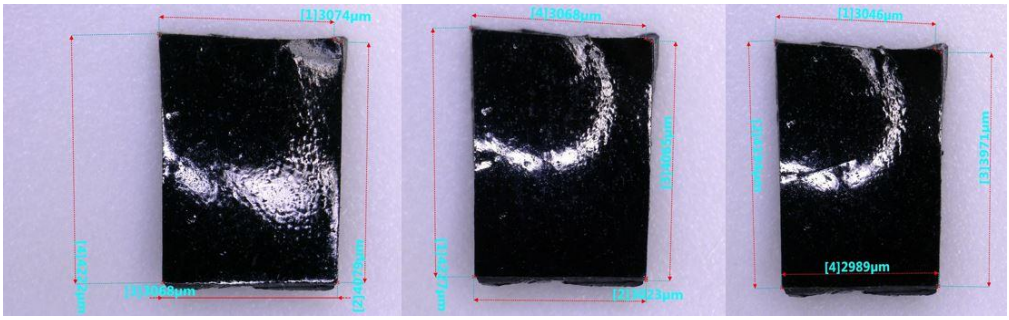

Figure A-S 4 Dry dimensions of rectangular polymer sample (PVA-SS25) after boiling in water, redrying, and repeating the process. From left to right: first round, second round and third round of this process. There is no significant change within experimental error.

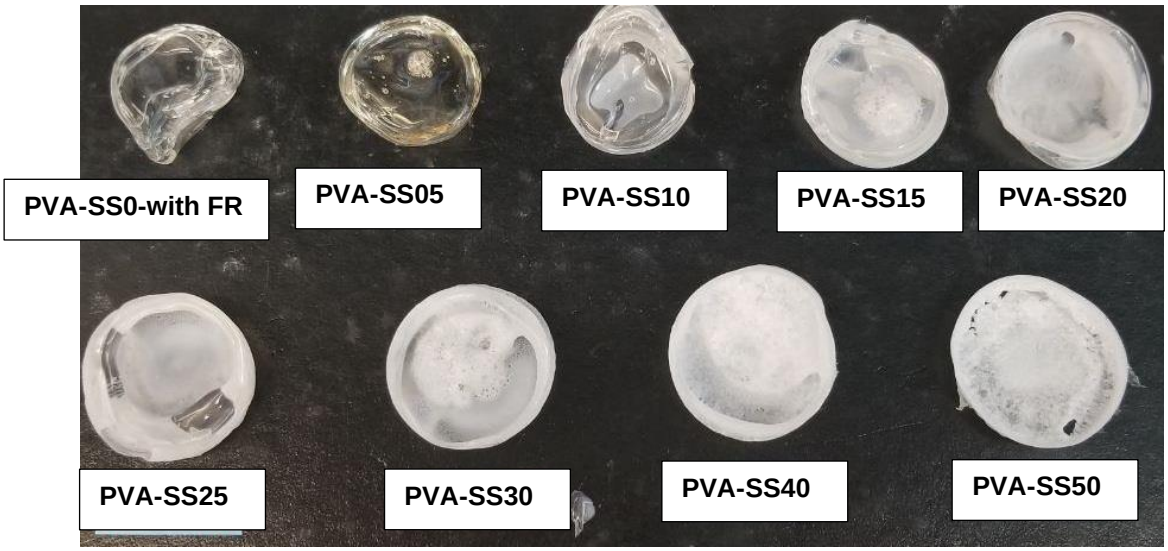

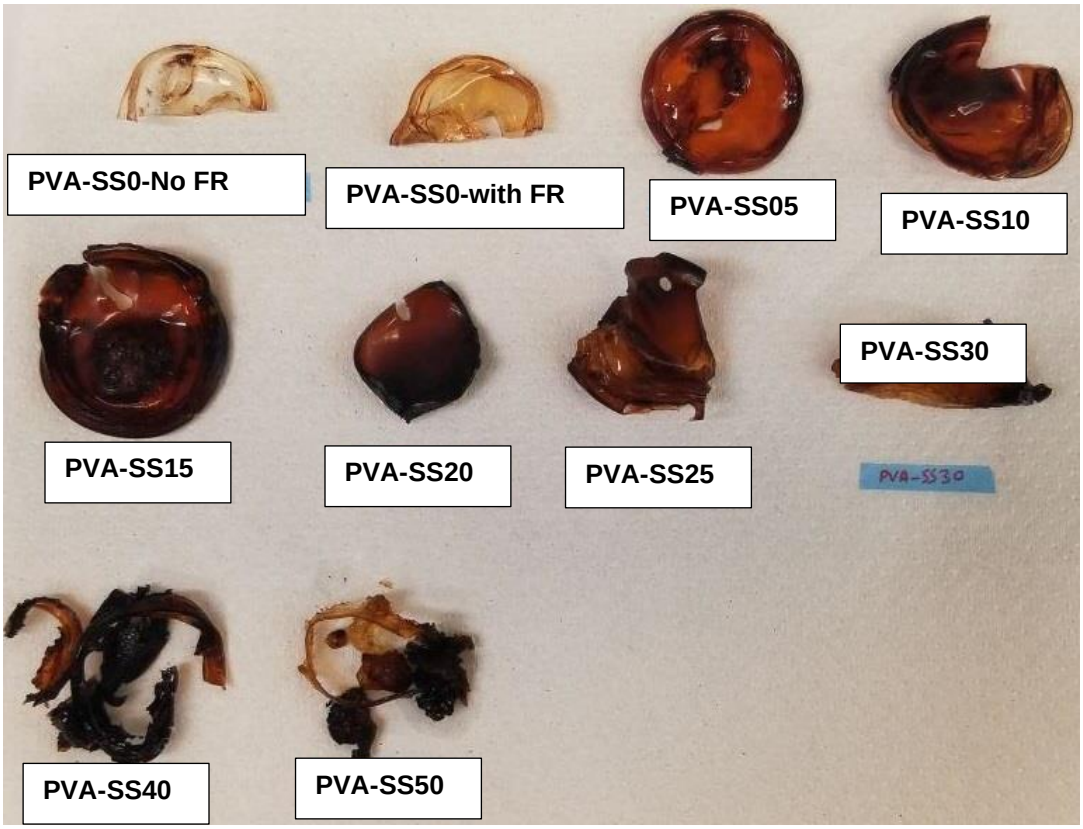

Figure A-S 5 PVA-SS0 to PVA-SS50 polymers. Top: PVA-SS0 to PVA-SS50 polymers Na^+-form, before annealing and conversion to H^+ form. Bottom: After conversion to H^+- form and 2 hours of annealing at 120 °C.

Visible Spectral Absorption Measurement

A 50 W quartz-halogen lamp was used as the light source and a back-thinned TE-cooled CCD spectrometer (Exemplar pro, BWTEK, https://bwtek.com/products/exemplar-pro/) was used as the detector. Both the source and detector were equipped with SMA terminated fiber optic, which snugly fit inside a 3 mm i.d. PTFE guide tube. The annealed H^+-form polymer membranes were soaked overnight in water to be fully hydrated. Disks, ~2.9 mm ϕ, ranging in thickness from just under 1 mm to just over 2

mm, were punched out with a cork borer and the thickness was measured with a micrometer. The polymer disc was simply sandwiched between the source and detector optical fibers using the PTFE tube as a guide; an even pressure was maintained while the spectra was collected. The reference light data was collected without the membrane in place but with about the same separation between the fibers. This is not a perfect substitute for an optically transparent membrane of the same refractive index and thickness and this limitation of the reported absolute absorbance data in Figures B-S6 and S7 should be kept in mind.

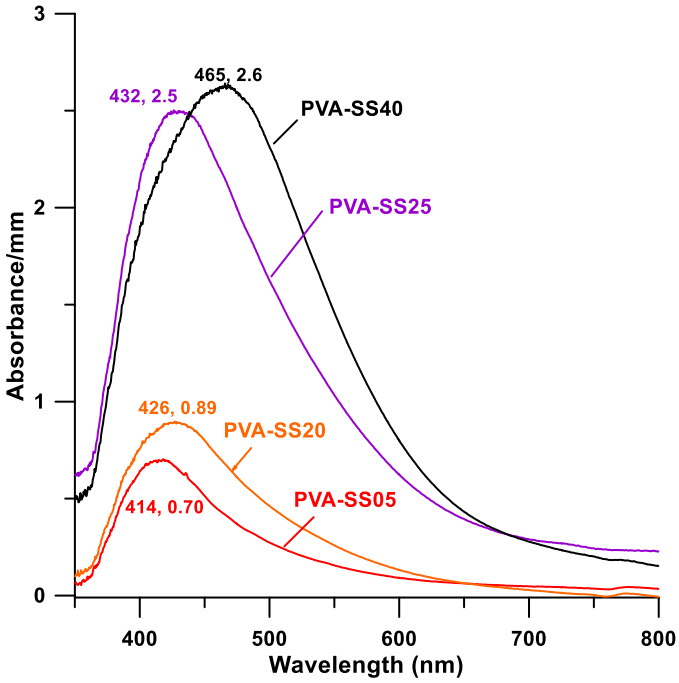

Figure A-S 6 Spectral absorption of selected PVA-SS polymers (initially containing nominally 5, 20, 25, and 40% SSNa), converted to H^+-form and annealed for 1 h at 120° C. Each curve also shows the wavelength of maximum absorption followed by the maximum absorbance/mm recorded

(λ_{max}, A_{max}/mm). Both increase with increasing SS content. Actual thickness of the polymers measured ranged from ~1 mm (for the two higher SS content polymers) to ~ 2 mm (for the two lower SS content polymers). Note that general opacity increases across the wavelength span as the SS content increases.

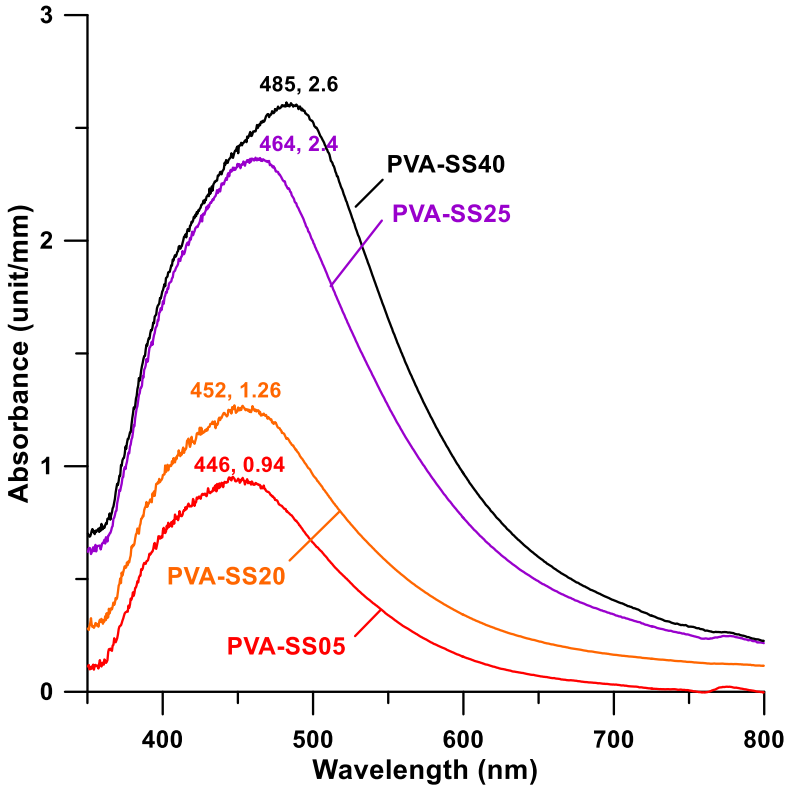

Figure A-S 7 Same as Figure A-S6, except after annealing for 2 h at 120 ° C. λ_{max}, A_{max}/mm are listed as before. The absorption maximum has red-shifted in all cases, compared to the 1 h annealed samples. The absorbance has also increased noticeably for the two lower SS content samples; the absorbance is too high for the two higher SS content samples for a difference to be measured with significance, especially considering that the samples being measured are different (not the same

1 h annealed sampled measured after another hour of annealing). Actual thickness of the polymers measured ranged from ~1 mm (for the two higher SS content polymers) to ~ 2 mm (for the two lower SS content polymers).

Figure A-S 8 Phase separation occurs if a PVA solution is put through repeated-freeze-thaw cycles. A simple way to visualize this is to incorporate a very hydrophilic dye. In the illustration, Nigrosin was incorporated in the PVA solution. The photograph depicts the result after three freeze-thaw cycles. Experiment and photograph courtesy of Payton A. Wasemiller.

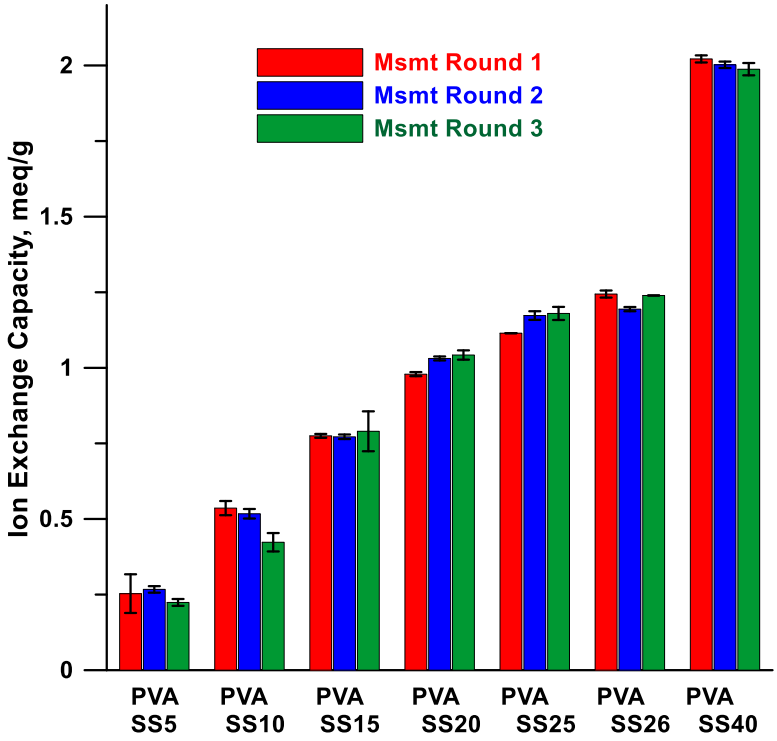

Figure A-S 9 Sequential triplicate measurement of ion exchange capacity of a particular polymer sample , one for each composition. Note that in repeated IEC measurement, the same polymer sample is initially treated with excess base for a long period, washed with acid for long periods (at least ten times), and this entire process is repeated twice more – any loss of the ionomer will readily show up as a loss in IEC as measurements continue. The error bars indicate ± 1 standard deviation. These data show no statistically significant trend red>blue>green as would occur on a washout loss.

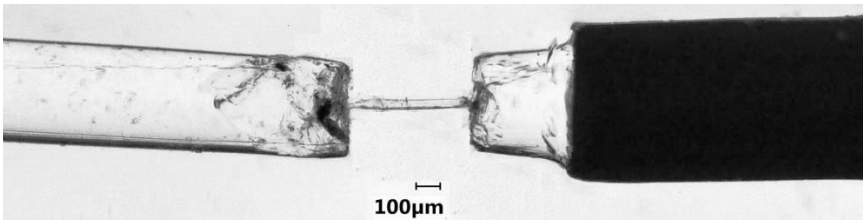

Figure A-S 10 A ~0.5 mm long, 0.03 mm dia. microchannel in PVA-SS25.

The outer channels are ~400 µm diameter. The right contains a 635 µm (0.025 in.) o.d. PEEK capillary that fits tightly into the elastomeric polymer; the connection readily withstands 300 psi.

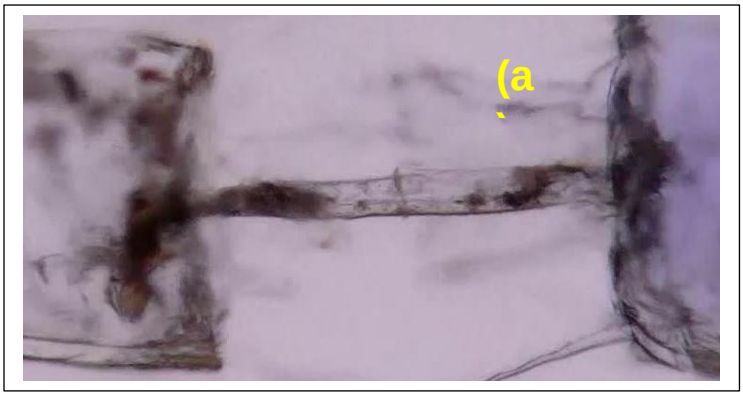

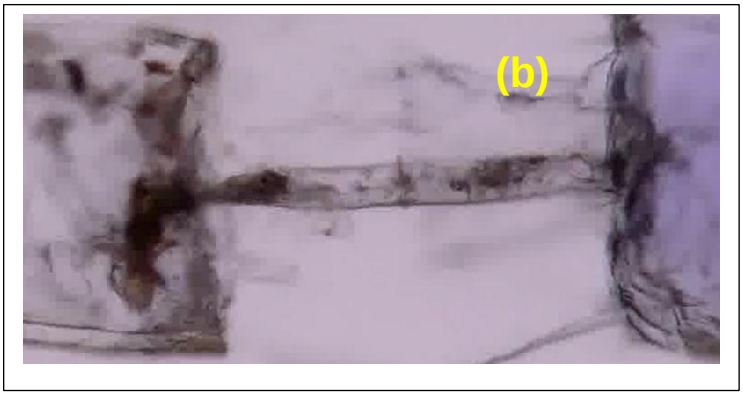

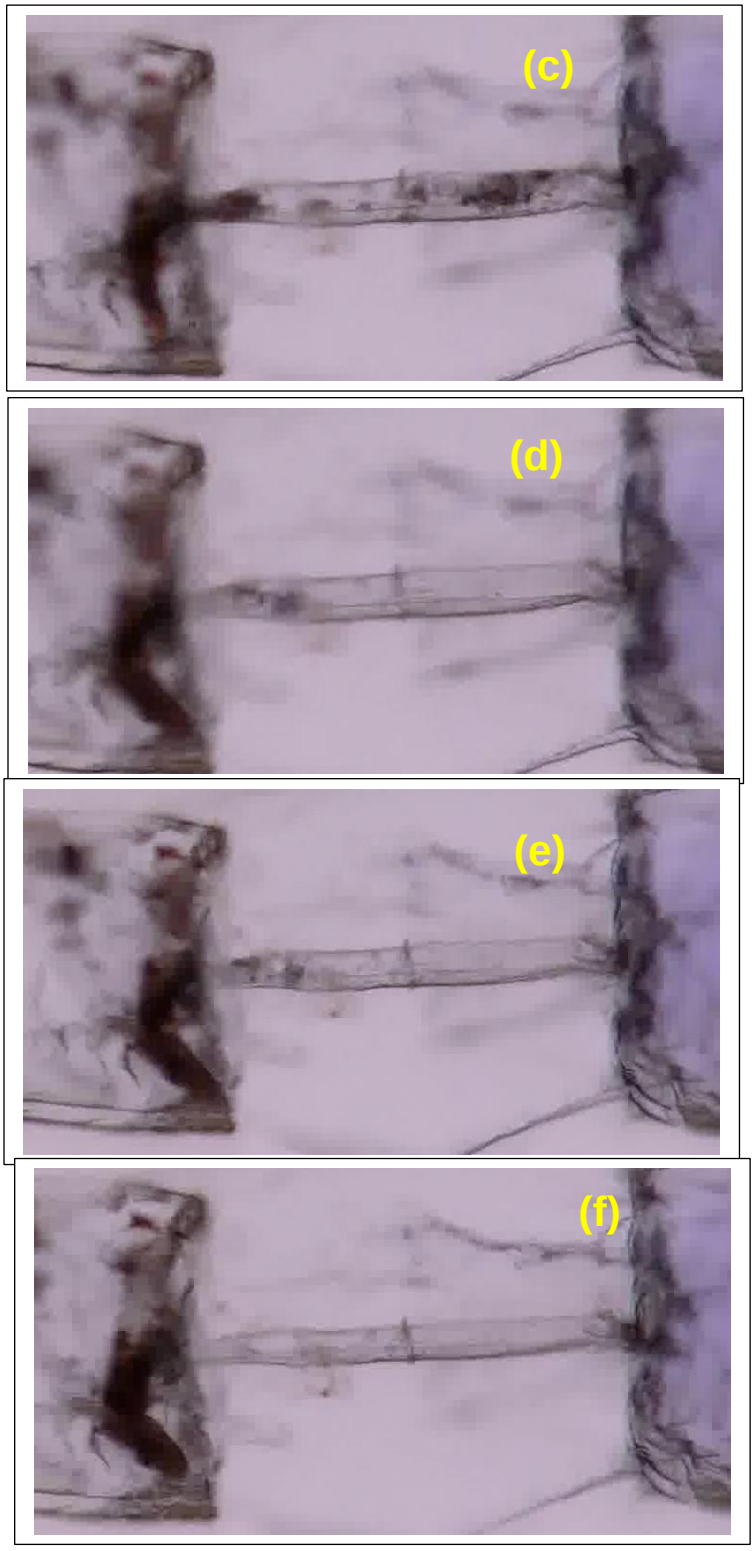

Figure A-S 11 Water was pumped from the left to right at 1 μL/min using a Milligat pump (low flow rate, high pressure version, www.globalfia.com). The pump is capable of low nL/min flow rates and pressures to 1 kpsi.

Panels (a) –(e) occur in that sequence and from beginning to end are 9 s apart. Panel (a) starts where the majority of the particles have clumped at the exit end, a smaller clump is just past the entrance of the microchannel. By (b) pressure has accumulated (the careful observer will note channel enlargement near the exit clump) and movement has started. Much of the exit clump has fallen into the exit channel – the velocity is much lower there and it does not really move in the exit channel. The clump near the inlet is dispersing. In (c) there is further movement of the exit clump and parts of the inlet clump can now be seen downstream. In (d) and (e) the exit clump is gone, and the remains of the entry clump approaches the exit. In (f) the channel is clear; the particles have accumulated in the low velocity exit channel like extruded debris.

Appendix B

SUPPORTING INFORMATION FOR CHAPTER 4

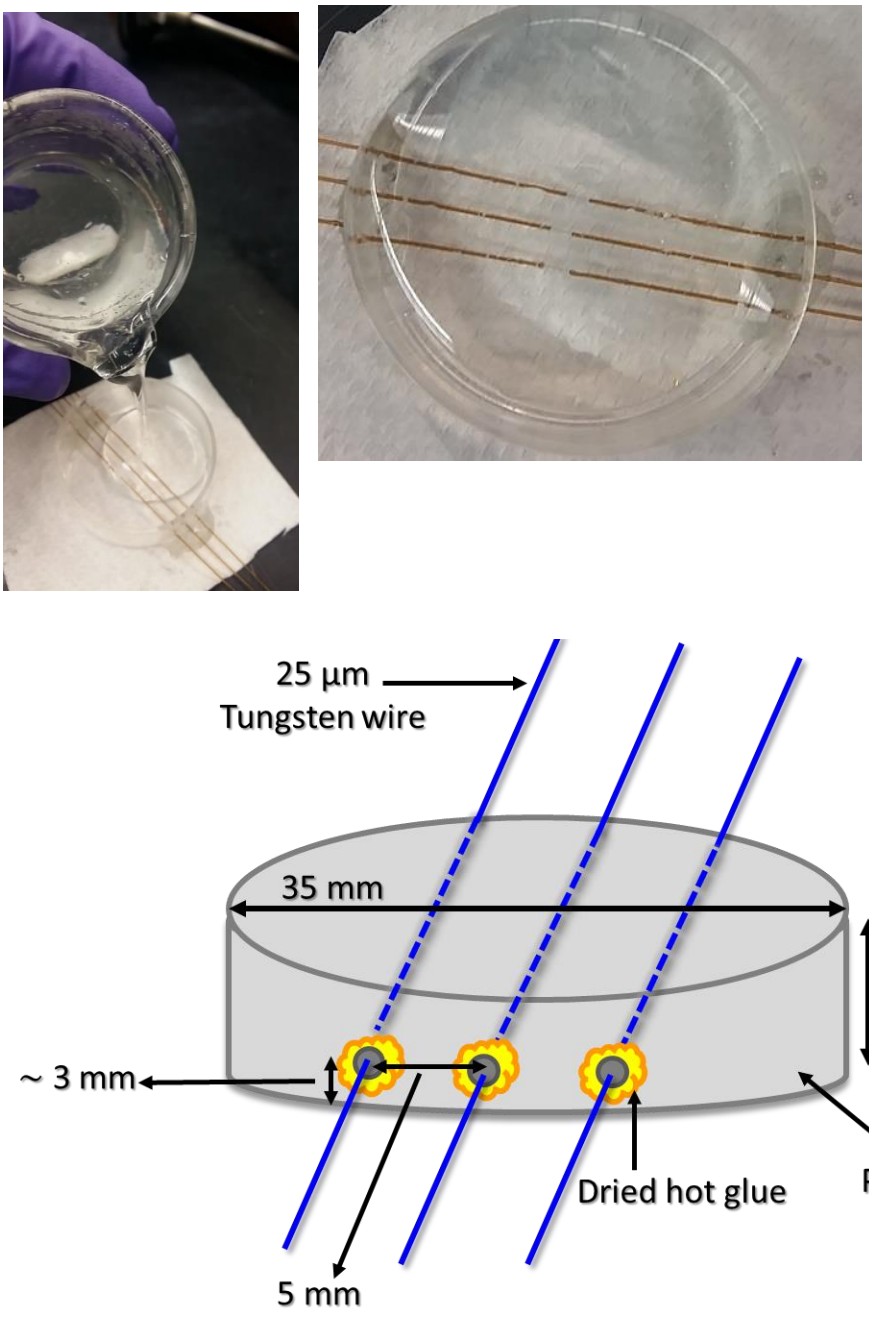

Figure B-S 1 Casting the (pre)polymer solution around a tungsten wire mandrel.

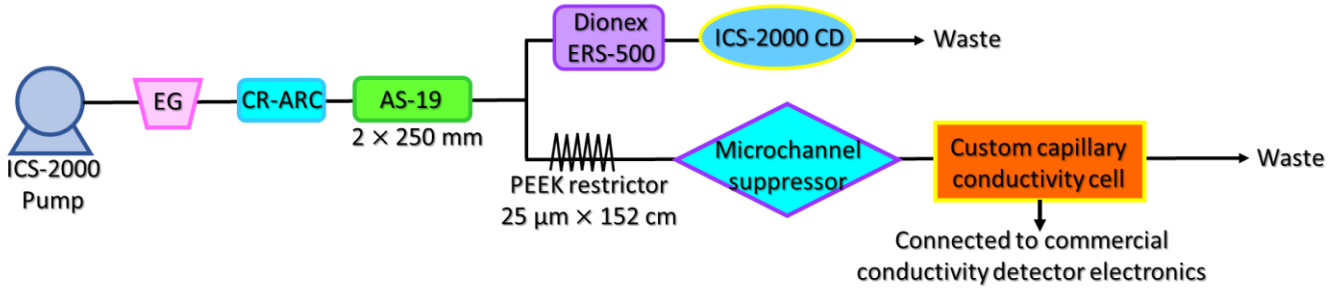

Figure B-S 2 The test arrangement of measuring the background conductance.

MS Operating Conditions

	5 mL/min	250 mL/min
Spray Voltage (V)	-3000	-3500
Vaporizer Temp (°C)	80	250
Sheath Gas Pressure	30	25
Ion Sweep Gas Pressure	0.6	0.2
Auxiliary Gas Pressure	5	5
Capillary Temperature (°C)	225	325
Skimmer Offset	0	0

Do the pressures have any units

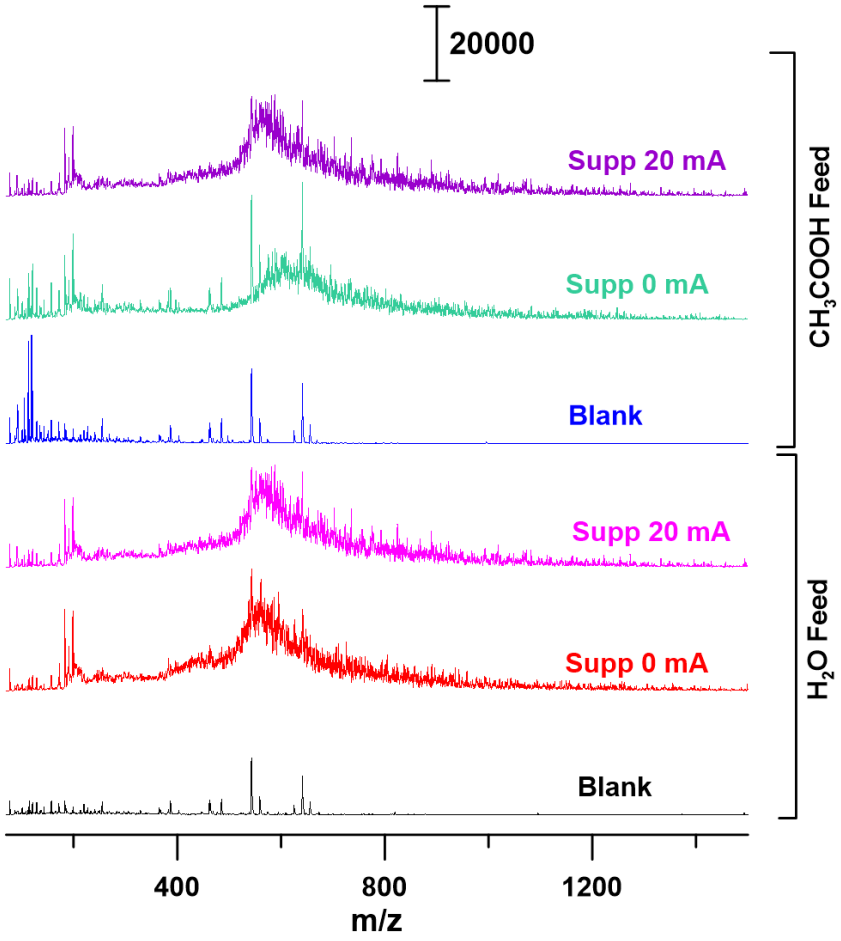

Figure B-S 3 Raw ion chromatograms for pumping DI water (bottom) and 0.01% HOAc (top) pumped into the MS at 5 μL/min (i) directly (black/blue traces) (ii) through the ERS-500 suppressor with 0 (red and green traces) and 20 mA (pink and purple traces) drive currents.

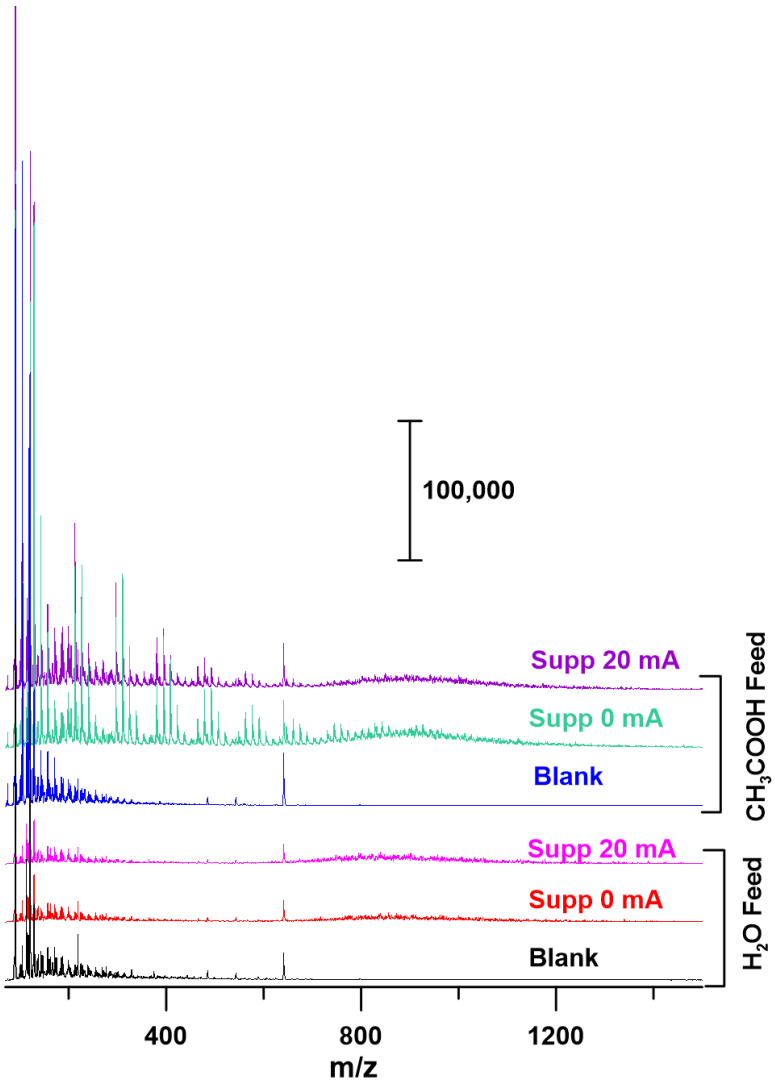

Figure B-S 4 Raw ion chromatograms for pumping (a) DI water and (b) 0.01% HOAc pumped into the MS at 250 μL/min (i) directly (ii) through the ERS-500 suppressor with 0 and 20 mA drive currents

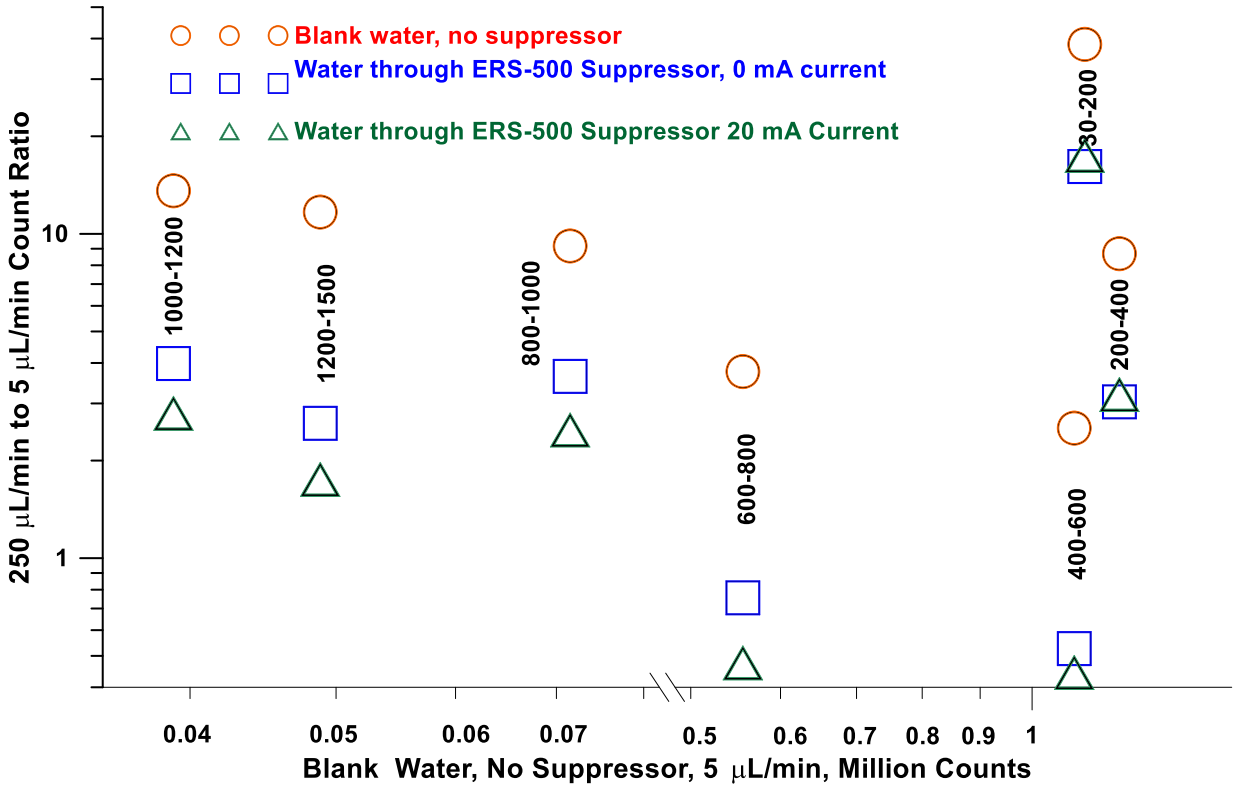

Figure B-S 5 The ratio of counts at 250 μL/min to that at 5 μL/min flow of water for (a) blank water directly into the MS, red circles; (b) via ERS-500 suppressor, no current, blue squares; (c) via ERS-500 suppressor, 20 mA current, green triangles, vs. blank water counts at 7 different mass ranges: 30-200, 200-400, 400-600, 600-800, 800-1000, 1000-1200 and 1200-1500.

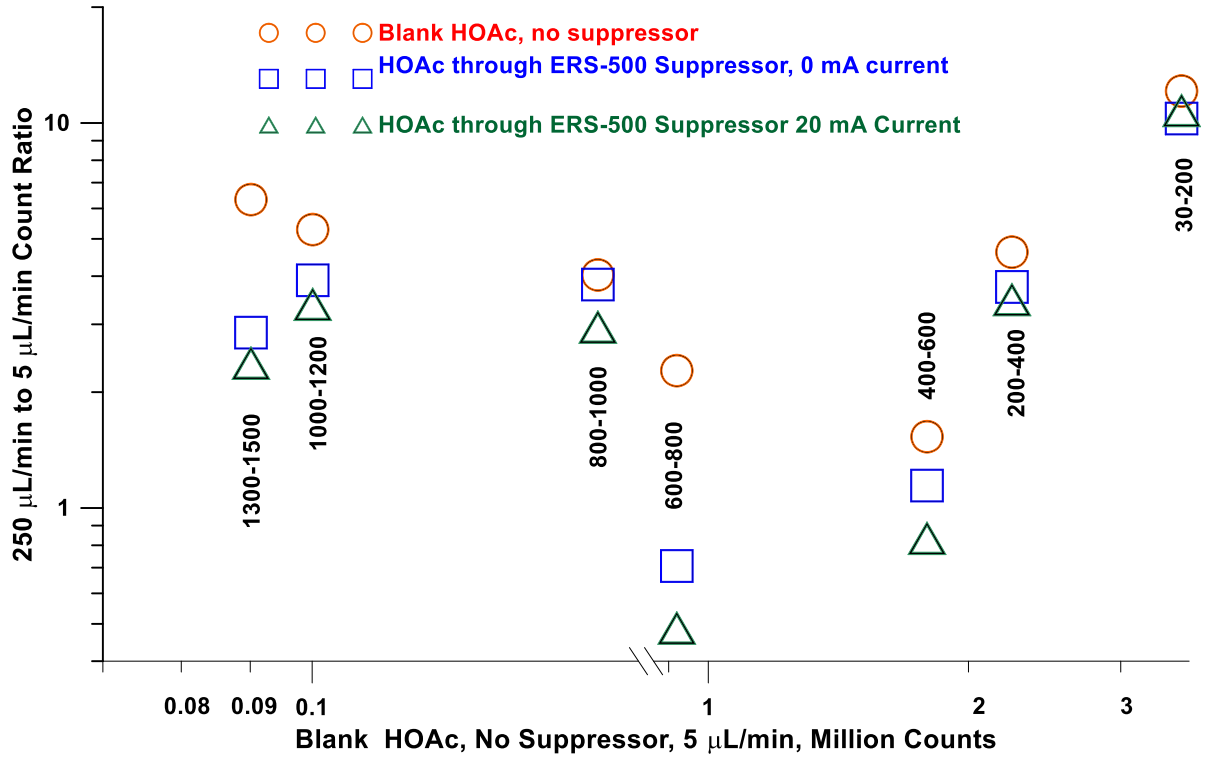

Figure B-S 6 The ratio of counts at 250 μL/min to that at 5 μL/min flow of 0.01% HOAc for (a) blank HOAc directly into the MS, red circles; (b) via ERS-500 suppressor, no current, blue squares; (c) via ERS-500 suppressor, 20 mA current, green triangles, vs. blank HOAc counts at 7 different mass ranges: 30-200, 200-400, 400-600, 600-800, 800-1000, 1000-1200 and 1200-1500.

Table B-S 1 Water: Ratio of Counts at 250 vs 5 μL/min in Different Mass Ranges

(Numerical Data for Figure B-S5)

		250:5 μL/min Count Ratio		
	5 μL/min	Direct	Via	Via
m/z Range	direct counts	Water	ERS-500	ERS-500
	millions		0 mA	20 mA
30-200	1.11	38.4	16.1	17.4
200-400	1.19	8.7	3.0	3.2
400-600	1.09	2.5	0.5	0.4
600-800	0.56	3.8	0.8	0.5
800-1000	0.07	9.2	3.6	2.5
1000-1200	0.04	13.6	4.0	2.8
1200-1500	0.05	11.7	2.6	1.7

Table B-S 2 0.01% HOAc: Ratio of Counts at 250 vs 5 μL/min in Different Mass Ranges

(Numerical Data for Figure B-S6)

		250:5 μL/min Count Ratio		
	5 μL/min	Direct	Via	Via
m/z Range	direct counts	0.01% HOAc	ERS-500	ERS-500
	millions		0 mA	20 mA
30-200	3.53	12.1	10.3	10.8
200-400	2.25	4.6	3.8	3.5
400-600	1.79	1.5	1.1	0.8
600-800	0.92	2.3	0.7	0.5
800-1000	0.16	4.0	3.8	3.0
1000-1200	0.10	5.3	3.9	3.4
1200-1500	0.09	6.3	2.9	2.4

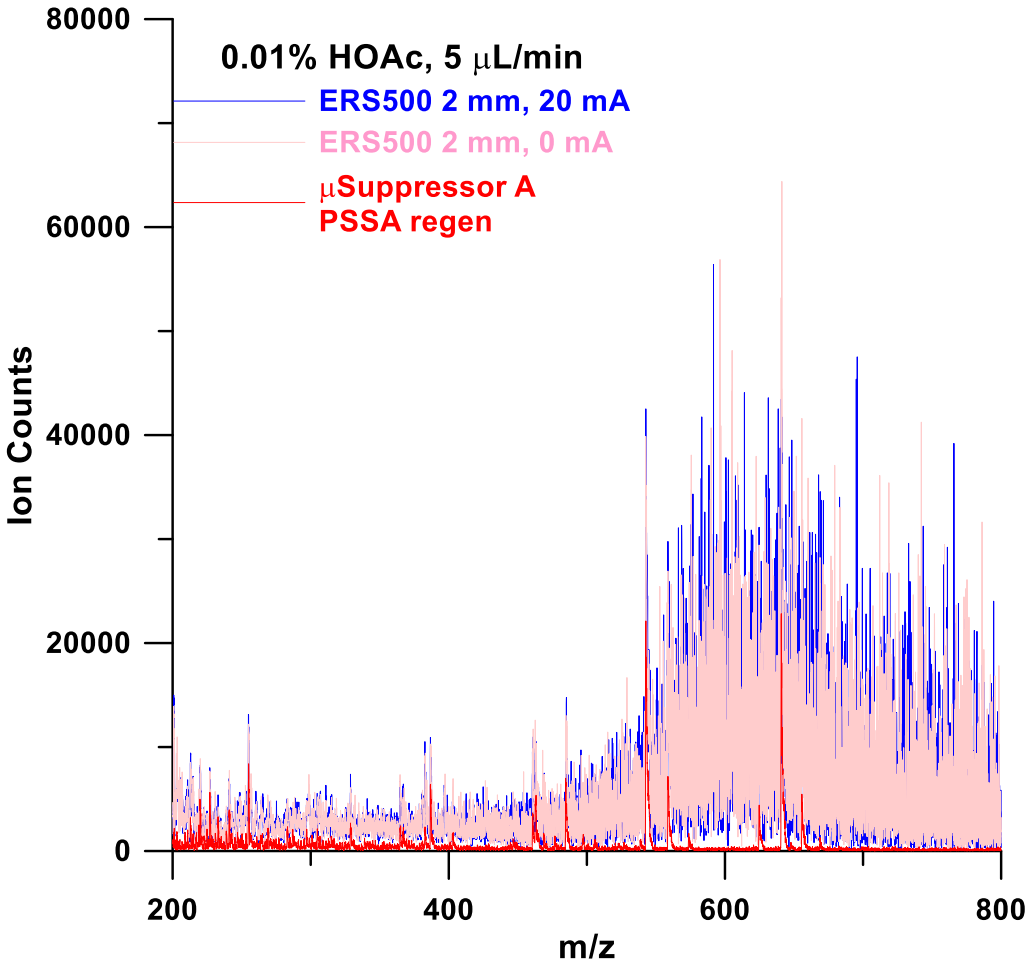

Figure B-S 7 MS response to 0.01% HOAc, through µsuppressor A (dark red trace) and ERS-500 effluents (0 mA: flesh colored trace, 20 mA: blue trace), all at 5 µL/min. This figure is equivalent to Figure 4-2 in the main text, except this is for 0.01% HOAc.

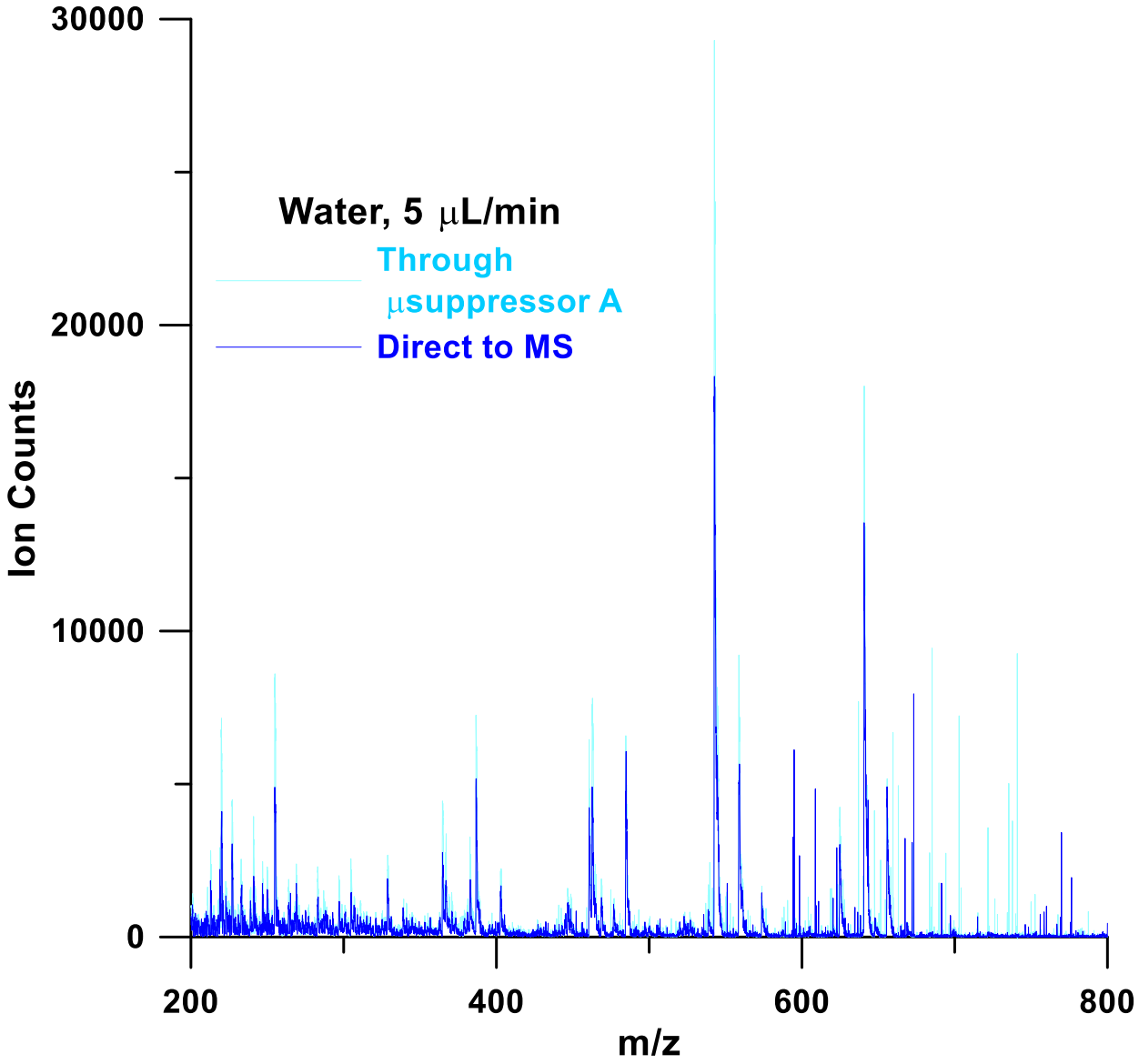

Figure B-S 8 MS response of water direct into the MS or through microsuppressor A shows that with rare exceptions (perhaps in the m/z 675-750 range), the same peaks are present in both cases.

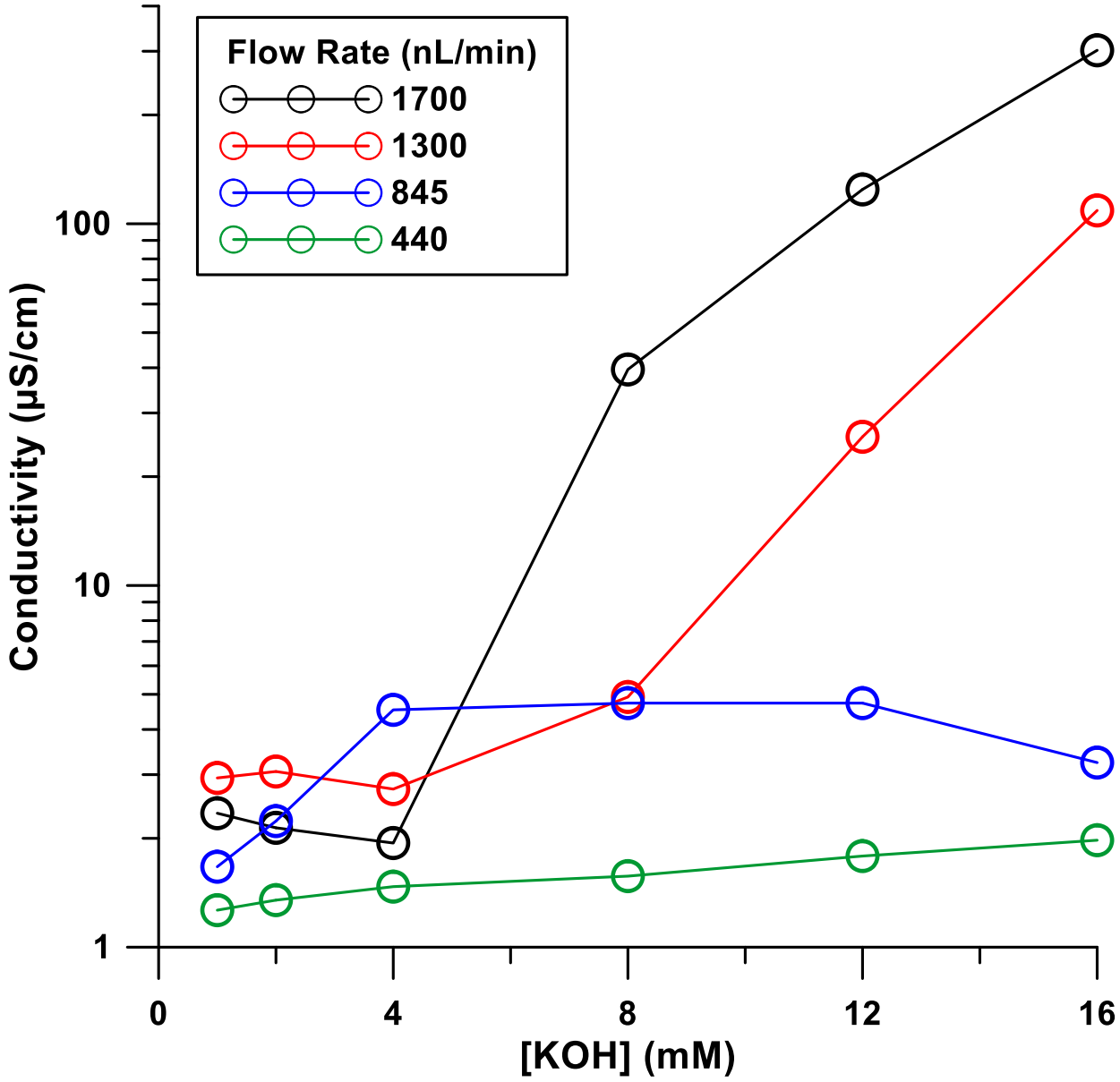

Figure B-S 9 Suppressed background conductance (SBC) at different flow rates from µsuppressor A.

References

(1) Small, H.; Stevens, T. S.; Bauman, W. C. *Anal. Chem.* **1975**, 47 (11), 1801–1809.

(2) Buchberger, W. W. *TRAC - Trend Anal. Chem.* **2001**, 20 (6–7), 296–303.
(3) Huang, W.; Dasgupta, P. K. *Anal. Chem.* **2016**, 88 (24), 12021–12027.
(4) Stevens, T.S.; Davis, J.C.; Small, H; Anal. Chem. 1981, 53, 1488-1492.

(5) Stevens, T.S.; Jewett, G. L.; Bredeweg, R. A. *Anal. Chem.* **1982**, 54, 1206-1208.

(6) Stevens, T.S.; Jewett, G.L.; Bredeweg, R.A.; Westover, L.B.; Small, H. European patent application no. 82201155.7, publication no. 0 075 371, Al, September 17, **1982**.

(7) Gupta, S.; Dasgupta, P. K. *J. Chromatogr. Sci.* **1988**, 26, 34-38.

(8) Hanaoka, Y.; Murayama, T.; Muramoto, S.; Matsuura, T.; Nanba, A. *J. Chromatogr. A*. **1982**, 239, 537-548.

(9) Dasgupta, P.K. *Anal. Chem.* **1984**, 56, 96-103.

(10) Dasgupta, P.K. *Anal. Chem.* **1984**, 56, 96-103.

(11) Waiz, S.; Cedillo, B.M.; Jambunathan, S.; Hohnholt, S.G.; Dasgupta, P.K.; Wolcott, D.K. *Anal. Chim. Acta*. **2001**, 428, 163-171.

(12) EMD Millipore Corp. SeQuant CARS and SAMS. https://www.emdmillipore.com/US/en/products/analytics-sample-prep/chromatography-for-analysis/ion-chromatography/cars-and-sams/0UKb.qB.u.UAAAE_zvB3.Lxi,nav

(13) Dasgupta, P.K.; Bligh, R.Q.; Mercurio, M.A. *Anal. Chem.* **1985**, 57, 484-489.
(14) Dasgupta, P. K. *Anal. Chem.* **1984**, 56, 769-772.

(15) Stillian, J. *LC Mag*. **1985**, 3, 802-812.

(16) Liu, Y.; Srinivasan, K.; Pohl, C.; Avdalovic, N. *J. Biochem. Biophys. Methods.* **2004**, 60, 205-232.

(17) Rokushika, S.; Qiu, Z.Y.; Hatano, H. *J. Chromatogr. A.* **1983**, 260, 81-87.

(18) Sjögren, A.; Boring, C.B.; Dasgupta, P.K. *Anal. Chem.* **1997**, 69, 1385-1391.

(19) Boring, C.B.; Dasgupta, P.K.; Sjögren, A. *J. Chromatogr. A.* **1998**, 804, 45-54.

(20) Boring, C.B.; Poruthoor, S. K.; Dasgupta, P.K. *Talanta*. **1999**, 48, 675-684.

(21) Kubáň, P.; Dasgupta, P.K.; Pohl, C.A. *Anal. Chem.* **2007**, 79, 5462-5467.

(22) Huang, X.; Dasgupta, P.K. *Anal. Chim. Acta*. **2011**, 689, 155-159.

(23) Huang, X.; Foss, F.W.; Dasgupta, P.K. *Anal. Chim. Acta*. **2011**, 707, 210-217.

(24) Rocklin, R.D.; Slingsby, R. W.; Pohl, C. A. *J. Liq. Chromatogr.* **1986**, 9, 757-775.
(25) Smith, F.C.; Chang, R.C.; Stevens, T.S. *Anal. Chem.* **1980**, 9, 197-217.
(26) Fritz, J.S. *Anal. Chem.* **1987**, 59, 335A-344A>

(27) Okada, T. *Anal. Chem.* **1988**, 60, 1666-1669.

(28) Okada, T; Dasgupta, P.K. *Anal. Chem.* **1989**, 61, 548-554.

(29) Tian, Z.W.; Hu, R.Z.; Lin, H.S.; Hu, W.L. *J. Chromatogr. A.* **1988**, 439, 151-157.

(30) Srinivasan, K.; Pohl, C. A. US Patent 6,425,284, July 30, **2002**.

(31) Tian, Z.W.; Hu, R.Z.; Lin, H.S.; Wu, J.T. *J. Chromatogr. A.* **1988**, 439, 159-163.

(32) Ohta, K.; Matsui, H.; Tanaka, K. *Bunseki Kagaku*. **1990**, 39, 457-461.
(33) Strong, D.L.; Dasgupta, P.K. *Anal. Chem.* **1989**, 61, 939-945.

(34) Strong, D.L.; Ung Joung, C.; Dasgupta, P.K. *J. Chromatogr. A.* **1991**, 546, 159-173.

(35) Rabin, S.; Stillian, J.; Barreto, V.; Friedman, K.; Toofan, M. *J. Chromatogr. A.* **1993**, 640, 97-109.

(36) Hu, R.Z.; Weng, Y.H.; Lai, L.M.; Chen, J.C.; Lin, Q. *Chromatographia*. **2003**, 57, 471-474.
(37) Huang, W.; Hu, R.; Wu, S.; Pan, D. *Electrochemistry (Chinese)*. **2006**, 12, 439-441.

(38) Huang, W.; Hu, R.; Chen, H.; Su, Y. *Analyst*. **2011**, 136, 901-903.

(39) Huang, W.; Chen, H.; Su, Y.; Hu, R. *Talanta*. **2010**, 82, 1364-1370.

(40) Kar, S.; Dasgupta, P.K.; Liu, H.; Hwang, H. *Anal. Chem.* **1994**, 66, 2537-2543.

(41) Qi, D.; Okada, T.; Dasgupta, P. K. *Anal. Chem.* **1989**, 61, 1383-1387.

(42) Small, H.; Liu, Y.; Riviello, J.; Avdalovic, N.; Srinivasan, K. US Patent 6,325,976, December 4, **2001**.

(43) Masunaga, H.; Higo, Y.; Ishii, M.; Maruyama, N.; Yamazaki, S. *Anal. Sci.* **2012**, 28, 1071-1074.

(44) Srinivasan, K.; Bhardwaj, S.; Lin, R.; Pohl, C. Wiley, New York, NY, **2012**, 91-106.

(45) Bazinet, L.; Lamarche, F.; Ippersiel, D. *Trend Food Sci. Technol.* **1998**, 9, 107-113.

(46) Masunaga, H.; Higo, Y.; Ishii, M.; Maruyama, N.; Yamazaki, S. *Anal. Sci.* **2014**, 30, 477-482.

(47) Srinivasan, K.; Omphroy, B.K.; Lin, R.; Pohl, C.A. *Talanta*. **2018**, 188, 152-160.

(48) Liu, Y.; Barreto, V.M.B.; Pohl, C.A.; Avdalovic, N. US Patent 8,415,168, April 9, **2013**.

(49) Huang, W.; Dasgupta, P.K. *Anal. Chem.* **2016**, 88, 12021-12027.

(50) Zhang, M.; Dasgupta, P.K., Conductance or Admittance? October **2015**, 215.

(51) Dasgupta, P.K.; Bao, L. *Anal. Chem.* **1993**, 65, 1003-1011.

(52) Avdalovic, N.; Pohl, C.A.; Rocklin, R.D.; Stillian, J.R. *Anal. Chem.* **1993**, 65, 1470-1475.

(53) Chen, Y.; Srinivasan, K.; Dasgupta, P.K. *Anal. Chem.* **2012**, 84, 67-75.

(54) Chen, Y.; Edwards, B.L.; Srinivasan, K.; Dasgupta, P.K. *Anal. Chem.* **2012**, 84, 59-66.

(55)Srinivasan, K.; Avdalovic, N. US patent 6,808,608. October 26, **2004**.

(56) Yabe, K.; Motomura, Y.; Ishikawa, H.; Mizuniwa, T.; Ohmi,T. *Microcontamination.* **1989**, 7, 37-45.

(57) Strong, D.L.; Dasgupta, P.K.; Friedman, K.; Stillian, J.R. *Anal. Chem.* **1991**, 63, 480-486.

(58) Dasgupta, P.K.; Bligh, R.Q.; Lee, J.; D'Agostino, V. *Anal. Chem.* **1985**, 57, 253-257.

(59) Huang, S.; Gao, M.; Zhang, F.; Lu, Y.; Yang, B. *J. Chromatpgr. A.* **2019**.

(60) Sjögren, A.; Boring, C.B.; Dasgupta, P.K.; Alexander, J.N. *Anal. Chem.* **1997**, 69, 1385-1391.

(61) Dasgupta, P.K.; Yang, B.; Srinivasan, K.; Takeuchi, M. US Patent 7,632,404. 15 December, **2009**.

(62) Yang, B.; Zhang, F.; Liang, X. *Talanta*. *2009*, 79, 68-71.

(63) Strong, D. L.; Dasgupta, P. K. *J. Memb. Sci.* **1991**, 57, 321-336.

(64) Yang, B.; Takeuchi, M.; Dasgupta, P.K. *Anal. Chem.* **2008**, 80, 40-47.

(65) Yang, B.; Zhang, F.; Liang, X.; Dasgupta, P.K. *J. Chromatogr. A.* **2009**, 1216, 2412-2416.

(66) Lu, Y.; Zhou, L.; Yang, B.; Huang, S.; Zhang, F. *Anal. Chem.* **2018**, 90, 12840−12845.

(67) Lu, Y.; Zhao, L.; Lin, S.; Zhang, F.; Yang, B. *Analyst*. **2019**, 144, 2411-2415.

(68) Shelor, C.P.; Yoshikawa, K.; Dasgupta, P.K. *Anal. Chem.* **2017**, 89, 10,063-10,070.

(69) Sricharoen, P.; Limchoowong, N.; Shelor, C.P.; Dasgupta, P.K. *Anal. Chem.* **2019**, 91, 3636-3644.

(70) Chen, Y.; Barreto, V.; Woodruff, A.; Lu, Z.; Liu, Y.; Pohl, C. *Anal. Chem.* **2018**, 90, 10,910-10,916.

(71) Yang, B.; Chen, Y.; Mori, M.; Ohira, S.; Azad, A.K.; Dasgupta, P.K.; Srinivasan, K. *Anal. Chem.* **2010**, 82, 951-958.

(72) Thermo Fisher Scientific. Dionex™ ICS-4000 QD Charge Detector and Cell. https://www.thermofisher.com/order/catalog/product/078814

(73) Simons, R. *Nature*. **1979**, 280, 824-826.

(74) Mori, M.; Chen, Y.; Ohira, S.; Dasgupta, P.K. *Talanta*, **2012**, 102, 44-52.

(75) Shen, G.; Chen, F.; Lu, Y.; Zhang, F.; Yang, B. *Anal. Chim. Acta*. **2016**, 943, 131-135.

(76) Ohira, S.; Kuhara, K.; Kudo, M.; Kodama, Y.; Dasgupta, P.K.; Toda, K. *Anal. Chem.* **2012**, 84, 5421-5426.

(77) Ohira, S.; Kuhara, K.; Shigetomi, A.; Yamasaki, T.; Kodama, Y.; Dasgupta, P.K.; Toda, K. *J. Chromatogr. A*. **2014**, 1372, 18-24.

(78) Ohira, S.; Hiroyama, Y.; Nakamura, K.; Koda, T., Dasgupta, P.K.; Toda, K. *Talanta*. **2015**, 132, 228-233.

[79] Ohira, S.; Yamasaki, T.; Koda, T.; Kodama, Y.; Toda, K. *Talanta*. **2018**, 180, 176-181.

(80) Ohira, S.; Nakamura, K.; Shelor, C.P.; Dasgupta, P.K.; Toda, K. *Anal. Chem.* **2015**, 87, 11575-11580.

(81) Ohira, S.; Nakamura, K.; Chiba, M.; Dasgupta, P.K.; Toda, K. *Talanta*. **2017**, 164, 445-450.

(82) Karu, N.; Dicinoski, G.W.; Haddad, P.R. *TrAC-Trend Anal. Chem.* **2012**, 40, 119-132.

(83) Tanaka, K.; Fritz, J.S. *Anal. Chem.* **1987**, 59, 708-712.

(84) Berglund, I.; Dasgupta, P.K. *Anal. Chem.* **1991**, 63, 2175-2183.

(85) Berglund, I.; Dasgupta, P.K. *Anal. Chem.* **1992**, 64, 3007-3012.

(86) Srinivasan, K.; Saini, S., Avdalovic, N. US patent 6,752,927, June 22, **2004**.

(87) Srinivasan, K.; Saini, S., Avdalovic, N. US patent 7,618,535, November 17, **2009**.

(88) Caliamanis, A.; McCormick, M.J.; Carpenter P.D. *Anal. Chem.*, **1997**, 69, 3272-3276.

(89) Caliamanis, A.; McCormick, M.J.; Carpenter, P.D. *J. Chromatogr. A.* **1999**, 850, 85-98.

(90) Caliamanis, A.; McCormick, M.J.; Carpenter, P.D. *J. Chromatogr. A.* **2000**, 884, 75-80.

(91) Al-Horr, R.; Dasgupta, P.K.; Adams, R.L. *Anal. Chem.* **2001**, 73, 4694-4703.

(92) Berglund, I.; Dasgupta, P.K.; Lopez, J.L.; Nara, O. *Anal. Chem.* **1993**, 65, 1192-1198.

(93) Sjögren, A.; Dasgupta, P.K. *Anal. Chem.* **1995**, 67, 2110-2118.

(94) Kadjo, A.F.; Liao, H.; Dasgupta, P.K.; Kraiczek, K.G. *Anal. Chem.* **2017**, 89, 3893-3900.

(95) Sjögren, A.; Dasgupta, P.K. *Anal. Chim. Acta.* **1999**, 384, 135-141.

(96) Dasgupta. P.K.; Tarter, J. G., Ed., Marcel Dekker, **1987**, 191-367.

(97) Mishra, S.K.; Dasgupta, P.K. *Anal. Chem.* **2010**, 82, 3981-3984.

(98) Pankratova, N.; Cuartero, M.; Cherubini, T.; Crespo, G.A.; Bakker, E. *Anal. Chem.* **2017**, 89, 571-575.

(99) Sateanchok, S.; Pankratova, N.; Cuartero, M.; Cherubini, T.; Grudpan, K.; Bakker, E. *ACS sensors*. **2018**, 3, 2455-2462.

(100) Davis, J.C.; Peterson, D.P. *Anal. Chem.* **1985**, 57, 768-771.

(101) Dasgupta, P.K.; Gupta, V.K. *Environ. Sci. Technol.* **1986**, 20, 524-526.

(102) Hwang, H.; Dasgupta, P.K. *Mikrochim. Acta*. **1985**, 87, 77-87.

(103) Hwang, H.; Dasgupta, P.K. *Anal. Chem.* **1986**, 58, 1521-1524.

(104) Davis, T.A. Encyclopedia of Desalination and Water Resources, Membrane Processes- Vol. II, Unesco-EOLSS.

(105) Blaedel, W.J.; Haupert, J.T. *Anal. Chem.* **1966**, 38, 1305-1308.

(106) Cox, J.A.; DiNunzio, J.E. *Anal. Chem.* **1977**, 49, 1272-1275.

(107) Cox, J.A.; Twardowski, Z. *Anal. Chem.* **1980**, 52, 1503-1505.

(108) Cox, J.A.; Olbrych, E.; Brajter, K. *Anal. Chem.* **1981**, 53, 1308-1309.

(109) Cox, J.A.; Cheng, K. *Anal. Chem.* **1978**, 50, 601-602.

(110) Akretche, D.; Kerdjoudj, H. *Talanta*. **2000**, 51, 281-289.

(111) Hichour, M.; Persin, F.; MolÃ©nat, J.; Sandeaux, J.; Gavach, C. *Desalination*. **1999**, 122, 53-62.

(112) Durmaz, F.; Kara, H.; Cengeloglu, Y.; Ersoz, M. *Desalination*. **2005**, 177, 51-57.

(113) Kir, E.; Alkan, E. *Desalination*. **2006**, 197, 217-224.

(114) DiNunzio, J.E.; Jubara, M. *Anal. Chem.* **1983**, 55, 1013-1016.

(115) Cox, J.A.; Tanaka, N. *Anal. Chem.* **1985**, 57, 2370-2373.

(116) Cox, J.A.; Gajek, R.; Litwinski, G.R.; Carnahan, J.; Trochimczuk, W. *Anal. Chem.* **1982**, 54, 1153-1157.

(117) Cox, J.A.; Tanaka, N. *Anal. Chem.* **1985**, 57, 383-385.

(118) Cox, J.A.; Tanaka, N. *Anal. Chem.* **1985**, 57, 383-385.

(119) Cox, J.A.; Dabek-Zlotorzynska, E. *Anal. Chem.* **1987**, 59, 534-536.

(120) PauláThomas, C.L. *Analyst.* **1989**, 114, 759-769.

(121) Dasgupta, P.K. *ACS Adv. Chem. Ser.* **1993**, 232, 41-90.

(122) Dasgupta, P.K.; Pawliszyn, J. (Ed.) Wilson and Wilson's Comprehensive Analytical Chemistry Series, vol. 37, Elsevier, Amsterdam, The Netherlands **2002**, 97-160.

(123) Ferm, M. *Atmos. Environ.* **1979**, 13, 1385-1393.

(124) Dasgupta, P.K. *Atmos. Environ.* **1984**, 18, 1593-1599.

(125) Dasgupta, P.K.; Phillips, D.A. *Sep. Sci. Technol.* **1987**, 22, 1255-1267.

(126) Berg, J. M.; James, D. L.; Berg, C. F.; Toda, K.; Dasgupta, P. K. *Anal. Chim. Acta*. **2010**, 664, 56-61.

(127) Genfa, Z.; Dasgupta, P.K.; Cheng, Y.S. *Atmos. Environ.* **1991**, 25A, 2717-2729.

(128) Fan, Q.; Dasgupta, P.K. *Anal. Chem.* **1994**, 66, 551-556.

(129) Li, J.Z.; Dasgupta, P.K.; Genfa, Z.; Hutterli, M.A. *Field Anal. Chem. Technol.* **2001**, 5, 2-11.

(130) Li, J.Z.; Dasgupta, P.K.; Luke, W.T. *Anal. Chim. Acta*. **2005**, 531, 51-68.

(131) Dasgupta, P.K.; Li, J.Z.; Zhang, G.; Luke, W.T.; McClenny, W.A.; Stutz, J.; Fried, A. *Environ. Sci. Technol.* **2005**, 39, 4767-4783.

(132) Eom, I.Y.; Li, Q.Y.; Li, J.Z.; Dasgupta, P.K. *Environ. Sci. Technol.* **2008**, 42, 1221-1226.

(133) Rappenglück, B.; Dasgupta, P.K.; Leuchner, M.; Li, Q.Y.; Luke, W. *Atmos. Chem. Phys.* **2010**, 10, 2413-2424.

(134) Li, Y.; Shao, M.; Lu, S.; Chang, C.C.; Dasgupta, P.K. *Atmos. Environ.* **2010**, 44, 2632-2639.
(135) Genfa, Z.; Dasgupta, P.K. *Anal. Chem.* **1992**, 64, 517-522.

(136) Zhu, Q.Z.; Li, Q.G.; Lu, J.Z.; Xu, J.G. *Anal. Lett.* **1996**, 29, 1729-1740.

(137) Matsubara, C.; Kawamoto, N.; Takamura, K. *Analyst*. **1992**, 117, 1781-1784.

(138) Zhang, G.; Dasgupta, P.K.; Sigg, A. *Anal. Chim. Acta*. **1992**, 260, 57-64.

(139) Li, J.; Dasgupta, P.K. *Anal. Chem.* **2000**, 72, 5338-5347.

(140) Li, J.; Dasgupta, P.K. *Anal. Chim. Acta.* **2001**, 442, 63-70.

(141) Li, J.; Dasgupta, P.K. *Anal. Sci.* **2003**, 19, 517-523.

(142) Li, J.; Dasgupta, P.K.; Tarver, G.A. *Anal. Chem.* **2003**, 75, 1203-1210.

(143) Toda, K.; Ohira, S.; Tanaka, T.; Nishimura, T.; Dasgupta, P.K. *Environ. Sci. Technol.* **2004**, 38, 1529-1536.

(144) Takeuchi, M.; Dasgupta, P.K.; Dyke, J.V.; Srinivasan, K. *Anal. Chem.* **2007**, 79, 5690-5697.
(145) Takeuchi, M.; Yoshioka, K.; Toyama, Y.; Kagami, A.; Tanaka, H. *Talanta*. **2012**, 97, 527-532.
(146) Gas sample dryers. https://www.permapure.com/products/gas-sample-dryers/
(147) Leckrone, K.J.; Hayes, J.M. *Anal. Chem.* **1997**, 69, 911-918.
(148) Pleil, J.D.; Oliver, K.D.; McClenny, W.A. *Air Poll. Contr. Assoc. J.* **1987**, 37, 244-248.

(149) Iacomini, C.S.; Harrell, J.; Lopez, J. 45th International Conference on Environmental Systems, **2015**.

(150) Fitzgerald, N.; Tyson, J.F.; Leighty, D.A. *J. Anal. At. Spectrom.* **1988**, 13, 13-16.

(151) Yang, J.; Conver, T.S.; Koropchak, J.A.; Leighty, D.A. *Spectrochim. Acta B*. **1996**, 51, 1491-1503.

(152) Huan, Y.; Zhou, J.; Peng, Z.; Cao, Y.; Yu, A.; Zhang, H.; Jin, Q. *J. Anal. At. Spectrom.* **2000**, 15, 1409-1411.

(153) Sundin, N.G.; Tyson, J.F.; Hanna, C.P.; McIntosh, S.A. *Spectrochim. Acta B.* **1995**, 50, 369-375.

(154) Haberhauer-Troyer, C.; Rosenberg, E.; Grasserbauer, M. *J. Chromatogr. A.* **1999**, 852, 589-595.
(155) Welp, L.R.; Keeling, R.F.; Weiss, R.F.; Paplawsky, W.; Heckman, S. *Atmos. Meas. Tech.* **2013**, 6, 1217-1226.

(156) Yang, C.; Zhao, W.; Fang, B.; Xu, X.; Zhang, Y.; Gai, Y.; Zhang, W.; Venables, D. S.; Chen, W. *Anal. Chem.* **2018**, 90, 3307-3312.

(157) Yang, C.; Zhao, W.; Fang, B.; Yu, H.; Xu, X.; Yu, H.; Xu, X.; Zhang, Y.; Gai, Y.; Zhang, W.; Chen, W.; Fittschen, C. *Anal. Chem.* **2019**, 91, 776-779.

(158) Huang, S.Y.; Fedkiw, P.S. *Sep. Sci. Technol.* **2016**, 51, 2932-2939.

(159) Neves, L.A.; Benavente, J.; Coelhoso, I.M.; Crespo, J.G. *J. Memb. Sci.* **2010**, 347, 42-52.

(160) Sun, D.; Zhou, J. *AIChE J.* **2013**, 59, 2630-2639.

(161) Neves, L.A.; Coelhoso, I.M.; Crespo, J.G. *J. Memb. Sci.* **2010**, 360, 363-370.

(162) Chaiyo, S.; Mehmeti, E.; Žagar, K.; Siangproh, W.; Chailapakul, O.; Kalcher, K. *Anal. Chim. Acta.* **2016**, 918, 26-34.

(163) Taurková, P.; Svoboda, M.; Musil, S.; Matoušek, T. *J. Anal. At. Spectrom.* **2011**, 26, 220-223.

(164) Gong, Q.; Demerjian, K.L. *J Air Waste Mgmt Assoc.* **1995**, 45, 490-493.
(165) Burns, W.F.; Tingey, D.T.; Evans, R.C.; Bates, E.H. *J. Chromatogr. A.* **1983**, 269, 1-9.
(166) Zhu, C.; Bright, F.V.; Wyatt, W.A.; Hieftje, G.M. *J. Electrochem. Soc.* **1989**, 136, 567-570.

(167) Patil, Y.P.; Seery, T.A.P.; Shaw, M.T.; Parnas, R.S. *Ind. Eng. Chem. Res.* **2005**, 44, 6141-6147.
(168) Sadaoka, Y.; Matsuguchi, M.; Sakai, Y.; Murata, Y. *Sens. Actuators B*. **1992**, 7, 443-446.

(169) Raimundo Jr., I.M.; Narayanaswamy, R. *Analyst*. **1999**, 124, 1623-1627.

(170) Weiss, M.N.; Srivastava, R.; Groger, H. *Electronics Lett.* **1996**, 32, 842-843.

(171) Huang, P.H. *Sens. Actuator.* **1988**,13, 329-337.

(172) Morris, D.R.; Sun, X. *J. Appl. Polym. Sci.* **1993**, 50, 1445-1452.

(173) Wang, H.; Feng, C.; Sun, S.; Segre, C.U.; Stetter, J.R. *Sens. Actuator B*. **1997**, 40, 211-216.

(174) Feng, C.D.; Sun, S.L.; Wang, H.; Segre, C.U.; Stetter, J.R. *Sens. Actuators B.* **1997**, 40, 217-222.

(175) Keidel**,** F.A. *Anal. Chem.* **1959**, 31, 2043-2048.

(176) Huang, H.; Dasgupta, P.K. *Anal. Chem.* **1990**, 62, 1935-1942.
(177) Su, X.; Xingguo, X.; Dallas, T.; Gangopadhyay, S.; Temkin, H.; Wang, X.; Walulu, R.; Li, J.; Dasgupta, P.K. *Talanta.* **2002**, 56, 309-321.
(178) Kuban, P.; Berg, J.M.; Dasgupta, P.K. *Anal. Chem.* **2004**, 76, 2561-2567.

(179) Star, A.; Han, T.R.; Joshi, V.; Stetter, J. R. *Electroanalysis*. **2004**, 16, 108-12.

(180) Huang, H.; Dasgupta, P.K.; Ronchinsky, S. *Anal. Chem.* **1991**, 63, 1570-1573.

(181) Chen, H.W.; Wu, R.J.; Chan, K.H.; Sun, Y.L.; Su, P.G. *Sens. Actuators B*. **2005**, 104, 80-84.

(182) Su, P.G.; Sun, Y.L.; Lin, C.C. *Sens. Actuators B*. **2006**, 115, 338-343.

(183) Wu, R.J.; Sun, Y.L.; Lin, C.C.; Chen, H.W.; Chavali, M. *Sens. Actuators B*. **2006**, 115, 198-204.

(184) Sheng, L.; Dajing, C.; Yuquan, C. *Nanotechnology*. **2011**, 22.

(185) Huang, H.; Dasgupta, P.K. *Anal. Chem.* **1992**, 64, 2406-2412.
(186) Merle, G.; Wessling, M.; Nijmeijer, K. *J. Memb. Sci.* **2011**, 377, 1-35.

(187) Varcoe, J.R.; Atanassov, P.; Dekel, D.R.; Herring, A.M.; Hickner, M.A.; Kohl, P.A.; Kucernak, A.R.; Mustain, W.E.; Nijmeijer, K.; Scott, K.; Xu, T.; Zhuang, L. *Energy Environ. Sci.* **2014**, 7, 3135-3191.

(188) Gao, Y.; Xu, W.; Mason, B.; Oakes, K.D.; Zhang, X. *Electrochim. Acta.* **2017**, 246, 707-711.

(189) Chen, Z.; Wang, P.; Chang, H. *Anal. Bioanal. Chem.* **2005**, 382, 817-824.

(190) Wang, P.; Chen, Z.; Chang, H. *Sens. Actuator B Chem.* **2006**, 113, 500-509.
(191) Zhu, Z.; Lu, J.J.; Almeida, M.I.; Pu, Q.; Kolev, S.D; Liu, S. *Microchimica Acta.* **2015**, 182, 1063-1070.

(192) Bakker, E.; Bühlmann, P.; Pretsch, E. *Chem. Rev.* **1997**, 97, 3083-3132.

(193) Bühlmann, P.; Pretsch, E.; Bakker, E. *Chem. Rev.* **1998**, 98, 1593-1688.

(194) Zdrachek, E.; Bakker, E. *Anal. Chem.* **2019**, 91, 2-26.
(195) Bakker, E. *Encyclopedia of Analytical Science*. **2019**, 3rd ed., 231-251.

(196) Bakker, E.; Pretsch, E. In Electroanalytical Chemistry: A Series of Advances: Volume 24. A.J. Bard, C.G. Zoski, Eds. CRC press, **2017**, 2-73.

(197) Tanaka, Y. 17 - Bipolar membrane electrodialysis, in: Y. Tanaka (Ed.), Ion exchange membranes (Second Edition), Elsevier, Amsterdam, **2015**, 369-392.

(198) Luo, T.; Abdu, S.; Wessling, M. *J. Membr. Sci.* **2018**, 555, 429-454.

(199) Adams, B. A.; Holmes, E. L. *J. Soc. Chem. Ind*. **1935,** 54, 1-6.

(200) Yee, R.; Rozendal, R. A.; Zhang, K.; Ladewig, B. P. *Chem. Eng. Res. Design* **2012**, 90, 950-959.

(201) Kim, D. S.; Cho, H. I.; Kim, D. H.; Lee, B. S.; Lee, B. S.; Yoon, S. W.; Kim, Y. S.; Moon, G. Y.; Byun, H.; Rhim, J. W. *J. Memb. Sci.* **2009,** 342, 138-144.

(202) Dasgupta, P. K.; Maleki, F. *Talanta.* **2019**, 204, 89-137.

(203) www.permapure.com Last accessed June 1, **2020**.

(204) Dasgupta, P. K. *Anal. Chem.* **1984**, 56, 96-103.

(205) Huang, W.; Dasgupta, P. K. *Anal. Chem.* **2016**, 88, 12,021 - 12,027.

(206) Kuban, P.; Dasgupta, P. K.; Pohl, C. A. *Anal. Chem.* **2007**, 79, 5462-5467.

(207) Higa, M.; Nishimura, M. *Bull. Soc. Sea. Water Sci. Jpn.* **2010**, 64, 244-249.

(208) Kim, K.; Lee, S.; Han, N. W. *Polym. J.* **1993**, 25, 1295-1302.

(209) Rudra, R.; Kumar, V.; Kundu, P. P. *RSC Adv.* **2015,** 5, 83,436-83,447.

(210) Barui, A.; Pal, K.; Banerjee, I., eds. pp 55-90, Elsevier, **2018**.

(211) Kang, M.; Choi, Y.; Moon, S. *J. Memb. Sci.* **2002**, 207, 157-170.

(212) Kang, M. S.; Cho, S. H.; Kim, S. H.; Choi, Y. J.; Moon, S. H. *J. Memb. Sci.* **2003,** 222, 149-161.

(213) Kang, M.; Kim, J. H.; Won, J.; Moon, S.; Kang, Y. S. *J. Memb. Sci.* **2005**, 247, 127-135.

(214) Nitanan, T.; Akkaramongkolporn, P.; Rojanarata, T.; Ngawhirunpat, T.; Opanasopit, P. *Int. J. Pharm.* **2013,** 448, 71-78.

(215) Kim, D. S.; Park, H. B.; Rhim, J. W.; Lee, Y. M. *Solid State Ionics* **2005,** 176, 117-126.

(216) Tsai, C. E.; Lin, C. W.; Hwang, B. J. *J. Power Sources* **2010**, 195, 2166-2173.

(217) Tsai, C. E.; Lin, C. W.; Rick, J.; Hwang, B. J. *J. Power Sources* **2011**, 196, 5470-5477.

(218) Kamjornsupamitr, T.; Sangthumchai, T.; Youngme, S.; Martwiset, S. *Int. J. Hydrogen Energy* **2018**, 43, 11190-11201.

(219) Fogle, M. W. US Patent 3,275,575, September 27, **1966**.

(220) Mollá, S.; Compañ, V., 2011. *J. Memb. Sci.* **2011,** 372, 191-200.

(221) Tiwari, B. R.; Noori, M. T.; Ghangrekar, M. M. *Mater. Chem. Phys.* **2016,** 182, 86-93.

(222) Sharma, D. K. Li, F.; Wu, Y. N. *Coll. Surf. A* **2014,** 457, 236-243.

(223) Yang, J. M.; Wang, N. C.; Chiu, H. C. *J. Memb. Sci.* **2014,** 457, 139-148.

(224) Hao, J.; Gong, M.; Wu, Y.; Wu, C.; Luo, J.; Xu, T. *J. Hazard. Mater.* **2013**, 244, 348-356.

(225) Yang, Y.; Shi, Z.; Holdcroft, S. *Macromolecules* **2004**, 37, 1678-1681.

(226) Gu, S.; He, G.; Wu, X.; Guo, Y.; Liu, H.; Peng, L.; Xiao, G. *J. Memb. Sci.* **2008,** 312, 48-58.

(227) Wu, Y.; Hao, J.; Wu, C.; Mao, F.; Xu, T. *J. Memb. Sci.* **2012,** 423, 383-391.

(228) Wu, C. S.; Lin, F. Y.; Chen, C. Y. Chu, P. P. *J. Power Sources* **2006,** 160, 1204-1210.

(229) Beydaghi, H.; Javanbakht, M.; Kowsari, E. *Ind. Eng. Chem. Res.* **2014,** 53, 16621-16632.

(230) Volkov, V. I.; Dobrovolsky, Y. A.; Nurmiev, M. S.; Sanginov, E. A.; Volkov, E. V.; Pisareva, A. V. *Solid State Ionics* **2008,** 179, 148-153.

(231) Hao, J.; Wu, Y.; Ran, J.; Wu, B.; Xu, T. *J. Memb. Sci.* **2013,** 433*,* 10-16.

(232) Uragami, T.; Nakamura, R.; Sugihara, M. *Makromol Chem. Rapid Comm.* **1982**, 3, 467-470.

(233) Lebrun, L.; Da Silva, E.; Metayer, M. *J. Appl. Polym. Sci.* **2008,** 84, 1572-1580.

(234) Sahu, A. K.; Selvarani, G.; Bhat, S. D.; Pitchumani, S.; Sridhar, P.; Shukla, A. K.; Narayanan, N.; Banerjee, A.; Chandrakumar, N. *J. Memb. Sci.* **2008**, *319*, 298-305.

(235) Abd El-Kader, K. M. *J. Appl. Polym. Sci.* **2003,** 88, 589-594.

(236) Wu, X.; Wang, X.; He, G.; Benziger, J. *J. Polymer Sci. B: Polym. Phys.* **2011,** 49, 1437-1445.

(237) Gardner, C. L.; Anantaraman, A. V. *J. Electroanal. Chem.* **1998,** 449, 209-214.

(238) Misra, B. N.; Mehta, I. K.; Khetarpal, R. C. *J. Polym. Sci. Polym. Chem.* **1984**, 22, 2767-2775.

(239) Misra, B. N.; Chandel, P. S.; Dogra, R. *J. Polym. Sci. Polym. Chem.* **1978**, 16, 1801-1805.

(240) Hassan, C. M.; Peppas, N. A. Springer, **2000**. 37-65.

(241) Tretinnikov, O. N.; Sushko, N. I. *J. Appl. Spectrosc.* **2015,** 81,1044-1047.

(242) Yang, C.; Srinivasan, S.; Bocarsly, A. B.; Tulyani, S.; Benziger, J. B. *J. Memb. Sci*. **2004**, 237, 145-161.

(243) Napoli, L.; Franco, J.; Fasoli, H.; Sanguinetti, A. *Int. J Hydrogen Energy* **2014,** 39, 8656-8660.

(244) Sone, Y.; Ekdunge, P.; Simonsson, D. *J. Electrochem. Soc*. **1996**, 143, 1254 -1259.

(245) Slade, S.; Campbell, S. A.; Ralph, T. R.; Walsh, F. C. *J. Electrochem. Soc.* **2002,** 149, A1556-A1564.

(246) Liu, L.; Chen, W.; Li, Y. *J. Memb. Sci.* **2016,** 504, 1-9.

(247) Kohlraursch, F.; Maltby, M. E. Das Elecktrische Leitvermögen wäβriger Lösungen von Alkalichloriden und Nitraten. *Wiss Abhdlgen. D. Phys. T. Reichsansalt* **1900,** *3,* 156-227.

(248) Nafion N115, N117, N1110. Product Bulletin P-12. Last accessed April 20, **2020**.

(249) Zook, L. A.; Leddy, J. *Anal. Chem.* **1996,** 68*,* 3793-3796.

(250) Eisenberg, H.; Mohan, G. R. *J. Phys. Chem.* **1959,** 63,.671-680.

(251) Jordan, D. O.; Kurucsev, T.; Martin, M. L. *Trans Faraday Soc.* **1969,** 65, 606-611.

(252) Stellwagen, N. C., Gelfi, C.; Righetti, P. G. *Biopolymers* **1997**, 42, 687-703.

(253) Dawson, L. R.; Golben, M.; Leader, G. R.; Zimmerman Jr, H. K. *J. Phys. Chem.* **1951**, 55, 1499-1502.

(254) Dietrich, O. Last accessed May 25, **2020**.

(255) Suresh, G.; Scindia, Y. M.; Pandey, A. K.; Goswami, A. *J. Memb. Sci.* **2005,** 250, 39-45.

(256) Chouhan, B.; Shelor, C. P.; Huang, W.; Chen, Y.; Dasgupta, P. K. *Anal. Chem.*, **2020,** 92, 5561-5568.

(257) Spindler, M.; Herold, S.; Acker, J.; Brachmann, E.; Oswald, S.; Menzel, S.; Rane, G. *Thin Solid Films*, **2016,** 612*,* 322-326.

(258) Small, H.; Stevens, T. C.; Bauman, W. *Anal. Chem.* **1975**, *47* (11), 1801–1809.

(259) Dasgupta, P. K.; Maleki, F.. *Talanta* **2019**, *204*, 89–137.

(260) Srinivasan, K.; Omphroy, B. K.; Lin, R.; Pohl, C. A. *Talanta* **2018**, *188*, 152–160.

(261) Rokushika, S.; Zong, Y. Q.; Zhuo, L. S.; Hatano, H. *J. Chromatogr. A.* **1983**, *280*, 69–76.

(262) Sjögren, A.; Boring, B. C.; Dasgupta, P. K.; Alexander IV J. N. *Anal. Chem.* **1997**, *69*, 1385–1391.

(263) Boring, C. B.; Dasgupta, P. K.; Sjögren, *J. Chromatogr.* **1998,** *804,* 45-54.

(264) Kuban, P.; Dasgupta, P. K. *J. Sep. Sci.* **2004,** *27,* 1441-1457.

(265) Sedyohutomo, A.; Lim, L. W.; Takeuchi, T. *J. Chromatogr. A* **2008,** *1203,* 239-242.

(266) Huang, W. *Anal. Chim. Acta* **2021,** *1143,* 210–224.

(267) Huang, W.; Plistil, A.; Stearns, S., Dasgupta, P. K. *Talanta Open,* **2021,** *3*, 100029.

(268) Kuban, P.; Dasgupta, P. K.; Pohl, C. A. *Anal. Chem.* **2007,** *79,* 5462–5467.

(269) Huang, X. J.; Dasgupta, P. K. *Anal. Chim. Acta* **2011,** *689*, 155–159.

(270) Huang, X. J.; Foss, F.; Dasgupta, P. K. *Anal. Chim. Acta* **2011,** *707,* 210–217.

(271) Huang, W.; Dasgupta, P. K. *Anal. Chem.* **2016,** *88*, 12021–12027.

(272) Chouhan, B.; Shelor, C.P.; Huang, W.; Chen, Y.; Dasgupta, P. K. *Anal. Chem.* **2020**, *92*, 5561–5568.

273 Maleki, F.; Dasgupta, P. K. *Anal. Chem.* **2020**, *92*, 13378–13386.

(274) Qi, D.; Okada, T.; Dasgupta, P. K. *Anal. Chem.* **1989,** *61*, 1383-1387.

(275) Tan, S.; Laforgue, A.; Bélanger, D. *Langmuir* **2003**, *19*, 744–751.

(276) Kraytsberg, A.; Ein-Eli, Y. *Fuels* **2014**, *28*, 7303–7330.

(277) Kusoglu, A.; Weber, A. Z. *Chem. Rev.* **2017**, *117*, 987–1104.

(278) Kreuer, K. D. *Chem. Mater.* **2013**, *26*, 361–380.

(279) Liao, H.; Dasgupta, P. K. *Anal. Chem.*, **2016,** *88*, 2198–2204.

(280) Huang, W.; Pohl, C. A.; Dasgupta, P. K. *J. Chromatogr A* **2018,** *1550,* 75-79.

(281) Dasgupta, P. K. *Anal. Chem.* **1984,** *56*, 96-103.

(282) Gormley, P. G.; Kennedy, M. *Proc. R. Ir. Acad., Sect. A* **1949,** *52*, 163-169.

(283) McKays, W.; Crawford, M. E. 2nd ed.; McGraw-Hill, New York, 1980. pp 66-68.

(284) Dasgupta, P. K.; Bligh, R. Q.; Lee, J.; D'Agostino V. *Anal. Chem*. **1985,** *57*, 253-257.

(285) Stevens, T. S.; Davis, J. C.; Hamish, S. *Anal. Chem.* **1981,** *53*, 1488–1492.

(286) Stevens, T. S.; Jewett, G. L.; Bredeweg, R. A. *Anal. Chem.*, **1982,** *54*, 1206–1208.

(287) Karu, N.; Dicinoski, G. W.; Haddad, P. R. *TrAC Trends Anal. Chem.,* **2012,** *40,* 119-132.

(288) Al-Horr, R.; Dasgupta, P. K.; Adams, R. L. *Anal. Chem.* **2001,** *73,* 4694-4703.

(289) Gjerde, D. T.; Fritz, J. S.; Schmuckler, G. *J. Chromatogr. A* **1979,** *186*, 509-519.

(290) Okada, T.; Kuwamoto, T. *Anal. Chem.* **2001,** *57*, 829-833.

(291) Zhang. M.; Dasgupta, P. K. Issue 215, October 2015. http://q-more.chemeurope.com/q-more-articles/215/conductance-or-admittance.html

(292) Zhang, M.; Stamos, B. N.; Dasgupta, P. K. *Anal. Chem.* **2014,** *86,* 11,547-11,553.

(293) Huang, W.; Chouhan, B.; Dasgupta, P. K. *Anal. Chem.,* **2018,** *90,* 14,561-14,568.

(294) Kadjo, A. F.; Dasgupta, P. K.; Shelor, C. P. *Anal. Chem.*, **2020,** *92,* 6391-6400.

(295) Golay, M. J. E. *Anal. Chem.* **1968**, *40*, 382-384.

(296) Blumberg, L. M. *J. Chromatogr. A,* **2017,** *1524*, 303-306.

(297) Christian, G. D.; Dasgupta, P. K.; Schug, K. A. *Analytical Chemistry.* 7th Ed. Wiley, 2014. Ch 21. pp. 678-679.

Biographical Information

Fereshteh Maleki earned her B. Sc. in chemical engineering from University of Kerman (UK) in Iran in 2009. After that, she did her studies in M. Sc. in chemical engineering at the University of Isfahan ended in 2011. Next, she worked for 4 years as a chemical product development manager in a rubber/plastic chemical additive company. Next, she came to the United States and joined the University of Texas at Arlington accepting the offer to pursue her Ph.D. in analytical chemistry in fall 2015. She joined Professor Purnendu K. Dasgupta's group by end of the fall of 2015 working in the field of ion chromatography focusing on developing novel moldable ion-exchange polymer to fabricate capillary size suppressors. She developed a microsuppressor for open tubular ion chromatography from a novel moldable high capacity ion-exchange polymer.